UNIVERSITÀ DEGLI STUDI DI PALERMO

Dottorato di Ricerca in Ingegneria Civile, Ambientale e dei Materiali
Dipartimento di Ingegneria
Settore Scientifico Disciplinare ICAR/07

VOLUMETRIC BEHAVIOUR OF SOILS EXPERIENCING WIDE CHANGES IN THE DEGREE OF SATURATION

IL DOTTORE
Ing. Vincenzo Butticè

LA COORDINATRICE
Prof.ssa Ing. Antonina Pirrotta

IL TUTOR
Prof. Ing. Alessio Ferrari

CICLO XXXIII
ANNO CONSEGUIMENTO TITOLO 2021

Index

Ringraziamenti

È estremamente complesso tradurre in parole dei ringraziamenti che siano all'altezza di esprimere la gratitudine e il riconoscimento verso le persone che mi hanno accompagnato in questo percorso triennale.

Desidero ringraziare il mio Tutor, il Prof. Alessio Ferrari, persona di elevata caratura professionale e umana, per avermi dato la possibilità di intraprendere questo percorso di ricerca e per avermi guidato in questi anni. È stato un onore lavorare per tre anni al suo fianco. Un ringraziamento anche al Dott. Ing. Marco Rosone, per il suo costante supporto, e al Prof. Maurizio Ziccarelli, per i suoi preziosissimi consigli. Ringrazio il Prof. Calogero Valore, colui che mi ha spinto ad intraprendere la strada della Ricerca e che, per questo, non riuscirò mai a smettere di ringraziare. Un Ringraziamento alla Coordinatrice, la Prof.ssa Pirrotta, per l'impegno profuso per noi Dottorandi.

Un ringraziamento speciale ad un pilastro del laboratorio di Geotecnica dell'Università degli Studi di Palermo, il Dott. Giovanni Sapienza, lavoratore instancabile e sempre disponibile nel fornire il suo supporto tecnico.

Doverosi sono i ringraziamenti al Prof. Tomasz Hueckel della Duke University, per avermi accolto nel suo gruppo di ricerca. Durante le tante discussioni avute ho potuto beneficiare della sua vasta cultura, che ha influenzato il mio percorso di Dottorato e dalla quale ho tratto diversi spunti per la stesura di questa tesi.

Ringrazio sinceramente anche il Prof. Manolis Veveakis per i suoi suggerimenti e al Dott. Boleslaw Mielniczuk per il suo supporto tecnico. Ma ci tengo a ringraziare tutto il gruppo della Duke che, oltre a supportarmi scientificamente, hanno rappresentato la mia famiglia durante i sei mesi statunitensi. Dunque, nuovamente grazie a Tomasz e Margaret, Manolis e Nicoletta, Bolo, Carolina, Hadrien e Alex.

Ci tengo a ringraziare anche il Prof. Guido Gottardi per la proficua collaborazione instaurata in questi anni, la quale costituisce una parte importante del mio lavoro di ricerca, e l'Ing. Carmine Gerardo Gragnano per la disponibilità e il supporto scientifico datomi.

Un affettuoso ringraziamento va a Vincent, il quale mi ha accolto nella sua casa e ha costantemente cercato di sopperire alla distanza della mia famiglia. Una persona speciale, premurosa e sempre disponibile ad aiutare il prossimo. Farà per sempre parte della mia famiglia. Alla mia amica/collega Silvia, per la sua costante vicinanza e supporto morale, per il suo prezioso aiuto profuso nella stesura di questa tesi.

Adesso i ringraziamenti più difficili, perché rivolti alle persone più vicine: ai miei genitori, guide perpetue nella mia vita, ai miei fratelli Giuseppe e Matteo, a Enzo e Gabriella, Irene e Daniele, Davide, Eleonora, Giuseppe, Salvatore, Rosaria, Stefano, Giovanna e Giuseppina.

Infine, voglio ringraziare la mia futura moglie, Mariachiara, parte integrante della mia vita da tredici anni, con cui ho sempre condiviso le decisioni che mi hanno permesso di essere quello che sono oggi. Persona straordinaria, propulsore della mia carriera, la quale mi ha supportato nei momenti più difficili e sopportato il mio "aver poco tempo" e il mio essermene andato a più di 7.700 km per seguire la carriera; a te va il ringraziamento più grande.

Abstract

The new challenges dictated by global warming and the increase of the drylands impose us to highlight the volumetric behaviour of the unsaturated soils when they approach the dry state and to investigate the role of the soil water retention curve on the evolution of the elastic domain. Nevertheless, some models, especially those expressed in terms of effective stress, take into account only the link between the water retention curve and the Loading-Collapse curve (LC) in the transition from saturated to unsaturated state and the relationship between the two curves has never been fully investigated.

In this thesis, the behaviour of unsaturated soils in a wide range of degree of saturation was analysed. Different materials were tested and to cover the suction range, which is expected to be different, a combination of suction-control and suction measurement techniques was used (e.g. negative water column, axial translation, vapour equilibrium).

The new equation proposed to model the compressibility coefficient is able to model the elastic domain in the entire range of the degree of saturation (from saturated to dry state).

A thorough analysis on the new shape of the yield curve is also reported. The new shape is consistent to the classical soils mechanics approach, which suggests that the yield stress at saturated condition is almost the same of the yield stress at dry state. In addition, the characteristics points of the new yield curve are related to the characteristic points of the water retention curve.

The mathematical link between the soil water retention curve and the Loading-Collapse curve suggests that also a mathematical link between the elastic domain and other soil properties (e.g. Pore Size Distribution and Relative Permeability function) exist and they are easily obtainable.

In order to properly understand the hydro-mechanical behaviour of unsaturated soils, especially granular soils, the evolution of the capillary force and water pressure inside the water bridge between two or three spheres or cylinders was analysed. The evolution of the water pressure during evaporation tests and separation tests was for the first time measured directly using a micro-burette

and compared with the Laplace's pressure calculated from the measured bridge curvatures along the process. The agreement between the two measures was well. Starting from the saturated state, as the drying process proceeds the negative capillary pressure increase up to a maximum point, after which the suction decrease until the rupture of the meniscus. After rupture, the capillary pressure is equal to zero, like in the case of the saturated pore. However, to understand the macro-behaviour of unsaturated soils and then to explain the trend of the compressibility coefficient with suction, it is necessary to consider the attractive stress relaxion in multi-grain assemblies as the cumulation of microscale forces and processes from capillary water bridge. For these reasons the evolution of the capillary force during a drying process was also determined, which allowed to determine a qualitative link between the micro- and macro-scale was obtained.

The new framework of the Loading – Collapse curve was validated on a natural undisturbed soil. The tested soil (a sandy silt) has been picked up from the embankment of the river Secchia. Due to continuous river level fluctuations and changing climatic and environmental conditions, flood embankment materials experience frequent variations in degree of saturation and suction values. Such variations strongly impact the earthwork performance both in terms of seepage and stability conditions. For these reasons, a detailed characterization of the material behaviour in unsaturated conditions was carried out. Experiments were designed in order to highlight the response of the involved soil in terms of changes in matric suction and confining stress. All tests were performed on undisturbed samples from the embankment. Obtained results enabled, to quantify the evolution of the yield stress with suction, to validate the new equation proposed for the evolution of the compressibility coefficient, to assess the collapse upon wetting behaviour, to get detailed information on the water retention behaviour and to define the relative permeability of the soil.

Riassunto

Le nuove sfide dettate dal riscaldamento globale e l'aumento della desertificazione ci impone di evidenziare il comportamento dei terreni parzialmente saturi quando raggiungono la condizione di terreno asciutto e di studiare l'influenza della curva di ritenzione del terreno sull'evoluzione del dominio elastico. Tuttavia, alcuni modelli, specialmente quelli espressi in termini di tensioni efficaci, tengono in conto l'influenza della curva di ritenzione sull'evoluzione della Loading-Collapse curve (LC), ma solo nella transizione tra terreno saturo e terreno parzialmente saturo e la relazione tra le due curve non è mai stata pienamente investigata.

In questa tesi, attraverso un accurato lavoro sperimentale è stato analizzato il comportamento dei terreni parzialmente saturi in un ampio range del grado di saturazione. Sono stati testati diversi materiali e per coprire i range di suzione, i quali sono attesi molto differenti in funzione del materiale, sono stati utilizzati diverse combinazioni di tecniche per il controllo e la misura della suzione (e.g. colonna d'acqua negativa, traslazione degli assi, equilibrio del vapore).

La nuova equazione proposta per modellare il coefficiente di compressibilità è idonea a descrivere l'evoluzione della tensione di snervamento nell'intero campo del grado di saturazione (dalla condizione satura a quella asciutta). Nella tesi è riportata anche una dettagliata analisi della forma della curva di snervamento. La nuova forma è consistente con l'approccio della Meccanica Classica, il quale mostra che la tensione di snervamento del terreno saturo è pressoché uguale alla tensione di snervamento del terreno asciutto. In aggiunta, i punti caratteristici della nuova curva di snervamento sono stati correlati con i punti caratteristici della curva di ritenzione.

La correlazione matematica tra la curva di ritenzione del terreno e la Loading – Collapse curve suggerisce anche una correlazione tra il dominio elastico del terreno e altre proprietà meccaniche (e.g. curva della distribuzione delle dimensioni dei pori e la permeabilità relativa) e che sono facilmente determinabili.

Al fine di comprendere in modo compiuto il comportamento idro-meccanico dei terreni parzialmente saturi, con particolare riferimento ai terreni granulari, è stata analizzata l'evoluzione della pressione all'interno di un menisco capillare tra due o tre sfere o cilindri. L'evoluzione della pressione capillare durante test di evaporazione e separazione è stata per la prima volta misurata direttamente attraverso una micro-buretta e comparata con la pressione capillare calcolata utilizzando l'espressione di Laplace. L'agreement tra le due curve è ottimo. Partendo dalla condizione satura, durante il processo di drying le misure mostrano innanzitutto un aumento della suzione fino ad un punto di massimo, superato il quale la suzione decresce fino alla rottura del menisco. La rottura rappresenta il punto in cui la pressione capillare è uguale a zero, stesso che si ottiene anche quando i pori sono completamente saturi. Tuttavia, per comprendere il comportamento dei terreni parzialmente saturi alla macro-scale e interpretare fisicamente l'evoluzione del coefficiente di compressibilità con la suzione, è necessario considerare gli stress di attrazione in un sistema formato da diversi grani come l'effetto cumulato di forze alla micro-scale e processi dovuti alla presenza dei menischi. Per questa ragione è stata determinata anche l'evoluzione della forza capillare durante un processo di drying, la quale ha permesso di determinare un link qualitativo tra il comportamento alla micro-scale e alla macro-scale.

Il nuovo framework per la Loading – Collapse è stato validato su un terreno naturale e indisturbato. Il terreno testato (un limo sabbioso) è stato prelevato dall'argine del fiume Secchia. A causa delle continue fluttuazioni del livello del fiume e delle variazioni delle condizioni climatiche e ambientali, gli argini sono sottoposti a frequenti variazioni del grado di saturazione e di conseguenza della suzione. Tali variazioni influenzano fortemente il comportamento delle opere di materiale sciolto sia in termini di filtrazione che di stabilità. Per questo motivo è stato pianificato un dettagliato programma sperimentale che fosse in grado di evidenziare la risposta meccanica del terreno sotto diverse condizioni di suzione e tensione di confinamento. Tutti i test sono stati eseguiti su campioni indisturbati provenienti dall'argine. I risultati ottenuti hanno permesso di quantificare l'evoluzione della tensione di snervamento al variare della suzione, di validare la nuova equazione proposta per

modellare l'evoluzione del coefficiente di compressibilità con la suzione, di valutare il collasso per imbibizione, di dare informazioni dettagliate sulla curva di ritenzione e di definire la permeabilità relativa del terreno.

List of Symbols

Greek symbols

$\alpha(s)$	Suction – dependent parameter	-
β	Parameter which controls the rate of increase of soil compressibility with suction	-
β_H	Coefficient of the compressibility for the plastic part of the degree of saturation	-
β_s	Parameter which accounts the swelling tendency of the assemblages	-
$\varepsilon_s, \varepsilon_s^e, \varepsilon_s^p$	Total, elastic and plastic deviatoric strains	-
$\varepsilon_v, \varepsilon_v^e, \varepsilon_v^p$	Total, elastic and plastic volumetric strains	-
ε_{vs}^e	Elastic volumetric strain induced by changes in suction	-
ε_{vs}^p	Plastic volumetric strain associated with the SI yield surface	-
ε_{vs}	$\varepsilon_{vs}^e + \varepsilon_{vs}^p$	-
$\varepsilon_{v(p-u_a)}^e$	Elastic volumetric strain induced by changes in net mean stress	-
$\varepsilon_{v(p-u_a)}^p$	Plastic volumetric strain associated with the LC yield surface	-
$\varepsilon_{v(p-u_a)}$	$\varepsilon_{v(p-u_a)}^e + \varepsilon_{v(p-u_a)}^p$	-
η	Parameter that defines the proportion between the compression and the swelling coefficient	-
ζ	Parameter	-
θ	Coefficient of the compressibility	-
$\lambda(0)$	Compressibility parameter for change in net mean stress for virgin states in saturated conditions	-
$\lambda(s)$	Compressibility parameter for change in net mean stress for virgin states	-
λ_0	Compressibility parameter for change in net mean stress for virgin states in saturated conditions	-
λ_d	Compressibility parameter for change in net mean stress for virgin states in dry conditions	-
λ_m	Compressibility parameter for change in net mean stress at low confining stresses	-
λ_s	Compressibility parameter for change in suction for virgin states	-
λ_{se}	Slope of the $S_r - e$ curve under constant suction larger than the air-entry value	-
λ_{sr}	Slope of the wetting/drying curves in the plain S_r – ln s	-
$\lambda(s_{eq})$	Compressibility parameter for change in mean equivalent stress for virgin state	-
$\lambda_{in}(s_{eq})$	Compressibility parameter for change in mean equivalent stress for virgin state at low confining stress	-
π_H	Material parameter	-
σ	Total stress	Pa

σ'	Effective stress	Pa
σ_{net}	Net stress	Pa
σ^*	Bishop's stress	Pa
$\hat{\sigma}$	Translated stress	Pa
$\sigma_0(s)$	Suction stress	-
ϕ	Dissipation component	-
ψ	Total suction	Pa
ψ_2	Component of the Helmholtz free energy that depends on plastic strain	-
Ω	Material parameter	-

Latin symbols

A	Ratio of impedance of the ceramic disc	-
a	Constant equal to the maximum $\sigma_0(s)$ of the soil for infinite suction	-
a_r	Suction correspondent to the residual void ratio	kPa
a_1	Material parameter	-
a_s	Material parameter	kPa
A(s)	Suction – dependent parameter	-
b	Parameter controlling point of maximum potential collapse	-
C_c	Compression coefficient	-
C_s	Swelling coefficient	-
C_u	Uniformity coefficient	-
c	Coupling parameter	-
d	Material parameter	-
e	Void ratio	-
e_1	Void ratio just before the inundation	-
e_a	Air void ratio	-
e_m	Microstructural void ratio	-
e_m^*	Intra-assemblage void ratio	-
e_{wh}	Residual water ratio	-
e^p	Plastic void ratio	-
G_s	Specific gravity	-
I_e	Collapse Index	
k	Elastic compressibility parameter for changes in net mean stress	-
k_1	Parameter that controls the path traced by the corner between the LC and the SD yield curves during a wetting stage producing yielding on the SD	-
k_2	Parameter that controls the magnitudes of the shifts in the primary drying and primary wetting curves caused by plastic volumetric strains.	-
$k(0)$	Elastic compressibility parameter for change in net mean stress in saturated conditions	-
$k(s)$	Elastic compressibility parameter for change in net mean stress in unsaturated conditions	-
k_{sr}	Slope of the scanning curve in the plane S_r – ln s	-
k_s	Elastic compressibility parameter for changes in suction	-

K_H	Elastic modulus	Pa
K_{ref}	Bulk elastic modulus	Pa
L	Specimen height	m
m	Fitting parameter	-
M	Parameter	-
n	Fitting parameter	-
n^e	Nonlinearity exponent	-
$N(s)$	Specific volume at $p = p^c$	-
p	Total mean stress	Pa
$p\text{-}u_a$	Net mean stress	Pa
$(p - u_a)_0$	Yield stress	Pa
$(p - u_a)_0^*$	Yield stress for saturated conditions	Pa
P_{atm}	Atmospheric pressure	Pa
p^c	Reference state o critical pressure	Pa
p'_{ref}	Reference mean stress	Pa
p'_c	Effective yield stress	Pa
p'_{c0}	Effective yield stress at saturation condition	Pa
p'_{cr}	Critical state pressure	Pa
p'_{cr0}	Initial critical state pressure	Pa
r	Constant related to the maximum compressibility of the soil	-
r_1	External radius of curvature of the meniscus	m
r_2	Internal radius of curvature of the meniscus	m
r_{iso}	Radius of mobilisation of the isotropic mechanism	-
R	Universal gas constant	J/(mol K)
RH	Relative humidity	%
s	Matric suction	Pa
s*	Modified suction	Pa
s_{air}	Air entry value	Pa
s_D	Actual drying yield suction	Pa
s_{eq}	Equivalent suction	Pa
s_e	Air entry value	kPa
s_0	Reference yield suction	Pa
S_r	Degree of saturation	-
S_r^0	Degree of saturation at zero suction	-
S_r^e	Elastic component of the degree of saturation	-
S_r^{eff}	Effective degree of saturation	-
S_r^M	Macroscopic degree of saturation	-
S_r^m	Microscopic degree of saturation	-
S_r^p	Plastic component of the degree of saturation	-
$S_{r,cluster}$	Degree of saturation of the cluster	-
$S_{r,res}$	Residual degree of saturation	-

T	Temperature	K
T_l	Coefficient of the surface tension of liquid-gas interface	-
T_s	Coefficient of the surface tension of solid-gas interface	-
T_{sl}	Coefficient of the surface tension of solid-liquid interface	-
T_{su}	Surface tension	N/m
u_a	Pore air pressure	Pa
u_w	Pore water pressure	Pa
v	Specific volume	-
v_w	Specific water volume	-
v_{mol}	Molar volume of liquid water	m^3/mol
V	Volume of the specimen	m^3
V_w	Total water volume exchanged during a water pressure change	m^3
w	Water content	-
w_l	Liquid limit	-
w_n	Natural water content	-
w_p	Plastic limit	-
W, W^e, W^p	Total, elastic and plastic work input	-

Abbreviations

ACMEG	Advanced Constitutive Model for Environmental Geomechanics, unsaturated extension
ATT	Axial Translation Technique
BBM	Barcelona Basic Model
BExM	Barcelona Expansive Model
CPTU	Piezocone Penetration Test
ESEM	Environmental Scanning Electron Microscope
HAEV	High Air-Entry Value
ICL	Intrinsic Comprension Line
LC	Loading – Collapse
MIP	Mercury intrusion porosimetry
MCC	Modified Cam – Clay
NCL	Normal Compression Line
NL	Neutral Line
SD	Suction - Decrease
SI	Suction - Increase
SWRC	Soil Water Retention Curve
URL	Unloading-Reloding Line
VET	Vapour Equilibrium Technique

1. Introduction

Drylands cover about 41% of the Earth's surface (Reynolds et al. 2007) and many model predictions show that they will experience an accelerated expansion in the range of 11-23% by the end of the 21st century (Huang et al. 2015). The main cause of this increase is due to climate change. However, the on-going pattern of climate change will not only raise in temperature but will also intensify the water cycle, reinforcing existing patterns of water scarcity and abundance, increasing the risk of droughts and floods.

Climate changes are likely to lead to changes in soil conditions. For the scenario predicted for many areas of the World, where the winter becomes wetter, but summer becomes drier, this will result in greater extremes of wetting and drying (Toll et al. 2012). Recent researchs investigated the soil responses to climate change. Many works are focused on the stability of natural slopes (e.g. Briceno et al. 2007, Dehn et al. 2000, Dixon et al. 2006, Huggel et al. 2010, Laloui et al. 2010, McInnes et al. 2007) on the temperature-induced instability in permafrost region (e.g. Gruber and Haeberli, 2007, Harris, 2005) on geotechnical infrastructure (e.g. Vardon, 2014).

However, regarding the potential impacts on the soils due to long-term drying (i.e. increase in temperature along with drought) the recent experimental works are only focused on the desiccation cracking (e.g. Peron et al. 2008, 2009) and shrinkage (Hu et al. 2008,2009). But, long-term drying could also affect the mechanical behaviour of soils. Donald (1956) indeed has shown that the available shear strength of unsaturated sandy soils tends after an initial increase, to the shear strength in saturated condition once the degree of saturation decreases significantly.

However, regarding the volumetric behaviour of unsaturated soils, the existing elasto-plastic models take into account only the transition between the saturated and partially saturated state. In addition, many models for partially saturated soils does not take into account the hydraulic properties of the soils and for this reason, they are called *uncoupled models* (e.g. Alonso et al. 1990, Wheeler &

Sivakumar 1995, Gens and Alonso 1992, Alonso et al. 1994, 1998, Sun et al. 2000, 2003, Georgiadis et al. 2005, Rampino et al. 2000).

In contrast, the models using the effective stress like stress variable (e.g. Wheeler et al. 2003, Sun et al. 2010, Nuth and Laloui 2007) are called *coupled models* and they are able to describe also the hydraulic behaviour of unsaturated soils. For instance, in the ACMEG-s model (Nuth and Laloui 2007) the shape of the elastic-domain is strictly linked to the water retention curve. In fact, in the saturated domain (up to the air-entry) the pores remain filled with water so that the capillary mechanisms are not activated and a positive suction can take place without affecting the yield stress that remains equal to its saturated value.

This research is focused on the relationship between the water retention curve and the Loading-Collapse curve. In particular, it is explored the link between the water retention curve and the evolution of the compressibility coefficient with suction. As known, the yield stress is strictly linked to the compressibility coefficient of the soil which in turn depends on the water retention curve. One of the stabilizing effects recorded in unsaturated soils is due to the capillary effect which is caused by the presence of a curved air-water interface (meniscus) in the large pores (macropores). However, also the water stored in the micropores could affect the hydro-mechanical behaviour, and then the compressibility of the soil. This physical mechanism is called absorption effect which is caused by exchangeable cation hydration, mineral surface or crystal interlayer surface hydration. Obviously, the shape of the water retention effect depends on the structure of the soil (mono or double structure). Consequently, to better understand the hydro-mechanical behaviour of unsaturated soil it was necessary to evaluate the experimental response of different kinds of material from a macro- and micro-scale point of view.

1.1 Objectives and outline of the thesis

In this thesis, a systematic approach was used to analyse the hydro-mechanical behaviour of partially saturated soils in a wide range of the degree of saturation. In particular, this thesis aims to:

- analyse the limit of the elasto-plastic models for unsaturated soils in the literature to describe the transition between partially saturation and dry state;

- shed light over the evolution of the yield stress over the entire range of the degree of saturation from an experimental perspective;

- link the mechanical behaviour of the soils to their hydraulic properties;

- propose a new equation to improve the existing frameworks;

- provide a microscopic interpretation of the hydro-mechanical behaviour of unsaturated soils and to link the features at micro-scale to the geomechanical properties at macro-scale.

In order to carefully investigate and analyse the hydro-mechanical behaviour of unsaturated soils from saturated to dry state, this research work is organised as follows:

Chapter 2 reports a review of the many elasto-plastic models for unsaturated soils in the literature. The review is organized by dividing the frameworks according to the stress state variable used.

Chapter 3 is devoted to the experimental characterisation of the volumetric behaviour of unsaturated soils. In order to describe different mechanical behaviour, three different soils were tested (quartz sand, Speswhite kaolin and a scaly clay). To cover the suction range, which is expected to be different for the tested materials, a combination of suction-control and suction measurement techniques was used. To complete in a properly manner the experimental characterization of the soils, the hydraulic properties are also determined.

Chapter 4 presents a new framework to model the soil compressibility which is able to describe the evolution of the yield stress in the entire range of the degree of saturation. The proposed equation models the evolution of the compressibility coefficient with suction and depends on the soil water

retention curve of the materials, permitting to obtain in a simple way a coupled hydro-mechanical model for partially saturated soils.

Chapter 5 reports the experimental characterization carried out at the micro-scale. The experimentation was performed at the Duke's Multiphysics Geomechanics Lab (MGLab) under the supervision of Prof. Tomasz Hueckel and thanks to the precious contribution of Prof. Manolis Veveakis and PhD. Boleslaw Mielniczuk. A new experimental device is designed for the measurements of the water pressure inside the water bridge between two grains. The effects of the evolution of the capillary pressure on the volumetric behaviour of the soils at macro-scale are analysed. In addition, using a MatLab code, the evolution of the capillary force is determined.

Chapter 6 is devoted to the experimental characterization of natural undisturbed soil. The first part of the chapter reports the experimental results carried out on the material from the embankment of the river Secchia. The volumetric response, water retention behaviour, potential collapse and hydraulic conductivity are investigated in a wide range of suction. In the second part of the chapter, the experimental results are used to validate the new framework proposed to model the evolution of the compressibility coefficient from saturated to dry state.

Finally, **Chapter 7** summarizes the conclusion and the main achievements of this thesis. Suggestion for future works on modelling of unsaturated soils.

2. Elasto-plastic models for unsaturated soils

2.1 Stress State variables for unsaturated soils

The development of constitutive models for partially saturated soils is strictly linked to the discussion on effective stress. Historically, the study carried out by Bishop (1959) is considered the first theoretic and experimental work proposed in order to extend the classical definition of the effective stress (Terzaghi 1936). Bishop (1959) proposed to add a portion of suction to the total stress to obtain a unique effective stress:

$$\sigma_{ij}^{'} = \sigma_{ij} - u_a \delta_{ij} + \chi (u_a - u_w) \delta_{ij} \tag{2.1}$$

where χ depends on the degree of saturation, assuming values between 0, in dryer condition, and 1, in saturated condition.

The major objection encountered by the Bishop's proposal was the impossibility of explaining the collapse upon wetting. This difficulty was soon recognised in early researches (e.g. Bishop and Blight 1963, Blight 1965, Burland 1965, Aitchison 1967). The only way to obtain a consistent representation of volumetric behaviour is by using two independent stress variables; total stress and suction were the parameters chosen by those authors.

Many elasto-plastic models were formulated using these two independent stress variables. In subsequent years, several authors had recourse to effective stresses in their constitutive models. Their formulations vary widely, but they essentially require two independent stress components: one is the effective stress alternatively to the net stress, and one is the suction.

In general, as well explained by Gens (1996), the two stresses variable used in the classical constitutive models for unsaturated soil could be summarized as follows:

$$\sigma_{ij} - u_a \delta_{ij} + \mu_1 (s,...) \delta_{ij}; \qquad \mu_1 (s,...) \delta_{ij} \tag{2.2}$$

where μ_1 is function of the suction and other variables (i.e the degree of saturation). Depending on the expression used to define μ_1, it is possible to divide the elasto-plastic models for partially saturated soils in three classes:

1. $\mu_1 = 0$;
2. $\mu_1 = \mu_1(s)$;
3. $\mu_1 = \mu_1(s, S_r)$.

The first case corresponds to the use of the mean net stress. With this choice, the stress path is simple to define, but the hydraulic behaviour of unsaturated soils cannot be described. In fact, these models are able to consider only the irreversible volumetric behaviour of soils without taking into account the variations of the degree of saturation or water content. These models are called *uncoupled models* (e.g. Alonso et al. 1990; Wheeler and Sivakumar, 1995; Gens and Alonso, 1992; Alonso et al. 1994, 1998; Rampino et al. 2000; Wheeler, 1996).

In the second group, the stress variable includes explicitly the suction (e.g. Loret and Khalili, 2002, Sun et al. 2000, 2003; Georgiadis et al. 2005). In this case, the representation of the stress paths is not as simple as it is in the first group and the hydraulic behaviour is not represented in a complete manner, being not possible to take into account the hysteresis of the soil water retention curve.

The third group consists of models using the effective stress as stress variable. The use of the effective stress provides many advantages such as simple shape of the yield surfaces and strain increments easily integrable with a relatively small number of integration constant. These advantages justify the major complexity to work with the effective stresses compared to the classical choice of mean net stress (e.g. Wheeler et al. 2003, Sun et al. 2010, Sheng et al. 2004, Nuth and Laloui, 2007).

2.2 Models in terms of net stress

2.2.1   The Barcelona Basic Model (Alonso et al. 1990)

The first elasto – plastic critical state model was proposed in a qualitative manner by Alonso et al. (1987), while the mathematical framework was reported in Alonso et al. (1990).

The elasto-plastic model for partially saturated soil proposed by the authors was born as an extension of the Modified Cam-Clay (MCC) model by Roscoe and Burland (1968) for partially saturated and unexpansive soils.

To define the elastic domain of unsaturated soils, Alonso et al. (1987) introduced two yield curves: the Loading Collapse curve (LC) and the Suction Increase curve (SI).

Plastic volumetric strains were predicted for any stress path involving expansion of the yield curve. Yielding on the LC yield curve could be caused by an increment of mean net stress (loading path) or by decrement of suction (wetting path) or both. The SI yield curve was introduced to represent the irreversible compression that occurred when the suction was increased above the previous maximum value. This model was the first elasto-plastic model able to reproduce some of the basic behaviour of unsaturated soil, such as swelling and collapse upon wetting.

In order to validate the model, the authors used different stress paths. In fact, analysing the loading paths at constant suction, Alonso et al. (1990) observed a mechanical behaviour, in terms of variation of specific volume, similar to the behaviour of saturated soils. In full correspondence with the behaviour of saturated soils, the virgin state line is expressed as follows:

$$v = N(s) - \lambda(s) \ln \frac{p - u_a}{p^c} \qquad (2.3)$$

where p^c is a reference stress state for which $v = N(s)$ and $\lambda(s)$ is the compressibility parameter for changes in net mean stress for the virgin state of the soil. The variations of the specific volume on loading paths (at constant suction) inside the elastic region is given by:

$$dv = -k \frac{d(p - u_a)}{(p - u_a)} \qquad (2.4)$$

where k is the elastic compressibility parameter for changes in net mean stress. Alonso et al. (1990) consider that the compressibility parameter $\lambda(s)$ depends on the suction, while the elastic compressibility parameter k is considered independent of the applied suction. In the same way, when the suction changes at constant net stress inside the elastic domain, the variation of the specific volume is defined as follows:

$$dv = -k_s \frac{d(u_a - u_w)}{(u_a - u_w) + p_{atm}} \tag{2.5}$$

where k_s is the elastic compressibility parameter for changes in suction, and the atmospheric pressure is added to the suction to avoid infinite values as suction approaches zero.

Equation 2.3 also defines the state boundary surface in the space $(p - u_a):(u_a - u_w):v$ where the volumetric plastic deformations occur. In addition, equations 2.4 and 2.5 represent the elastic surface constrain of equation 2.3, which divides the elastic region from the impossible state. The intersection between these two surfaces in the plane $(p - u_a):(u_a - u_w)$ defines the yield curves. Therefore, the yield curve, called Loading-Collapse curve, defines the set of yield points for the corresponding value of suction (Fig. 2.1).
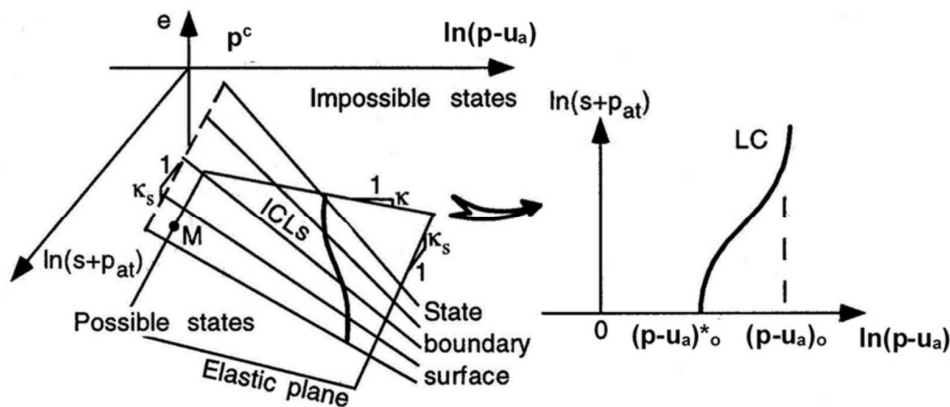

Figure 2.1 Determination of the Loading – Collapse curve from the ICLs curve (Figure from Vaunat et al. 2000).

As reported in Figure 2.2 it is possible to relate the yield stress corresponding to a generic value of suction, $(p - u_a)_0$, with the yield stress for saturated state $(p - u_a)_0^*$.
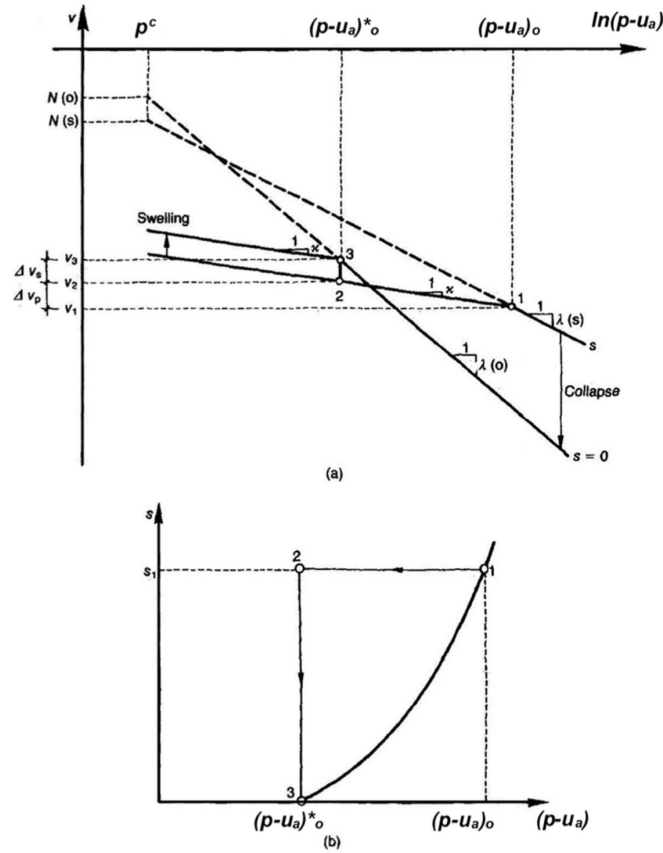
Figure 2.2 Relationship between the yield stresses $(p-u_a)_0$ and $(p-u_a)_0^*$: (a) compression curves for saturated and partially saturated soil; (b) stress path and yield curve in $(p-u_a):s$ stress plane (Figure from Alonso et al. 1990).

The stress path reported in Figure 2.2 is composed by an unloading path (1-2) at constant suction, and a wetting path at constant mean net stress. Mathematically, this stress path could be expressed taking into account equation 2.3 and subtracting the equations 2.4 and 2.5, as follows:

$$N(s)-\lambda(s)\ln\frac{(p-u_a)_0}{p^c}+k\ln\frac{(p-u_a)_0}{(p-u_a)_0^*}+k_s\ln\frac{(u_a-u_w)+p_{atm}}{p_{atm}}=N(0)-\lambda(0)\ln\frac{(p-u_a)_0^*}{p^c} \quad (2.6)$$

which provides a relationship between the yield stress and the suction as a function of some reference value and some soil parameters.

To simplify the expression the authors assumed that (Fig. 2.2 (a)):

$$\Delta v(p^c)\Big|_s^0 \, N(0)-N(s)=k_s\ln\frac{s+p_{atm}}{p_{atm}} \quad (2.7)$$

In other words, Alonso et al. (1990) impose that p^c is the net stress at which one may reach the saturated virgin state, starting at partially saturated condition, through a wetting path which involves only elastic swelling.

Introducing equation 2.7 into equation 2.6, the Loading – Collapse curve equation is obtained:

$$\frac{(p-u_a)_0}{p^c} = \left[\frac{(p-u_a)_0^*}{p^c}\right]^{[\lambda(0)-k]/[\lambda(s)-k]} \tag{2.8}$$

Alonso et al. 1990 proposed an asymptotic equation to model the compressibility parameter $\lambda(s)$:

$$\lambda(s) = \lambda(0)\{(1-r)\exp(-\beta s)+r\} \tag{2.9}$$

where r is a constant related to the maximum compressibility of the soil and β is a parameter that controls the rate of increase of soil compressibility with suction. Figure 2.3 reports the shape of Loading – Collapse curves, for different values of r and β.
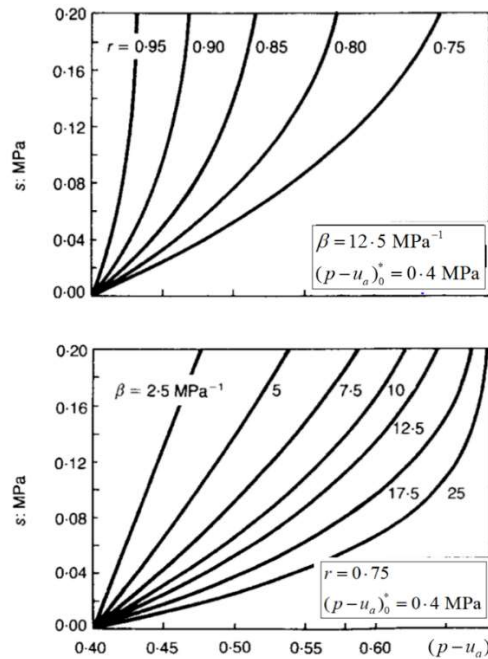
Figure 2.3 Shape of the LC yield curve for different values of the parameters r and β (Figure from Alonso et al. 1990).

As clearly reported in Figure 2.3, the parameters r and β influence the shape of the LC curve. It means that the compressibility parameter $\lambda(s)$ plays a key role in unsaturated modelling.

As reviewed before, a drying path may also induce plastic deformation. Alonso et al. (1990) proposed that whenever the soil reaches a maximum previously attained value of the suction s_0, irreversible strains will begin to develop:

$$s = s_0 = \text{constant} \tag{2.10}$$

The two yield curves, LC and SI, enclose the elastic region in the plane $(p - u_a) : s$, as shown in Figure 2.4.
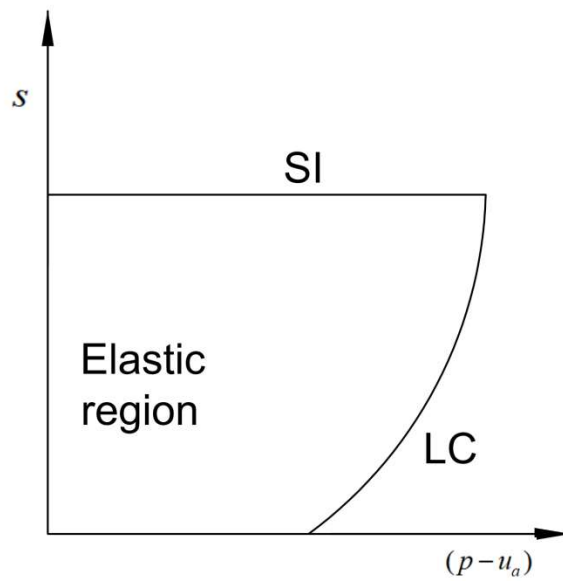

Figure 2.4 Shape of the LC yield curve for different values of the parameters r and β.

According to equation 2.4, a loading path in the elastic region will induce a compressive volumetric deformation given by:

$$d\varepsilon^e_{v(p-u_a)} = -\frac{dv}{v} = -\frac{k}{v}\frac{d(p-u_a)}{(p-u_a)} \tag{2.11}$$

Once the net mean stress $(p - u_a)$ reaches the yield value $(p - u_a)_0$, the total volumetric deformation could be expressed from equation 2.3, as:

$$d\varepsilon_{v(p-u_a)} = -\frac{dv}{v} = -\frac{\lambda(s)}{v}\frac{d(p-u_a)_0}{(p-u_a)_0} \tag{2.12}$$

and, therefore, the irreversible component of volumetric strain will be given by:

$$d\varepsilon_{v(p-u_a)}^p = \frac{\lambda(s)-k}{v}\frac{d(p-u_a)_0}{(p-u_a)_0} \tag{2.13}$$

The plastic volumetric deformation could be expressed also taking into account the equation (2.8) as follows:

$$d\varepsilon_{v(p-u_a)}^p = \frac{\lambda(0)-k}{v}\frac{d(p-u_a)_0^*}{(p-u_a)_0^*} \tag{2.14}$$

In the same way, a drying or wetting path inside the elastic region caused elastic volumetric strain:

$$d\varepsilon_{vs}^e = \frac{k_s}{v}\frac{ds}{(s+p_{atm})} \tag{2.15}$$

and, if the SI curve is reached, the total and the plastic volumetric deformation will be given by:

$$d\varepsilon_{vs} = -\frac{\lambda_s}{v}\frac{ds_0}{(s_0+p_{atm})} \tag{2.16}$$

$$d\varepsilon_{vs}^p = \frac{\lambda_s-k_s}{v}\frac{ds_0}{(s_0+p_{atm})} \tag{2.17}$$

The plastic deformations control the position of the LC and SI curves through equation 2.14 and 2.17 (Fig 2.5). The two hardening equations imply an independent motion of both yield curves. However, some experimental evidence carried out by Josa et al. (1987) suggests a coupling between them. For this reason, Alonso et al. (1990) proposed a simple way to couple both yield curves.

They proposed to consider the position of the two yield curves depending on the total plastic volumetric deformation $d\varepsilon_v^p = d\varepsilon_{vs}^p + d\varepsilon_{v(p-u_a)}^p$. Then, from the equation 2.14 and 2.17, the coupled hardening law proposed by Alonso et al. (1990) could be expressed as follows (Fig. 2.6):

$$\frac{d(p-u_a)_0^*}{(p-u_a)_0^*} = \frac{v}{\lambda(0)-k}d\varepsilon_{v(p-u_a)}^p \tag{2.18}$$

$$\frac{ds_0}{s_0+p_{atm}} = \frac{v}{\lambda_s-k_s}d\varepsilon_{vs}^p \tag{2.19}$$
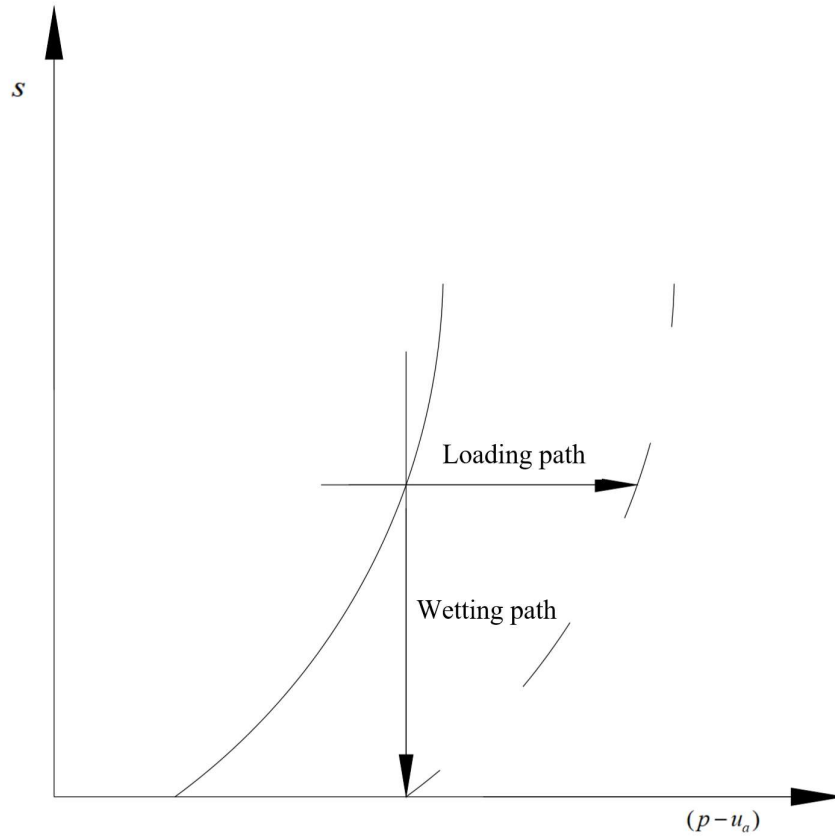
Figure 2.5 Yielding curves for load-collapse behaviour of unsaturated soil.
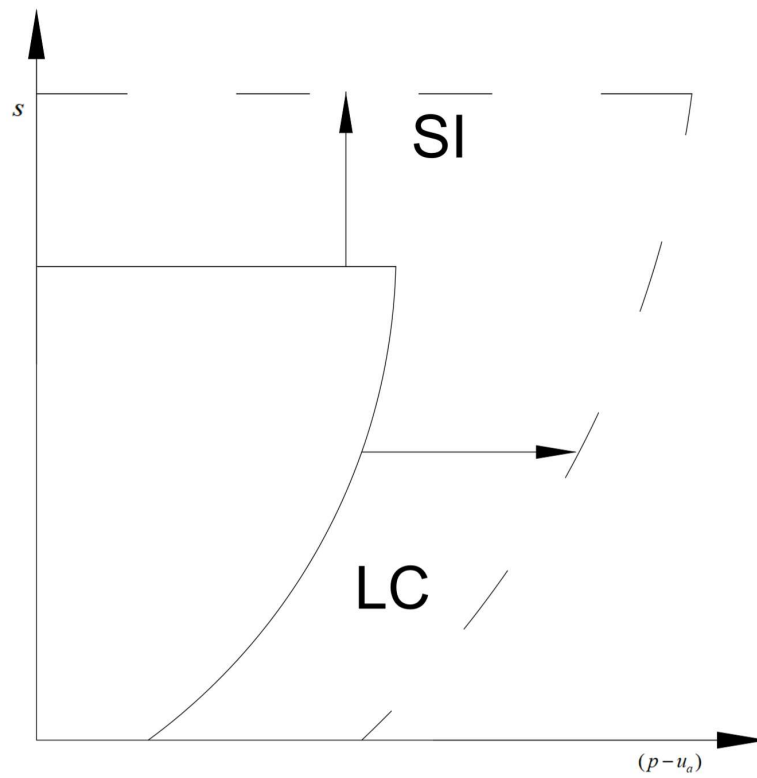

Figure 2.6 Coupling between the LC and SI yield curves.

2.2.2 The model of Wheeler and Sivakumar (1995)

After Alonso et al. (1990), many authors presented other constitutive models (e.g. Wheeler and Sivakumar (1995); Gens and Alonso (1992); Alonso et al. (1994), (1998); Rampino et al. (2000) and Wheeler (1996)).

The model proposed by Wheeler and Sivakumar (1995) was validated using the triaxial tests carried out by Sivakumar (1993) on samples of unsaturated compacted kaolin Speswhite. Wheeler and Sivakumar (1995) modified the BBM model introducing new constitutive relations, in order to improve the flexibility of the model. The authors proposed a new equation for the virgin state line:

$$v = N(s) - \lambda(s) \ln \frac{p - u_a}{p_{atm}}$$
(2.20)

Both the slope $\lambda(s)$ and the intercept $N(s)$ were assumed parameters of the models and were calculated, with best-fit, by taking average value of slope and intercept from tests that were taken to sufficiently high values of mean net stress to define properly the linear relationship of the equation (2.20). Therefore, Wheeler and Sivakumar (1995) did not propose any laws to model the variation of $\lambda(s)$ and of $N(s)$. In contrast, equations 2.7 and 2.9 proposed by Alonso et al. (1990) provided a limitation of these parameters.

In conclusion, the approach proposed by Wheeler and Sivakumar (1995) permitted to obtain a model more flexible than BBM. Considering the new equation for the virgin compression line (2.20) and the equations 2.4 and 2.5, the new equation of the Loading – Collapse curve is given by:

$$N(s) - \lambda(s) \ln \frac{(p - u_a)_0}{p_{atm}} + k \ln \frac{(p - u_a)_0}{(p - u_a)_0^*} + k_s \ln \frac{s + p_{atm}}{p_{atm}} = N(0) - \lambda(0) \ln \frac{(p - u_a)_0^*}{p_{atm}}$$
(2.21)

This equation is similar to equation 2.6 proposed by Alonso et al. (1990), the only difference is the presence of atmospheric pressure instead of the parameter p^c and therefore the hardening laws are still valid.

2.2.3 The BExM model By Gens and Alonso (1992)

Gens and Alonso (1992) presented an extension of the BBM model to describe the mechanical behaviour of unsaturated expansive soils. In fact, the BBM model is not able to reproduce the large swelling strains exhibited by expansive soils. The important improvement introduced by the authors was the incorporation of the microstructural effects in the formulation.

The extended framework is based on considering two levels: a microstructural level that corresponds to the active clay minerals where physicochemical interaction phenomena predominate (as the first hypothesis the authors considered this level saturated even when the soil as a whole is in an unsaturated state); a macrostructural level that accounts for the larger-scale structure of the soil.

The basic point of the BexM model (Gens and Alonso, 1992) is that the deformations of the microstructure are able to affect the macrostructural level, while the reverse is not true.

In fact, a microstructural swelling will affect the soil skeleton, increasing its macrostructural void ratio. This irreversible volume change leads in turn to a movement of the LC to the left (a softening in hardening plasticity terms) in response to the new structural arrangements. In contrast, a microstructural shrinkage does not cause any macrostructural volume change, and then any movements of the LC. From these hypothesises, the authors define a new curve named Neutral Loading line (NL) (or Suction Decreased (SD) Alonso et al. 1994) (Fig. 2.7): this line separates stress paths, causing swelling from stress paths, causing compression. The reductions in suction or pressure will lead to microstructural expansion, whereas an increase in suction or pressure will bring about microstructural compression. It should be pointed out that depending on the microstructural theory adopted, a different inclination of the neutral loading line could perhaps be obtained in some suction-stress regions.

2.2.4 Suction Increase curve (SI) and Suction Decrease curve (SD) Alonso et al. (1994) & Alonso (1998)

Alonso et al. (1994) and Alonso (1998) supposed the existence of the opposite of the SI curve. This new yield curve is reached when the microstructure reaches the limit of the reduction of volume that can affect the behaviour of the macrostructure. Instead, the SI introduced by Alonso et al. (1994) has an inclination of 45° because it is linked to the behaviour of the microstructure (it is a consequence of the theory of the double layer to model the microstructure) hypothesized saturated. Thanks to the equation adopted by Alonso et al. in (1994) to link the SD and SI, the model is able to predict the irreversible deformations recorded during a wetting-drying cycles.
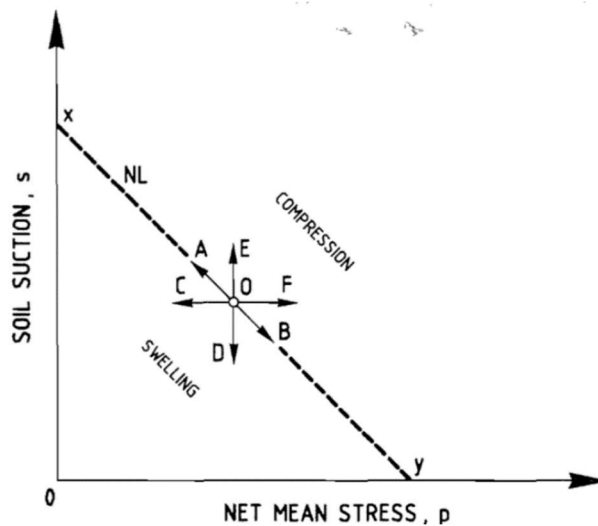
Figure 2.7 Microstructural behaviour. Neutral Loading line (NL) separating compression from swelling regions (Figure from Gens and Alonso, 1992).

2.2.5 Correction on swelling coefficient by Rampino et al. (2000)

All the models shown so far consider the swelling coefficient independent of the level of suction applied. Clearly, this is a simplifying hypothesis. Rampino et al. (2000) considered that the swelling index, k, is not constant with the suction, but they observed that it exhibits a small decrease with an increase in suction, following the same law of $\lambda(s)$ and using the same value of r and β. After Rampino et al. (2000), the new equation of Loading – Collapse curve becomes:

$$\left[\lambda(s) - k(s)\right] \ln \frac{(p - u_a)_0^*}{p^c} =$$
$$= \left[\lambda(0) - k(0)\right] \ln \frac{(p - u_a)_0^*}{p^c} + N(s) - N(0) + k_s \ln \frac{s + p_{atm}}{p_{atm}}$$

(2.22)

Or in a simplified form:

$$\frac{(p - u_a)_0}{p^c} = \left[\frac{(p - u_a)_0^*}{p^c}\right]^{[\lambda(0) - k(0)]/[\lambda(s) - k(s)]}$$

(2.23)

2.2.6 The coupled hydro-mechanical model by Wheeler (1996)

The main omission of the BBM and other formulations was the lack of a specific model to describe the variation of the water content or the degree of saturation due to changes of stresses and/or suction (Gens et al. 2006). In fact, in the BBM model, the hydraulic behaviour is simply defined in terms of a state surface.

The issue of the hydraulic component of the constitutive model was first addressed by Wheeler (1996). The author described a constitutive law that addresses the irreversible behaviour of unsaturated soils upon wetting and drying, with particular attention to the phenomenon of hydraulic hysteresis using the specific water volume $v_w = 1 + S_r e = 1 + w G_s$ as volumetric state variable. The use of the specific water volume permits to link the hydraulic and mechanical behaviour using the same model structure of the BBM through the function:

$$e_a = f[(s), (p - u_a)_0^*]$$

(2.24)

where e_a is the air void ratio and $f[(s),(p-u_a)_0^*]$ is defined, in accordance to Wheeler and Sivakumar (1995), as follows:

$$f[(s),(p-u_a)_0^*] = A(s) + \alpha(s) \cdot \ln \frac{d(p-u_a)_0^*}{(p-u_a)_0^*}$$

(2.25)

The specific water volume is given by subtracting the air void ratio from the overall specific volume:

$$v_w = v - e_a = v - A(s) + \alpha(s) \cdot \ln \frac{d(p-u_a)_0^*}{(p-u_a)_0^*}$$

(2.26)

where $A(s)$ and $\alpha(s)$ are suction-dependent parameters.

Using these modifications, the model proposed by Wheeler (1996) is able to predict the variation of specific water content during wetting and drying cycles and loading and unloading cycles. The limitation of the model is that it considers the same value of elastic compressibility parameter both in terms of specific volume and specific water volume, this means that for elastic stress paths the variations of the two specific volumes coincide. To get out from this limitation, an equation that takes into account the reversible deformation of air void ratio could be used, instead of equation 2.26.

2.3 Models in terms of "equivalent" effective stress

2.3.1 The model in terms of mean "translated" stress by Sun et al. (2000, 2003)

Interesting is the model presented by Sun et al. (2000). In this model, the authors introduced a new kind of stress tensor variable called translated stress tensor. In fact, the influences of suction on the mechanical behaviour of partially saturated soil are taken into account in the model using a parameter named suction stress $\sigma_0(s)$, which is added to the net stress. Sun et al, (2000) defined the general translated stress tensor $\hat{\sigma}_{ij}$ for unsaturated soil as follows:

$$\hat{\sigma}_{ij} = \sigma_{tij} - u_a \delta_{ij} + \sigma_0(s)\delta_{ij} \tag{2.27}$$

The authors assumed a hyperbolic equation to describe the relation between $\sigma_0(s)$ and s with the initial slope being unit (Fig. 2.8):

$$\sigma_0(s) = \frac{s}{1 + \dfrac{s}{a}} \tag{2.28}$$

where a is a constant equal to the maximum $\sigma_0(s)$ of the soil for an infinite suction, which depends on the type of soil (Escario and Juca, 1989). The value of a is calculated from the imposed s and the measured corresponding $\sigma_0(s)$ for a given partially saturated soil.
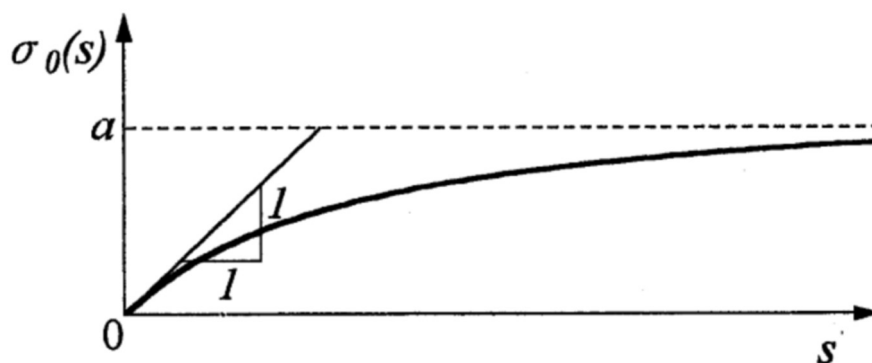
Figure 2.8 Relationship between suction and suction stress (Figure from Sun et al. 2000).

However, the suction stress is not able to take into account the hysteretic hydraulic behaviour of the soil. Indeed, the suction stress may be different at the same suction under drying and wetting

conditions while Sun et al. (2000) assume for the sake of simplicity in this model a unique relationship for the suction stress.

Sun et al. (2000) consider, to define the model in isotropic stress state, the compression curves for saturated and partially saturated soils in the $e - \ln \hat{p}$ and $e^p - \ln \hat{p}$ planes. Where e^p is the sum of the initial void ratio $e_i(s)$ and the plastic void ratio incremental de^p due to change in $\hat{p}$. In this manner the authors may express the normal compression line for saturated soil in the following way:

$$e = e_i(0) - \lambda(0) \ln \frac{p_0^*}{p_i} \qquad (2.29)$$

And the normal compression line for unsaturated soil with a constant suction s is expressed by:

$$e = e_i(s) - \lambda(s) \ln \frac{p_0 + \sigma_0(s)}{p_i} = e_i(s) - \lambda(s) \ln \frac{\hat{p}_0}{p_i} \qquad (2.30)$$

where p_i is a reference net stress, and p_0^* and p_0 are the yield stresses on the normal compression lines for saturated and unsaturated soils respectively in the isotropic stress.

In contrast to others authors, Sun et al. (2000) assume that exists a normal compression line between void ratio e and mean effective stress $\hat{p}_0$ for a given partially saturated soil and suction and adopt the linear $e \sim \ln \hat{p}$ relationship because $\hat{p}$ is considered to be the mean effective stress for unsaturated soils. This assumption is similar to the normal compression line, between void ratio and mean effective stress, in the Cam-Clay Model.

The variation of the $e \sim \ln p$ curves in this model is similar to the framework of Wheeler and Sivakumar (1995) and in contrast to the proposal of Alonso et al. (1990). In fact, in this model the authors consider that the normal compression lines for different values of suction gather to the point N (Fig. 2.9a) with an increase of the mean effective stress, while Alonso et al. (1990) propose that the normal compression lines for different suction diverge with an increase of the mean net stress.

(a) In e~ln p̂ plane
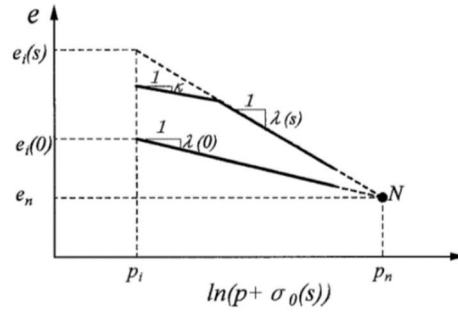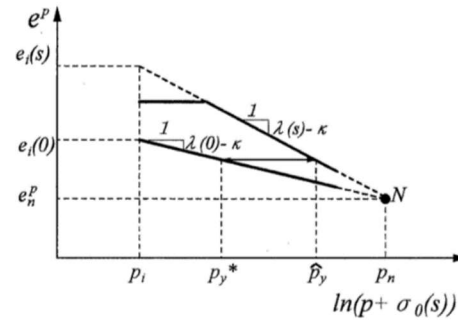
(b) In e^P~ln p̂ plane

Figure 2.9 Relationship between compression curves for saturated and unsaturated soils (Figure from Sun et al. 2000).

The point N in Figure 2.9(a) is considered to be invariable when suction changes. This condition implies that no collapse occurs at the state of point N, then it must exist a single point N that all the normal compression lines pass through. The coordinate of point N can be obtained considering two lines, a first one at zero suction and a second one whit suction s.

$$\begin{cases} p^c = p_i e^{(e_i(0)-e_i(s))/(\lambda(0)-\lambda(s))} \\ e^c = \dfrac{1}{\lambda(0)-\lambda(s)}(e_i(s)\lambda(0)-e_i(0)\lambda(s)) \end{cases} \tag{2.31}$$

Considering the assumption shown in Figure 2.9(a), the amount of collapse varies with the mean net stress as shown in Figure 2.10
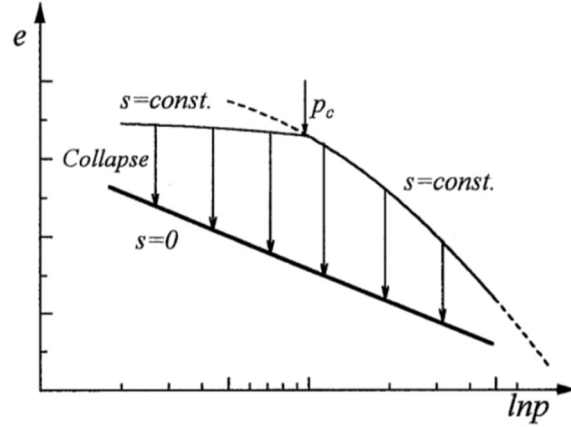
Figure 2.10 Collapse at different mean stresses and states (Figure from Sun et al. 2000).

When the mean net stress is less than the initial yield stress, the volume reduction induced by the suction reduction from s to zero increases with the increase in the imposed mean net stress. When the mean net stress is greater than the initial yield stress, the volume reduction induced by the suction reduction from s to zero decreases with the increase in the imposed mean net stress.

The equation 2.29 can be rewritten by using the coordinate of point N as

$$e = e^c - \lambda(s) \ln \frac{p_0 + \sigma_0(s)}{p^c} \tag{2.32}$$

Differentiating the equation 2.32 it is possible to obtain the increment of void ratio in the following form:

$$de = \frac{\partial e}{\partial p_0} dp_0 + \frac{\partial e}{\partial \sigma_0(s)} = \frac{-\lambda(s)}{p_0 + \sigma_0(s)} dp_0 + \left(\lambda_s \ln \frac{p^c}{p_0 + \sigma_0(s)} - \frac{\lambda(s)}{p_0 + \sigma_0(s)} \right) d\sigma_0(s) \tag{2.33}$$

In which $\lambda(s)$ is assumed to be linear with regard to $\sigma_0(s)$

$$\lambda(s) = \lambda(0) + \lambda_s \sigma_0(s) \tag{2.34}$$

As shown in Figure 2.9(b) Sun et al. (2000) assumed that the swelling coefficient k of saturated and unsaturated soils are the same. In this case, from the same plastic volumetric strain, the following equation can be obtained:

$$(\lambda(s)-k)\ln\frac{p^c}{p_0+\sigma_0(s)} = (\lambda(0)-k)\ln\frac{p^c}{p_0^*} \qquad (2.35)$$

Substituting equation 2.34 into equation 2.35, and solving for p_0, gives:

$$p_0 = p^c\left(\frac{p_0^*}{p^c}\right)^{(\lambda(0)-k)/(\lambda(0)-k+\lambda_s\sigma_0(s))} - \sigma_0(s) \qquad (2.36)$$

Equation 2.36 is the equation of Loading – Collapse curve for the model of Sun et al. (2000). As we

can see the form of the equation is very similar to Alonso et al. (1990), where the suction stress is a

parameter to define the rate of increase of yield stress for unsaturated soil.

In a successive work, Sun et al. (2003) modified the equation of the Loading – Collapse curve. They

conducted a series of experimental test on unsaturated compacted soils with different initial densities.

Results obtained by a test of isotropic compression and collapse tests on compacted Pearl-clay show

that the slope of the normal compression line of unsaturated soil depends by suction and void ratio

corresponding to initial yield stress. For these reasons, the authors rewrote the coordinates of point N

as follows:

$$\begin{cases} p^c = p_i e^{(e_0(0)-e_0(s))/(\lambda(0)-\lambda(s,e_0))} \\ e^c = \dfrac{1}{\lambda(0)-\lambda(s,e_0)}(e_0(s)\lambda(0)-e_0(0)\lambda(s,e_0)) \end{cases} \qquad (2.37)$$

where $e_0(0)$ and $e_0(s)$ are the void ratios corresponding to initial yield translated stress, $\hat{p}_0(s)$ on the

normal compression lines of saturated and unsaturated soil respectively, and $\lambda(s,e_0)$ is given by:

$$\lambda(s,e_0) = \frac{e_0(s)-e^c}{\ln\dfrac{\hat{p}^c}{\hat{p}_0(s)}} \qquad (2.38)$$

In analogy to equation 2.34, equation 2.38 can be rewritten as follows:

$$\lambda(s,e_0) = \lambda(0)+\lambda(e_0)\sigma_0(s) \qquad (2.39)$$

Considering the condition assumed in the equation 2.35:

$$(\lambda(s,e_0)-k)\ln\frac{p^c}{p_0+\sigma_0(s)}=(\lambda(0)-k)\ln\frac{p^c}{p_0^*} \tag{2.40}$$

solving the equation 2.40 for p_0, it gives:

$$p_0 = p^c\left(\frac{p_0^*}{p^c}\right)^{(\lambda(0)-k)/(\lambda(s,e_0)-k)} - \sigma_0(s) \tag{2.41}$$

The model predictions and the test data carried out by Sun et Al. (2003) show that the initial yield stress curve moves towards right when initial void decrease, according to tests results of Maatouk et al. (1995), and the effect of suction on the initial yield stress decrease with increasing the initial density (i.e. the denser the specimen) the steeper is the initial yield curve.

2.3.2 The model of Georgiadis et al. (2005)

Georgiadis et al. (2005) presented a new expression for the LC curve based on a new formulation for the stress variables: $\tilde{\sigma} - s_{eq}$;

where $\tilde{\sigma} = \bar{\sigma} + s_{air}$, $\bar{\sigma}$ is the net stress, s_{air} is the air entry value and s_{eq} is the equivalent suction defined as the difference between the suction and the air entry value of suction $\left(s_{eq} = s - s_{air}\right)$

According to the BBM (Alonso et al. 1990), considering an elastic stress path joining two points lying on the same surface, at $s_{eq} > 0$ and $s_{eq} = 0$ the following expression is obtained:

$$N(0) - \lambda(0)\ln\frac{(p-u_a)_0^*}{p^c} =$$

$$= N(s_{eq}) - \lambda(0)\ln\frac{(p-u_a)_0}{p^c} + \lambda_m\left(\frac{(p-u_a)_0}{p^c}\right)^{-b}\ln\frac{(p-u_a)_0}{p^c} + k\ln\frac{(p-u_a)_0}{(p-u_a)_0^*} + k_s\ln\frac{s_{eq}+p_{atm}}{p_{atm}} \tag{2.42}$$

where λ_m is a parameter related to soil compressibility at low confining stress that can be calculated by the initial slope of the isotropic compression line, $\lambda_{in}(s_{eq})$.

The slope of isotropic compression line of unsaturated soils is defined as follows:

$$\mathrm{d}v = -\lambda(s_{eq})\frac{d(p-u_a)_0}{(p-u_a)_0} \Rightarrow \lambda(s_{eq}) = -(p-u_a)_0\frac{dv}{d(p-u_a)_0} \tag{2.43}$$

Considering:

$$v = N(s_{eq}) - \lambda(0) \ln \frac{(p-u_a)_0}{p^c} + \lambda_m \left(\frac{(p-u_a)_0}{p^c} \right)^{-b} \ln \frac{(p-u_a)_0}{p^c}$$ (2.44)

and

$$\Delta v = \Delta v_e = N(0) - N(s_{eq}) = k_s \ln \frac{s_{eq} + p_{atm}}{p_{atm}}$$ (2.45)

The equation 2.43 can be rewritten as follows:

$$\lambda(s_{eq}) = \lambda(0) - \lambda_m \left(\frac{(p-u_a)_0}{p^c} \right) \left(1 - b \ln \frac{(p-u_a)_0}{p^c} \right)$$ (2.46)

The initial slope of the isotropic compression line, $\lambda_{in}(s_{eq})$, is obtained by setting $(p-u_a)_0 = p^c$ in equation 2.43

$$\lambda(s_{eq}) = \lambda(0) - \lambda_m$$ (2.47)

The authors assumed that the initial slope of the isotropic compression line, $\lambda_{in}(s_{eq})$, is given by a similar equation used by Alonso et al. (1990)

$$\lambda_{in}(s_{eq}) = \lambda(0) \left[(1-r) e^{-\beta s_{eq}} + r \right]$$ (2.48)

Combining equation 2.47 and equation 2.48 the expression of λ_m is obtained

$$\lambda_m = \lambda(0)(1-r)(1-e^{-\beta s_{eq}})$$ (2.49)

So, also in this case, an exponential expression for the compressibility coefficient is adopted. Combining equation 2.43 and equation 2.45, the expression of LC curve, according to Alonso et al. (1990), is expressed as follows:

$$\frac{(p-u_a)_0^*}{p^c} = \left[\frac{(p-u_a)_0}{p^c} \right]^{[1-(\lambda_m \frac{(p-u_a)}{p^c})^{-b}]/(\lambda(0)-k)]}$$ (2.50)

In conclusion, the model presented by Georgiadis et al. (2005) takes into account the nonlinearity of the partially saturated isotropic compression line and the soil is treated as fully saturated for suction lower s_{air}.

2.4 Hydro-mechanical models in terms of effective stress

2.4.1   Coupling of hydraulic hysteresis and stress-strain behaviour, Wheeler et al. (2003)

Wheeler et al. (2003), based on Buisson and Wheeler (2000), presented a fully coupled elastoplastic

model that takes into account the hydraulic hysteresis.

The framework is based on consideration of the main physical processes involved. Considering the

Figure 2.11, two elasto-plastic processes are considered:

1. the mechanical process of straining of the soil skeleton under changes of applied stresses, with

    elastic strains attributed to elastic deformation of soil particles and packets, and plastic strains

    attributed to slippage at interparticle or inter-packet contacts. Slippage at contact is controlled

    by tangential and normal components of the contact forces. The contact forces are influenced

    by externally applied total stresses and by pore pressure in the surrounding voids. Wheeler et

    al. (2003) consider also that the slippage at contacts will be inhibited by meniscus water, which

    produces an additional component of normal force at the contact and therefore meniscus water

    provides a stabilizing effect. The authors consider that the slippage can produce both plastic

    volumetric strain and plastic shear strain.

2. The second elasto-plastic phenomenon is the hydraulic process of water inflow and outflow

    to individual voids. Plastic change of S_r can be produced during a wetting or drying. The

    authors consider the movement of interfaces between the water in the void and the air. During

    a drying process the radius of curvature of the interfaces decreases, and the interfaces move

    from position 1 to position 2, as shown in Figure 2.11. This movement is modelled as a

    reversible, then elastic, process. If a drying process causes an increase of suction beyond a

    critical value, air will break through into the void. This air breakthrough into a void during a

    drying process is an irreversible process, because the void will not immediately re-flood with

    water if the suction is reduced slightly. In the same way, the flooding of a void with water

    during wetting is also treated as an irreversible process. Then both air breakthrough into a

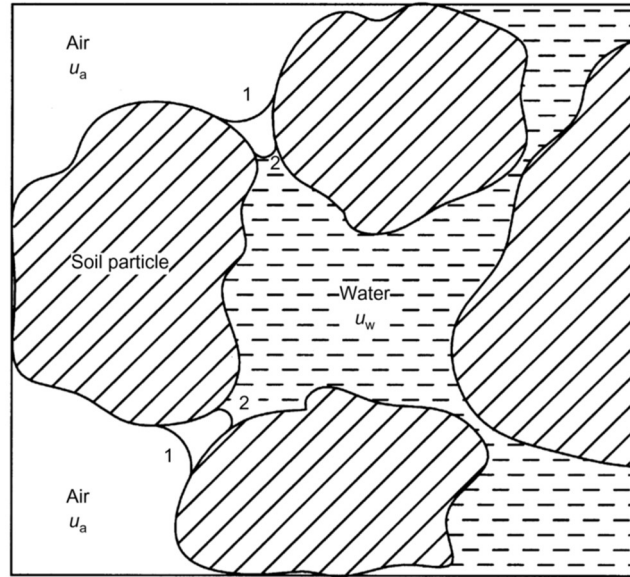void during drying and water flooding a void during wetting cause plastic change of degree of saturation.

Figure 2.11 Movements of air-water interfaces (Figure from Wheeler et al. 2003).

To model the hydro-mechanical behaviour in a coupled manner, the authors adopted Bishop's stress and modified suction, as follows:

$$\begin{cases} \sigma_{ij}^* = \sigma_{ij} - \left[S_r u_w + (1 - S_r) u_a \right] \delta_{ij} \\ s^* = ns = n(u_a - u_w) \end{cases} \tag{2.51}$$

The weighting factors of S_r and $(1 - S_r)$, applied to the pore water pressure and pore air pressure respectively, can be considered as representing the portion of the total void occupied by bulk water and by air respectively. But the Bishop's stress alone is not able to represent the stabilising influence provided by the presence of meniscus water lens, hence the authors introduced the second stress variable s^*. Clearly, the appropriate work-conjugate strain increment variables are $d\varepsilon_{ij}$ and $-dS_r$ and therefore, for the simplified stress state of triaxial test, the equation of work input dW can be written as:

$$dW = p^* d\varepsilon_v + q d\varepsilon_s - s^* dS_r \tag{2.52}$$

where $d\varepsilon_v$ and $d\varepsilon_s$ are the increments of volumetric strain and shear strain respectively, q is the deviator stress, and p^* is the mean Bishop's stress.

The process of slippage at inter-particle or inter-packet contacts is associated with a LC surface. The shape of the LC curve can be derived by considering the influence of suction within meniscus water on inter-particle slippage.

Figure 2.12 shows the proposed elastic domain by Wheeler et al. (2003), for isotropic stress states. The elastic domain, rectangular region, is enclosed by the three yield curves. Yielding on the LC curve produces plastic volumetric strains but it is assumed to cause no plastic change of S_r . In contrast, yielding on the SI or on the SD curves produces plastic change of S_r , but it is assumed to cause no plastic volumetric strain.

(a)   (b)
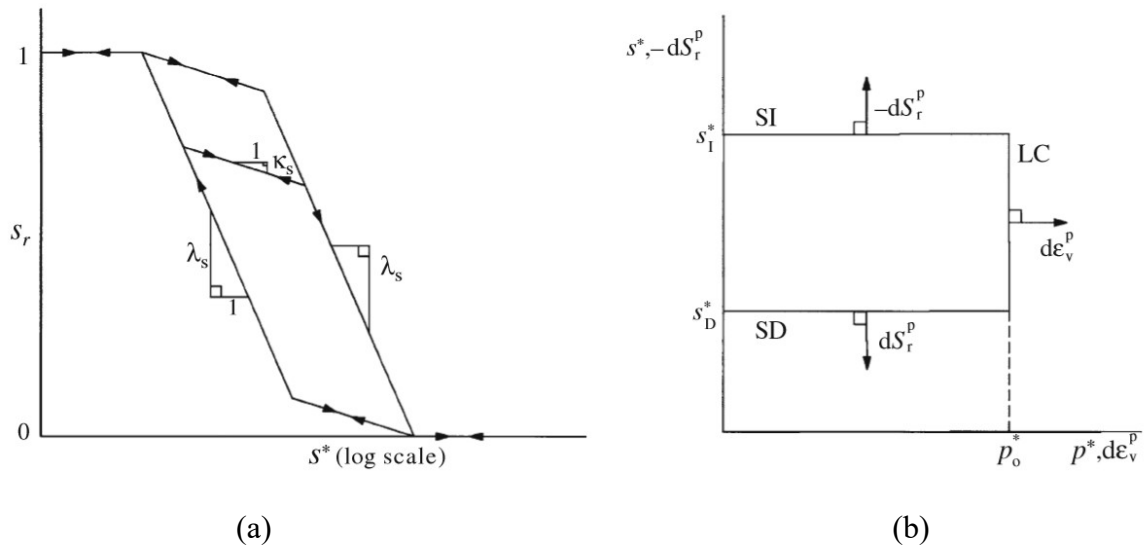
Figure 2.12 (a) Model for retention behaviour (b) LC, SI, SD yield curves for isotropic stress state (Figure from Wheeler et al. 2003).

The coupled movements of the various yield curves are central to the model of Wheeler et al. (2003) and they can be resumed as followed:

1. Yielding on the Loading – Collapse curve causes plastic volumetric strain, which produces coupled upward movements of SI and SD curves.

2. Yielding on the Suction Increase curve causes plastic decrements of S_r , which produce coupled upward movement of the SD curve and outward movement of the LC curve.

3. Yielding on the Suction Decrease curve causes plastic increments of S_r, which produce coupled downward movement of the SI curve and inward movement of the LC curve.

Yield curve equations for the LC, SI and SD curves are given respectively by:

$$\begin{cases} p^* = p_0^* \\ s^* = s_I^* \\ s^* = s_D^* \end{cases} \tag{2.53}$$

Where p_0^*, s_I^* and s_D^* define the current position of the three curves.

Elastic volumetric strain increments are given by:

$$d\varepsilon_v^e = \frac{k dp^*}{vp^*} \tag{2.54}$$

Instead, plastic volumetric strain increments, caused by yielding on only the LC curve, they are given by:

$$d\varepsilon_v^p = \frac{(\lambda - k) dp_0^*}{vp_0^*} \tag{2.55}$$

The flow rule for the LC curve and the elastic increments of degree of saturation are given respectively by:

$$\frac{dS_r^p}{d\varepsilon_v^p} = 0 \tag{2.56}$$

$$dS_r^e = -\frac{k_s ds^*}{s^*} \tag{2.57}$$

If yielding occurs on only the SI or SD yield curve, plastic changes of S_r are given by:

$$dS_r^p = -(\lambda_s - k_s) \frac{ds_I^*}{s_I^*} = -(\lambda_s - k_s) \frac{ds_D^*}{s_D^*} \tag{2.58}$$

The flow rule for the SI or SD corresponds to

$$\frac{d\varepsilon_v^p}{dS_r^p} = 0 \tag{2.59}$$

When yielding on only the SI or SD curve, coupled movements of the LC yield curve are given by:

$$\frac{dp_0^*}{p_0^*} = k_1 \frac{ds_I^*}{s_I^*} = k_1 \frac{ds_D^*}{s_D^*} \tag{2.60}$$

where k_1 is a parameter that controls the path traced by the corner between LC and SD yield curves during a wetting stage producing yielding on the SD curve.

When yielding on only the LC curve, coupled movements of SI and SD curves are given by:

$$\frac{ds_I^*}{s_I^*} = \frac{ds_D^*}{s_D^*} = k_2 \frac{dp_0^*}{p_0^*} \tag{2.61}$$

where the second coupling parameter, k_2, controls the magnitude of the shifts in the primary drying and primary wetting curves caused by plastic volumetric strains.

In general, the overall movement of the LC curve is given by the sum of any direct movement caused by yielding on the LC curve itself and any coupled movement produced by yielding on Suction Increase or Suction Decreased curve:

$$\frac{dp_0^*}{p_0^*} = \frac{vd\varepsilon_v^p}{(\lambda - k)} - \frac{k_1 dS_r^p}{(\lambda_s - k_s)} \tag{2.62}$$

Similarly, overall movements of the SI or SD curves are given by the sum of any direct movements caused by yielding on the SI or SD curve and any coupled movements produced by yielding on the LC curve:

$$\frac{ds_I^*}{s_I^*} = \frac{ds_D^*}{s_D^*} = -\frac{dS_r^p}{(\lambda_s - k_s)} - \frac{k_2 vd\varepsilon_v^p}{(\lambda - k)} \tag{2.63}$$

Equation 2.62 and 2.63 can be combined to give general expression for the plastic strain increments:

$$\begin{cases} d\varepsilon_v^p = \dfrac{(\lambda - k)}{v(1 - k_1 k_2)}\left(\dfrac{dp_0^*}{p_0^*} - k_1 \dfrac{ds_D^*}{s_D^*}\right) \\[4mm] dS_r^p = \dfrac{-(\lambda_s - k_s)}{(1 - k_1 k_2)}\left(\dfrac{ds_D^*}{s_D^*} - k_2 \dfrac{dp_0^*}{p_0^*}\right) \end{cases} \tag{2.64}$$

In summary, the framework proposed by Wheeler et al. (2003) is able to model plastic changes of degree of saturation that they influenced the stress-strain behaviour, and volumetric strains influence the water retention behaviour. The model involved also the coupling between hydraulic hysteresis and mechanical behaviour.

2.4.2 The extension of the BBM to takes into account the hydraulic hysteresis (Sheng et al. 2004)

In the same way proposed by Wheeler et al. (2003), Sheng et al. (2004) presented a new model, showing that it can be cast in the thermodynamic framework proposed by Collins and Houlsby (1997). In this model, the authors used the Bishop's stress and the suction as stress variables. Although the use of modified suction provides some benefit in the thermodynamical considerations, there is no essential difference between the two stress quantities (Gens et al. 2006).

The hysteretic water retention model is composed of a wetting and a drying curve with scanning curves (Fig. 2.13).
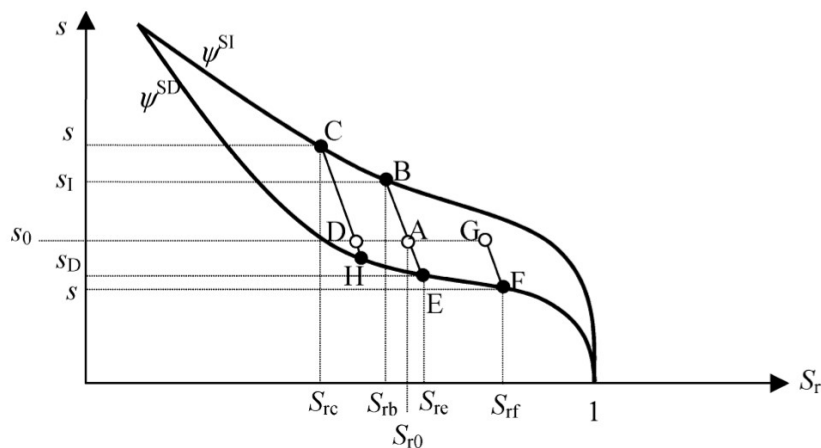
Figure 2.13 Model for retention behaviour (Figure from Sheng et al. 2004).

However, the hydraulic model does not take into account the dependency on the void ratio.

The innovative assumption proposed by Sheng et al. (2004), is that the main wetting curve corresponds to the SD curve, while the main drying curve corresponds to the SI curve. The LC equation proposed by the authors is given by:

$$\frac{p_0'}{p^c} = \left[\frac{p_0^{'*}}{p^c}\right]^{[\lambda(0)-k]/[\lambda(s)-k]} + S_r s \tag{2.65}$$

It should be noted that the second term on the right side of equations 2.65 is due to the transformation of the net stress to the constitutive stress (Jommi, 2000).

However, the three yields surface are not coupled but move independently of each other.
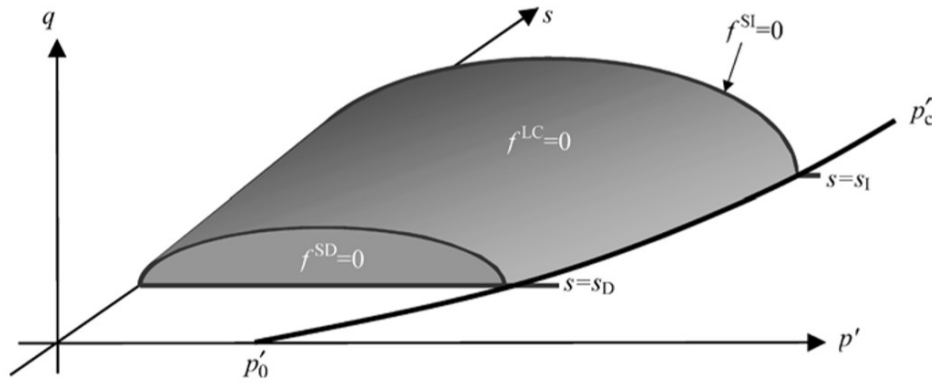
Figure 2.14 Yield surfaces (Figure from Sheng et al. 2004).

Neglecting the air compressibility, the plastic component of the work input rate can be expressed:

$$dW^p = (\sigma')^T d\varepsilon^p + ns dS_r^p \tag{2.66}$$

For uncoupled materials, where the elastic modulus is independent of the plastic strains, the plastic work increment can be decomposed into two components (Collins and Hilder 2002):

$$dW^p = d\psi_2 + d\phi \tag{2.67}$$

where ψ_2 is the part of the Helmholtz free energy that depends on plastic strains only and $d\phi$ is the dissipation increment. In terms of triaxial stress states, the plastic work is also expressed as:

$$dW^p = p_0' d\varepsilon_v^p + q d\varepsilon_\gamma^p + ns dS_r^p \tag{2.68}$$

Only the last term of the equation (1.68) is relevant to yielding in the SI or SD yield surface, thus the movements of the LC curve does not link to S_r^p. In addition, to find the first two terms, the authors assume that the irreversible volumetric and irreversible deviator strains are caused only by yielding at LC curve. Clearly, this is a strong restriction on the role of the SI and SD curves. Then:

$$dW^p = \left(\frac{1}{2} p_0^{'} d\varepsilon_v^p + (ns_{SI} dS_r^p \text{ or } ns_{SD} dS_r^p) \right) + \left(\frac{1}{2} p_0^{'} \frac{(d\varepsilon_v^p)^2 + \frac{M^2}{\zeta}(d\varepsilon_\gamma^p)^2}{\sqrt{(d\varepsilon_v^p)^2 + \frac{M^2}{\zeta}(d\varepsilon_\gamma^p)^2}} \right) \qquad (2.69)$$

where ζ and M are parameters of the model. The terms within the first brackets are all integrable and give zero in a closed loop.

Therefore, they are the contribution of the plastic strain work from the free energy and they correspond to $d\psi_2$. The term within the second brackets is not integrable because it involves the plastic shear strain. This term thus corresponds to the dissipation function $d\phi$.

Equation 2.69 indicates that the yielding at the SI and SD yield surfaces does not contribute to the plastic dissipation, but only to the plastic work. This means that all plastic work associated with a plastic increment of the degree of saturation is stored and can be recovered during a reversed plastic increment of saturation. This plastic work is very much the same as the ''locked-in elastic energy'' due to the shift or back stress.

Finally, note that $p_0^{'}$ is independent of the pore water pressure. A consequence of this is the non-convexity of the LC yield curve at high degree of saturation (Fig. 2.15). This non-convexity is inevitable, thus, forcing the convexity of the LC curve in the unsaturated state will inevitably cause a discontinuity in the first order derivative of the yield surface at transition point.

Due to the non-convexity and vertices of the yield surfaces, Sheng et al. (2004) suggested that the incremental stress-strain relations should be solved using explicit integration methods.
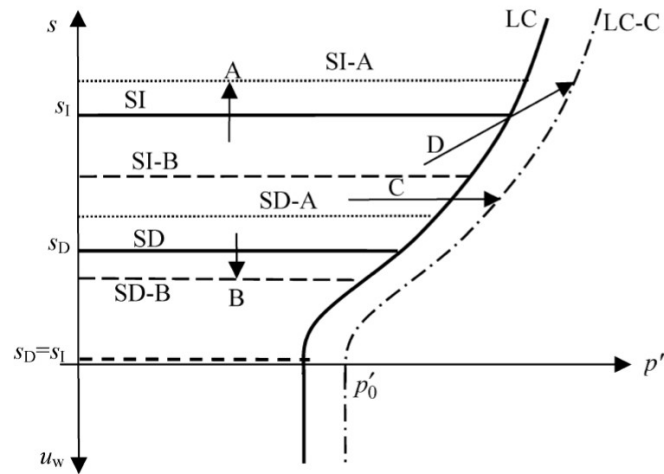
Figure 2.15 Non-convexity shape of the LC curve and hardening under different stress paths (Figure from Sheng et al. 2004).

2.4.3 The compression index as a function of the effective degree of saturation (Zhou et al. 2012a, 2012b, 2018)

Zhou et al. (2012a) showed an alternative approach to model the volumetric behaviour of unsaturated soils. As showed also in this thesis, the volume change behaviour is usually interpreted and modelled in term of stress and suction. The choice of the suction as a variable is done for simplicity because it is a variable that can be controlled during the common laboratory tests (e.g. controlled suction oedometric tests). However, Zhou et al. (2012a) showed that this approach suffers some limitations and they present an alternative approach for interpreting unsaturated soil behaviour.

The authors proposed a new volume change equation in the plane of effective stress vs effective degree of saturation. The equation of the effective degree of saturation used by Zhou et al. (2012a) is similar to the one proposed by Alonso et al. (2010) and it is given by:

$$S_r^e = \frac{S_r - S_{r,res}}{S_r^0 - S_{r,res}} \tag{2.70}$$

where $S_{r,res}$ is the residual degree of saturation and S_r^0 is the degree of saturation at zero suction which usually is equal to 1, but for some particular material it could be less (Sun et al. 2007).

Using the effective degree of saturation instead of the degree of saturation, the Bishop effective stress becomes:

$$\sigma_{ij}^{'} = \sigma_{net,ij} + S_r^e s \delta_{ij} \tag{2.71}$$

To describe the volume change behaviour of unsaturated soil in the plane $v - \ln p^{'}$ the authors assume:

$$v = N - \lambda\left(S_r^e\right) \ln p^{'} \tag{2.72}$$

where the compression index is assumed to be function of the effective degree of saturation. The authors suggest to interpolate the compression index from compression indices for the saturated and dry state:

$$\lambda\left(S_r^e\right) = \lambda_0 - \left(1 - S_r^e\right)^{a_1}\left(\lambda_0 - \lambda_d\right) \tag{2.73}$$

where λ_0 is the compression index for saturated state ($S_r^e = 1$), λ_d is the compression index for the dry state ($S_r^e = 0$), and a_1 is a fitting parameter.

The equation (1.72) cand be rewritten as follows:

$$-dv = \lambda\left(S_r^e\right)\frac{dp^{'}}{p^{'}} + \frac{\partial\lambda\left(S_r^e\right)}{\partial S_r^e}\ln p^{'}dS_r^e \tag{2.74}$$

Using this approach the authors give a better explanation to the non-linear change of soil compressibility under constant suction. In fact, the volume change behaviour is affected by two components: the first component is due to the stress change and the second component is due to the change of the effective degree of saturation. If the effective degree of saturation is fixed (only for loading path at saturated or dry condition) the second component will degenerate to zero. During a loading path at constant suction the second term of the equation (2.74), which describes the debonding effect, is always larger than zero since $dS_r^e \geq 0$. Although $\lambda\left(S_r^e\right)$ is less than λ_0, the apparent slope of the compression curve for an initially unsaturated soil can still be larger than its saturated counterpart. The irreversible volumetric strain can be calculated as follows:

$$\varepsilon_v^p = \frac{\lambda\left(S_r^e\right) - k}{N}\ln p^{'} \tag{2.75}$$

or in function of the yield stress for saturated condition:

$$\varepsilon_v^p = \frac{\lambda_0 - k}{N} \ln p_0'$$

(2.76)

The LC curve can be obtained combining the equation (2.75) and (2.76):

$$p' = \left(p_0'\right)^\beta$$

(2.77)

where:

$$\beta = \frac{\lambda_0 - k}{\lambda\left(S_r^e\right) - k}$$

(2.78)

Due to the hydraulic hysteresis and the hydro-mechanical coupled behaviour, the LC curve is not easy to plot in the plane mean net stress vs suction. To predict the hysteretic saturation variation with stress and suction Zhou et al. (2012a) proposed also an alternative method for. In this case too, the authors prefer using the effective degree of saturation instead of the degree of saturation. The equation that describes the change of the effective degree of saturation is given by:

$$dS_r^e = \frac{\partial S_r^e}{\partial s} ds + D_e d\varepsilon_{v\sigma_{net}}$$

(2.79)

where D_e is a general function that defines the effect of volumetric strain on the effective degree of saturation caused by a net stress change ($d\varepsilon_{v\sigma_{net}}$). The first term of the right side of the equation 2.79 describes the change of the effective degree of saturation under a constant net stress, while the second one describes the change of the effective degree of saturation due to the net stress under a constant suction. Due to the hysteretic hydraulic behaviour a simply choice is to plot the LC curve in the plane mean effective stress vs effective degree of saturation as shown in Fig. 2.16
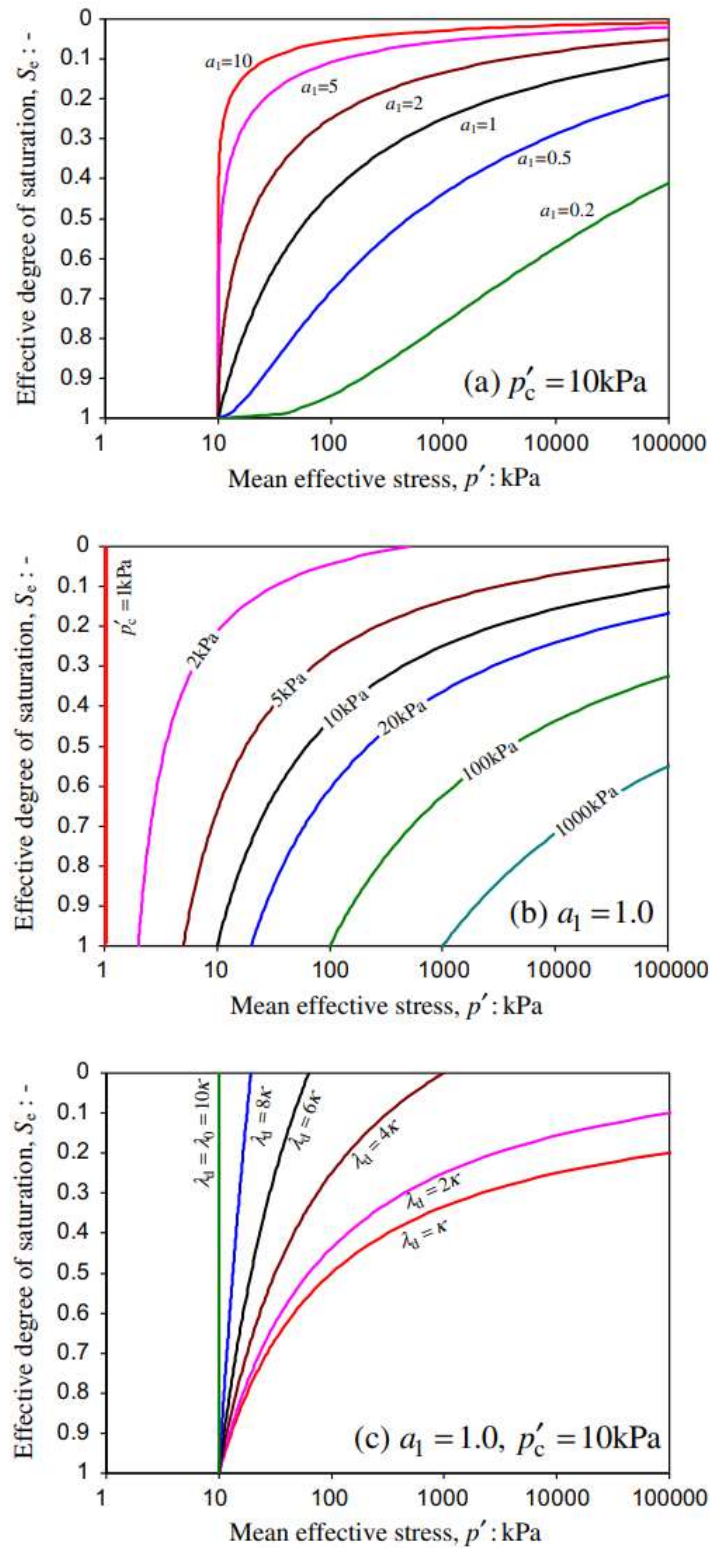
Figure 2.16 LC curve in the plane of mean effective stress vs effective degree of saturation: (a) variation of the yield curve with a_1,(b) variation of the LC curve with the saturated yield stress, (c) variation of the LC curve with λ_d (Figure from Zhou et al. 2012b).

In conclusion the model proposed by Zhou et al (2012a,b) represents a fully coupled model that can take into account the bi-directional hydro-mechanical interaction and that is able to describe the non-linear compressibility of the soil under constant suction continuously and smoothly.

Successively, Zhou et al. (2018) modified the previous framework. They divided the degree of saturation into two components: the degree of capillary saturation (S_r'), based on the capillary water, and the degree of adsorptive saturation (S_r''), based on the adsorbed water.

Using the degree of capillary saturation instead of the effective degree of saturation and introducing:

$$\lambda = \lambda_0 - \left(1 - S_r'\right)^c \left(\lambda_0 - \lambda_d\right) \tag{2.80}$$

$$k = k_0 - \left(1 - S_r'\right)^c \left(k_0 - k_d\right) \tag{2.81}$$

where c is a coupling parameter which can be determined by a drying test, the new equation that describes the evolution of the yield stress with suction is given by:

$$p_0' = \left(p'\right)^{1 - \left(1 - S_r'\right)^c} \tag{2.82}$$

2.4.4   Constitutive model with consideration of inter-particle bonding (Hu et al. 2014)

Hu et al. 2014 proposed a physically-based constitutive model for partially saturated soils able to consider the bonding effect of water menisci at inter-particle contacts. In a similar way proposed by Gallipoli et al. (2003), the authors introduced the effect of the capillary bonding in their elasto-plastic constitutive model.

In the original formulation (Gallipoli at al. 2003), the magnitude of the effect of the water menisci (ξ) was given by:

$$\xi = f(s) \cdot (1 - S_r) \tag{2.83}$$

where $f(s)$ represented the ratio of the inter-particle attraction at the two suction of s and zero (ideal case of a water meniscus located at the contact between two identical spheres, see Figure 1.17). This lead to a unique relationship between the bonding variable ξ and the ratio e / e_s, where e is the void

ratio calculated at the same value of average skeleton stress in unsaturated condition, and e_s is calculated in saturated condition.
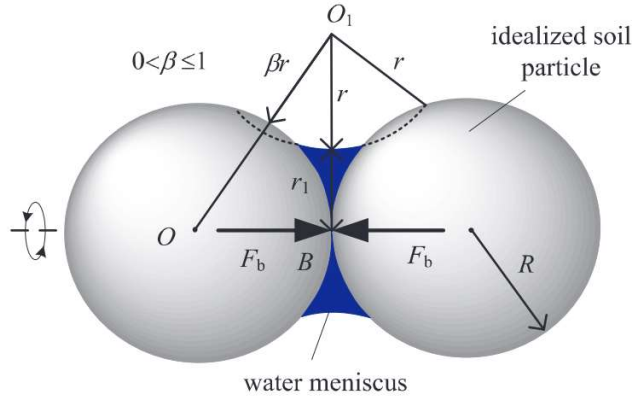
Figure 2.17 Water meniscus between two identical contacting spheres scheme (Figure from Hu et al. 2014).

Hu et al. (2014) improved the original constitutive model proposed by Gallipoli et al. (2003), in order to reproduce many features of unsaturated soils, using a small number of parameters and adopting a different approach to define the bonding effect.

Considering the Figure 2.17, the authors, using geometrical considerations, defined the relationship between the radius of curvature of the air-water interface r and the radius of the gorge of the meniscus r_1 as follows:

$$(\beta r + R)^2 = R^2 + (r + r_1)^2 \tag{2.84}$$

where β is a parameter that decreases with increasing values of the contact angle and R is the radius of the spheres.

Neglecting the weigth of the water bridge, the bonding force due to the water meniscus is given by:

$$F_b = \pi r_1^2 s + 2\pi r_1 T_s \tag{2.85}$$

where T_s is the surface tension of water and s is the suction calculated using the Young-Laplace equation $s = p_a - p_w = T_s \left(\dfrac{1}{r} - \dfrac{1}{r_1} \right)$.

The bonding stress σ_b can be written as follows:

$$\sigma_b = \frac{2\pi\beta T_s}{R} \cdot \frac{\left(1 - S_r^{1/4}\right)}{g(e)} \tag{2.86}$$

In other words, the authors consider the bonding stress as a product of two components. The first component depends on the contact angle, the surface tension and the radius of the spheres, while the second one depends on the degree of saturation and the void ratio and it represents the evolution of the bonding stress during isothermal deformation. In this way, the authors defined the dimensionless second term as the bonding factor related to the magnitude of the bonding stress:

$$\zeta = \frac{\left(1 - S_r^{1/4}\right)}{g(e)} \tag{2.87}$$

Differently from what proposed by Gallipoli et al. (2003), the bonding factor proposed by Hu et al. (2014) is based on the assumption that the bonding force exists for any two contacting soil particles while Gallipoli et al. (2003) considered that only a portion of contacting particles are subjected to bonding force.

Two constitutive variables were used in the model proposed by Hu et al. (2014): the effective stress, defined from the expression of Bishop's stress (Bishop, 1959) introducing the degree of saturation as weighting factor, and the bonding factor (equation 2.87) to take into account the presence of the inter-particle water menisci.

To describe the effect of inter-particle bonding on the irreversible volumetric behaviour, Hu et al. (2014), in a way similar to that proposed by Gallipoli et al. (2003), introduced the following empirical equation:

$$\frac{e}{e_s} = h(\zeta) = 1 + a\zeta^b \tag{2.88}$$

which describes the increasing of e/e_s with the bonding factor. In the equation 2.88, e and e_s are the void ratios in the unsaturated and saturated state at the same value of average skeleton stress. a and b are fitting parameters.

The void ratio under unsaturated condition can be expressed as:

$$e = \frac{e}{e_s} \cdot e_s = h(\zeta) e_s \tag{2.89}$$

The authors consider the elastic change in void ratio as a function of the change of mean average skeleton stress (equation 2.90), but they neglect the elastic strains induced by changes of the bonding factor for changes of saturation under constant average skeleton stress. In their opinion, this assumption is best suited to describe the behaviour of silt or low plasticity clays. However, for highly expansive soils further examinations to take into account the development of elastic strains due to changes of bonding factor are necessary.

$$de = -k \frac{dp^{'}}{p^{'}} \tag{2.90}$$

Combining the equation 1.90 with the equation of the normal compression line in the $\ln p^{'} - e_s$ plane, given by:

$$e_s = e_s(p^{'}) = N - \lambda \ln p^{'} \tag{2.91}$$

the expression of the normal compression surface is obtained:

$$e = h(\zeta)(N - \lambda \ln p^{'}) \tag{2.92}$$

The expression of the yield curve f, given by the intersection of the elastic domain with the normal compression surface, is given by:

$$f\left(p^{'}, \zeta, p_c^{'}(0)\right) = \left(h(\zeta)\lambda - k\right)\ln p^{'} - (\lambda - k)\ln p_c^{'}(0) - N\left(h(\zeta) - 1\right) = 0 \tag{2.93}$$

where $p_c^{'}(0)$ is the mean yield averange skeleton stress under saturated conditions.

The irreversible change of void ratio is obtained by subtracting the elastic change from the total canghe as follows:

$$\Delta e^p = \Delta e - \Delta e^e = \left[e_s(p_2^{'})h(\zeta_2) - e_s(p_1^{'})h(\zeta_1)\right] - \Delta e^e \tag{2.94}$$

where $p_1^{'}, \zeta_1$ and $p_2^{'}, \zeta_2$ are the average skeleton stress and bonding factors corresponding to the starting and the end points of a stress path, respectively.

The three-dimensional representation of the elastic domain is reported in Figure 2.18.

$$f=q^2-M^2p'[p_c'(\zeta, p_c'(0))-p']=0$$

$$p_c'(\zeta, p_c'(0))=\exp\left\{\frac{(\lambda-\kappa)\ln p_c'(0)+N(h(\zeta)-1)}{h(\zeta)\lambda-\kappa}\right\}$$
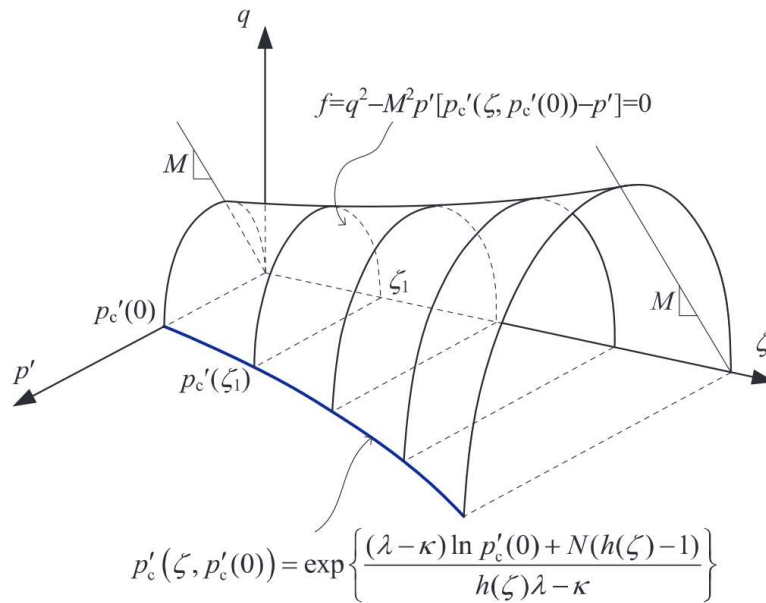
Figure 2.18 Three-dimensional view of yield surface (Figure from Hu et al. 2014).

The model proposed by Hu et al. 2014 can be extended at the triaxial states, in a similar way proposed by Alonso et al. (1990). In this case, the authors are able to introduce only one yield surface; in this way they are able to reduce the number of parameters of the model.

The model is able to take into account the bonding effect of the water menisci. The yield curve is represented in the plane average skeleton stress vs bounding factor, the shape of it is convex and the yield stress increases monotonically with the bouding factor.

In other words, the mechanical behaviour of the soil is assumed governed by two mechanisms: the action of the average skeleton stress acting on the soil skeleton and the stabilizing action of the normal force axerted at the inter-particle contacts by water menisci.

2.4.5 Coupling of hydraulic hysteresis and stress-strain behaviour for expansive soils (Sun et al. 2010)

Sun et al. (2010) proposed a new framework in terms of effective stress to model the hydro-mechanical model of unsaturated expansive soils. The framework proposed by the authors is based on the existing hydro-mechanical model for non-expansive soils proposed by Sun et al. (2007). The existing model used by the authors is a reformulation of the BBM model by Alonso et al. (1990) in terms of effective stress, thus the similarity of the equation of the LC curve proposed by Sun et al. (2007) with the LC equation proposed by Alonso et al. (1990):

$$\frac{p_0^{'}}{p^c} = \left[\frac{p_0^{'*}}{p^c}\right]^{[\lambda(0)-k]/[\lambda(s)-k]} \tag{2.95}$$

where $p_0^{'}$ is the Bishop's effective stress calculated using the degree of saturation as a weighting parameter.

The only significant modification that the authors introduced in this model was the expression of $\lambda(s)$:

$$\lambda(s) = \lambda(0) + \frac{\lambda_s s}{s + p_{atm}} \tag{2.96}$$

where λ_s is a material parameter for identifying the change of $\lambda(s)$ with suction s.

The water-retention curves of unsaturated expansive soils at different void ratio are expressed in Fig. 2.16, which are similar to those used for non-expansive soils (Sun et al. 2007) and they are given by:

$$dS_r = -\lambda_{se}de - B\frac{ds}{s} \tag{2.97}$$

where λ_{se} is the slope of the $S_r - e$ curve under constant suction larger than the air-entry value (Sun et al. 2007) and

$$B = \begin{cases} k_s & \text{Scanning curve} \\ \lambda_{sr} & \text{Main wetting/drying curve} \end{cases} \tag{2.98}$$

where k_s and λ_{sr} are the slopes of the scanning and wetting/drying curves (Fig. 2.19).
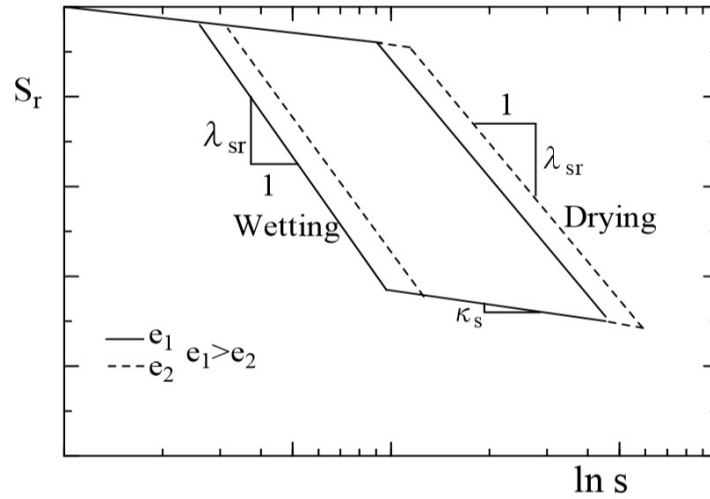
Figure 2.19 Water-retention behaviour at different constant void ratios (Figure from Sun et al. 2007).

The equation of the LC curve is the same proposed by Sun et al. (2007) (equation 2.95), while to model the variation of compressibility, Sun et al. (2010) used the same equation proposed by Alonso et al. (1990) (equation 1.9).

The framework proposed by Sun et al. (2010) is similar to the BBM model substituting the increment of the net stress with the following:

$$dp' = dp + S_r ds + s dS_r \qquad (2.99)$$

Finally, the proposed model by Sun et al. (2010) requires twelve parameters. There are three parameters to describe the water retention behaviour, λ_{sr}, k_s, and S_{rw}^0, which are determined by the measured water-retention curve. The parameter λ_{se} reflects the hydraulic and mechanical coupling behaviour, and it is determined by plotting e against S_r from results of isotropic compression test on unsaturated soil at a constant suction.

2.4.6 The ACMEG-s model by Nuth and Laloui (2007)

The Advanced Constitutive Model for Environmental Geomechanics, unsaturated extension (ACMEG-s) was proposed by Nuth and Laloui (2007). It consists of two independent parts: mechanical and retention.

The stress and strain framework is defined by Nuth and Laloui (2008a):

$$\begin{Bmatrix} \sigma'_{ij} = \sigma_{net\,ij} + S_r s \delta_{ij} \\ s = u_a - u_w \end{Bmatrix} \text{ and } \begin{Bmatrix} \varepsilon_{ij} \\ S_r \end{Bmatrix} \tag{2.100}$$

Each of the strain variables is likely to be affected by either the mechanical stress or the retention stress. The formulation of the stress-strain model is based on the monotonic part of the Hujeux model (1979). The increments of total strain are again decomposed into two components (elastic and plastic):

$$d\varepsilon_v^e = \frac{dp'}{K_{ref} \left(\dfrac{p'}{p'_{ref}} \right)^{n^e}} \tag{2.101}$$

where K_{ref} is the bulk elastic modulus at reference mean stress p'_{ref} and n^e is the nonlinear exponent, assuming values between 0 and 1. The yield surface is defined by:

$$\tilde{f}_{iso} = p' - r_{iso} \cdot d \cdot p'_{cr} \tag{2.102}$$

where p'_{cr} is the critical state pressure, d is a material parameter and r_{iso} is the radius of mobilisation of the isotropic mechanism.

Volumetric irreversible strains are generated following the NCL whose slope is defined by that of the CSL:

$$\ln \frac{p'_{cr}}{p'_{cr0}} = \theta \varepsilon_v^p \tag{2.103}$$

where p'_{cr0} is the initial critical state pressure and θ is the coefficient of the compressibility, and it is expressed as:

$$\theta = \tilde{\theta}(s) = \theta_0 + \Omega s \tag{2.104}$$

where Ω is a material parameter.

In the ACMEG-s model the critical state pressure is linked to the yield stress:

$$p_c' = d \cdot p_{cr}' \qquad (2.105)$$

From the previous elements, the first level of coupling between the retention variables and the mechanical stress-strain model is automatically featured. Nuth and Laloui (2007) introduced a second level of capillary effects. This second level permits to account the increase of the yield stress with suction.

$$\begin{cases} \tilde{p}_c'(s) = p_{c0}' & \text{for } 0 < s < s_e \\ \tilde{p}_c'(s) = p_{c0}' \left[1 + \gamma_s \log\left(\dfrac{s}{s_e}\right) \right] & \text{for } s > s_e \end{cases} \qquad (2.106)$$

where p_{c0}' is the yield stress at saturated condition, γ_s is a material parameter, and s_e is the air entry value.

The shape of the LC, defined in equation 2.106, is reported in Fig. 2.20. Equations 2.104 and 2.106 define the second level of coupling between the retention behaviour and mechanical behaviour.
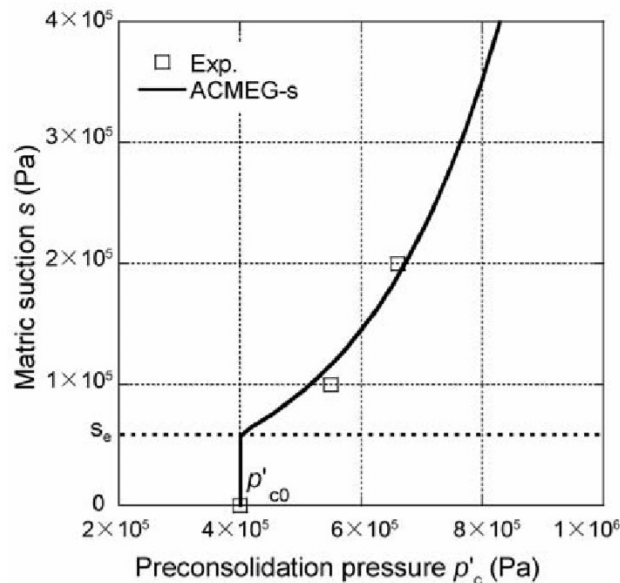
Figure 2.20 Shape of LC yield curve with experimental points carried out by Geiser (1999) (Figure from Nuth and Laloui 2007).

The elasto-plastic model for the soil water retention curve is proposed in Nuth and Laloui 2008b. The model is shown in Fig 2.21.
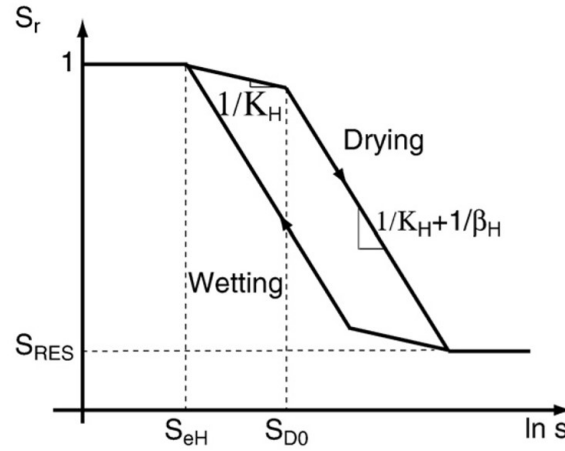
Figure 2.21 The ACMEG-s model for the Soil Water Retention Curve (Figure from Nuth et al. 2010).

The degree of saturation is decomposed into two parts (elastic and plastic):

$$dS_r = dS_r^e + dS_r^p \tag{2.107}$$

The elastic parts can be expressed by:

$$dS_r^e = \frac{ds}{K_H(s/s_e)} \tag{2.108}$$

where K_H is an elastic modulus.

If the suction remains lower than the updated air entry value, then the degree of saturation equals one, with no elastic increment. If the residual state is reached, then the elastic increment also becomes null. The elastic domain is delimitated by the yield surface:

$$f = \left\| \ln(s) - \ln(s_D) + \frac{1}{2}\left[\ln(s_{D0}) - \ln(s_e) \right] \right\| - \frac{1}{2}\left[\ln(s_{D0}) - \ln(s_e) \right] \tag{2.109}$$

where s_D is the actual drying yield suction and s_{D0} is the reference yield suction. The drying yield suction represents the maximum suction experienced by the material along a drying part (in the same way of the Suction Increase). Because a similar threshold exists upon wetting (capillary hysteresis) the equation 2.109 defines a yield surface that evolves with kinematical hardening, i.e., upon suction increase or decrease.

The plastic part of the degree of saturation is defined:

$$\ln \frac{s_D}{s_{D0}} = \beta_H S_r^p \tag{2.110}$$

where β_H is the coefficient of compressibility for the plastic part of the degree of saturation. The coupled model is introduced via air entry value. The principle is to update this variable as a function of the volumetric strain computed from the stress-strain model:

$$s_e = s_{e0} + \pi_H \varepsilon_v \tag{2.111}$$

where s_{e0} is the reference air entry value and π_H is a material parameter. The last equation shows that the hysteresis maintains the same aperture independent of the level of air entry. Using a logarithmic scale for suction, the equation becomes:

$$s_{D0} = \frac{s_{DI} \cdot s_e}{s_{e0}} \tag{2.112}$$

In conclusion, the ACMEG-s model is able to take into account the nonlinear elasticity and it is able to satisfactory predict the conventional features of the behaviour of unsaturated soils such as oedometric unsaturated compressions. Moreover, the advanced use of the loading collapse curve is favourable to simulate more complex stress paths, such as hydraulic cycles or constrained and confined tests. The model proposed by Nuth and Laloui (2007) describes the water retention capability and the mechanical behaviour in a coupled manner. The elasto-plastic volumetric changes within the porous medium incorporate the effects of water saturation and capillary pressure, or suction.

2.5 Summary and Conclusion

The review on the state of the art of the hydro-mechanical modeling of partially saturated soils allows to highlight the main disadvantages and advantages of each model.

First of all, it has been explained how the choice of variables is also a topic of discussion among the various authors. On this point, it should be considered that the partially saturated condition is only one of the states of soils, and therefore it is necessary to define a unique set of variables able to describe the entire stress state of the soils whatever its degree of saturation would be.

The literary models are divided, in function of the stress state variables used, into three groups. Obviously, all groups present some advantages and disadvantages. One common difficulty of the models is to describe the volume changes of unsaturated soil in terms of a single stress variable. The volume change behaviour is one of the most important properties of the partially saturated soils and the volume change equation underpins the evolution of the yield stress with suction and the water retention behaviour. In addition, one of the main differences between the models is the consequence of the volume change equation. Consequently, also the equation used to describe the evolution of the elastic domain with the suction should be consistent with the volume change equation.

In addition, when interested in a coupled hydro-mechanical model, the volume variations along the water retention curve should be taken into account. Neglecting these volume variations could lead to an incorrect prediction of the degree of saturation and volume changes.

The expressions used by the models to define the LC are either direct fitting of the yield stress or depending on the compressibility index (Table 2.1). However, even in the latter case, the curve that defines the change of the compressibility coefficient with suction is a direct fitting of the values obtained experimentally. In other words, whatever model is considered, the LC is always defined by a fitting and it is not determined by an equation that takes into account the physics of the problem. Considering, for example, the expression that define the change of the compressibility coefficient with suction, many models introduce an exponential equation. The use of exponential equation is equivalent to saying that the compressibility of the soil decreases monotonically as the suction

increases, and therefore the compressibility of a dry soil is much lower than the compressibility of the same soil in a saturated condition.

This conclusion does not find consistent physical confirmation. In fact, if for example we consider a sand, its compressibility when it is in dry state will certainly be lower than when it is in partially saturated conditions, lacking the additional contribution given to compressibility by the menisci. It is evident that the models present in the literature are not very suitable for describing the behavior of partially saturated soils in correspondence with the transition between partially saturated and dry state.

Instead, the transition from the saturated to the partially saturated state is often modeled (especially by models that use effective stresses as a stress variable) using a non-convex model. Obviously, non-convexity implies higher computational work. In this case, to correctly code the finite element model it is necessary to add an explicit stress integration scheme.

Ultimately, no model in the literature sheds light on the transition from unsaturated to dry states.

Clearly, this aspect must be adequately investigated both from an experimental and a modeling point of view. It is also necessary to verify whether the models in the literature are able to represent the hydro-mechanical behavior of unsaturated soils in the entire range of the degree of saturation, and to investigate the transition from partially saturated to dry state.

Table 2.1 Proposed Loading-Collapse curve equations by different authors.

Loading – Collapse curve equations	
Models in term of net stress	
Reference	**Equation**
Alonso et al. (1990)	$$\frac{(p-u_a)_0}{p^c} = \left[\frac{(p-u_a)_0^*}{p^c}\right]^{[\lambda(0)-k]/[\lambda(s)-k]}$$
Wheeler and Sivakumar (1995)	$$\frac{(p-u_a)_0}{p_{atm}} = \left[\frac{(p-u_a)_0^*}{p_{atm}}\right]^{[\lambda(0)-k]/[\lambda(s)-k]}$$
Rampino et al. (2000)	$$\frac{(p-u_a)_0}{p^c} = \left[\frac{(p-u_a)_0^*}{p^c}\right]^{[\lambda(0)-k(0)]/[\lambda(s)-k(s)]}$$
Models in term of "equivalent effective stress"	
Sun et al. (2000)	$$p_0 = p^c \left(\frac{p_0^*}{p^c}\right)^{(\lambda(0)-k)/(\lambda(0)-k+\lambda_s\sigma_0(s))} - \sigma_0(s)$$
Sun et al. (2003)	$$p_0 = p^c \left(\frac{p_0^*}{p^c}\right)^{(\lambda(0)-k)/(\lambda(s,e_0)-k)} - \sigma_0(s)$$
Georgiadis et al. (2005)	$$\frac{(p-u_a)_0^*}{p^c} = \left[\frac{(p-u_a)_0}{p^c}\right]^{[1-(\lambda_m\frac{(p-u_a)}{p^c})^{-b}]/(\lambda(0)-k)]}$$
Models in term of effective stress	
Wheeler et al. (2003)	$$p^* = p_0^*$$
Sheng et al. (2004)	$$\frac{p_0'}{p^c} = \left[\frac{p_0'^*}{p^c}\right]^{[\lambda(0)-k]/[\lambda(s)-k]} + S_r s$$
Zhou et al. (2012a), (2012b)	$$p' = \left(p_0'\right)^{\beta}$$
Zhou et al. (2018)	$$p_0' = \left(p'\right)^{1-\left(1-S_r'\right)^c}$$
Sun et al. (2010)	$$\frac{p_0'}{p^c} = \left[\frac{p_0'^*}{p^c}\right]^{[\lambda(0)-k]/[\lambda(s)-k]}$$
Nuth and Laloui (2007)	$$\begin{cases} \tilde{p}_c'(s) = p_{c0}' & \text{for } 0 < s < s_e \\ \tilde{p}_c'(s) = p_{c0}'\left[1+\gamma_s \log\left(\frac{s}{s_e}\right)\right] & \text{for } s > s_e \end{cases}$$

3. Experimental study on the yield stress from saturated to dry state

3.1 Introduction

This chapter is devoted to analyze the evolution of the yield stress from saturated to dry state. As known, wide areas of the earth's surface, like the Mediterranean Area, are subjected to significant variations of the degree of saturation during the year, and the soils could reach the complete dryness. For these areas, the study of the transition from saturated to dry states is relevant. In this chapter, it is precisely analysed, from an experimental perspective, the behaviour of unsaturated soils in a wide range of degree of saturation (from saturated to dry state). In order to describe different mechanical behaviour three different soils were tested (quartz sand, Speswhite kaolin and a scaly clay). To cover the suction range, which is expected to be different for the tested materials, a combination of suction-control and suction measurement techniques were used (e.g. negative water column, axial translation, vapour equilibrium). The obtained results enabled us to get detailed information on the water retention behaviour curves and to quantify the evolution of the yield stress with suction for the three materials. This extensive characterization work sheds light over the evolution of the yield stress over the entire range of degree of saturation. The obtained results, according to the classical soils mechanics approach, show that the yield stress does not increase monotonically with the suction and the yield stress at saturated condition is almost the same of the yield stress at dry state. A similar trend could be observed also for other geotechnical properties of unsaturated soils (e.g. shear strength). In addition, the new shape of the yield curve (LC curve) suggests that it could be reached by a drying path. To verify the hardening of the LC curve caused by a drying path, a special controlled-suction oedometric test was planned and carried out. The results confirm the new kind of hardening of the Loading-Collapse curve. This extensive campaign could be used as a basis for a new elasto-plastic framework for partially saturated soils, which will be able to anticipate the hydro-mechanical behaviour of the soils when they approach the dry state.

3.2 Experimental LCs curve – literature review

The volumetric response in partially saturated conditions has been determined experimentally for a variety of soils. Figure 3.1 depicts a collection of the LC curve determined by different authors. Data are shown both in terms of effective and net stress, keeping the original interpolations of the authors.

1. Silty soil - Maatouk et al. (1995)
2. Kaolin Bentonite - Sharma (1998)
3. Kaolin Speswhite - Wheeler & Sivakumar (1995)
4. Pearl Clay - Sun et al. (2003)
5. Matramo silty sand - Rampino et al. (2000)
6. Kaolin Speswhite - Sivakumar et al. (2010)
7. Silty clay - Oliviero (2016)
8. Kaolin Malaysia - Thu et al. (2007)
9. Volcanic ash - Ferrari et al. (2013)

10. Seprolite without cementation - Leroueil & Barbosa (2000)
11. Sand soil - Vilar & Rodrigues (2011)
12. Seprolite with 2% of cementation - Leroueil & Barbosa (2000)
13. Scaly clay - Airò et al. (2010)

Figure 3.1. Collection of Loading – Collapse curves.

Interestingly, all data show a monotonic increase of yield stress with the suction and then a monotonic increase of the LC curve. However, the experimental LC curves reported in Fig. 3.1 cover a limited part of the water retention behaviour. In fact, analysing the water retention curves, when they are available, it comes to light that generally the degree of saturation is between 1.00 and 0.60

Only Thu et al. (2007) have presented results at low value of the degree of saturation. The authors have performed tests on coarse kaolin made by Malaysia Kaolin, and have explored a range of degree of saturation 1.00-0.30. However, in this case too, the transition from unsaturated to dry state is not described.

The experiments conducted by Villar and Rodrigues (2011) investigated the hydro-mechanical behaviour of Brazilian sand soil presenting double porosity structure. But in this case the authors carried out the yield point of material in the range of the degree of saturation 0.35-0.25.

The experimental yield points showed by Lerouil and Barbosa (2000) show a different trend. In fact, the yield point obtained at high level of suction (500 kPa), is less than the yield point carried out at 300 kPa of suction. Nonetheless, the LC curve proposed by the authors increase monotonically with the suction.

So far, surprisingly, no tests at very low degree of saturation (in the range of 0.20-0) were conducted, and then the transition between unsaturated and dry state has never been studied. However, wide areas of the earth's surface are subjected to significant variations of the degree of saturation. In the areas, classified as arid or sub-arid zone (i.e. the Mediterranean area), in which the annual evaporation from the ground surface exceeds the annual precipitation, the soil could reach the complete dryness state. Obviously, for these soils the study of the transition from unsaturated state to dry state is relevant. However, the classical models presented in literature have been calibrated using the experimental points shown in Fig. 3.1, and therefore, for this reason, they are not validated to describe the transition from saturated to dry states. Moreover, all models proposed show that the LC curve increases monotonically with suction, in contrast with a classical geomechanical point of view, according to which the behavior of dry soils has to be similar to the saturated one, providing that the hydro-mechanical response is described in terms of effective stress. For instance, Donald (1956), studying the behavior of a sand, has shown that the available shear strength of the unsaturated soils tends, after an initial increase, to the shear strength in saturated state once suction increase significantly. It is reasonable to expect a similar behavior also for the evolution of yield stress with suction.

The aim of this chapter is, thus, to analyse in a complete manner the hydro-mechanical behaviour of unsaturated soil, shedding light over the evolution of the yield stress over the entire range of degree of saturation. For this reason, an intensive experimental program was carried out with the aim to cover a variety of soils in a wide range of the degree of saturation.

3.3 Materials and methods

Three soils with different geotechnical characteristics were tested: a quartz sand, a Speswhite kaolin and a scaly clay.

For each of them, a series of controlled-suction oedometric tests were conducted in order to determine the yield stress evolution in a wide range of suction. Complementary, for each material, information on the water retention behaviour was first collected, to select the suction values for the oedometric tests.

The following sections show the material properties, summarized in Tab. 3.1 (physical and water retention characteristics), and the experimental techniques (specimen preparation and apparatus layouts).

3.3.1   Quartz sand

The quartz sand used is a uniform sand (C_u= 1.4 ÷ 1.6) with grain size in the range of 0.07 ÷ 0.85 mm (Figure A1 – Appendix A) and a specific gravity of 2.65. Prior to testing, the sand was washed using distilled water and dried to eliminate the presence of fines.

The water retention curve was obtained using the negative water column technique. Specimens with dimensions of 60 mm in diameter and 20 mm in height were prepared in saturated conditions by wet pluviation in de-aired and distilled water at the target initial void ratio of 0.77 corresponding to a relative density equal to 0.48 ($e_{max} = 0.897$, $e_{min} = 0.634$). Sand raining was performed in three levelled layers to maximize the uniformity of the density (Raghunandan et al. 2012). The specimen was sitting on a high air-entry value ceramic disk (nominal air-entry value of 100 kPa), which was connected to a burette used to impose the negative water pressure. Water content changes of the specimens were also monitored through the burette (resolution of ± 0.17%). Starting from the saturated condition, the suction was increased maintaining a constant total vertical stress of 1.75 kPa. Suction was increased in steps from 0 to 16.6 kPa, following a geometric series. Each suction equalization phase was considered ended when no more variations of the water level in the burette and no more settlements

were registered. A twin burette, insulated from the specimen, was used to monitor and correct the

evaporated water volumes. The layout of the device is depicted in Fig. 3.2.
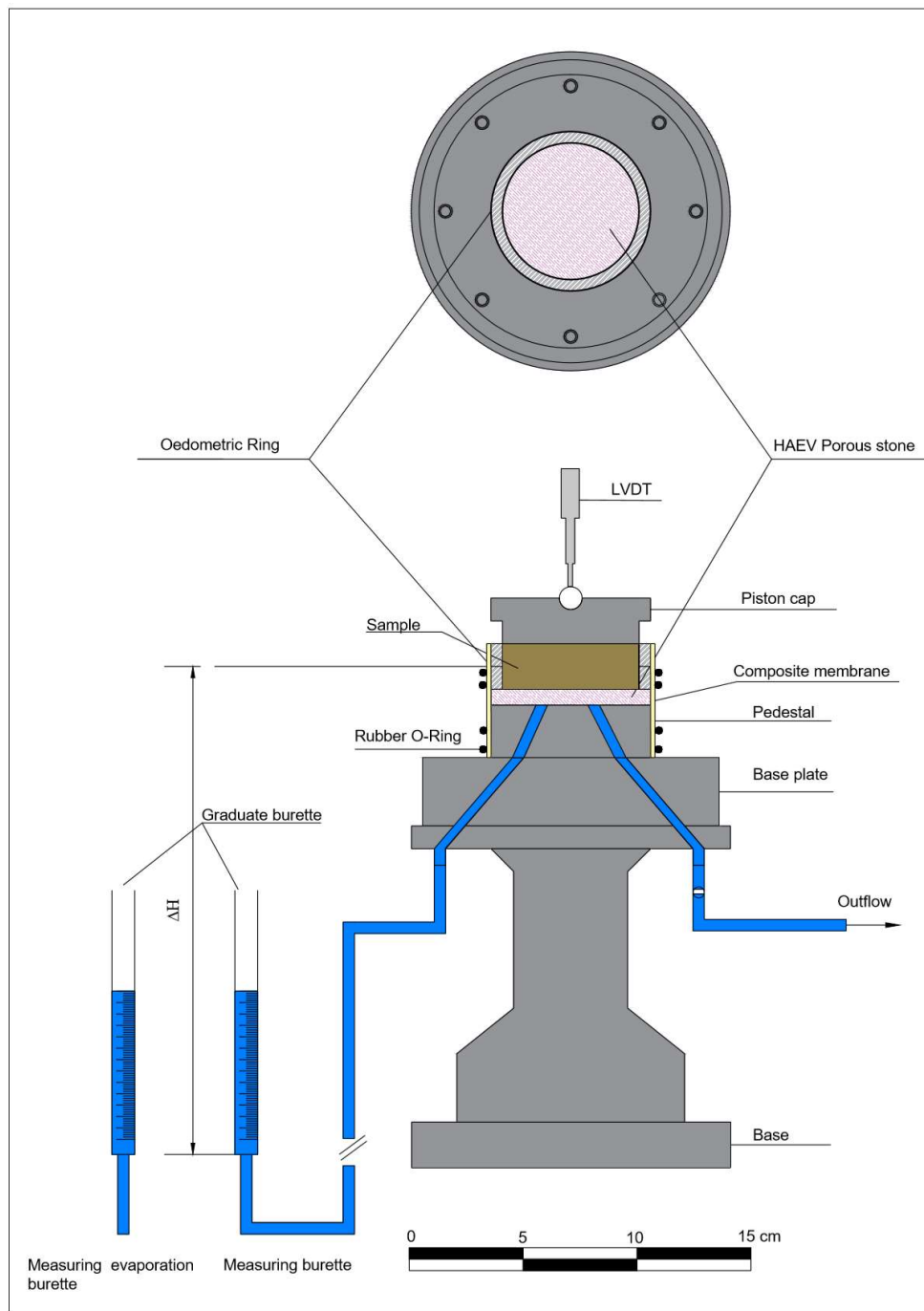
Figure 3.2. Layout of the device used to determine the water retention behaviour of the quartz sand operating with the negative water column technique.

The maximum variation in void ratio measured during the imposed drying was -0.001, so that the obtained curve will be referred to the reference void ratio at preparation. The experimental points on the plane (S_r, s) were fitted in Fig. 3.6a using the expression (Van Genuchten, 1980):

$$S_r = S_{r,res} + \frac{1 - S_{r,res}}{\left[1 + \left(\alpha s\right)^n\right]^m}$$

(3.1)

where $S_{r,res}$ is the residual degree of saturation, and α, n, m are fitting parameters. The best-fitting was obtained with the parameters $\alpha = 0.46 \text{ kPa}^{-1}$, $n = 3.38$, $m = 0.74$ and $S_{r,res} = 0.01$.

The same technique was also used to perform the controlled-suction oedometric tests in the suction range of $0 \div 16.6$ kPa; in this case the specimens (11 mm high and 33 mm in diameter) were sitting on a cellulose microporous membrane with a thickness of 0.1 mm (PALL – Supor® 450). The membrane, with a nominal pore size of 0.45 μm (corresponding to an air-entry value of 250 kPa) and permeability of $2 \cdot 10^{-8}$ m/s, was placed between the specimen and the drainage disk of the apparatus, and connected to the burette used to impose the suction. During all the test phases, the position of the burette was continuously adjusted in order to maintain a constant value of imposed suction. The vertical total stress was applied in steps, using a dead-weight loading frame, from a minimum of 30 kPa to a maximum of 12 MPa. Vertical displacement was measured with a resolution of 1 μm. The layout of the controlled-suction oedometer cell operating with the negative water column is reported in Fig. 3.3.

A total of nine specimens were used to perform seven controlled-suction oedometric tests and two tests in saturated condition. Starting from the saturated condition, the suction was initially imposed keeping the vertical total stress equal to 30 kPa. The suction values for the tests were identified on the base of the water retention curve depicted in Fig.1a. The selected values (1.8, 4.0, 4.9, 5.2, 8.8, 9.0, 16.6 kPa) allowed to cover the complete range of the degree of saturation, from 1.0 (tests in saturated condition) to the residual value of 0.01 (suction equal to 16.6 kPa).
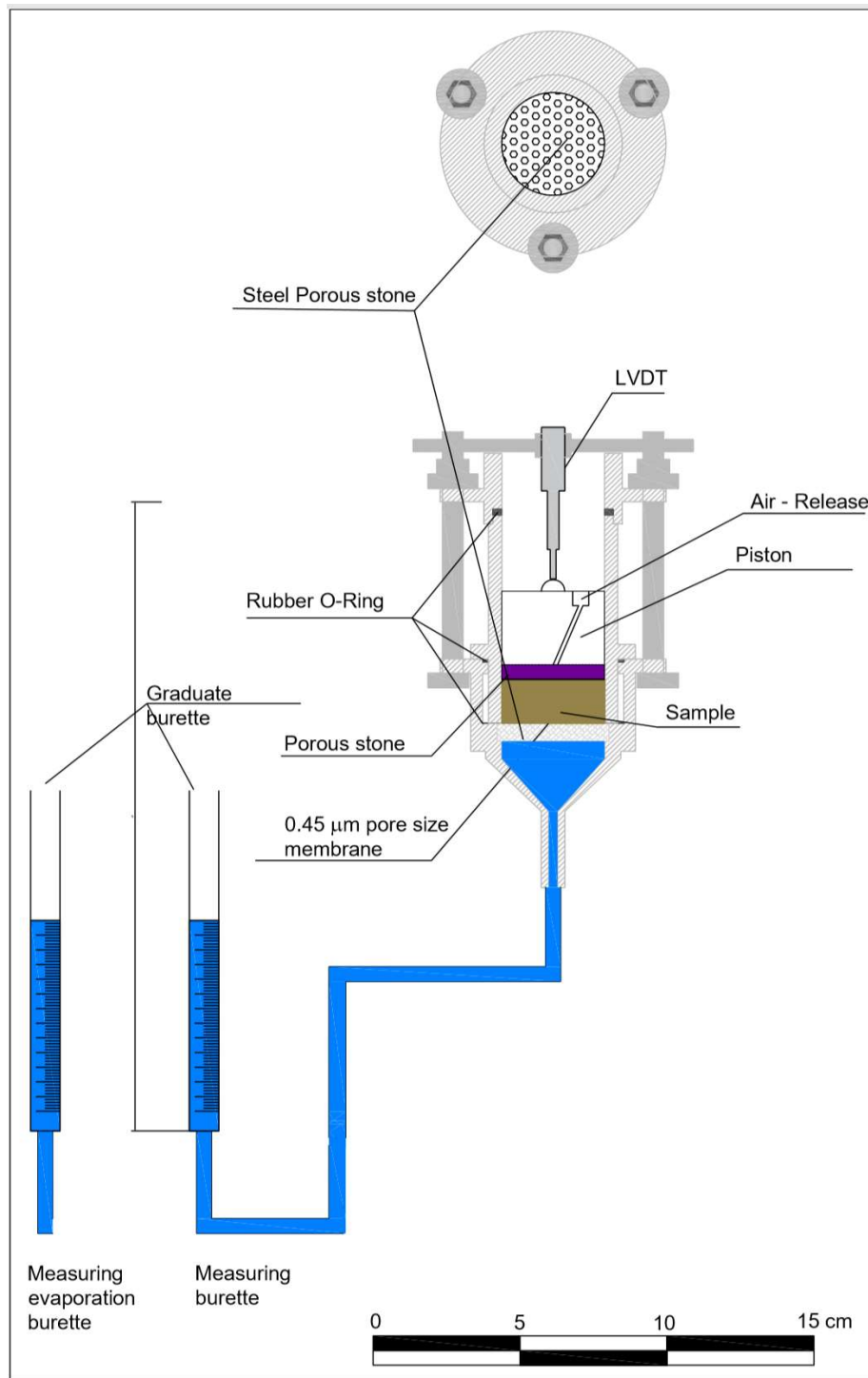
Figure 3.3. Layout of the controlled-suction oedometer cell operating with the negative water column technique.

The experimental points depicted in Fig.3.6a also include the equalization points obtained from the oedometric tests. After the initial equalization, suction was kept constant while performing loading-unloading cycle of vertical stress.

In addition, nineteen complementary oedometric tests at constant water content were conducted on specimens prepared at the reference void ratio. The sand was initially moisturized and stored in tiny hermetically closed glass jars (Frost and Park, 2003). Specimens were compacted by moist-tamping directly in an oedometric ring having a height of 20 mm and a diameter of 56 mm. The initial water content values were in the range of 0.05-29.6% (corresponding range of degree of saturation 0.01-1.00). Suction values were determined using the soil water retention curve depicted in Fig. 3.6a. The conventional porous bases of the oedometric cell were substituted with two impermeable disks. In addition, the entire cell was isolated from the external environmental by means of an impermeable membrane. The load was increased in steps up to a maximum vertical total stress of 6.0 MPa. During all these tests, the computed variations of the degree of saturation were limited (in the range of 0.3÷4.9%); in this sense, the tests will be analyzed with reference to the suction resulting from the average degree of saturation.

3.3.2 Speswhite kaolin

The tested Speswhite kaolin had a plastic limit equal to 35% and a liquid limit equal to 61%. The specific gravity was equal to 2.60. The clay fraction was 75% while the silt fraction was 25% (Figure A1 – Appendix A).

Air-dried kaolin powder was sprayed with distilled water to achieve a water content equal to 30%, and it was worked with a metallic spatula on a glass sheet. The material passing through a 1.18 mm aperture sieve was then selected. The moisturized material was stored for at least 24 hours to allow water content equalization.

All specimens were prepared by static compaction and suction conditioning, and they had a resulting void ratio in the range of 1.36±0.04.

The specimens used to determine the water retention curve (main wetting branch) had 37.4 mm in diameter and 6.8 mm in height. The water content after compaction was 26.2±0.1% and the initial suction of the as-compacted material was 850 kPa. The prepared specimens were subjected to air-drying in a room with a temperature of 21°C and relative humidity of 44% (corresponding total suction equal to about $\Psi = 110$ MPa). Then, the specimens were wetted by pure diffusion to different values of suction, putting them in closed jars in which NaCl solutions at different concentrations were placed. The NaCl solution concentrations were chosen according to Witteveen et al. (2013) in order to cover a suction range of $2 - 41$ MPa. Each suction equalization phase was considered as concluded when weight stabilised. During the drying and wetting processes, the measurements of the weight and dimensions (height and diameter) allowed to trace the evolution of the void ratio and degree of saturation.

The obtained data are depicted in Figure 3.6b in terms of degree of saturation vs. suction, along with data provided by Tarantino and De Col (2008) on specimens of Speswhite kaolin prepared with a similar technique at a similar void ratio (1.35). Figure 2.6b also shows the fitting of equation 3.1 using the parameters $\alpha = 0.001 \, \text{kPa}^{-1}$, $n = 0.80$, $m = 1.00$ and $S_{r,res} = 0.03$.

To determine the microstructural water void ratio of the material, a total of 9 water retention curves (6 main drying branches and 3 main wetting branches) were determined for different reference void ratio using the same technique described above. These water retention curves are depicted in the plane suction vs. degree of saturation in Fig. A2 (Appendix A).

To prepare the specimens for the controlled-suction oedometric tests, five samples were initially compacted in a rigid ring (60 mm in diameter and 20 mm in height); the resulting water content was 26.5±1.0%. The compacted samples were air-dried, while monitoring the volumetric strain and weight. After the air drying, one sample was re-wetted through the vapor phase in a closed environment with distilled water; from this sample a specimen was re-cored to be tested in a conventional oedometer (56 mm in diameter, 20 mm in height) in saturated conditions. A second

sample was equalized in a room with a temperature of 21 °C and relative humidity of 53% (target suction of 84.0 MPa); for this sample a specimen was obtained and tested in a conventional oedometer at the relative humidity of the room. For these two tests the maximum applied vertical total stress was 6.0 MPa.

The remaining three air-dried samples were re-wetted by pure diffusion using NaCl solutions at target suction values of 6.8, 8.7 and 41.0 MPa. Specimens for the controlled-suction oedometric tests were then re-cored from these samples; the specimens had dimensions of 50 mm in diameter and 20 mm in height. The selected suction range (6.8 - 84.0 MPa) was chosen in order to investigate the oedometric response in the range of the degree of saturation of 0.04 - 0.17, for which the water retention curve departs from the residual state (Figure 3.6b). During the loading-unloading phase the suction was maintained constant using the Vapour Equilibrium Technique (VET).

The circulation of the controlled-relative humidity vapour through the metallic porous bases of the cell was forced by a peristaltic pump (Fig. 3.4). The same NaCl solutions used for the equalization phase were used. The jars containing the salt solutions were weighted periodically in order to determine the variation of the water content of the specimens during the test. Loading-unloading paths were performed in steps by changing the total vertical stress in the range of $0 - 1.1$ MPa.
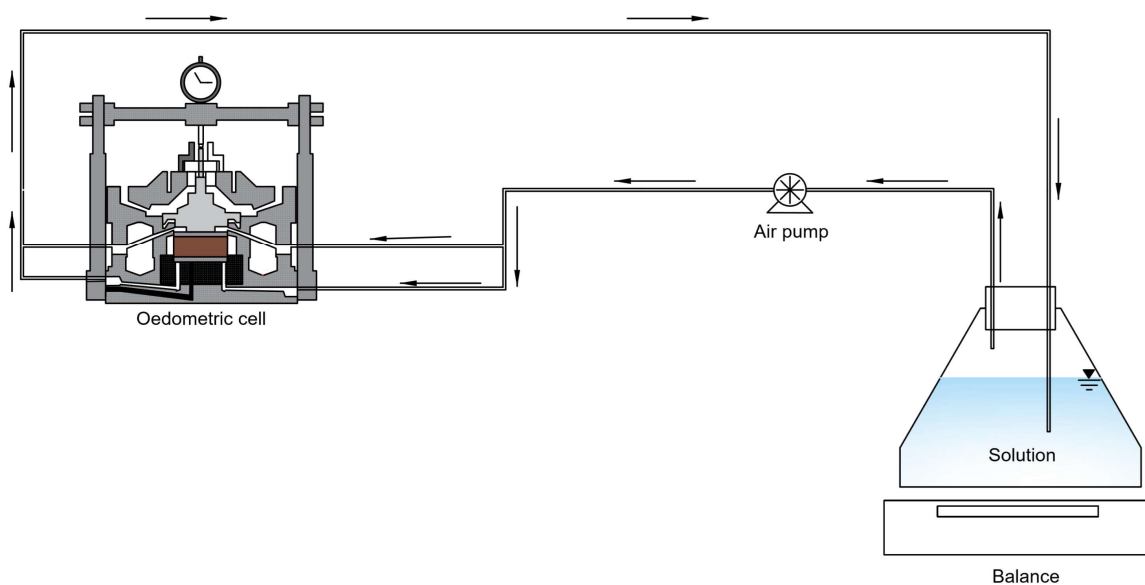
Figure 3.4. Layout of the controlled-suction oedometer cell operating with VET.

3.3.3 Scaly clay

In its natural state, the tested scaly clay is an over-consolidated clay characterised by the presence of interlocked stiff clayey angular fragments (named scales), having maximum dimensions of few centimeters. The material had plastic limit equal to 23% and a liquid limit of 62%. The specific gravity of scaly clay was equal to 2.75. Previous research work has been carried out to analyse the fabric proprieties of scaly clay and its evolution during compaction and suction changes (Airò Farulla et al. 2010, Airò Farulla and Rosone 2011). Moreover, the effect of the evolution of the microstructure on the volumetric and water retention behaviour was showed by Airò Farulla et al. (2007, 2011) and Ferrari et al. (2010).

The scaly clay at hygroscopic water content $w_h \approx 5\%$, was initially disaggregated by means of a rubber pestle. The material was sieved through a 4.75 mm aperture sieve. The fraction selected was constituted by scales, fragments of scales and powdered clay. The apparent grain size distribution of the specimens was characterized by a silt-size fraction of 3%, sand-size fraction of 42% and gravel-size fraction of 55% (Figure A1 – Appendix A). The passing material was sprayed with distilled water and stored for at least 24 hours to allow moisture equalization. The material was then statically compacted to a reference void ratio of 0.57±0.02; the resulting degree of saturation was in the range of 0.74±0.04 and initial suction was 2 MPa.

Additional equalization points of the scaly clay prepared with this technique were provided by Airò Farulla et al. (2011) for a reference void ratio of 0.57. The main drying and the main wetting retention curves depicted in Fig.2.6c were obtained using the expression proposed by Romero e Vaunat (2000):

$$S_r = \frac{e_{wh}}{e} + \frac{e - e_{wh}}{e}\left[1 + \frac{\ln\left(1 + \frac{s}{a}\right)}{\ln(2)}\right]\left[\frac{1}{1 + (\alpha s)^n}\right]^m \tag{3.2}$$

where e_{wh} and a are the residual water ratio (0.111) and the correspondent suction (110000 kPa) respectively. α, n, m are fitting parameters. The best-fitting parameter for the main-drying and main

wetting curve are $\alpha = 0.001\,\text{kPa}^{-1}$, $n = 1.62$, $m = 0.17$ and $\alpha = 0.01\,\text{kPa}^{-1}$, $n = 0.71$, $m = 0.31$ respectively.

Three samples were compacted in rigid rings having 60 mm in diameter and 20 mm in height. They were then dried by pure diffusion in glass jars to suction values of 2.2, 3.6, 9.7 MPa, using the technique described in the previous section. After equalization, specimens were re-cored (50 mm in diameter and 20 mm in height) from the samples; controlled-suction oedometric tests were then performed maintaining the same suction of equalization by vapour equilibrium control, in the same way described for the Speswhite kaolin.

Six additional specimens were statically compacted directly in the oedometric rings (diameter of 50-56 mm and 20 mm in height). Five specimens were used to carried out controlled-suction oedometric tests and one specimen was used for a conventional oedometric test in saturated condition. The suction-controlled tests were performed using the Axial Translation Technique (ATT) (Fig.3.5); suction was imposed keeping the air pressure constant in the cell and varying the water pressure at the bottom of the specimen through a High Air-Entry Value (HAEV) ceramic disc (air entry value equal to 1500 kPa). The pore water volume changes were measured by means of a burette and the measurements were corrected to take into account the air diffusions through and water evaporation from the ceramic disc (Airò Farulla and Ferrari, 2005). The imposed suction values were: 50, 100, 200, 400, 800 kPa (corresponding to a degree of saturation in the range of 0.77-0.88). For the specimens tested at the suction values equal to 50 and 100 kPa, the equalization was carried out in isochoric conditions, increasing the vertical total stress up to 270 kPa and 230 kPa; respectively. Loading-unloading cycles were then performed maintaining the suction constant and applying maximum vertical total stress of 2 MPa.

The specimen for the conventional oedometric test was saturated, preventing the swelling by applying a vertical total stress of 215 kPa. The maximum vertical total stress applied in the following loading-unloading cycle was 6.0 MPa.

Degree of saturation and suction before the loading-unloading cycles are depicted in Figure 3.6c along

with the water retention curves. The selected suctions allow to cover a range of the degree of

saturation of 0.53 - 1.00

Table 3.1. Physical properties and specimens characteristic of tested soils.

Material	Material properties						Specimens characteristic		
	G_s	w_l : %	w_p : %	f_{clay} : %	f_{silt} : %	f_{sand} : %	e_0	w_0 : %	s_0 : kPa
Quartz sand	2.65	-	-	-	-	100	0.77	28.9	0
Speswhite kaolin	2.60	61	35	75	25	-	1.36	26.5	850
Scaly clay	2.75	62	23	56	40	4	0.57	14.2	2000
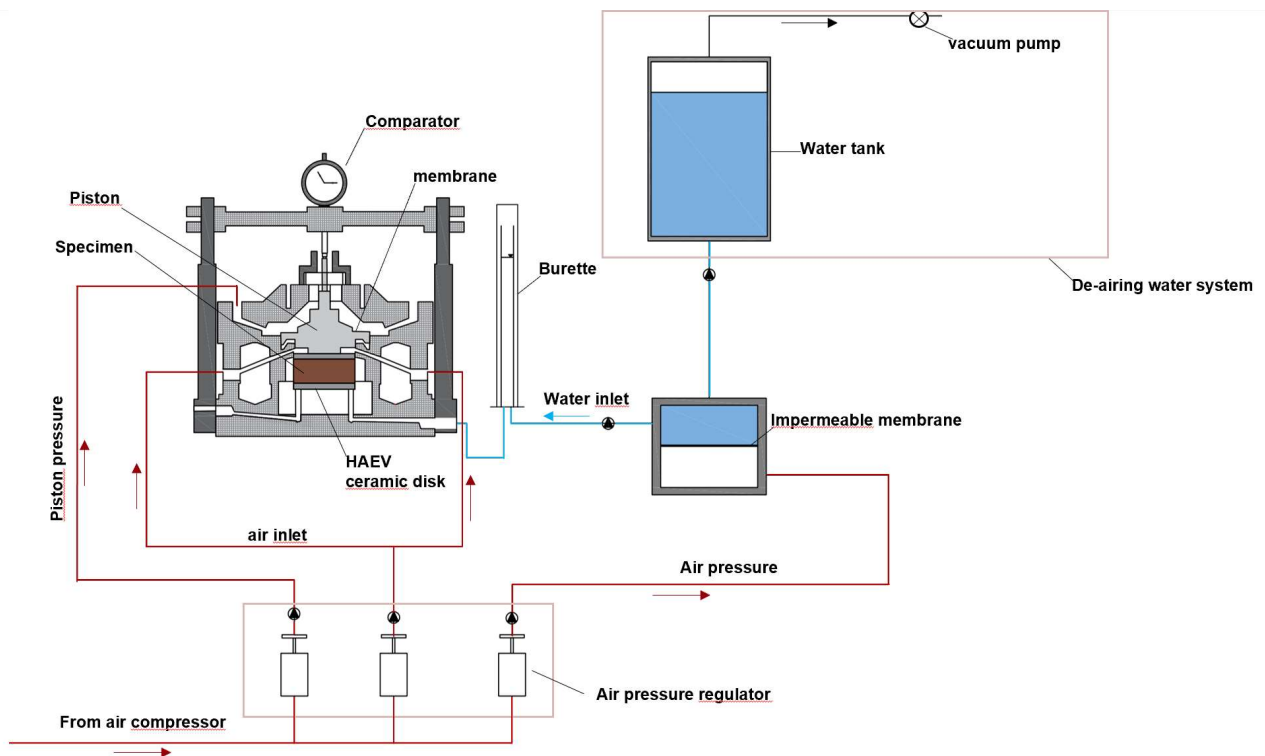
Figure 3.5. Layout of the controlled-suction oedometer cell operating with ATT.
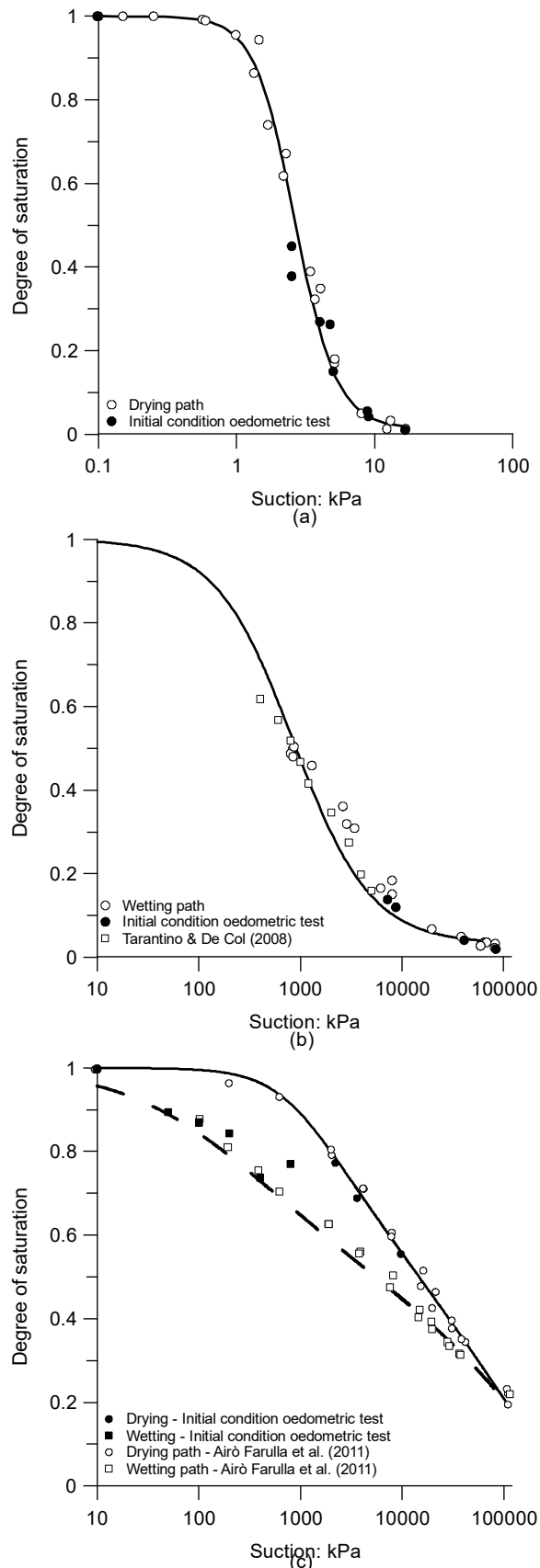
Figure 3.6. Water retention behavior of the tested materials: (a) main drying curve for quartz sand at a reference void ratio of e = 0.77; (b) main wetting curve for Speswhite kaolin for a void ratio in the range of 1.36±0.04; (c) main wetting and main drying curves for scaly clay for a reference void ratio of 0.60.

3.4 Experimental results

The results of the oedometric tests are reported and discussed in this section with reference to the vertical total stress. Yield stresses were determined in each performed tests using various methods (Casagrande, 1936, Pacheco Silva, 1970, Boone, 2010) in the plots we'll represent the yield stresses obtained with the method proposed by Boone (Boone, 2010), however, similar trends have been obtained also with the other methods.

For each material, selected oedometric curves are first presented in order to highlight the evolution of the yield stress with the imposed suction; the loading-collapse curves are then depicted considering the entire dataset. An interpretation of the results in terms of vertical effective stress is reported in the next section.

It is necessary to observe that the yield stress of granular soils does not coincide with the maximum effective overburden stress that the soil has sustained in the past. In fact, Atkinson (1990) suggests to use the term *yielding* only to describe the end of the elastic range, according to the classical meaning of yielding in continuum mechanics. For clayey soils, the yield stress is also called preconsolidation stress (Terzaghi et al. 1996), because it is equal to the maximum effective overburden stress that the soil sustained in the past. However, historically, the term yielding in soils mechanics has been used also to describe a clear change in stress-strain behavior (Vaughan 1985, 1990). With this regard, Vaughan (1988) defined two "*yield stress*" during his research on the mechanical behaviour of residual soils. Then, as reported before, for the granular soils two different yield stresses may be defined on the base of the volumetric behavior changes (Mesri and Vardhanabhuti 2009). The yield stresses for granular soils have been assumed to signal the abrupt onset of particle rearrangement and particle crushing (Coop and Lee 1993, McDowel and Bolton 1998, Nakata et al. 2001). The first point where the relationship between void ratio and effective vertical stress (in logarithmic scale) changes significantly it is recorded at low pressure (less of 15 MPa), and it is due to particle rearrangement into a more stable configuration; the second one is reached at high pressure (higher than 15 MPa),

and it is due to particle crushing (Mesri and Vardhanabhuti 2009). The first yield point does not depend only on the stress history, but it is strictly linked to the relative density. As known, it is possible to reach a very high value of relative density without a previously compaction (e.g. vibrating the sample).

In the explored range of confining stress (up to 12 MPa), the yielding mechanism is expected to be associated mainly to particle rearrangement. Grain crushing is limited as shown in Fig. 3.7, in which the grain size distributions of two tested specimens (maximum vertical stresses of 6 and 12 MPa) are compared with the initial one.
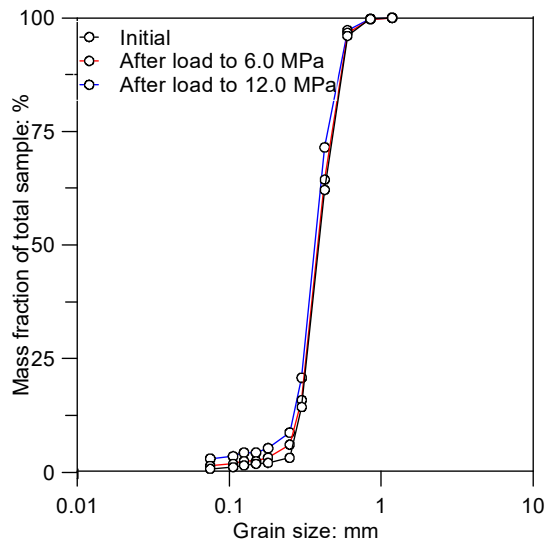
Figure 3.7. Grain size distribution pre and after compression.

Figure 3.8 shows the results of three oedometric tests on quartz sand. The oedometric curves refer to one of the saturated specimens (s=0), one controlled-suction specimen (s=5.2 kPa) and to a specimen at the residual degree of saturation (s=16.6 kPa). The curves clearly show that the yield stress at dried condition (s=16.6 kPa) is almost the same of the saturated one, instead for s=5.2 kPa, the oedometric curve shows a higher yield stress. Being the specimens prepared at the same relative density, the non-monotonic change of the yield stress has to be related to the effect of the suction. The other oedometric curves, obtained from controlled-suction oedometric tests and constant water content oedometric tests are reported in Fig. A3-A4 (Appendix A) respectively.
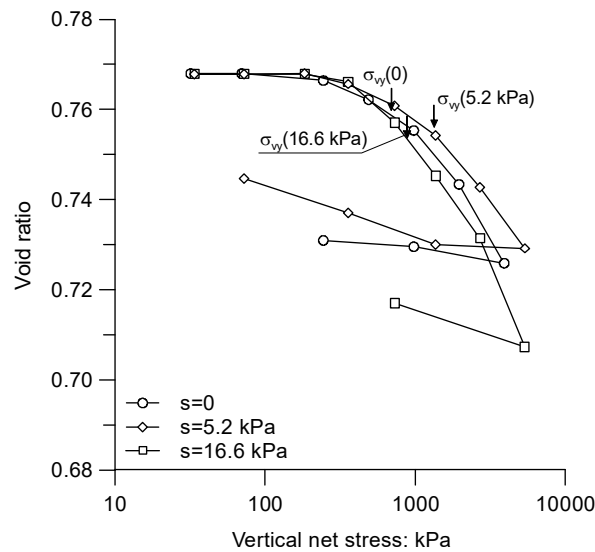
Figure 3.8. Selected controlled suction oedometric curves of quartz sand in terms of void ratio vs. vertical net stress; the arrows represent the values of the yield stresses obtained with the method of Boone (2010).

Figure 3.9 depicts, in the plane vertical net stress against suction, the yield points determined by means of controlled-suction tests and constant water content tests. The results clearly show that the yield stress does not increase monotonically with suction. Moreover, the constant water content tests were used to populate the trend of the yield stress vs suction, which is based on the results of the controlled-suction tests.

Similar results were obtained testing the Speswhite kaolin and scaly clay, as reported in Figures 3.10, 3.11, 3.12 and 3.13.

The complete set of the oedometric curves, obtained on the Speswhite kaolin and the scaly clay are depicted in Figures A5-A6 (Appendix A) respectively.
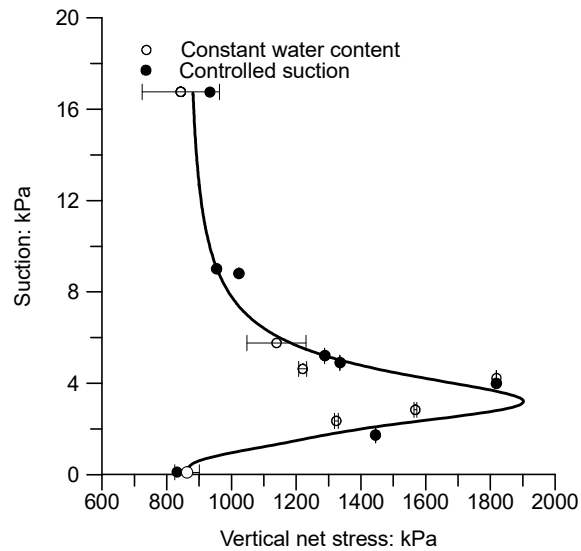
Figure 3.9. Yield points of quartz sand obtained by means of constant water content tests and suction controlled tests. Average value in term a both suction and vertical net stress, with error bar.
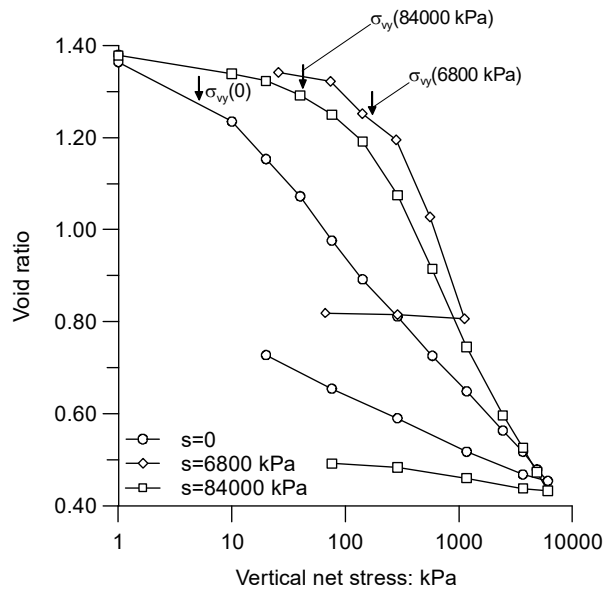
Figure 3.10. Selected controlled suction oedometric curves of Speswhite kaolin in terms of void ratio vs. vertical net stress; the arrows represent the values of the yield stresses obtained with the method of Boone (2010).
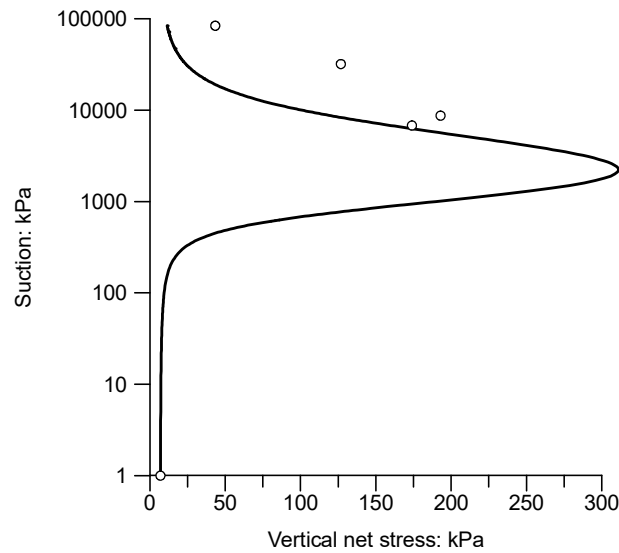
Figure 3.11. Yields points, in terms of vertical net stress and suction, determined by means of controlled suction oedometric tests on Speswhite kaolin.
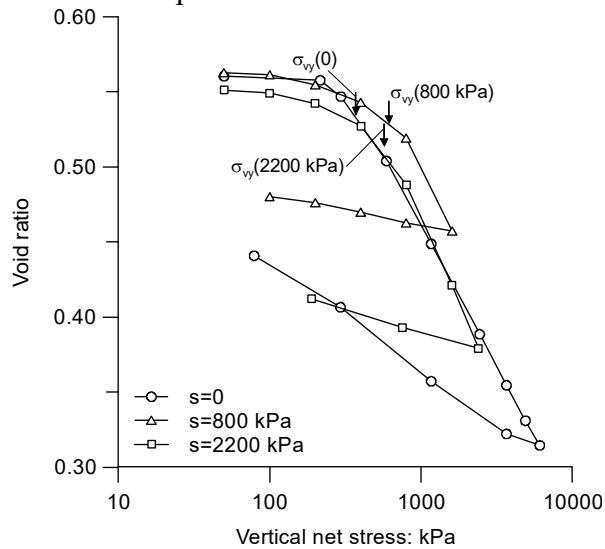
Figure 3.12. Selected controlled suction oedometric curves of scaly clay in terms of void ratio vs. vertical net stress; the arrows represent the values of the yield stresses obtained with the method of Boone (2010).
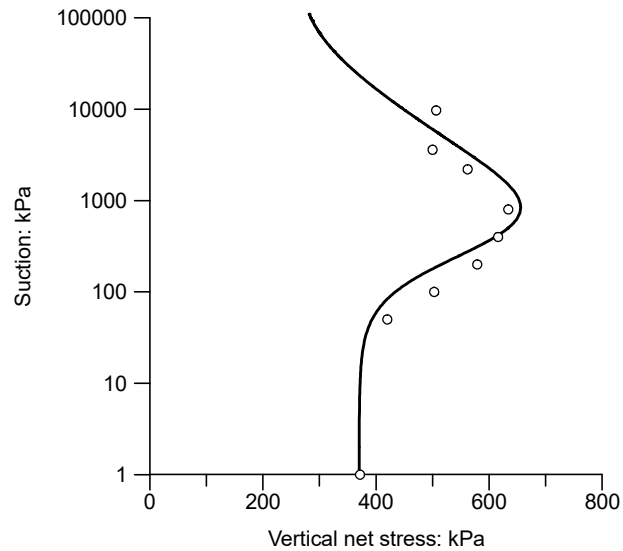
Figure 3.13. Yields points, in terms of vertical net stress and suction, determined by means of controlled suction oedometric tests on scaly clay.

The detailed test program used in this Thesis allowed us to determine the evolution of LC in a wide range of degree of saturation. After an initial increase, a maximum yield stress is observed for the three tested materials.

Then, the materials experience a continuous decrease of the yield stress, until they reach the dry state. This behaviour confirms the classical geomechanics assumption, which provides the same yield stress for saturated and dry soils.

In addition, this trend is consistent with the ones observed for other geotechnical properties of unsaturated soils, such as the shear strength and hydraulic conductivity (Bishop and Donald 1961, Donald 1956, Lins and Schanz 2005).

3.5 Effective stress

The findings reported above proved the snapback of the Loading-Collapse curve when it is defined in terms of net stress. However, the net stress is not the best variable to describe the hydro-mechanical behaviour of unsaturated soils. The oedometric tests on quartz sand were re-elaborated in terms of effective stress using the expression derived by Bishop (1959), assuming the χ parameter equal to the degree of saturation for the χ parameter:

$$\sigma_v^{'} = \sigma_{v,net} + \chi s \delta_{ij} \tag{3.3}$$

where $\chi = S_r$ and δ_{ij} is the Kroenecker's delta: $\delta_{ii} = 1$; $\delta_{i \neq j} = 0$.

However, the Bishop expression is unsuitable for clayey soils because they maintain significant degree of saturation under quite high suction. In this condition, the effective stress term unrealistically increases as suction increases. So, the oedometric curves obtained from tests on the Speswhite kaolin and Scaly clay were re-elaborated in terms of effective stress using the expression proposed by Alonso et al. (2010). This expression takes into account the hydro-mechanical behaviour of double structured clayey soils. The behaviour of these geomaterials is influenced by the fabric arrangement at the microstructural level in which it is possible to group the pores into two categories, according to their size: macropores and micropores. In function of the pores size, two distinct physical mechanisms are considered: the capillarity effect occurs due to the presence of a curved air-water interface in the large pores while the absorption effect caused by exchangeable cation hydration, mineral surface, or crystal interlayer surface hydration occur in the small pores. Then, the degree of saturation, S_r, could be separated into two contributions: a macroscopic degree of saturation S_r^{M}, which describes the occupation of macropores by water, and a microscopic degree of saturation S_r^{m}, which concerns the water within micropores.

In this way, Alonso et al. (2010) defined the effective degree of saturation as:

$$S_r^{eff} = \left\langle \frac{S_r - S_r^m}{1 - S_r^m} \right\rangle \tag{3.4}$$

Where $\langle x \rangle = 0.5 \left(x + |x| \right)$ defines the Macauley brackets, thus: $S_r^e = S_r$ if $S_r = 1$ and : $S_r^e = 0$ if $S_r = S_r^m$.

The effective stress becomes:

$$\sigma_v^{'} = \sigma_{v,net} + S_r^{eff} s \tag{3.5}$$

The microscopic degree of saturation of the Speswhite kaolin was calculated from the data presented by Tarantino and Tombolato (2005). For specimens of Speswhite kaolin prepared using the same technique used in this research, the authors have determined a microstructural water content (w_m) equal to 0.14, which is consistent with the value of 0.12 determined using the empirical equation suggested by Romero & Vaunat (2000), and the MIP data shown in Tarantino and De Col (2008). A microstructural water ratio, equal to 0.364, was calculated using the following equation:

$$e_{wm} = w_m G_s \tag{3.6}$$

The corresponding microstructural degree of saturation was calculated as follows:

$$S_r^m = e_{wm} / e \tag{3.7}$$

As a first approximation, the maximum value of water that could be stored in the micropores, was considered constant irrespective of the applied suction.

The approximation on the microstructural void ratio is unsuitable for active clay as the Scaly Clay. In fact, Rosone et al. (2016), showed that the microstructure of the scaly clay used in this work changes substantially with the suction. To quantify the evolution of the microstructure of compacted scaly clay upon suction changes, the authors suggested to use the equation proposed by Romero et al. (2011):

$$e_m = e_m^* + \beta \left(e_w - e_m^* \right) \tag{3.8}$$

Where the parameter β accounts for the swelling tendency of the assemblages and e_m^* represents the intra-assemblage void ratio corresponding to saturated micropores and empty macropores.

The equation provides a linear evolution of the microstructural void ratio e_m whit the amount of water stored in the material (expressed as the water ratio, e_w). The experimental results presented by Rosone

et al. (2016) from MIP and ESEM tests suggest a value of $e_m^* = 0.31$ and an interpolating slope $\beta = 0.19$ for the scaly clay used in this work. If $e_w < e_m$, $S_r = S_r^m$ and therefore the effective degree of saturation is equal to 0. If $e_w > e_m$, the micropores are supposed to be saturated, and the microstructural water ratio is calculated using the equation (3.8), imposing $e_{wm} = e_m$.

The experimental Loading-Collapse curves in terms of effective stress are reported in Fig. 3.14. In this case too, the yield stress does not increase monotonically with the suction, and the curves present a maximum point.
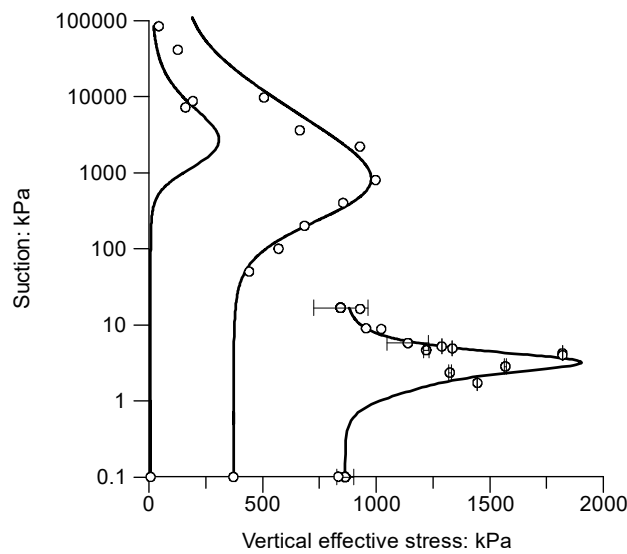
Figure 3.14. Loading – Collapse curves of tested materials in terms of effective stresses.

3.6 Hardening caused by drying

As known, the classical frameworks for unsaturated soils provide that the LC curve could be reached only by a loading path or by a wetting path. However, also a drying path could cause irreversible deformations which must be taken into account in the formulation of the model. For this reason, the classical models (e.g. BBM) need to define the Suction-Increase curve (SI).

The new shape of the Loading-Collapse curve presented in this research, suggests that it could be reached also by a drying process at high values of vertical net (or effective) stress. In order to analyse

the volumetric response of the unsaturated soil when it is subjected to drying at high level of vertical

stress, a controlled suction test was planned and carried out.

The test was carried out in a controlled–suction oedometer cell, operating with the vapour equilibrium

technique, on a compacted scaly clay with initial properties similar to the ones of the specimens

presented before (e = 0.56 and w = 14.5%). The stress path followed in the test is depicted in the

plane of vertical net stress against suction (Figure 3.15).
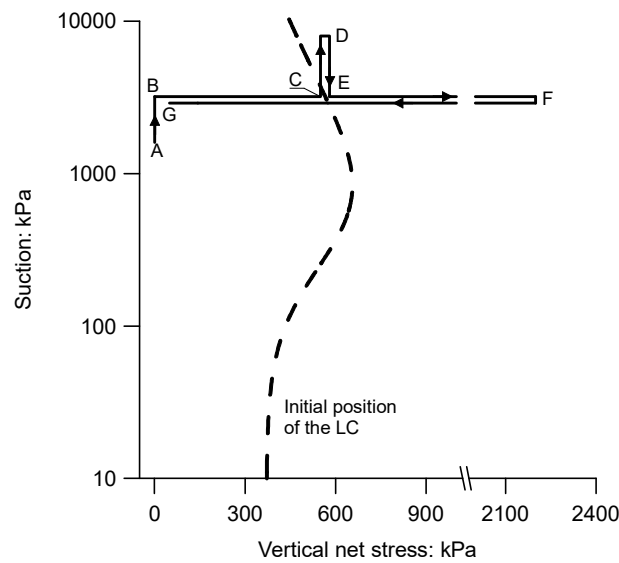
Figure 3.15. Stress path applied in controlled–suction oedometric test on a scaly clay sample.

Firstly, from the as-compacted condition, the tested sample was dried to 3600 kPa of suction (path

A-B). Starting from point B, the vertical net stress was increased in steps (B-C) at constant suction

up to 550 kPa; the sample was then dried at 7600 kPa (C-D) and wetted at 3600 kPa of suction (D-

E), in order to measure the volumetric plastic strain induced by the drying path. Finally, a loading-

unloading path (E-F-G) was applied with the aim to verify the new position of the Loading-Collapse

curve. In Figure 3.16 the test results are depicted in the plane suction against void ratio and vertical

net stress against void ratio. During the initial drying (A-B) no significant void ratio changes were

obtained (from 0.560 to 0.559). The loading path (B-C) defined the transition from the pre–yield to a

post-yield behavior. The yield point obtained in this loading path, referring to the initial position of

the LC curve, was also used to populate the experimental points depicted in Fig. 3.13. While, the

point C (in Figure 3.15) is a point of the new LC curve, due to the expansion of the elastic locus

induced by the loading path B-C. The new shape of the LC curve, showed in Figure 3.15, implies that

any loading or drying path from the point C causes plastic strains. As reported before, to verify this

last assumption the drying-wetting path (C-D-E) was applied. The reduction of the void ratio occurred

during the drying path (C-D) was not completely recovered during the subsequence wetting path (D-

E). This demonstrates that the point C was on the LC and an increase of suction caused plastic

deformation. The loading path (E-F) clearly identified a new yield point (E′). This confirms that the

drying-wetting path (C-D-E) induced the yielding of the material and the movement of the Loading-

Collapse curve. The hardening laws of the classical models provide that a drying path can cause

plastic deformations only if the SI is reached. In contrast, the new shape of LC curve implies that

plastic strains could be caused also by drying path at high level of vertical net of effective stress. It

means that to describe the hydro-mechanical behaviour of unsaturated soils in the entire range of

degree of saturation, also this aspect must be considered in the elastoplastic frameworks.
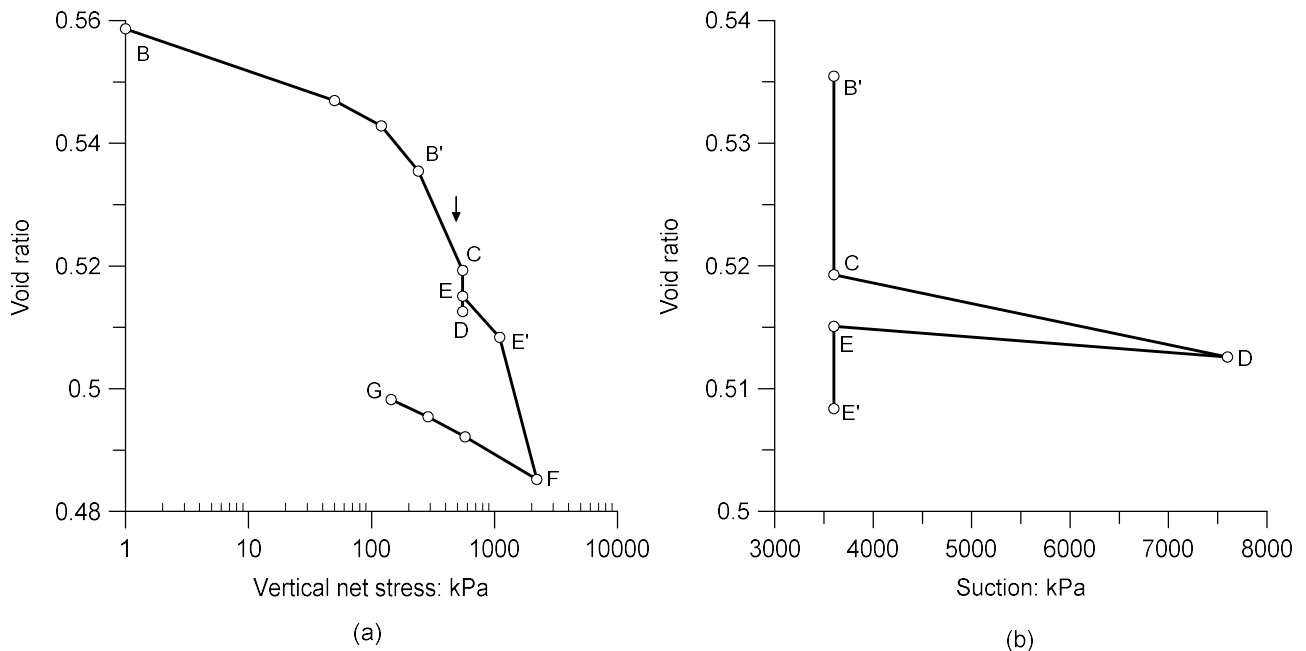
Figure 3.16. Results of the controlled-suction oedometric test following stress path reported in Figure 3.15.

3.7 Discussion

As discussed, the oedometric tests aimed to identify the LC; its position is the result of previously cumulated plastic volumetric strains, which, for clays can result from suction increase; in terms of the BBM model, this cumulation of plastic strain upon drying would correspond to the activation of the SI yield curve. Having this in mind, the preliminary air-drying on the samples before the re-wetting was performed in order to secure that all the specimens had gone through a similar hardening process; in this sense, all the loading/unloading tests allowed to detect yielding stresses that belonged to the same position of the LC.

In contrast to the previous tests on Speswhite kaolin, the air-drying after compaction was not performed for the scaly clay. The controlled-suction oedometric tests reported by Airò Farulla et al. (2010) show that also a wetting path at low confining pressure induces plastic volumetric strains that cause the LC curve to move to the left; in terms of the BExM model (Gens and Alonso, 1992), this corresponds to the Suction-Decrease yield curve. Therefore, for each suction change (increase or decrease) the LC curve evolves owing to plastic volumetric strain accumulation (activation of the SI or SD). For this reason, a preliminary air-drying/wetting cycle on the samples would not allow to induce a similar hardening process and therefore to fix the initial position of the LC.

3.8 Summary and conclusion

Despite significant areas of the earth's surface are subjected to very high variations of the degree of saturation, all constitutive models are calibrated for a restricted range of suction.

This chapter showed the results of an intensive experimental campaign aimed at assessing the evolution of the yield stress from saturated to dry state. To cover the high variability of soils, three materials with different hydro-mechanical behaviour were tested (the quartz sand, the Speswhite kaolin and the compacted scaly clay).

To determine the hydraulic behaviour of the soils, a combination of suction-control and suction measurement techniques were used. The controlled-suction oedometric tests carried out at different suction levels proved that, in contrast with the classical elasto-plastic frameworks for unsaturated soils, the yield stress does not increase monotonically with suction, instead the Loading-Collapse curves of three different materials presented a maximum point. Moreover, the yield stress for saturated condition is almost the same of the dried one. This trend is consistent with the Classical Soil Mechanics approach and with the ones observed for other geotechnical properties of unsaturated soils.

As shown in the chapter, previous experimentally Loading-Collapse curves, determined by different authors for a variety of soils, did not show this trend. Probably, this could be due to a lack of experimental yield points determined at very low degree of saturation.

The oedometric test results were analysed both in terms of vertical net stress and vertical effective stress. The choice of the expression of the effective stress is a matter of convenience, and different expressions were used in this paper. However, the choice of this stress variable did not affect the trend observed in the LC curve.

The new shape suggests that the Loading-Collapse curve could be activated also by a drying path. The results, obtained by a special planned stress path, show the hardening process of the LC when it is reached in a drying process.

In conclusion, the classical models are not able to describe the hydro-mechanical behaviour of unsaturated soil within the full range of degree of saturation. In order to model the hydro-mechanical response in a unified manner, a new framework is necessary. The new model has to consider that the yield stress does not increase monotonically with the suction and to provide that the Loading-Collapse curve could be reached by a drying path.

4. A new coupled hydro-mechanical framework to model the soil compressibility from saturated to dry state

4.1 Introduction

This chapter is focused on the relationship between the water retention curve and the LC curve. In particular, it is explored the link between the water retention curve and the evolution of the compressibility coefficient with suction. As known, the yield stress is strictly linked to the compressibility coefficient of the soil which in turn depends on the water retention curve. One of the stabilizing effects recorded in unsaturated soils is due to the capillary effect, caused by the presence of a curved air-water interface (meniscus) in the large pores (macropores). However, also the water stored in the micropores could affect the hydro-mechanical behaviour, and then the compressibility of the unsaturated soil. This physical mechanism is called absorption effect which is caused by exchangeable cation hydration, mineral surface or crystal interlayer surface hydration. Obviously, the shape of the water retention effect depends on the structure of the soil (mono or double structure).

In the ACMEG-s model (Nuth and Laloui 2007) the shape of the elastic-domain is strictly linked to the water retention curve. In fact, in the saturated domain (up to the air-entry value) the pores remain filled with water, so that the capillary mechanisms are not activated and a positive suction can take place without affecting the yield stress that remains equal to its saturated value. However, no other characteristic points of the water retention curve are linked with the shape of the Loading-Collapse curve. Probably, it is due to a limited calibration of this model. In fact, as shown in the previous chapter, all models are calibrated using experimental data carried out for a limited range of the degree of saturation (usually in the range of 1.00-0.60).

The experimental yield points reported in the previous chapter were determined performing controlled-suction oedometric tests covering the entire range of the degree of saturation and they showed other characteristic points (e.g. the snapback of the Loading-Collapse curve).

4.2 The role of the soil compressibility on the elasto-plastic models for unsaturated soils

The evolution of the compressibility coefficient with suction is usually modelled without taking into account the water retention behaviour. Many elasto-plastic frameworks for partially saturated soils used the empirical equation proposed by Alonso et al. (1990) to model the compressibility coefficient (eq. 2.9).

As shown by Alonso et al. (1990) the parameters β and r could be defined like a shape parameter of the model. In particular, equation 2.9 defines the shape of the Loading-Collapse curve (eq. 2.8).

It is possible to note that the only variable in equation 2.8 is the compressibility coefficient λ which is therefore the only parameter that influences the shape of the Loading-Collapse curve, as shown in Fig. 4.1.
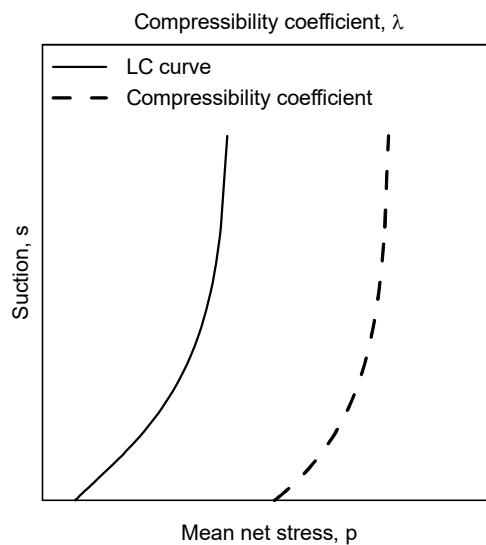
Figure 4.1. Comparison between the evolution of the yield stress and the compressibility using the framework proposed by Alonso et al. (1990).

Figure 4.1 shows that the monotonic increase (or decrease) of the compressibility coefficient implyies a monotonic increase of the yield stress with suction which would reach an unrealistic value at dry state. This is in contrast with the Classical Soil Mechanics points of view and the experimental points reported in the previous chapter.

4.3 The new framework for the soil compressibility

The compressibility coefficient λ, which represents the slope of the Normal Compression Line (NCL) in the plane $\ln p' - v$, was determined starting from the compression index C_c. In fact, the results reported in the previous chapter, having been obtained from oedometric tests, were plotted in the plane $\log \sigma'_v - v$ and then the response in compression was described using the compression index C_c. The main difference between the parameters λ and C_c is the conventional use of base-10 logarithm in the latter pair. The slope of the Normal Compression Line is simply related:

$$C_c = \lambda \ln 10 \cong 2.3\lambda \tag{4.1}$$

In the same way the slope of the Unloading-Reloding Line (URL) in the isotropic plane could be related to the URL in the oedometric plane as follows:

$$C_s = k \ln 10 \cong 2.3k \tag{4.2}$$

In figure 4.2 and figure 4.3 are reported the evolution of the yield stresses and the compressibility coefficients with suction respectively for the tested quartz sand.

The results are interpolated using different frameworks from literature. As shown, the classical models are not able to describe the hydro-mechanical behaviour for unsaturated soil in the entire range of suction (Figure 4.2).

The limit of these models depends from the inadequacy of the equation 2.9 to model the soil compressibility in a wide range of the degree of saturation (Figure 4.3).
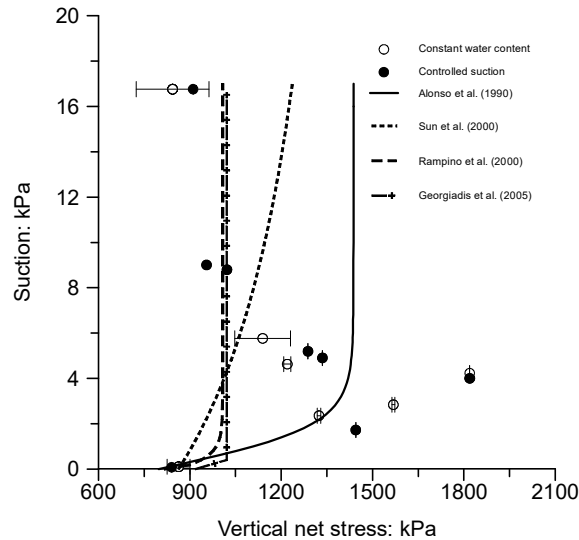
Figure 4.2. Experimental yield stress for the quartz sand represented in the plane vertical net stress vs suction, interpolated using different expressions for the Loading-Collapse curve.
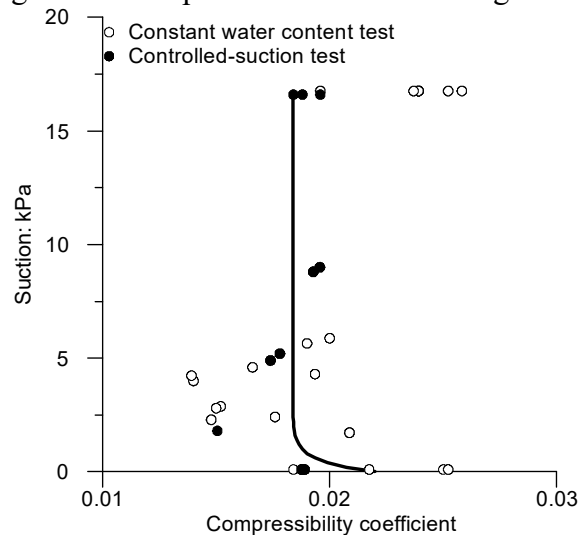
Figure 4.3. Evolution of the compressibility coefficient of the quartz sand with suction interpolated using the equation proposed by Alonso et al. (1990). Fitting parameter: $\lambda(0) = 0.022$, $r = 0.83$, $\beta = 2.15$.

A good equation to model the compressibility coefficient with suction must consider that:

- In the saturated state, suction is generated by the menisci at the surface, but the pore space remains filled with water, so the capillary mechanisms are not activated and the yield stress and the compressibility coefficient remains equal to the value at zero suction.

- Exceeding the value of the suction corresponding to the air-entry value, the water menisci inside the macropores appears. The stabilizing effect due to the menisci is reflected on the soil compressibility which decrease. As drying proceeds, meniscus curvature increases up to its

92

limit value. This value corresponds to the minimum compressibility coefficient and the maximum yield stress. Observing the experimental data in Figures 4.2 and 4.3, the value of the degree of saturation where the soil reaches its minimum compressibility corresponds to the inflection point of the soil water retention curve.

- After the inflection point of the soil water retention curve, the menisci will recede into the soil and the water remains isolated. Though the curvature of the meniscus, and then the stabilizing effect, into the smallest pores, is higher than the meniscus into bigger pores but, globally the capillary effect is smaller and then the compressibility coefficient increases again.

- When the soil reaches the dry state no stabilizing effect is present, and the compressibility of the soils is equal to the saturated one.

A function that respects all these characteristics is the first derivative of the soil water retention curve. The experimental points determined to describe the water retention behaviour of the quartz sand and the Speswhite kaolin were fitted using the Van Genuchten's equation, and its first derivative is expressed as follows:

$$S_r^{'} = \frac{\left(S_{r,res} - 1\right) nm(\alpha s)^n \left[(\alpha s)^n + 1\right]^{-m-1}}{s} \qquad (4.3)$$

While, the water retention curves of the scaly clay were determined interpolating the experimental points with the expression proposed by Romero e Vaunat (2000), and its first derivative is given by:

$$S_r^{'} = \left[\frac{e - e_{wh}}{e(a_r + s)\ln(2)}\right]\left[\frac{1}{e + e(\alpha s)^n}\right]^m - \left[\frac{e - e_{wh}}{e} + \frac{(e - e_{wh})\ln\left(1 + \frac{s}{a_r}\right)}{e\ln(2)}\right]\left[e\alpha mn(\alpha s)^{n-1}\left(\frac{1}{e + e(\alpha s)^n}\right)^{m+1}\right] \qquad (4.4)$$

The proposed equation to model the soil compressibility depends on the first derivative of the soil water curve and it is given by:

$$\lambda(s) = \lambda(0) + a_s S_r^{'}\left(\frac{s}{s_e}\right)^d \qquad (4.5)$$

where a_s is a scale parameter, d is a shape parameter and s_e is the air entry value (or exit, depending

on the chosen water retention curve). The parameter a_s can assume positive or negative values

depending on the trend of the compressibility coefficient. The two parameters permit to increase the

"flexibility" of the model.

As shown in Figure 4.4 the new equation is able to model the evolution of the soil compressibility

with suction. To model the evolution of the yield stress with suction in this work the equation

proposed by Rampino et al. (2000) was used (2.23). The authors observed that the swelling index k

is not constant with the suction but it exhibits a similar behaviour of $\lambda(s)$. As a first approximation

the swelling index could be imposed:

$$k(s) = \eta\lambda(s) \tag{4.6}$$

where η is a parameter that defines the proportion between the compression and the swelling

coefficient for the fixed value of suction. The parameter η was determined for each material and it is

reported in Table 4.1.

Substituting equation 4.5 into equation 2.23, the new shape of the LC is obtained (Figure 4.4). The

best-fitting parameters are reported in Table 4.1.
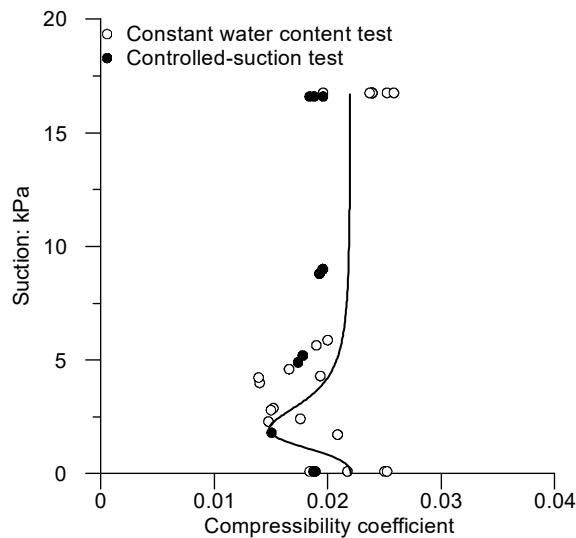
Figure 4.4. Evolution of the compressibility coefficient of the quartz sand with suction interpolated
using the proposed equation.
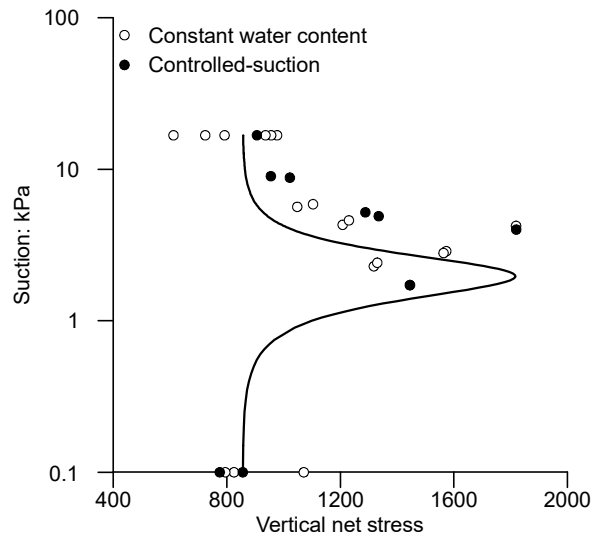
Figure 4.5. Experimental yield stress for the quartz sand interpolated using the new equation of the soil compressibility.

The new shape of the LC fitted well the experimental yield stress obtained for the quartz sand. Interestingly, the compressibility coefficient reaches its minimum value more or less in correspondence to the inflection point of the water retention curve as supposed previously.

In order to compare the capability of the new equation to model the compressibility coefficient and the BBM model by Alonso et al. (1990), the data provided by Wheeler and Sivakumar (1995) on kaolin samples were used. These data were most used to calibrate many elasto-plastic frameworks for partially saturated soils. The soil water retention curve of the material was obtained using the equalization points reported in Sivakumar (1993) and they were interpolated using the Van Genuchten's equation. The best-fitting was obtained with the parameters $\alpha = 0.078$ kPa^{-1}, $n = 1.16$, $m = 0.14$ and $S_{r,res} = 0.04$.

The comparison between the two models is depicted in Figure 4.6. As clearly shown, the fitting obtained using the proposed equation permits to interpolated better the evolution of the yield stress with suction. In addition, the new equation permits to shed light also the transition between the saturated and unsaturated state. In fact, the Loading-Collapse curve has an initial vertical state, this because initially the suction increase (meniscus formation at the surface) but the soil is still saturated

and the yield stress must be constant, according to the classical effective stress formulation provided by Terzaghi (1930). The best-fitting parameters used are reported in Table 4.1.

Figures 4.7 and 3.8 reported the result for the Speswhite Kaolin and the scaly clay respectively.
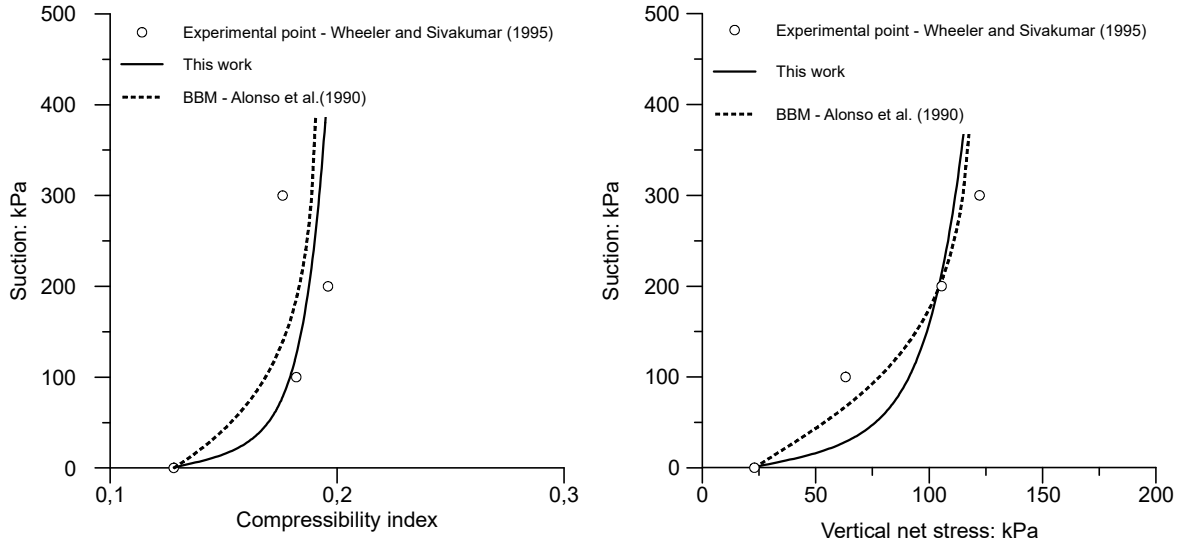
Figure 4.6. Comparison between the BBM model by Alonso et al. (1990) and the new framework: (a) Compressibility coefficient vs suction (b) Loading-Collapse curve. Parameter of the BBM model: $\lambda(0) = 0.128$, $\kappa = 0.025$, $r = 1.50$, $\beta = 0.01$, $p_0^* = 23$ kPa and $p^c = 1761$ kPa .
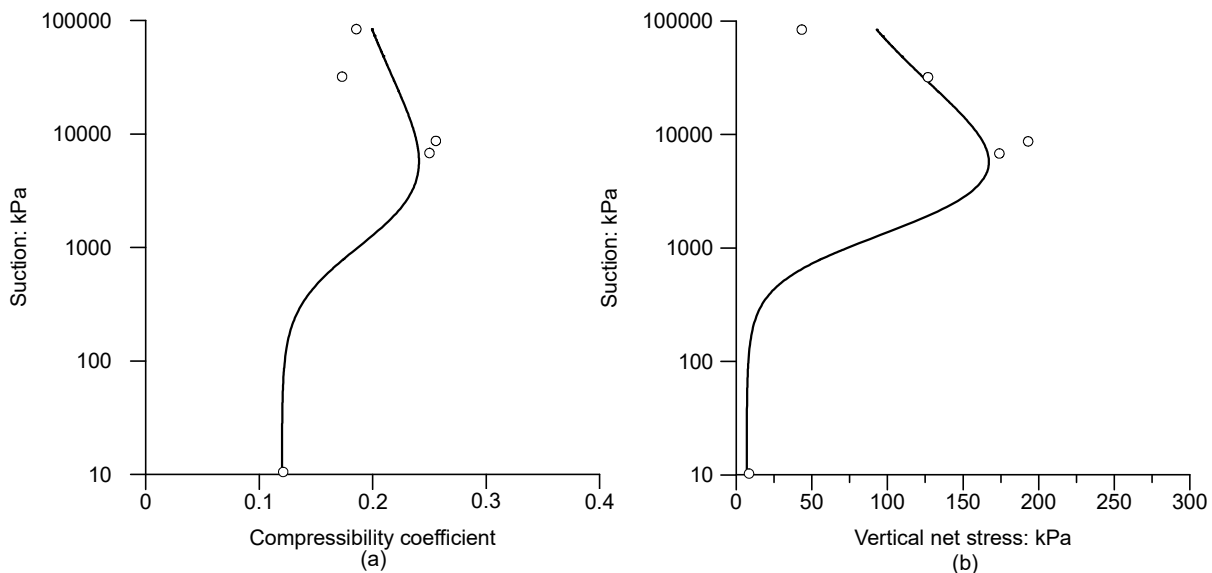
Figure 4.7. Experimental results obtained on Speswhite kaolin interpolated using the new equation: (a) Compressibility coefficient vs suction (b) Loading-Collapse curve.
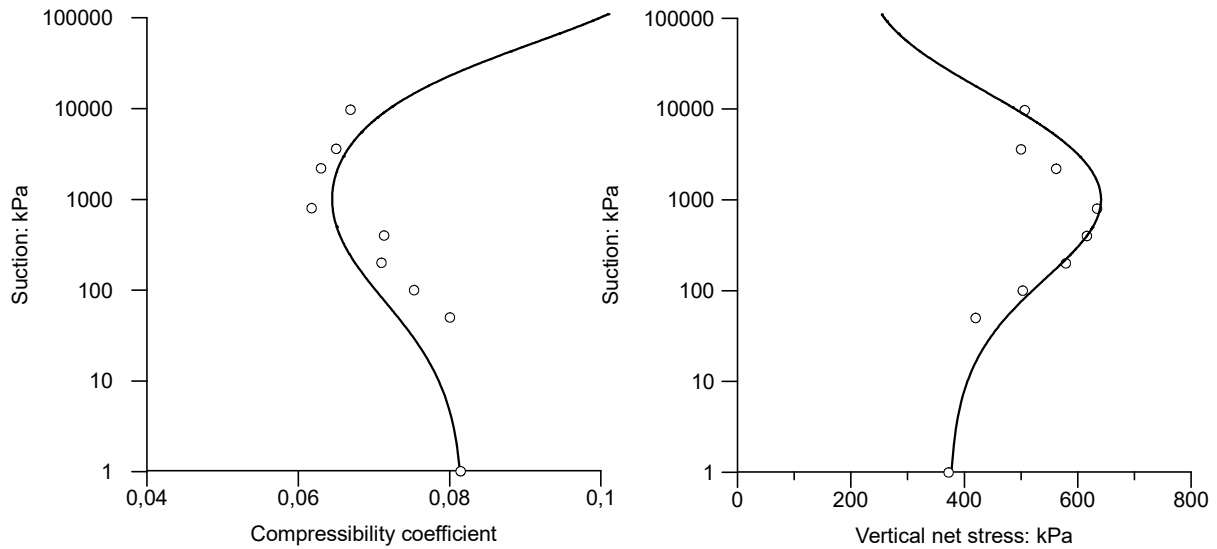
Figure 4.8. Experimental results obtained on scaly clay interpolated using the new equation.

To model the compressibility coefficient of the quartz sand, the main drying curve was chosen, while

for the Speswhite kaolin the main wetting curve was selected. The choice depends on the particular

suction path followed by the samples before the loading-unloading path. However, for the scaly clay,

the choice is not immediate. In fact, the samples tested at a value of suction lower than 2 MPa

followed a wetting path, while the other ones followed a drying path. It is clear that the main wetting

retention curve models better the results obtained after the wetting path while the main drying the

results obtained after the drying path. The main characteristic that most influences the shape of the

LC is the part of the retention curve that defines the transition between the saturated and partially

saturated state, as well as the shape closed to the inflection point. However, most of the tests on scaly

clay have been performed after a wetting process and for this reason the main wetting retention curve

was selected to model the evolution of the compressibility coefficient with suction.

The results depicted in Figures 4.4-4.8 show that the water retention curve plays a key role on the

hydro-mechanical behavior of unsaturated soils. In particular, the shape of the curve that describes

the evolution of the compressibility coefficient with the suction, and then the shape of the Loading-

Collapse curve, is strictly linked to the shape of the soil water retention curve. In fact, the saturated

state (horizontal part of the water retention curve) corresponds to the initial vertical part of the

Loading-Collapse curve. This result is consistent with the classical mechanical point of view, in fact up to the air entry value the soil is saturated and then the yield stress does not change. In the unsaturated state the yield stress initially increases. The rate of the increment of the yield stress depends on the slope of the retention curve in unsaturated state. This means that for the uniform soils (which have a uniformity coefficient close to 1), the *"bell"* is more flattened and the peak more pronounced. Theoretically, for the soils with a uniformity coefficient equal to 1 the amplitude of the bell is equal to 0. The last part of the water retention curve (residual state) influences the last part of the Loading-Collapse curve which describes the evolution of the yield stress when the soil approaches the residual state.

Table 4.1. Fitting parameter of the new framework.

Material	$\lambda(0)$	η	p_0^*: kPa	s_e kPa	a_s kPa	d	p^c: kPa
Quartz sand	0.220	0.20	863.0	1.25	0.02	0.115	180
Kaolin (data from Wheeler & Sivakumar, 1995)	0.128	0.15	23.0	5.10	-2.50	1.300	1015
Speswhite kaolin	0.120	0.23	6.8	142.00	-5.85	1.900	1924
Scaly clay	0.080	0.19	371.7	5.00	0.49	1.121	50

4.4 Validation of the compressibility coefficient equation and a new equation for the Loading-Collapse curve in terms of effective stress

In this section, the proposed equation is validated using the effective stress. The experimental results, on Speswhite kaolin and scaly clay, reformulated in terms of effective stresses are reported in the paragraph 3.5. Also in this case the compressibility coefficient was modelled using the proposed equation (4.5). To model the evolution of the yield stress with suction an equation similar to that suggested by Sun et al. (2010) was used (2.70), where the consideration on the swelling coefficient proposed by Rampino et al. (2000) was introduced (eq. 4.6). The value of the parameter η for each material is reported in Table 4.2.

Therefore, the equation of the Loading-Collapse curve in terms of effective stress is given by:

$$\frac{p_0'}{p^c} = \left[\frac{p_0'^*}{p^c}\right]^{[\lambda(0)-k(0)]/[\lambda(s)-k(s)]} \tag{4.7}$$

The results reformulated in terms of effective stress within the interpolations are depicted in Figures 4.9-4.10 while the best-fitting parameters are reported in Table 4.2.
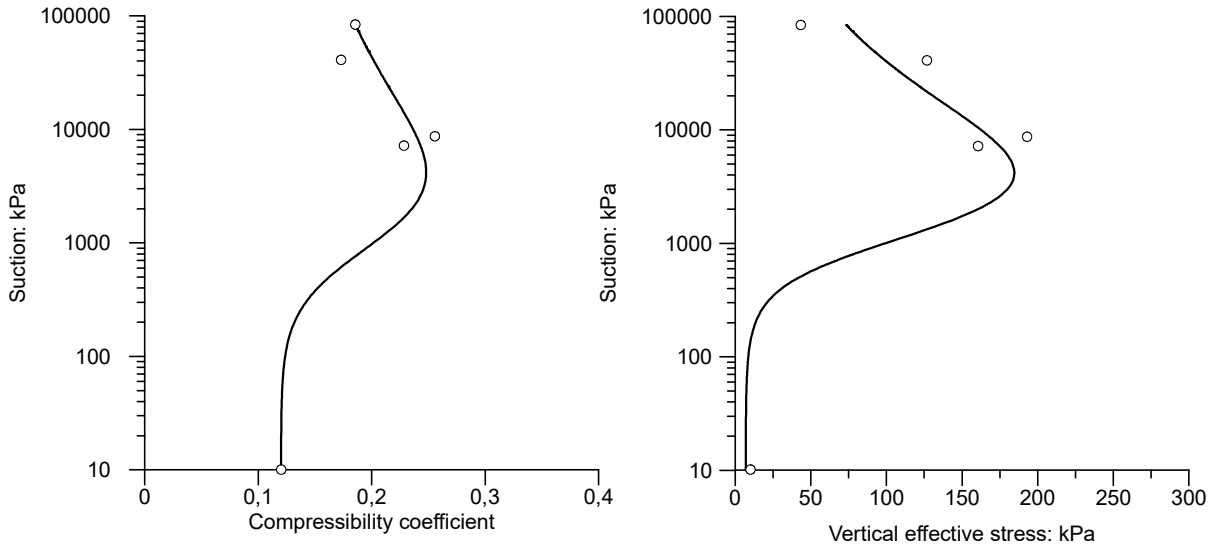
Figure 4.9. Experimental results obtained on Speswhite kaolin interpolated using the new equation: (a) Compressibility coefficient vs suction (b) Loading-Collapse curve.
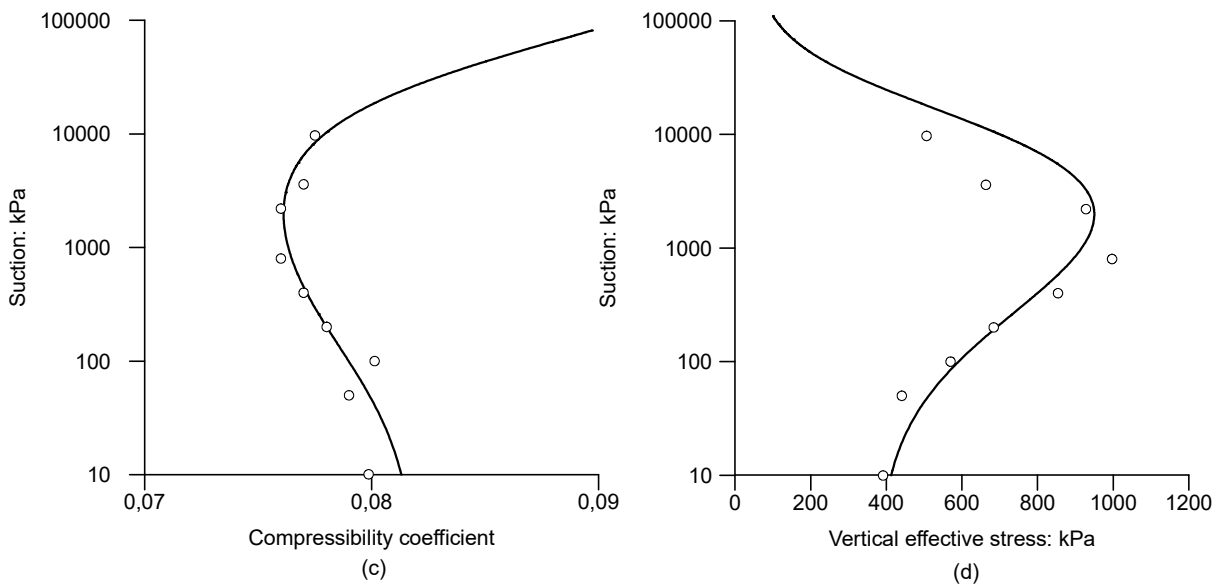
Figure 4.9. Experimental results obtained on scaly clay interpolated using the new equation; (a) Compressibility coefficient vs suction (b) Loading-Collapse curve.

Figures 4.9 and 4.10 show that the new equation for the compressibility coefficient and the new equation for the Loading-Collapse curve are able to interpret the hydro-mechanical behaviour of unsaturated soil in the entire range of the degree of saturation. Also in this case the shape of the water retention curve plays a key role and the same considerations exposed in the previous section for the results in terms of total stress are valid. The new equations are consistent with the classical mechanical point of view and confirm that the mechanical behaviour of unsaturated soils is strictly linked with the hydraulic component. In addition, as known, the water retention curve depends on differents sample properties like the Particle Size Distribution (PSD). The results permit to assert the strictly dependence of the evolution of the compressibility coefficient, and in consequence of the Loading-Collapse curve, from the soil water retention curve and the PSD. As known, it is possible to estimate the water retention curve using the particle size distribution (Cornelis et al. 2001, Hwang et al. 2011). Most approaches are regression models, lognormal distribution models or pore-solid fractal models (Hwang et al. 2011, Hwang and Choi, 2006, Kosugi, 1994, Perrier et al. 1999, Schaap et al. 1998). In a qualitative manner we could suppose that:

- from the PSD curve it is possible to determine the water retention curve;

- the shape of the evolution of the compressibility coefficient and the Loading Collapse curve is determined from the water retention curve;

- the position of these two curves is fixed using the results obtained from a saturated oedometric or isotropic compression.

In this way the entire hydro-mechanical framework of unsaturated soils could be extimated simply and quickly.

In the same manner, the Loading-Collapse curve could be linked to the relative permeability function, being both strictly linked to the water retention curve (e.g. Brooks and Corey, 1964, Mualem, 1986).

Table 4.2. Fitting parameter of the new framework.

Material	$\lambda(0)$	η	$p_0'^*$: kPa	s_e kPa	a_s kPa	d	p^c: kPa
Speswhite kaolin	0.120	0.21	6.8	142.00	-8.45	1.820	1796
Scaly clay	0.080	0.22	371.7	5.00	0.09	1.223	0.002

4.5 Summary and conclusion

Despite some models, especially those expressed in terms of effective stress, take into account the link between the water retention curve and the Loading-Collapse curve in the transition from saturated to unsaturated state, the relationship between the two curves has never been fully investigated.

The results of the controlled-suction oedometric tests were firstly used to determine the relationship between the water retention curve and the evolution of the compressibility coefficient with suction for each material. The new equation, proposed in this chapter, to model the curve compressibility coefficient vs. suction depends on the first derivative of the water retention curve. To verify the capability of the new expression, it was also used some data reported in literature.

In addition, the new equation, put into the classical equation of the Loading-Collapse curve, provides its snapback. The new shape is able to model the experimental yield points provided for the tested material and the data provided from the literature. In addition, a strict link between the soil water retention curve and the elastic domain was demonstrated.

The analysis of the shape of the Loading-Collapse curve reported in this chapter is consistent with the classical geomechanical point of view and it is physically correct.

The new equation of the compressibility coefficient was validated both in terms of total and effective stress.

5. Microscopic interpretation of the hydro-mechanical behaviour of unsaturated granular soils

5.1 Introduction

This chapter is devoted to the interpretation of the evolution of the compressibility coefficient and the yield stress at the micro-scale. The experimentation was performed at the Duke's Multiphysics Geomechanics Lab (MGLab) under the supervision of Prof. Tomasz Hueckel and thanks to the precious contribution of Prof. Manolis Veveakis and PhD Boleslaw Mielniczuk.

The first part of the chapter discusses the basic concepts of the water retention mechanism in capillary system with a specific focus on the water pressure inside a water bridge.

The experimental setups and procedures developed for the separation and evaporation tests are reported in the second part of the chapter. In particular, three set-ups were used to investigate the evolution of the water pressure inside a water bridge.

The results are compared with the water pressure obtained from Laplace's law analysing the evolution of the curvature of the water bridge.

In the third part, the image data on the curvature are used to determine the evolution of the capillary force during the evaporation process.

Finally, a qualitative link between the macro-scale behaviour and the micro-scale measurements is reported.

5.2 Water retention mechanisms in capillary system

The hydro-mechanical behaviour of unsaturated granular materials is strongly influenced by capillary forces acting between the grains. The most famous effect of the water on the granular soil is the possibility to build a "castle sand", that can only defy gravity as long as the sand is unsaturated. Therefore, in order to determine the local origin of the mechanical behaviour of unsaturated soil, and in particular unsaturated granular materials, it is necessary to know the capillarity force and how it

interacts with the grains (Richefeu et al. 2009). The water, in unsaturated geomaterials, is divided into two categories:

- the *meniscus water*, defined as the water at the inter-particle contacts around air-filled voids;

- the *bulk water,* defined as the water at the saturated sub-regions of the pore space.

The inter-particle contacts are usually divided in the same way into *"saturated"* contacts and *"meniscus"* contacts. For the first group, the slippage at the contact is controlled by the contact forces, which are controlled by the external load and by the pore water pressure in the surrounding void. In contrast, the menisci provide a stabilizing effect through an additional component of the normal force at the contact without an additional tangential force (Gallipoli et al. 2003, Wheeler et al. 2003). Meniscus and bulk water play a key role in the mechanical response of partially saturated soils by different mechanisms.

As known, the pressure difference across the liquid interface is given by the Young-La Place equation:

$$u_a - u_w = T\left(\frac{1}{r_1} - \frac{1}{r_2}\right) \tag{5.1}$$

where T is the surface tension, r_1 and r_2 are the principal radii of the curvature.

If the equilibrium contact angle of the liquid at the grain surface is zero, one speaks of complete wetting. In this case, the surface of the capillary bridge meets the grain surface tangentially. This is, however, not always the case.
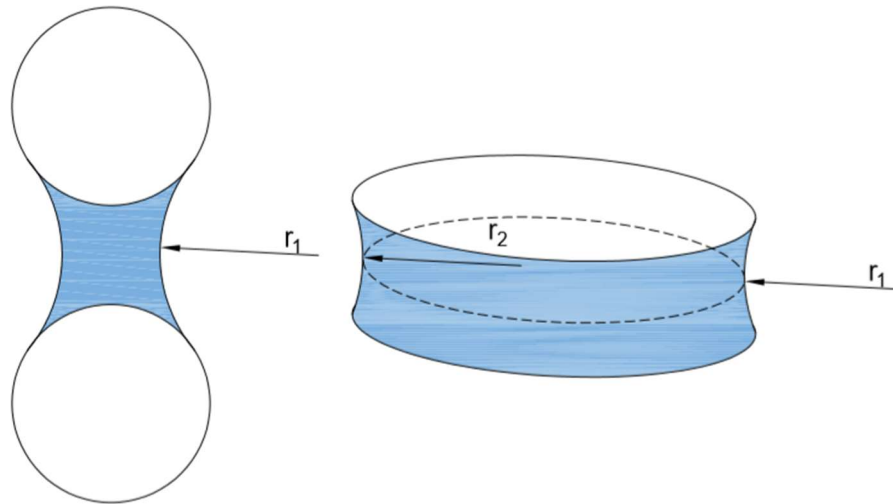
Figure 5.1 Meniscus contact.

In general, the contact angle is given by the Young–Dupre´ equation (Israelachvili 1992, Young 1805):

$$\cos \vartheta = \left(\frac{T_s - T_{sl}}{T_l} \right)$$
(5.2)

where T_s, T_{sl} and T_l are the coefficients of the surface tension of solid-gas, solid-liquid and liquid-gas interfaces respectively.

It is clear that the Laplace's pressure plays a key role to understand the hydro-mechanical behaviour of unsaturated soils. In addition, the study of the evolution of the water pressure inside the water meniscus and the others parameter at the micro-scale permits to evaluate the phenomena that occur during the transition from unsaturated to dry state.

To determine the Laplace's pressure, and then the curvature of the water meniscus different methods were developed.

The exact curvature of the water bridge could be calculated by numerical solution of the LaPlace-Young's equation (Liang et al. 1992, Molenkamp and Nazemi, 2003). Lian et al. (1992) showed that the difference between the numerical solution of the exact shape and the toroidal approximation is less than 10%, and so it is sufficient accurate for many practical experiments.

In Mielniczuk et al. (2015) are reported the calculations of the Laplace pressure, calculated from the measured bridge curvatures and its evolution during an evaporation process. As shown by Mielniczuk et al. (2015) the behaviour of the liquid bridge during the evaporation process is strongly dependent on the grain separation and many variables play a key role. In fact, the variables at micro-scale include: the Laplace's pressure, forces resulting from pressure, surface tension forces and the resultant total capillary force (Mielniczuk et al. 2014a, 2014b).

As showed in Mielniczuk et al. (2015) the rupture of the bridges is seen at large separations to occur quite early, at only 1/4–1/3 of the initial water volume evaporated. At a sub-microscopic scale of a single capillary bridge between two glass spheres show that the bridge gorge radius decreases much faster than the contact radius, distorting the original constant mean curvature bridge shape. Hence, the calculated Laplace pressure exhibits high gradients along the moving bridge external surface, most commonly with a high suction near the triple phase contact and positive pressure near the gorge suggesting a flow of liquid from the central area of the bridge, toward the solid contact, and then along with the solid toward the contact area. The flow is believed to contribute to contact pinning (Mielniczuk et al. 2014a).

The adhesion-force is composed of capillary pressure force acting over the liquid/solid contact surface area, and surface tension forces acting over the three-phase contact perimeter length. This is in contrast with most macro-scale phenomenological models, in which the only desaturation process variables affecting strength are suction and saturation. Both the contact surface area and contact perimeter length are reduced to zero upon complete liquid evaporation.

But, the water pressure inside the water meniscus and its evolution during an evaporation process has never been registered experimentally. A new device was designed to measure the pressure and its results were compared with the calculation of the Laplace pressure using the Laplace's law carried out using the image-processing.

5.3 Experimental test device layout and experimental test program

The new device designed to measure the water pressure/suction evolution during an air-drying path is reported in Figure 5.2. To measure the water pressure inside the water bridge a burette was used. The diameter of the burette was 1.6 mm. This diameter permits to not interfere with the water bridge evolution. In fact, for higher diameter, the water inside the burette could affect the test, and a flow from the burette to the water bridge was recorded. In contrast, if the diameter is smaller than 1.6 mm, the tension surface along the burette does not permit the movement of the meniscus inside the burette. During the tests the mass evolution is recorded by a balance, and the evolution of the water bridge and the meniscus were recorded by two cameras. The entire system was closed in a climate chamber with humidity and temperature control (Figure 5.3).

Different kinds of test were carried out: evaporation tests for two and three glass spheres, evaporation tests for three glass cylinders, and separation tests, in which the distance between the upper spheres and the lower spheres is continuously increased whit a velocity of 50 μm per minute.

5.4 Determination of the Laplace pressure by image-processing

The determination of the evolution of the water bridge during the evaporation tests was performed by image-processing. The Laplace's pressure was calculated in ten points of the water bridge (five for the left side and five for the right side).

To determine the external curvature for each point the circumference approximation was applied. The bridge profile was approximated with an arch of circumference in correspondence of each point obtained by the segmentation of the profile (Figure 5.4)
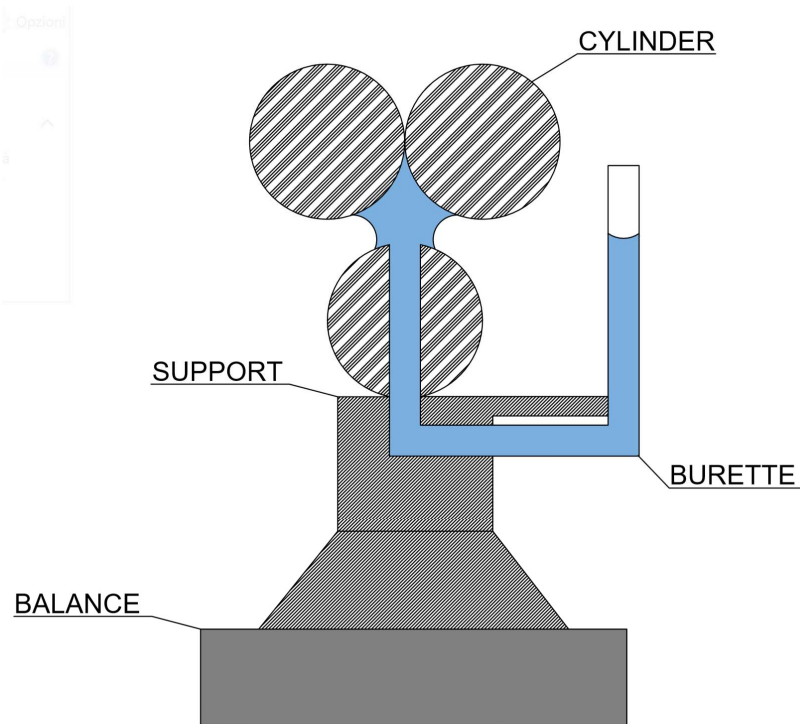
Figure 5.2 Experimental device for three spheres evaporation tests.

For each point, the coordinates and the radius of the circumference were deduced, and the correspondent curvatures were obtained using the follows equations:

$$k_1 = \frac{1}{r_1}$$

(5.3)

To calculate the internal curvature in each point two different approximations were used:

- Circumference approximation for the middle points of the profiles;

- Ellipse approximation for the other ones.

In fact, the "shape of the approximations" depends on the intersection between the plane normal to the point and the water bridge (hyperbolic paraboloid - Figure 5.5).

The intersection between the normal to the middle points and the hyperbolic paraboloid is a circumference (Fig. 5.6). To calculate the internal curvature is necessary to determine the curvature of the circumference in that point and then is sufficient to calculate the diameter of the gorge.
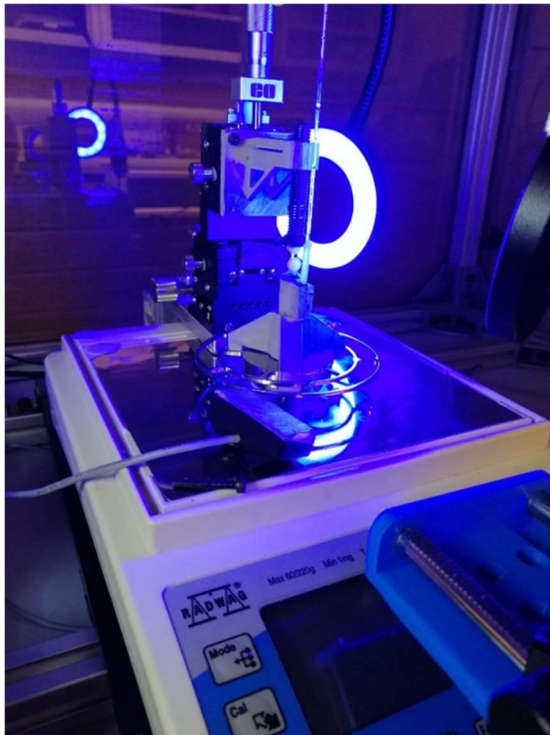
(a)   (b)

(c)

Figure 5.3 Test set-up: (a) Test device; (b) Particular of the burette; (c) Climate chamber set-up.
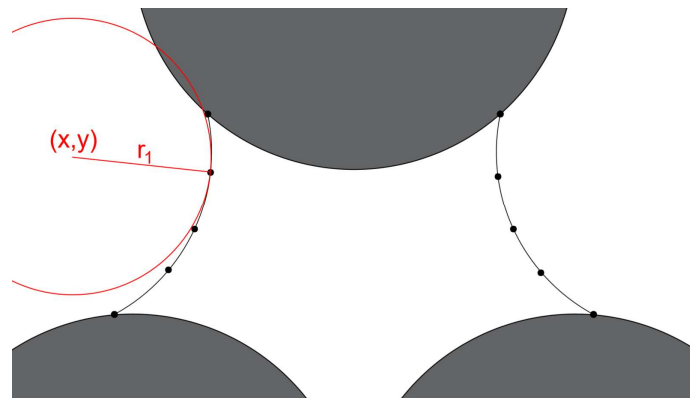
Figure 5.4 Calculation of the external curvature.
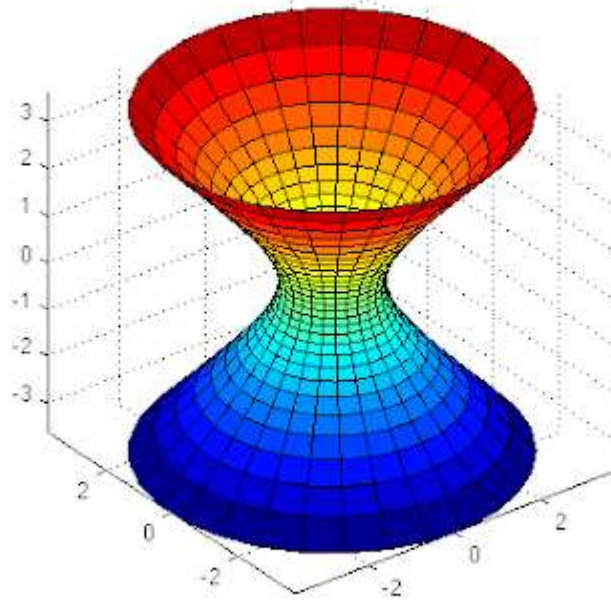
Figure 5.5 Water bridge 3D rapresentation.

The ellipse approximation is applied for the other points. At the beginning, it was calculated the slope of the normal of each point (Figure 5.7). The code used to process the images takes into account two different cases:

- The normal intersects the other side of the bridge (Figure 5.8);

- The normal does not intersect the other side of the bridge (Figure 5.9).

Known the ellipse, it is possible to calculate the internal curvature (equation 5.4) and then the Laplace's pressure (Figure 5.10).

$$k_2 = \frac{1}{r_2} = \frac{(\text{Length of major semi-axis})}{(\text{Length of minor semi-axis})^2} \qquad (5.4)$$

5.5 Processing of measurements from the burette by image-processing

Also the determination of the evolution of the meniscus inside the burette was performed by image-processing. The code used takes into account both the variation of the position of the meniscus and its curvature. Generally, at the beginning of the test the meniscus is flat. Initially, its curvature increases up to the maximum value, while its position remains unchanged. Once the maximum

curvature is reached, it remains constant while the position will begin to vary. When maximum

suction is exceeded, the pressure begins to increase, and the shape of the meniscus tends to be flat,

while its position varies slightly (Figure 5.11).
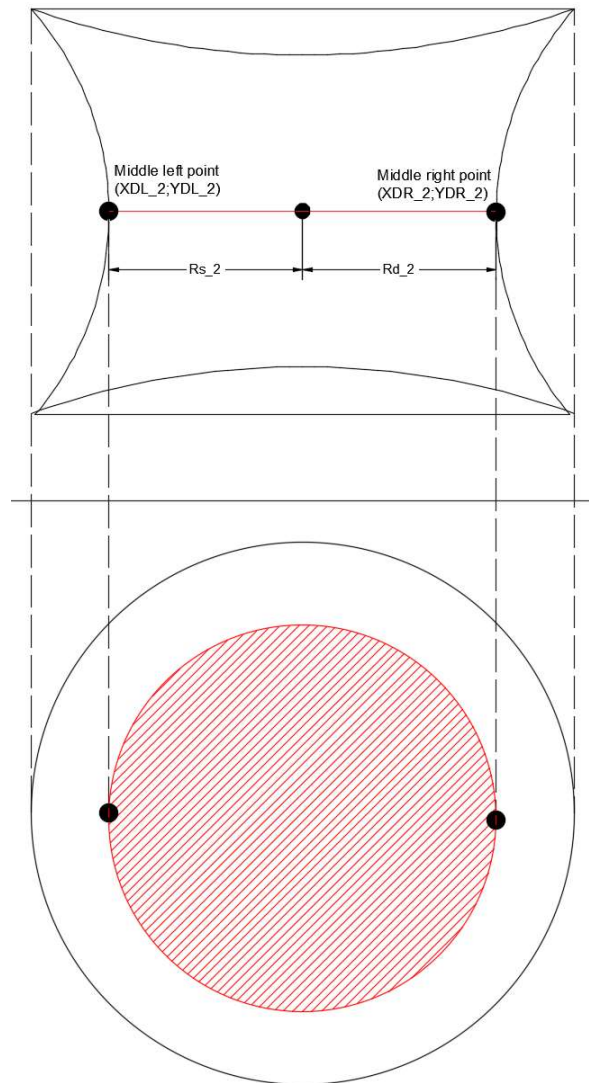
Figure 5.6 Calculation of the internal curvature for the middle points: Circumference approximation.
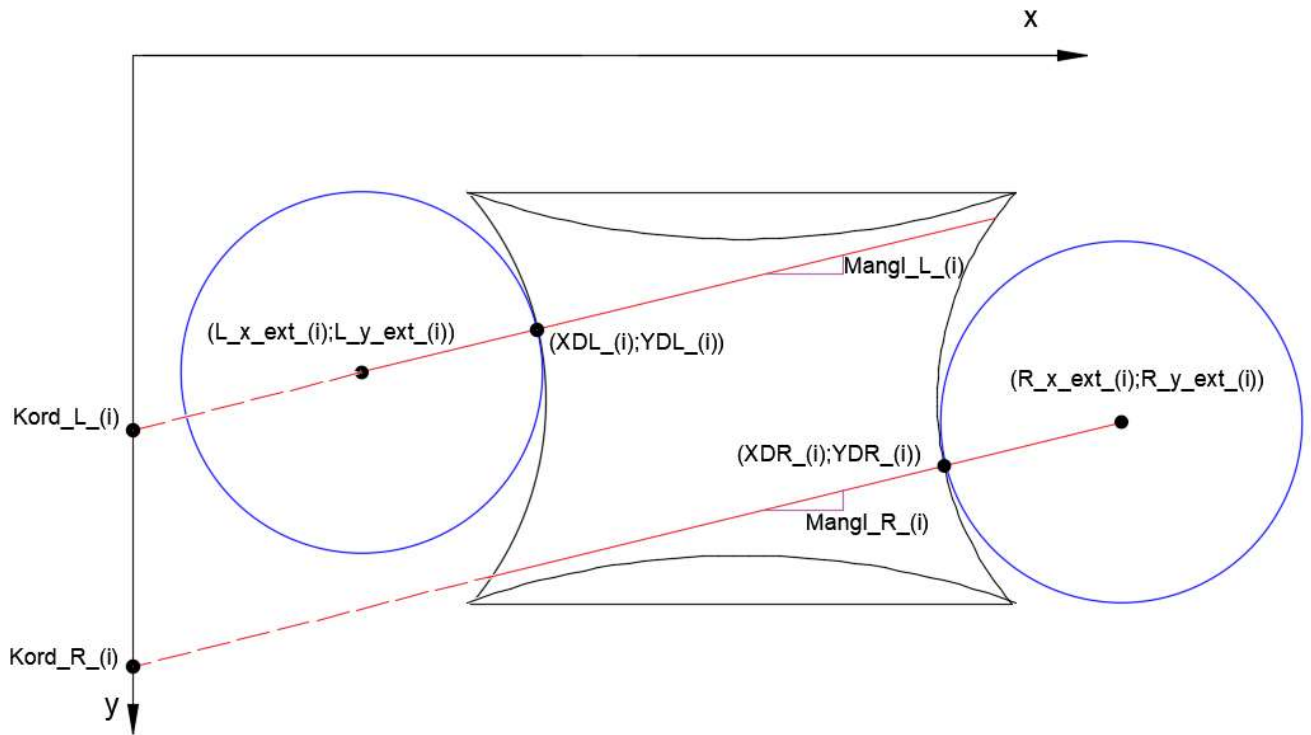
Figure 5.7 Calculation of the angular coefficient and the intercept of the normal.
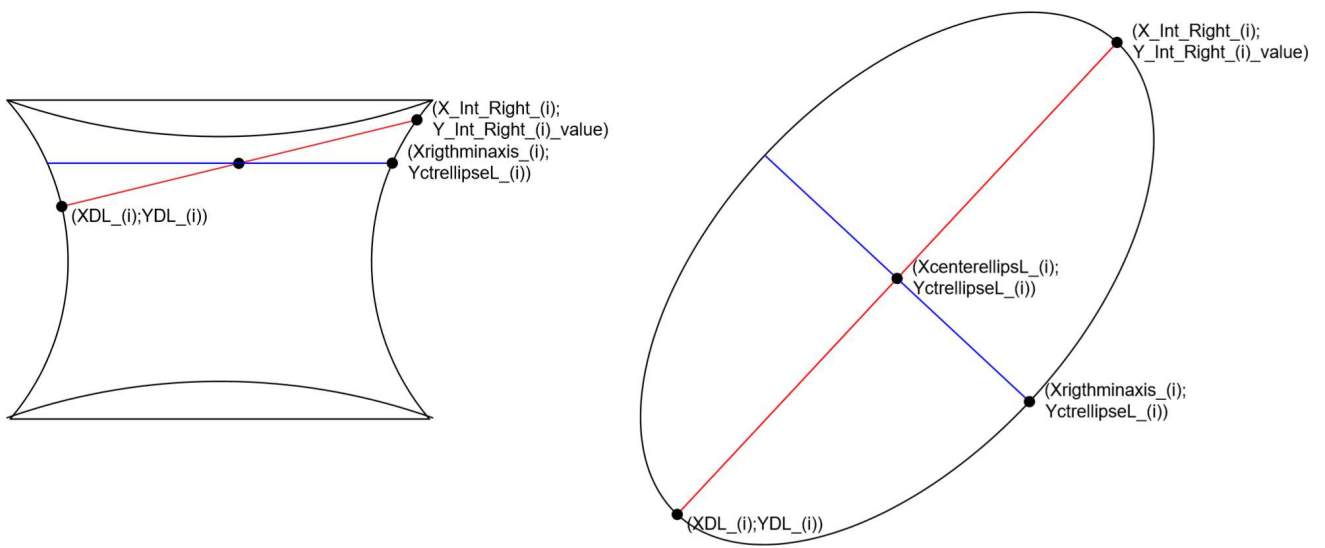
Figure 5.8 Case 1: Assonometric representation of the ellipse points.
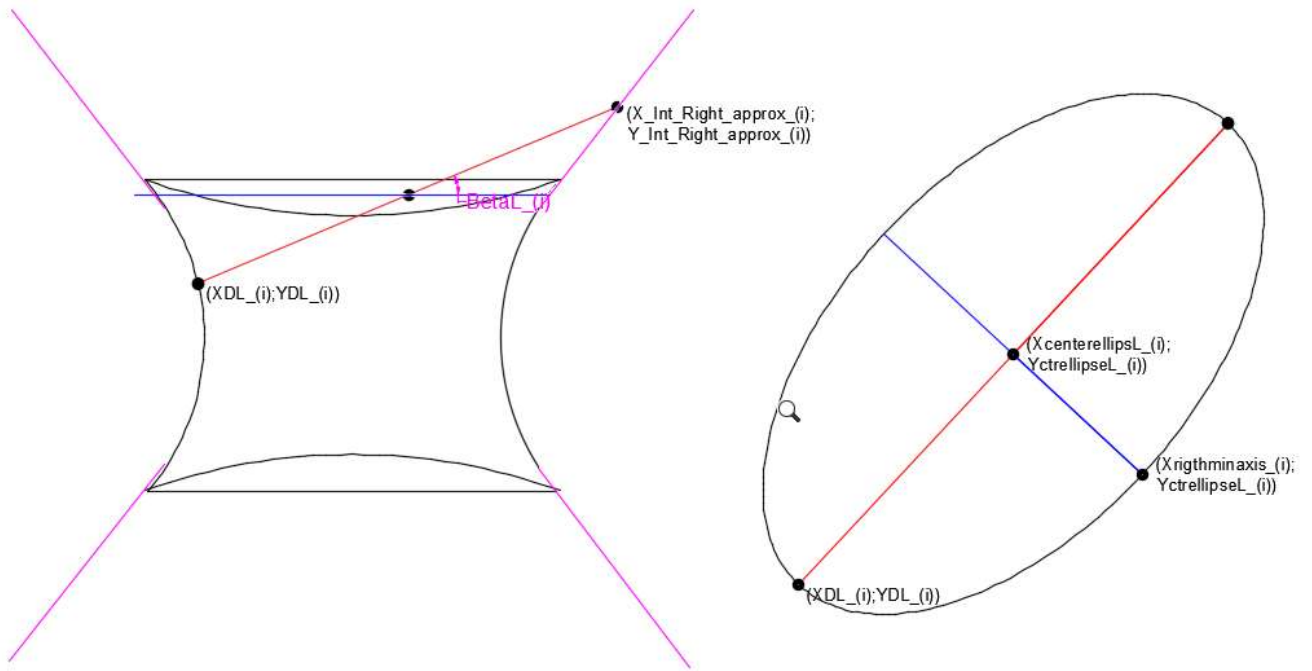
Figure 5.9 Case 2: Assonometric representation of the ellipse points.
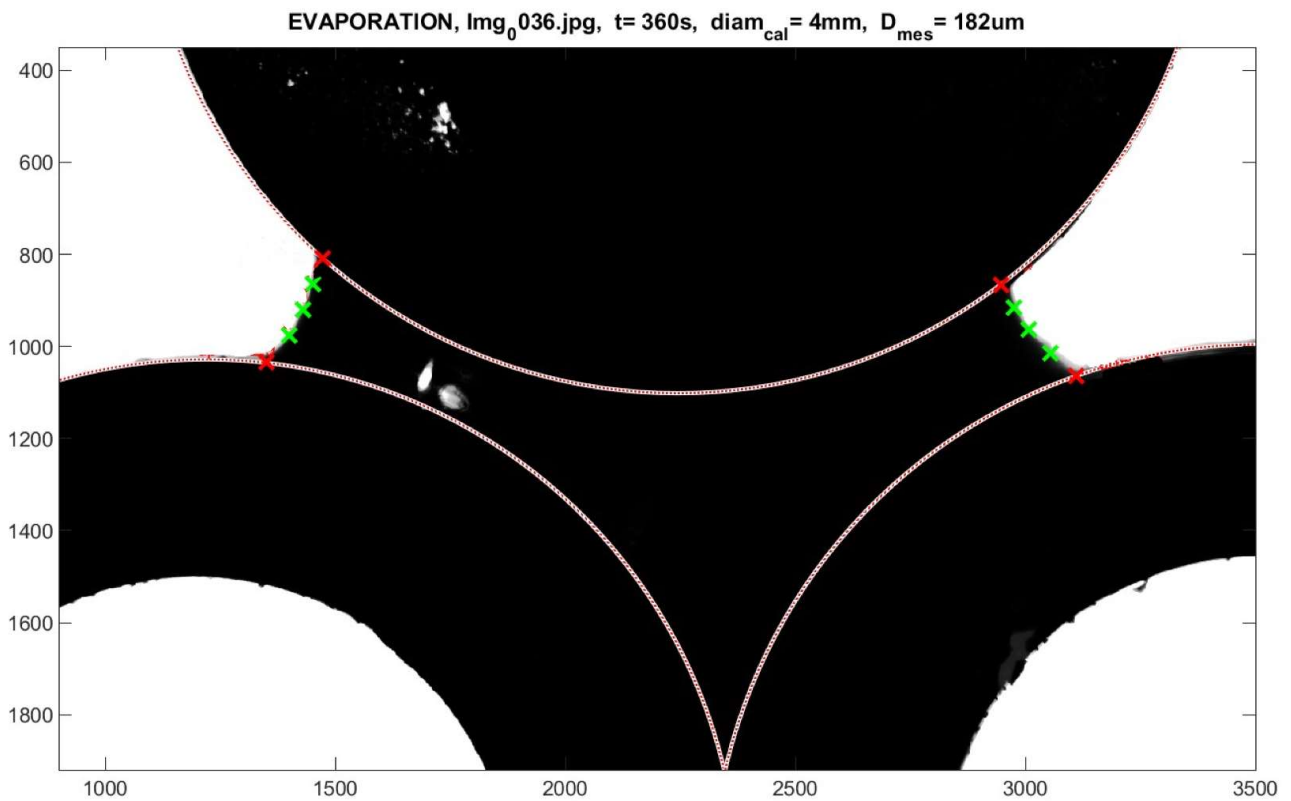
Figure 5.10 Determination of the Laplace pressure on the edges of the meniscus.
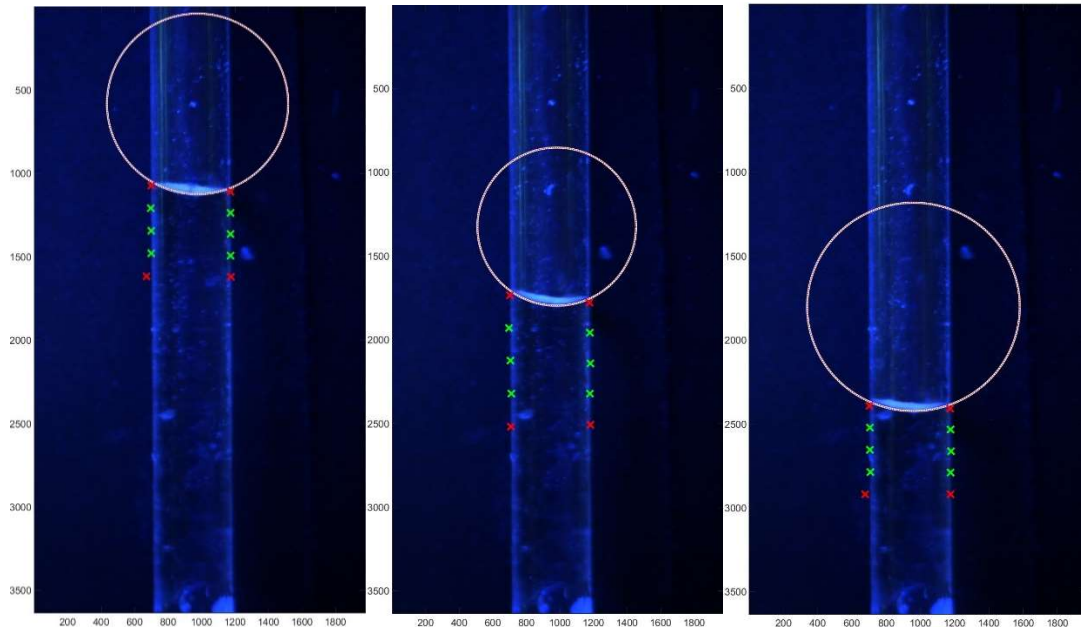
Figure 5.11 Evolution of the position and the curvature of the meniscus.

5.6 Evolution of Laplace pressure

In this section, the obtained results are reported in the plane time vs pressure for the evaporation tests while the results obtained from the separation tests are depicted in the plane distance vs pressure.

The experimentation aims to understand how capillary pressure evolves during a drying process. To do this, it was necessary to perform several tests and using different materials, to verify the correct functioning of the new device in all conditions.

The results measured experimentally by the burette are compared with the values obtained by calculating the pressure through Laplace's law. The figures show both the results obtained from the Laplace's law (average value calculated in the middle points of the meniscus) and the results obtained from the burette. A distinction will be carried out too in function of the kind of the tests (evaporation or separation tests) and the configuration of the device (two teflon spheres, two glass spheres, three glass spheres, three glass cylinders).

Initially, the Teflon spheres were selected to verify the functioning of the new device for different kinds of tests, distance between the spheres and velocity of the separation, because the material

permits to modify the layout and the set-up of the burette system easier than the glass. In addition, some tests, on three glass spheres, were also performed without the burette to depict the results in terms of the degree of saturation of the cluster. For all tests, the initial water volume was injected using a siring on the top sphere or cylinder.

After the injection, the upper sphere or cylinder was put in contact with the lower spheres or cylinder to form the water bridge (Figure 5.12).

For the separation tests, the distance was increased with constant velocity, while for the evaporation tests the reference distance was imposed after the formation of the water bridge.

Finally, the obtained results are used to give a qualitative explanation from a physical point of view of the shape of the LC obtained and commented in the previous chapters.

| (a) | (b) | (c) |
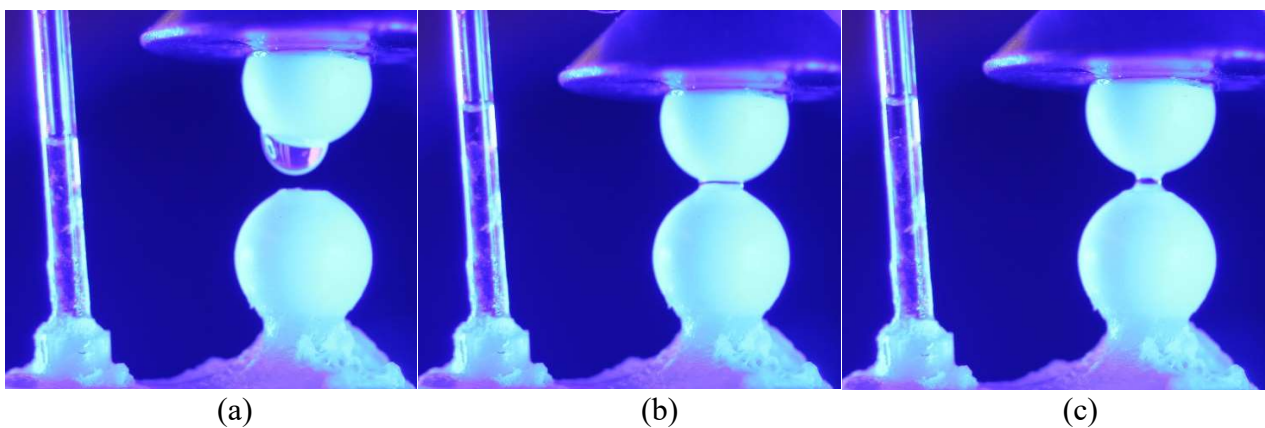
Figure 5.12 Set-up of the tests: (a) injection of the water; (b) formation of the water bridge; (c) setting of the distance between the spheres.

5.6.1 Separation test for two Teflon spheres

In Figure 5.13 are depicted the results obtained from separation test for two Teflon spheres. The Teflon spheres, having 6.35 mm in diameter and the water volume of the water bridge was 10 μl. The obtained results show a good agreement between the experimental measurements and the pressure calculated from the Laplace's law. The maximum difference between the two kinds of results is equal to 10 Pa.
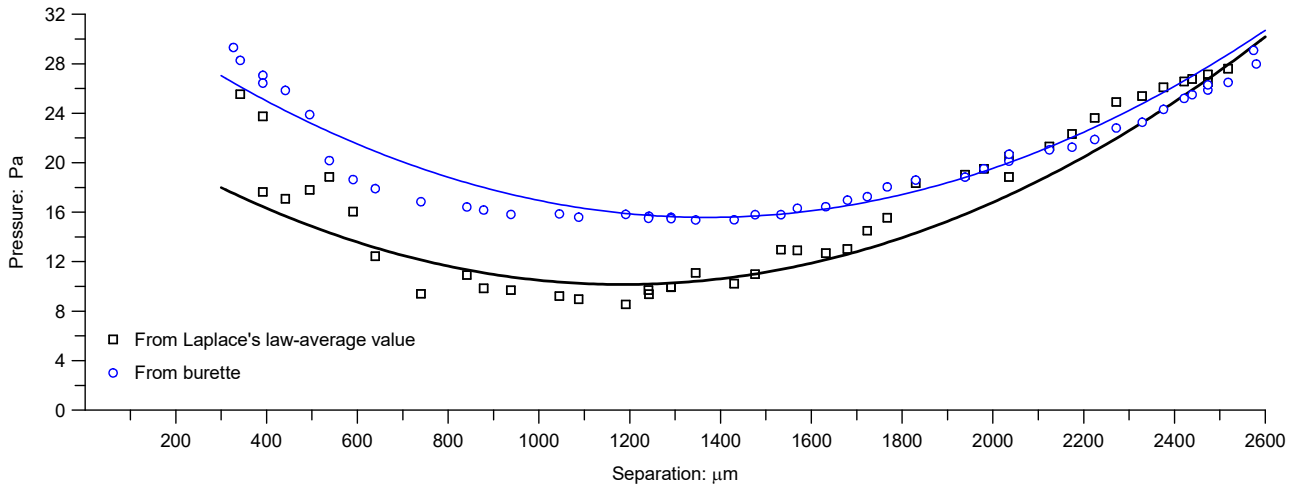
Figure 5.13 Separation test – Two Teflon spheres: Diameter of the spheres 6.35 mm, water volume of the water bridge 10 μl.

5.6.2 Evaporation test for two glass spheres

In Figure 5.14 are reported the results obtained by evaporation test for two glass spheres. The two spheres having 6.34 mm in diameter and the initial water volume was equal to 10 μl. The results show also in this case a good agreement between the experimental measures and the water pressure calculated using the Laplace's law. During the test, the suction increases up to 80 Pa after which decreases until the rupture.
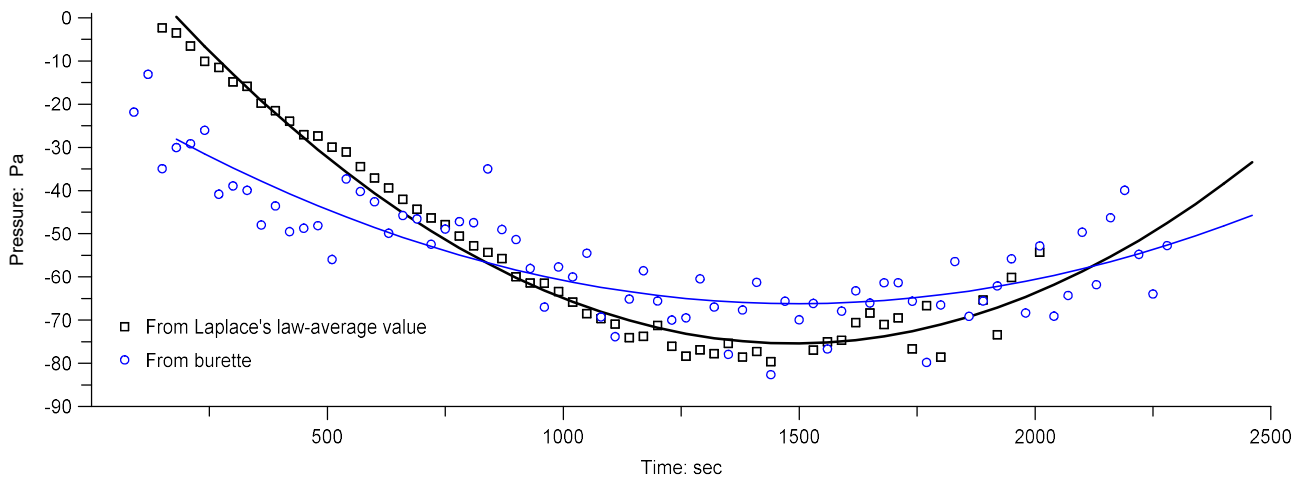

Figure 5.14 Evaporation test – Two glass spheres: Diameter of the spheres 6.34 mm, initial water volume of the water bridge 10 μl, distance between the spheres 800 μm.

5.6.3 Separation tests for two glass spheres

The results obtained by separation tests for two glass spheres (Figure 5.15) show a behaviour similar to the ones obtained for two Teflon spheres. The water bridge pressure reaches a positive value and

when the spheres reach a distance equal to 1600 μm, the rupture occurs. Obviously, the distance between the spheres at the rupture depends on different parameters such as the material of the spheres, the diameter, the velocity of the separation process, the initial water volume and the kind of fluid.
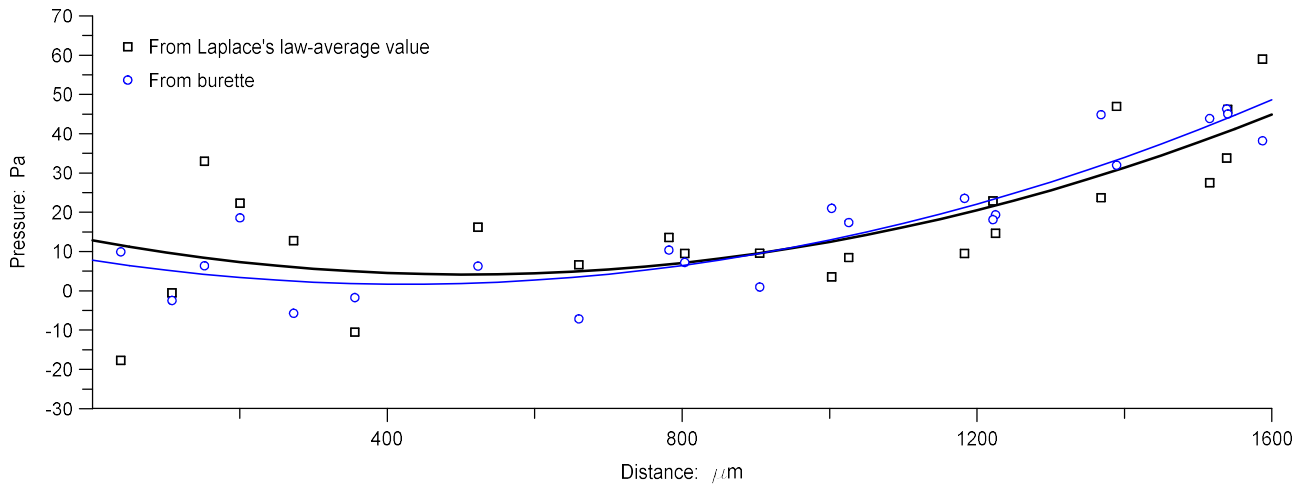
Figure 5.15 Separation test – Two glass spheres: Diameter of the spheres 6.34 mm, initial water volume of the water bridge 10 μl.

5.6.4 Evaporation tests for three glass spheres

The results of the evaporation tests carried out for three glass spheres are depicted in Figure 5.16. The Figure shows clearly the influence of the distance between the spheres on the pressure evolutions. In particular, it is possible to observe that the highest value of the suction is reached when the distance between the spheres is minimum. This behaviour is in agreement with the Laplace's law, in fact, when the water bridge is very tall the curvature k_2 is higher than the curvature k_1 and equation 5.2 provide a positive value. The curvature k_2 can also become higher than the curvature k_1 during the evaporation process when the radius of the internal ellipse or circumference (if we consider the middle point) becomes very small. In this case, initially, the suction increases until a maximum point, after which it decreases up to the rupture.

(a)

(b)

(c)
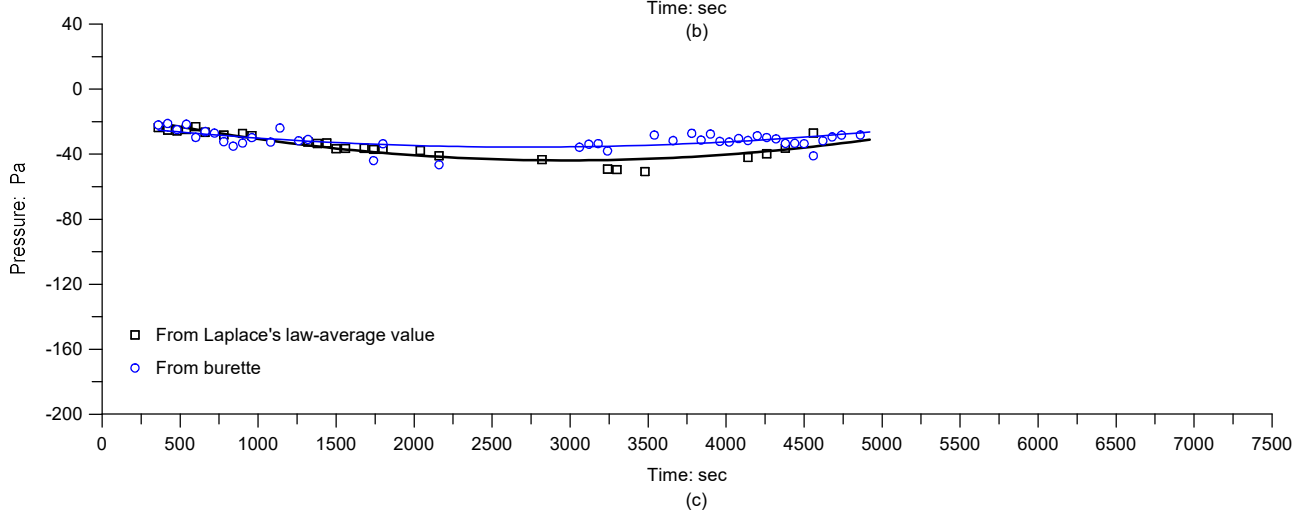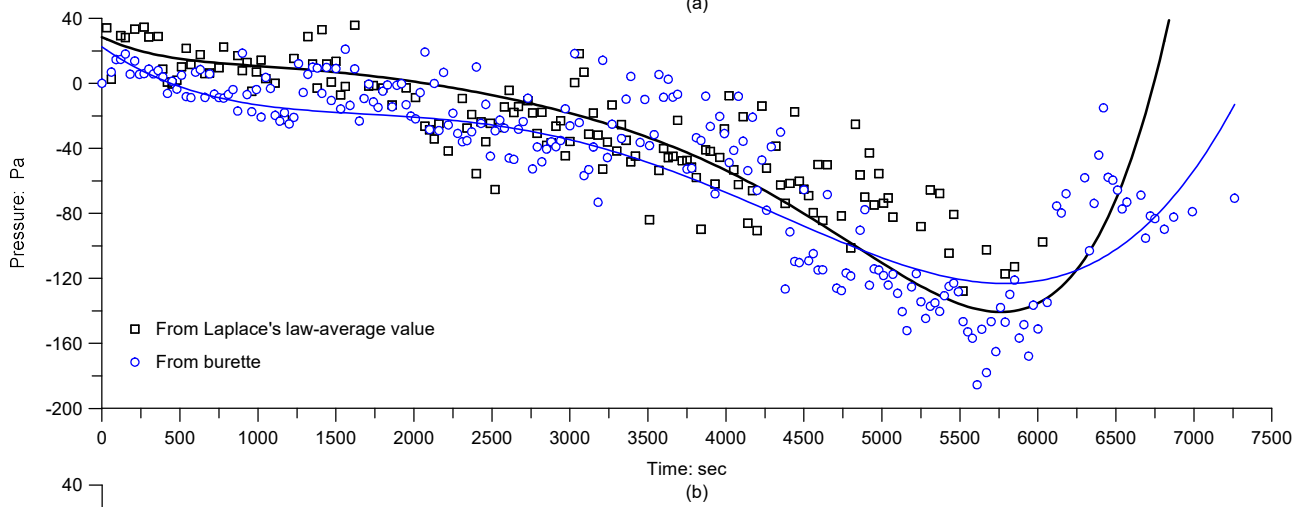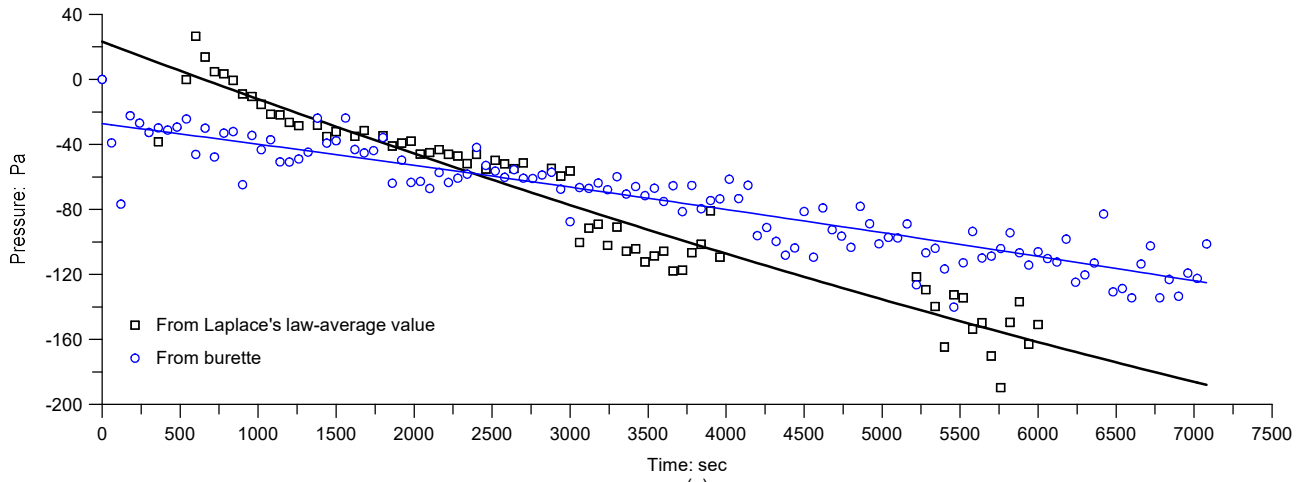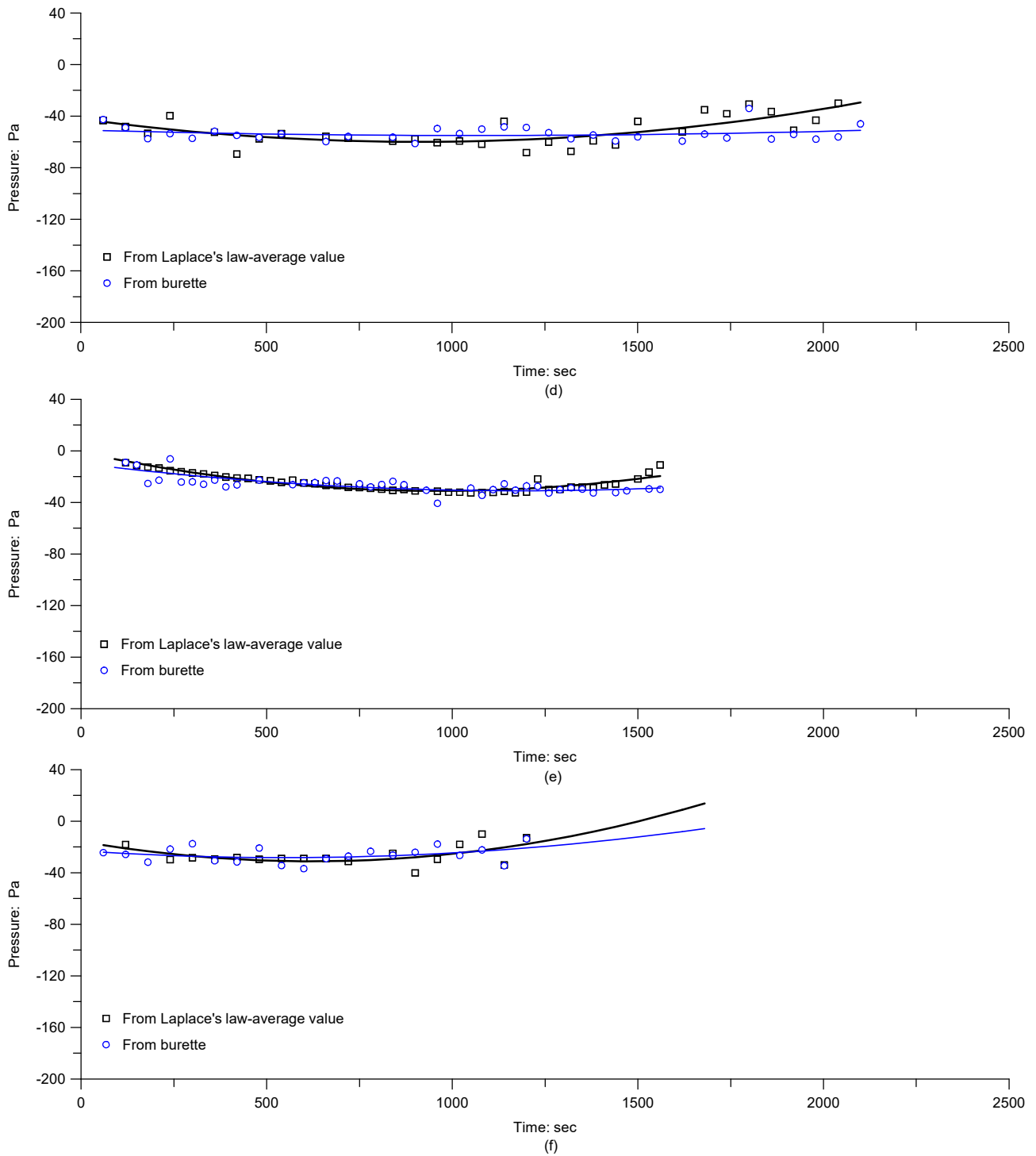
Figure 5.16 Evaporation tests – Three glass spheres: Diameter of the spheres 6.34 mm, initial water volume of the water bridge 10 μl, distance between the spheres: (a) 200 μm; (b) 800 μm; (c) 1400 μm; (d) 1500 μm; (e) 1600 μm; (f) 1800 μm.

5.6.5 Evaporation tests for three glass spheres without burette

Three evaporation tests for three glass spheres were repeated using a similar device but without the burette. These tests aimed to obtain the evolution of the *degree of saturation of the cluster* during the evaporation process. In fact, the burette could affect the measures of the mass evolution because, even if in minimal quantities, the evaporation could happen from the burette.

The degree of saturation of the cluster is defined as the ratio between the water volume and the initial water volume:

$$S_{r,cluster} = \frac{V_w}{V_{w,initial}}$$
(5.5)

The evaporation tests without the burette were performed imposing three different separations: 800 μm, 1100 μm and 1200 μm.

The results, depicted in Figure 5.17, show the strictly relation between the suction and distance, and then the relation between the suction and the shape of the meniscus. In particular, if the distance between the spheres decreases, the maximum suction value increases. In addition, for high value of the distance between the spheres the total amount of water that evaporates before the rupture decrease.

This behaviour is in agreement with the experimental measures of the suction in the soils. In fact, the air entry value and the maximum suction that a soil could sustain depends on the diameter of the void and the on the maximum length of the water bridge, that in these experiments on the spheres or cylinders is represented by the separation.
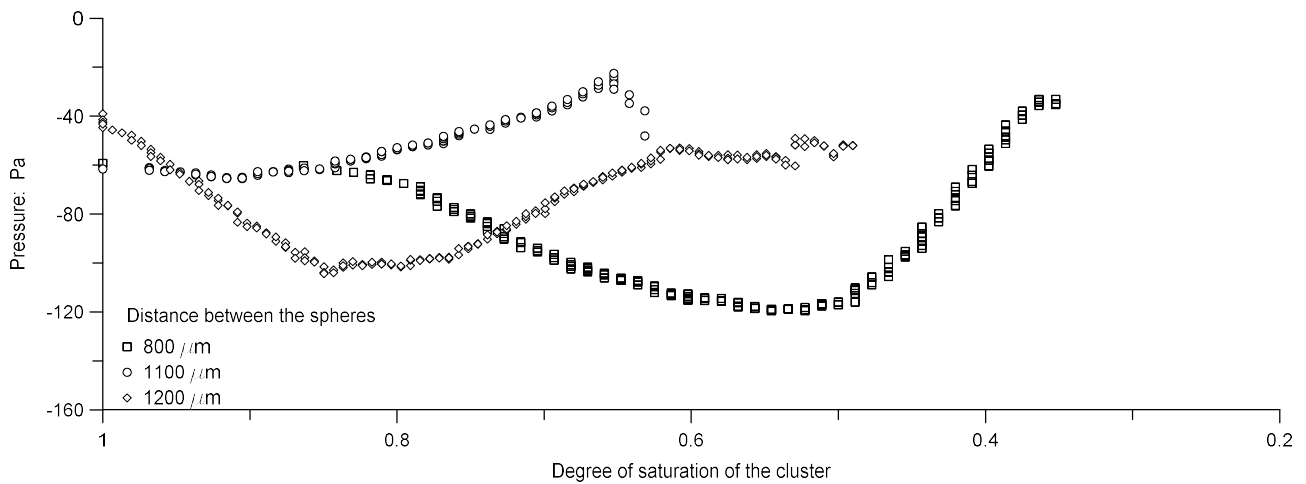
Figure 5.17 Evaporation tests – Three glass spheres without burette: Diameter of the spheres 6.34 mm, initial water volume of the water bridge 10 μl.

5.6.6   Evaporation tests for three glass cylinders

The last kind of tests carried out in this research programme was performed on three glass cylinders.

In particular, two evaporation tests setting a distance between the cylinders equal to 200 mm (Figure 5.18) and 2000 mm (Figure 5.19) were performed.

Also in this case the results show that the maximum value of the suction depends on the distance between the cylinders. Note that, in the last part of the tests the experimental measures of the suction by the burette are not in agreement with the results obtained from the Laplace's law.

This behaviour is due to the loss of contact between the burette and the water bridge. In fact, as the evaporation proceeds, the water bridge decreases its thickness and length. What can happen is that the water bridge moves from one cylinder to another, losing contact with the burette which is located in the center (Figure 5.20). Also the reduction of the length of the water bridge along the axis of the cylinder can cause the loss of contact with the burette which is also in the center in this case (Figure 5.20).
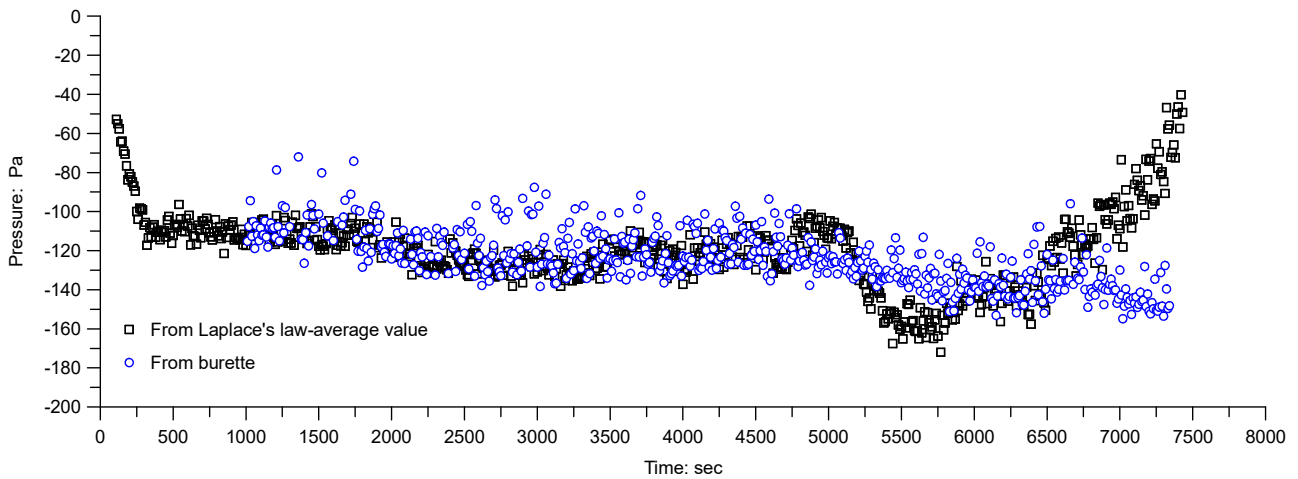
Figure 5.18 Evaporation tests – Three glass cylinders: Diameter of the cylinders 4.00 mm, initial water volume of the water bridge 10 μl, distance between the cylinders 200 μm.
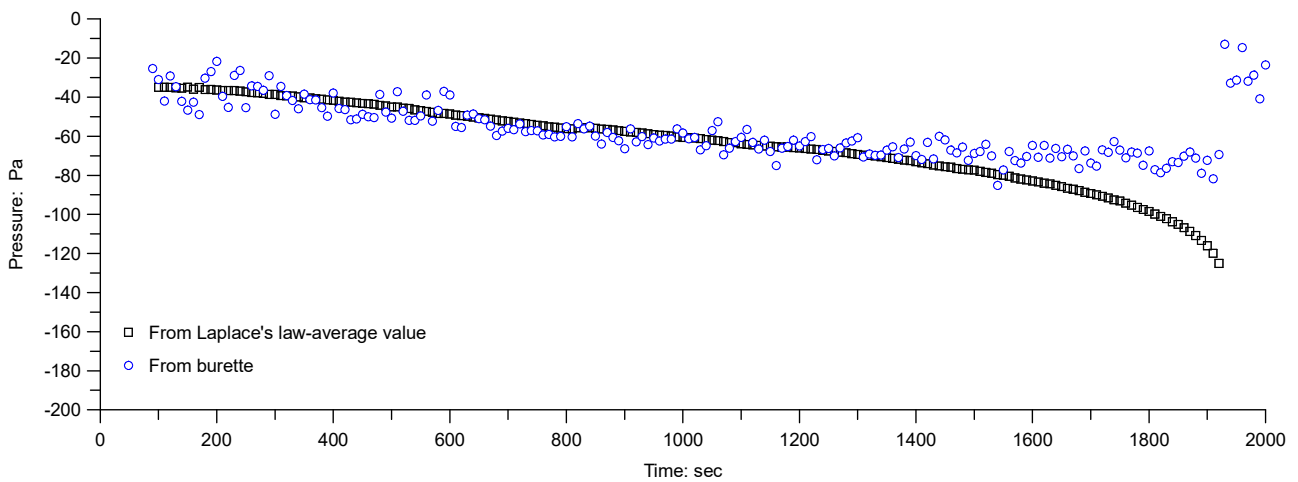
Figure 5.19 Evaporation tests – Three glass cylinders: Diameter of the cylinders 4.00 mm, initial water volume of the water bridge 10 μl, distance between the cylinders 2000 μm.
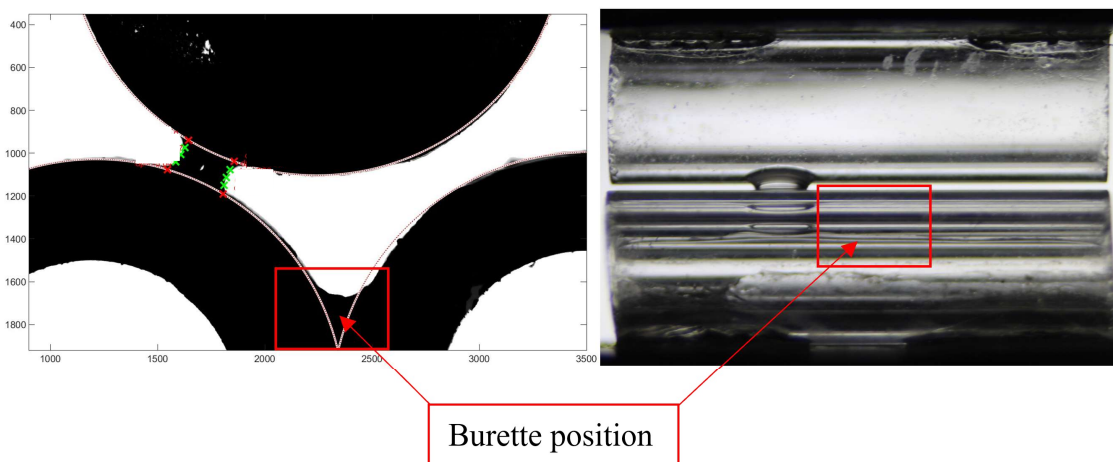
(a)   (b)

Figure 5.20 Loss of contact between the burette and the water bridge: (a) the water bridge moved on the left cylinder; (b) the water bridge moved from the center.

5.7 Evolution of capillary force

To understand the macro-behaviour of unsaturated soils and then to explain the trend of the compressibility coefficient with suction, it is necessary to consider the attractive stress relation in multi-grain assemblies as the cumulation of microscale force and processes from capillary water bridge. Hence, it is important to determine the evolution of the capillary force during a drying process. For this reason, the performed evaporation tests were also used to determine the evolution of the capillary force during a drying process. Haines (1926) proposed to attribute the force of capillary interaction entirely to the gas and liquid pressure difference resultant. However, Fisher (1926) proved that also the perimeter surface tension resultant plays a key role in the total force interaction.
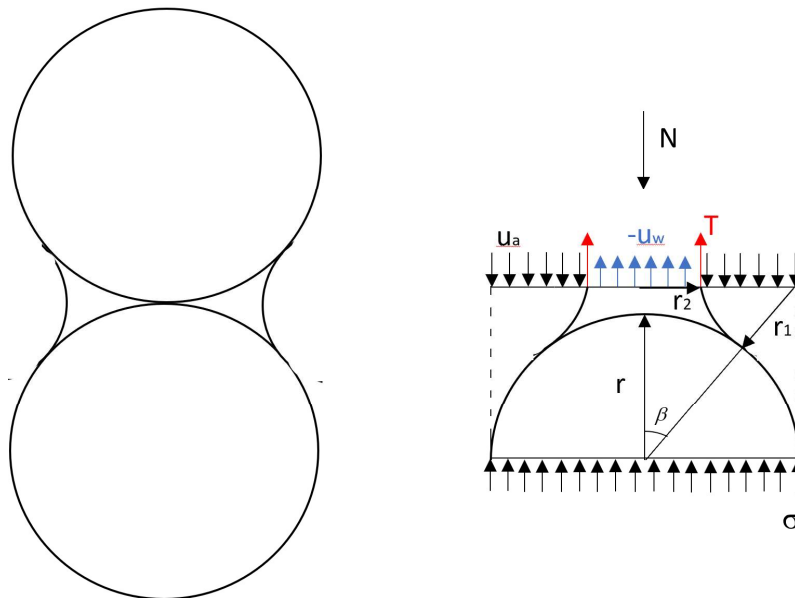
Figure 5.21 Equilibrium at the meniscus contact.

In Fisher's model, the total intergranular normal stress is obtained from the forces equilibrium across the horizontal plane passing through the inter-particle contact (Figure 5.21):

$$N = (\sigma - u_a) A + \left(A_w + P_w \left(\frac{r_1 r_2}{r_2 - r_1} \right) \right)(u_a - u_w)$$

(5.6)

where N is the intergranular force, σ is the total stress, A the total area, A_w and P_w are the wetted area and perimeter, respectively. In the pendular state (the state where the grains are not in contact)

the total intergranular force coincides with the forces generated by the meniscus (second term on the right-hand side of equation 5.6) called total capillary force. The total capillary force F_{CAP} is the sum of the force of liquid pressure difference resultant $F_{\Delta p}$ and the resultant surface tension force F_{ST}.

Conventionally, the capillary force is positive when it is attractive. If the volume of the liquid phase is very small, the gravity force is considered negligible (Butt and Kappl 2009, Willet et al. 2000, Mielniczuk et al. 2015).

The pressure resultant force between the grains in the pendular state is given by (Heines 1926, Oertli 1971):

$$F_{\Delta p} = -\pi r^2 \Delta p \tag{5.7}$$

where r is the radius of the meniscus in correspondence of the horizontal section considered for the equilibrium and Δp is the Laplace pressure.

The resultant surface tension force is defined as the vertical component of the surface tension acting at the perimeter of the meniscus (Fisher 1926, Willet et al. 2000 Soulié et al. 2006):

$$F_{ST} = 2\pi r T \cos \vartheta \tag{5.8}$$

where ϑ is the angle between the surface tension direction and the vertical axis and r is the radius of the meniscus in correspondence of the horizontal section considered for the equilibrium.
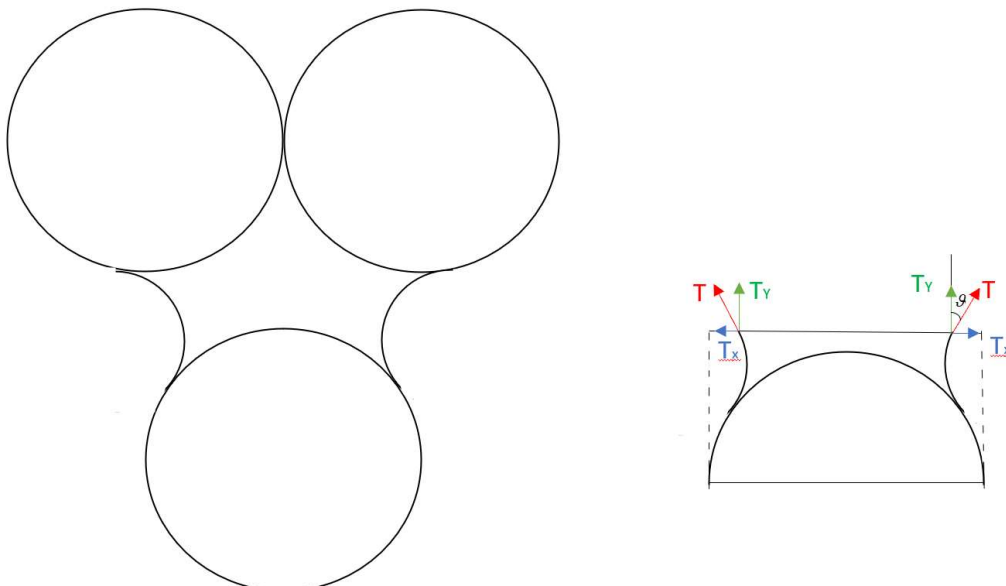
Figure 5.22 Direction of the surface tension acting at the perimeter of the meniscus.

In figures 5.23 – 5.27 are reported the results obtained in the previous section, reformulated in order to determine the evolution of the total capillary force.

The evolution of the capillary force determined for two glass spheres, reported in Figure 5.23, shows a maximum point. Note that the maximum point of the capillary force does not coincide with the maximum suction reached during the test (Figure 5.14). The position of the maximum point of the capillary force respect to the maximum value of suction depends on geometrical parameters, especially on the distance between the grains. Figure 4.24 clearly shows the impact of the distance between the grains on the trend of the capillary force during the evaporation tests (drying process). In particular for short bridge (distance between the grains equal to 200 μm, Figure 5.24 (a)), $F_{\Delta p}$ dominates the process and the capillary force reproduces the same trend showed by the suction evolution (Figure 5.16a). In this case, the maximux capillary force is reached at the rupture. For very tall water bridge (Figure 5.24f), F_{ST} dominates the process and the capillary force has its maximum value at the beginning of the evaporation process. For all intermediate conditions, the two contributions of the capillary force are comparable and its trend presents a maximum point.

Of particular interest are the results shown in figure 5.25, which highlights what happens when the water bridge jumps. In correspondence with the jumps of the water bridge or their breakage, there is a drastic decrease in the attractive force of the entire system, which therefore appears to be more labile. This is an important result to better understand how the global compressibility of a grain system, and then a granular soil, varies during a drying process.

The same considerations are available also for the tests on the cylinders reported in Figures 5.26 and 5.27. also in this case the most important parameter that influences the trend of the capillary force during the drying process is the distance between the cylinders and the eventual jump of the water bridge.
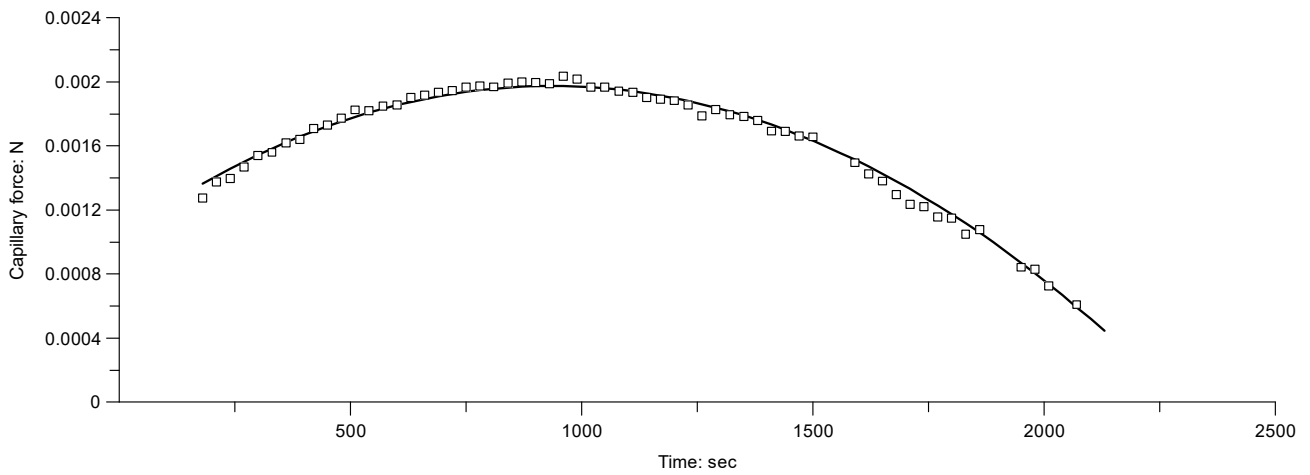
Figure 5.23 Evolution of the capillary force during an evaporation test – Two glass spheres: Diameter of the spheres 6.34 mm, initial water volume of the water bridge 10 µl, distance between the spheres 800 µm.

(a)

(b)

(c)
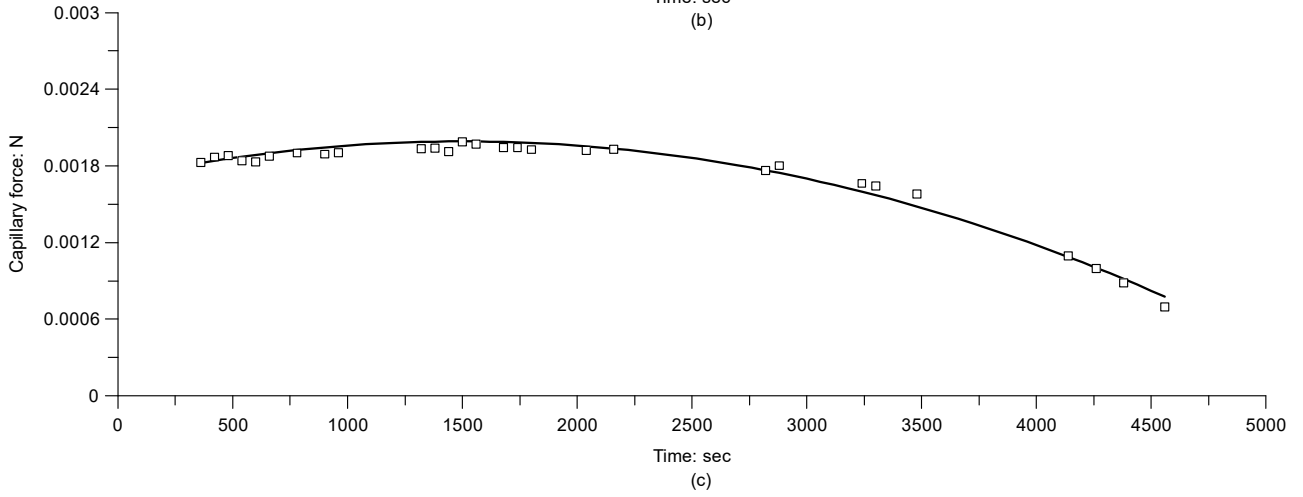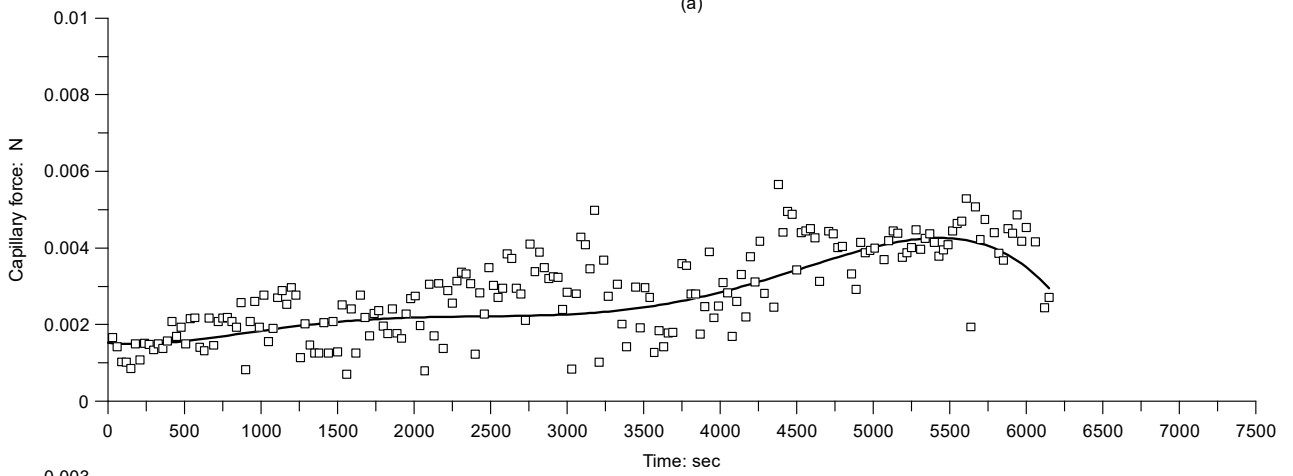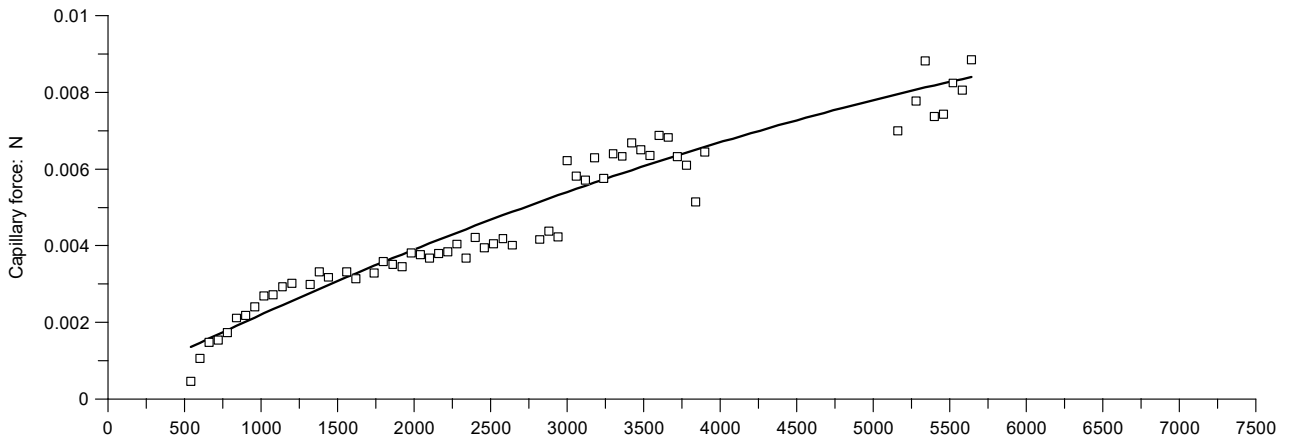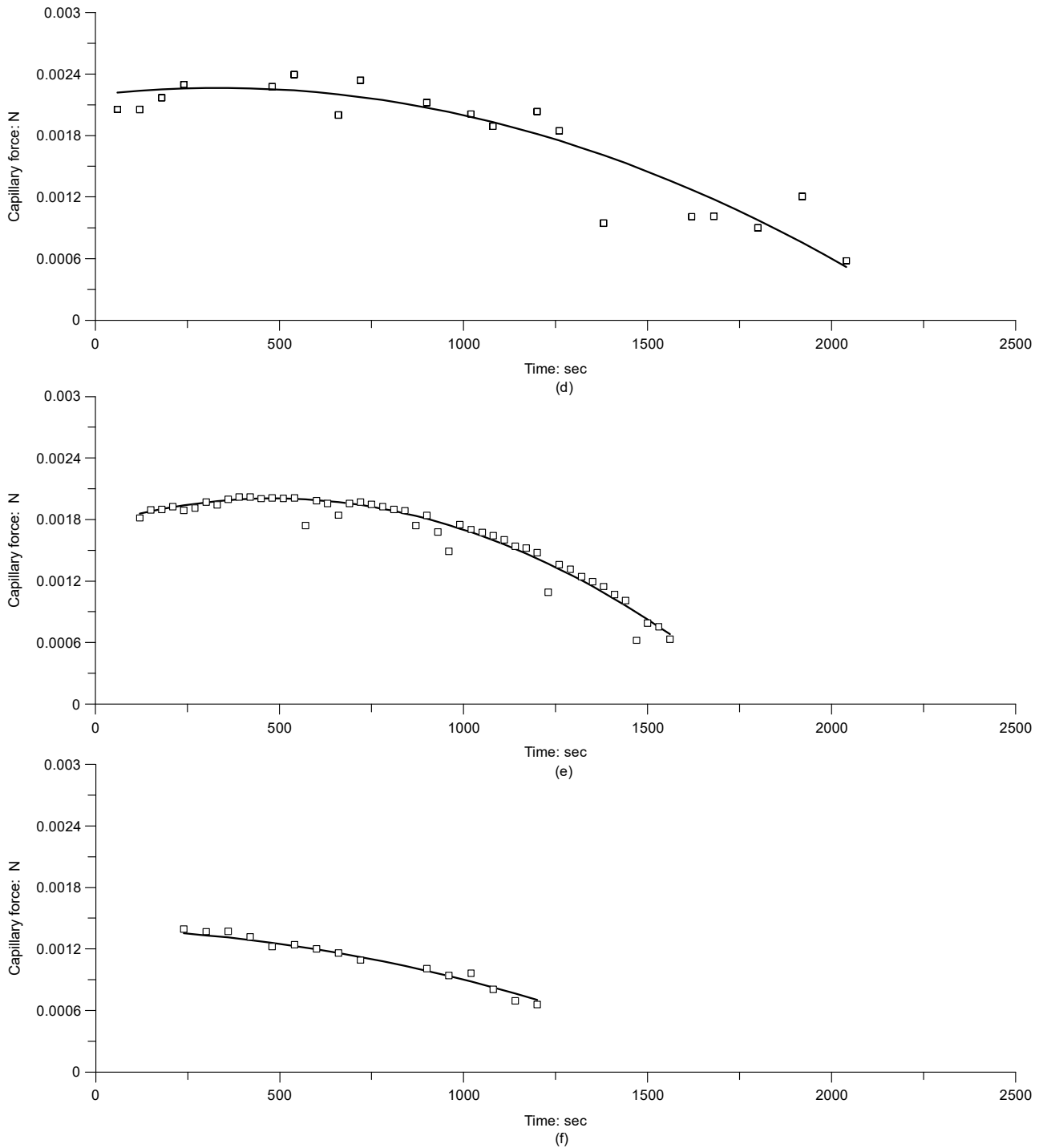
Figure 5.24 Evolution of the capillary force during evaporation tests – Three glass spheres: Diameter of the spheres 6.34 mm, initial water volume of the water bridge 10 μl, distance between the spheres: (a) 200 μm; (b) 800 μm; (c) 1400 μm; (d) 1500 μm; (e) 1600 μm; (f) 1800 μm.
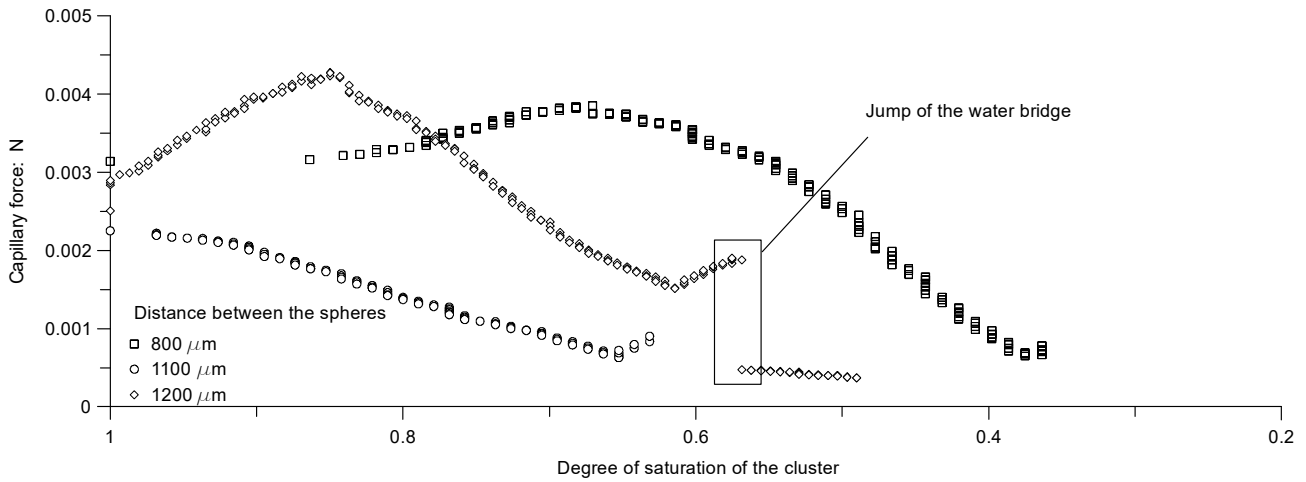
Figure 5.25 Evolution of the capillary force during evaporation tests – Three glass spheres without burette: Diameter of the spheres 6.34 mm, initial water volume of the water bridge 10 µl.
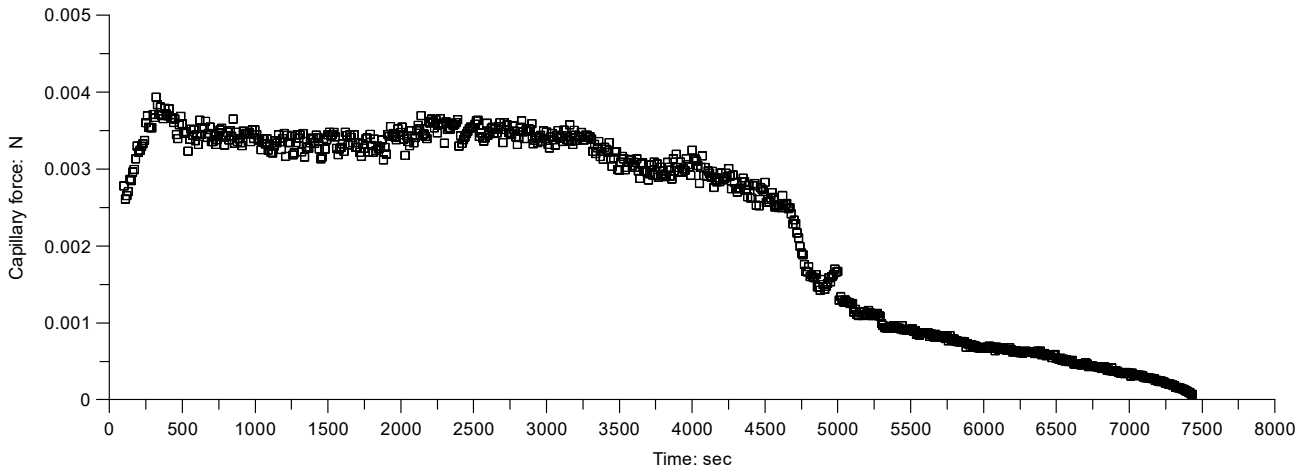
Figure 5.26 Evolution of the capillary force during evaporation tests – Three glass cylinders: Diameter of the cylinders 4.00 mm, initial water volume of the water bridge 10 µl, distance between the cylinders 200 µm.
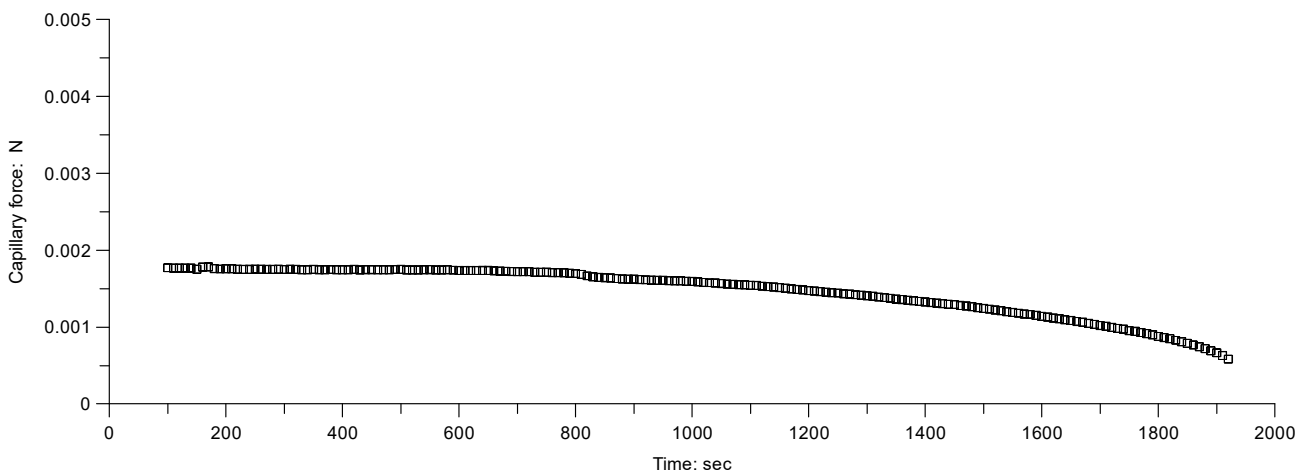
Figure 5.27 Evolution of the capillary force during evaporation tests – Three glass cylinders: Diameter of the cylinders 4.00 mm, initial water volume of the water bridge 10 μl, distance between the cylinders 2000 µm.

5.8 Interpretation of the results

Like many geomechanical properties, such as the shear strength, the apparent cohesion and the yield stress, also the capillary force increases during a drying process until a maximum value, after which it decreases.

Obviously, the evolution of the capillary force influences the mechanical behaviour of the soils. In fact, the menisci at inter-particle contacts generate an additional normal force that prevents the particle slip and limits the decrease in volume while the loading. This effect is named *"the stabilizing effect of the menisci"*. However, as shown in this chapter, the menisci can sustain a maximum value of suction, after which the rupture of the menisci occurs. Consequently, while the drying process proceeds some menisci break and the stabilizing effect decreases. Definitely, at the end of the drying process no stabilizing effect by menisci is present and then the geomechanical properties of dry geomaterials are equal to the saturated one.

This link between the micro-scale and the macro-scale could be better analysed considering Figure 5.28 as follows:

- In the saturated state, the suction is generated in the pore water with the degree of saturation still remaining equal to 1. In reality, the pore in contact with the atmosphere begins to empty due to the evaporation (Figure 5.28(a)). Note that, the results for the evaporation tests at the micro-scale are represented in terms of the degree of saturation of the cluster.

- As the drying process proceeds, the meniscus curvature at the interface will increase, the water pressure will further decrease and consequently the total capillary force increases. However, in the quasi-saturated state, the air phase is still discontinuous and not in direct contact with the surrounding air. The air-entry value corresponds to the point where the yield stress begins to increase.

- The partially saturated state is defined as the state where water menisci at the interface reach the limit curvature, menisci will recede into the soil and the air will enter the soil. In this state,

water and air will both be continuous in the pore space. So, in this state, some menisci (the

menisci in the small pores) are in the phase where the capillary force increases as drying

proceeds (red rectangle in Figure 5.28 (a)), the other one are in the phase where the generated

capillary force decreases as evaporation proceeds (green rectangle in Figure 5.28(a)). These

two different phases are reflected one the macro-scale behaviour. The yield stress, and then

the Loading – Collapse curve, will increase until the stabilizing effect provided by the pores

that are in the red phase are predominant over the green phase will be predominant. When the

green phase will be predominant over the red phase, the stabilizing effect provided by the

partially saturated condition will decrease.

- When the water remains isolated at the particle contact and is no longer continuous in the pore
space there is a small stabilizing effect (green rectangle in Figure 5.28 (a)), and the elastic
domain continues to decrease (green rectangle in Figure 5.28 (b)). At the residual condition
or the dry state in the case of granular soils, no stabilizing effect provided by menisci is present
and the mechanical properties of the soil are the same of the saturated one.

5.9 Summary and conclusion

The hydro-mechanical behaviour of unsaturated granular materials is strongly influenced by capillary

force acting between the grains. The most famous effect of the water on the granular soil is the

possibility to build a "castle sand", that can only defy gravity as long as the sand is unsaturated.

The experimental programme carried out in this chapter has permitted to measure the evolution of

the capillary pressure inside the meniscus. The experimental measures were compared with the results

obtained by the Laplace's law. The agreement between the experimental measurements, using the

new device with the burette system, and the pressure calculated from Laplace's law is well.

In addition, the experimental tests allowed us to determine the evolution of the capillary force during

a drying process. The results show a similar trend showed by many geomechanical properties: In

general, starting from the saturated state, as drying process proceeds, the attractive capillary force

increases up to a maximum point, after which it decreases until the rupture of the meniscus. After rupture, the capillary force is equal to zero, like in the case of the saturated pore.

The high number of the tests allowed also to highlight the influence of the distance between the grains on the trend of the capillary force during a drying process. In particular, if the distance between the grains is very small, the capillary force increases up to the rupture of the meniscus after which it becomes zero. If the water bridge is very tall, the resultant surface tension force dominates the process (the suction generates in the meniscus is small and then also the pressure resultant force).

Obviously, the macro-scale behaviour is influenced by the micro-scale behaviour, but to compare the two scales it is necessary to take into account the structure of the soil. In fact, the soil is formed by pores with different dimensions and then to link the micro-scale measurements to the macro-scale behaviour it is necessary to consider the rupture of the menisci, the maximum suction and the maximum capillary force resultant are not reached in the same time. This means that the behavior at the macro-scale is the result of an average of what happens at the micro-scale, and the link between the micro- and macro-scale must necessarily take into account the structure of the soil.

In this chapter the qualitative link between the micro- and macro-scale was obtained in order to explain the evolution of the yield stress with the suction. The same reasoning is applicable to other geomechanical properties such as the shear strength.

(a)

(b)
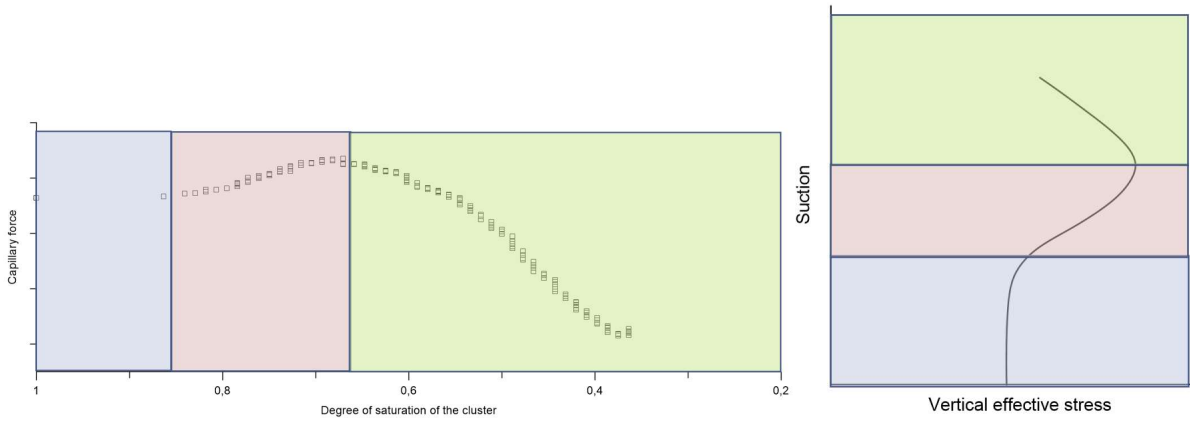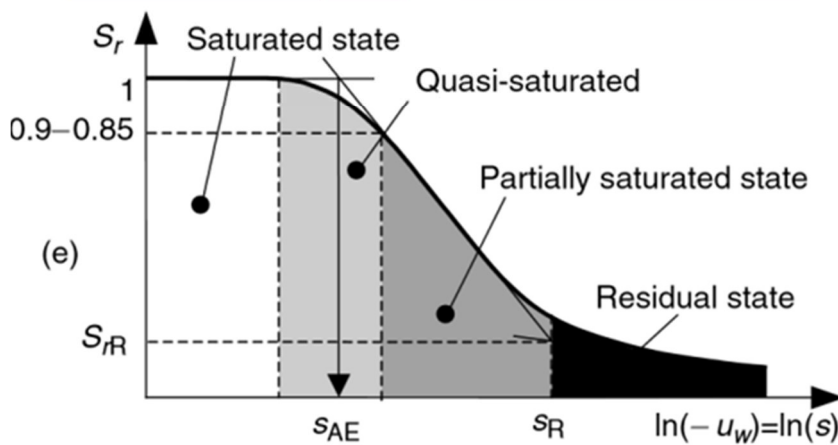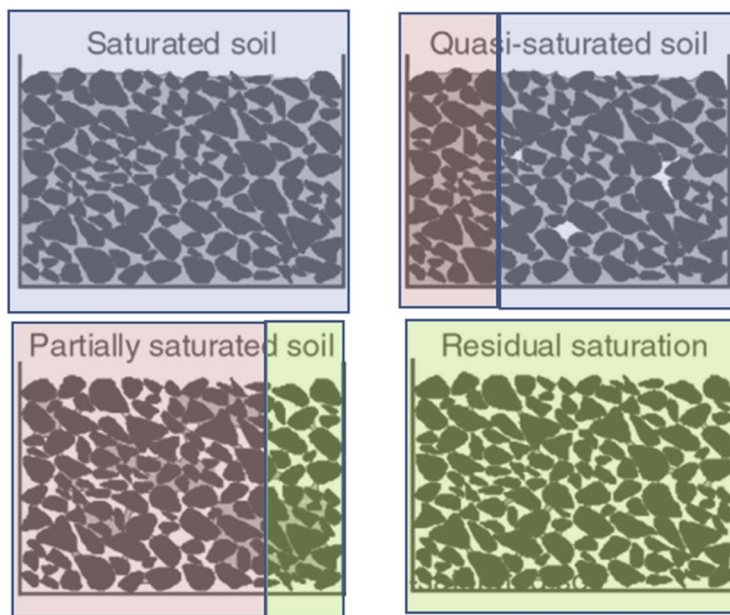
(c)

Figure 5.28 Hydro-mechanical behaviour of unsaturated soils – qualitative interpretation of the link between the micro- and macro scale: (a) evolution of the capillary pressure during an evaporation test; (b) Loading – Collapse curve; (c) State of saturation, Figure from Tarantino (2003) in Mechanics of Unsaturated Geomaterials, eds Laloui (2010).

6. Determination of the hydro-mechanical behaviour of an undisturbed natural soil: The case of study of the river Secchia

6.1 Introduction

River embankments are used to protect land, flood plains and humans from river flooding. As all earthen infrastructures, they are usually in partially saturated conditions. The degree of saturation and the suction could fluctuate as a result of river level variation, rainfall and evaporation. Obviously, the seepage and the stability of the embankments are strictly linked to these variations.

However, there is limited experience to perform a safety assessment of river embankments in unsaturated conditions. In addition, very few experimental evidence are available on the unsaturated behaviour of undisturbed soil samples from the embankments.

With the aim to highlight possible effects of partial saturation on the riverbank filling materials, this chapter presents results from an experimental investigation on undisturbed samples at different levels of matric suction. The experimental programme was designed and carried out in order to define the hydro-mechanical behaviour of the soil when subjected to variation in suction and vertical stress.

To cover the suction range was necessary to use a combination of several suction-control and suction-measurement techniques. The suction-controlled oedometric tests were performed to investigate the evolution of the elastic domain and the soil compressibility with suction. The results were also used to verify the new equation to model the soil compressibility, proposed in the previous chapter. In addition, the monitoring of the pore water volume changes induced by the suction changes allowed assessing the permeability function of the material. All tests were performed on undisturbed samples from an experimental site where recent studies have provided data on the hydraulic response of the river embankment (Gragnano et al. 2018, Gottardi et al. 2016) towards hydrometric fluctuations and atmospheric loadings. This extensive characterization work serves as a basis for the analysis of the embankment response under severe variations of river level and rainfall with high intensity, to evaluate the safety margins under transient seepage and the collapsibility of the river embankment.

6.2 Materials and methods

6.2.1   Experimental site and embankment features

The embankment section investigated is part of the river Secchia (Po tributary) retaining water infrastructure, North of Italy, which suffered a structural collapse happened in 2014 causing a flood that caused several damages and a victim.

The cross-section, analysed in this chapter, has an 11 m high crown, referred to the ground level. Riverside and landward slopes are 30° and 25°, respectively and the embankment crest is 4.6 m. On the river side there is a berm about 5.5 m wide and generally rich in vegetation. Several tests were carried out in order to characterize in detail the soil both from hydraulic and mechanical points of view (Gragnano et al. 2018, Gottardi et al. 2016). A set of four CPTU tests were performed in the area, two from the crest and two from the berm, along two adjacent cross-sections, enabling to identify the embankment stratigraphy and a preliminary mechanical characterization (Gragnano et al. 2018, Gottardi et al. 2016). Test results have shown that the embankment filling material mostly consists of alternating silt and sandy silt; in particular, three different soil-stratigraphy units were identified (D'Alpaos et al. 2014):

- *"**Unit AR:** the river embankment consists of alternating silt and sandy silt;*
- ***Unit B:** the foundation of the embankment consists of sandy silt and local clayey silt with horizontal stratification;*
- ***Units C:** clayey soil with local sandy silt intercalations.*

A schematic representation of the stratigraphy is depicted in Figure 5.1.

The boreholes have been also carried out for undisturbed soil sampling and installation of sensors for the monitoring of soil suction and water content at various depths in the berm and in the main embankment (Gragnano et al. 2019).

The undisturbed soil samples used in this research come from the borehole named TC2 and they were taken at the depth 5.00-5.50 m (TC2 – 5) and 6.00-6.50 m (TC2 – 6), as shown in Figure 6.1.
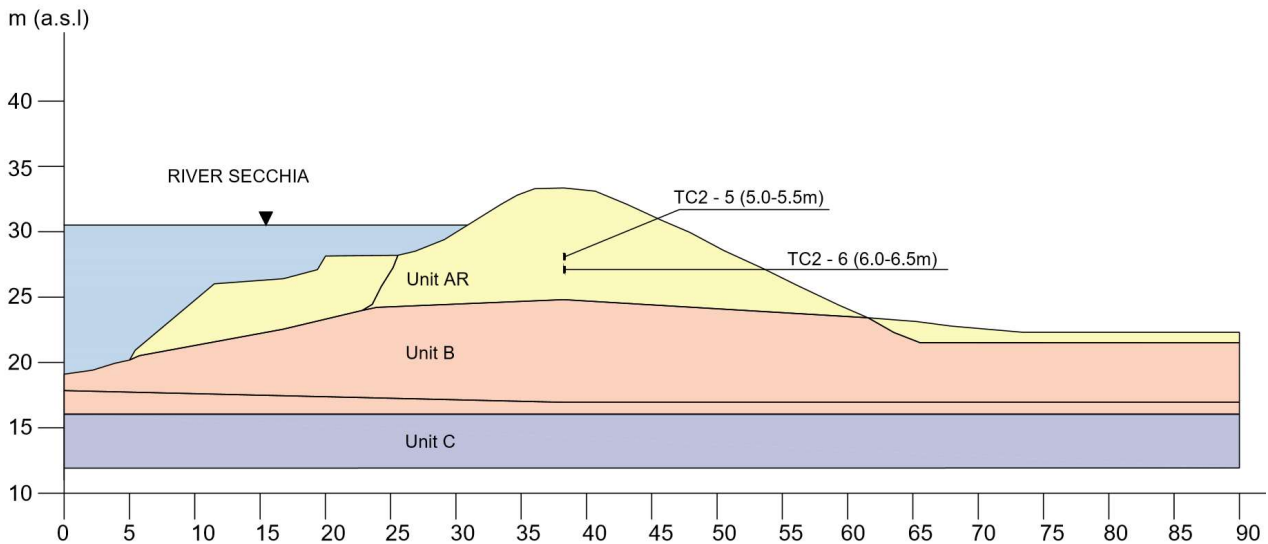
Figure 6.1. River embankments of the river Secchia: stratigraphy and position of the undisturbed soil samples used in this work.

6.2.2   Characterization of tested soil samples

The high variability of the soil is also present at the *"sample scale"*, as clearly shown in Figure 6.2.

The identification tests were also permitted to divide the tested soil into two groups: soil S_a and soil S_i. The grain size of the soil S_a presented a sand size fraction variable from 55.6 to 67.7%, while the silt fraction accounted for 22.3 to 30.5% and the clay fraction was around $9 \div 14\%$. The soil has been classified as a silty sand. The void ratio was in the range of $0.74 \div 1.24$ and the specific gravity was around $2.72 \div 2.74$. The soil had a plastic limit equal to 19.5% and a liquid limit equal to 29.8%. Generally, the soil S_a, in its natural condition, presented a low value of the degree of saturation (in the range of $19.8 \div 38.4\%$).

The sand fraction of the second unit, soil S_i, was in the range of $33 \div 45\%$, the silt fraction was variable from 35 to 51.5%, while the clay fraction was around $5.5 \div 20\%$. The soil has been classified as sandy silt. The sandy silt soil had a void ratio in the range of $0.57 \div 0.60$ and a specific gravity variable from 2.66 to 2.69. The plastic limit of the sandy silt was 17.5%, while the limit liquid was 27.2%. In its natural state the sandy silt presented an high value of the degree of saturation, in the range of $53.2 \div 57.8\%$.

The main physical properties are showed in Table 6.1.

Table 6.1. Physical properties of tested soils.

Depth [m]	G_s	w_l : %	w_p : %	f_{clay} : %	f_{silt} : %	f_{sand} : %	w_n : %	e_0	S_r : %	Unit
5.05	2.66	---	---	5.5	61.5	33.0	11.2	0.57	53.2	S_i
5.10	---	---	---	10.0	22.3	67.7	10.3	---	---	S_a
5.15	---	29.8	19.5	---	---	---	---	---	---	S_a
5.20	---	---	---	---	---	---	10.0	1.24	22.2	S_a
5.25	2.72	---	---	14.0	30.4	55.6	8.4	1.16	19.8	S_a
5.30	---	---	---	9.0	30.5	60.5	8.0	0.74	24.9	S_a
5.35	---	---	---	---	---	---	11.0	0.79	38.4	S_a
5.40	2.74	---	---	---	---	---	10.0	---	---	S_a
5.45	---	---	---	13.6	27.5	58.9	9.6	---	---	S_a
6.25	---	---	---	---	---	---	12.8	0.79	37.0	S_a
6.45	2.69	27.3	17.5	20.0	35.0	45.0	12.9	0.60	57.8	S_i

The water retention behaviour of the two units was determined using a combination of different suction-control and suction-measurement techniques. Both techniques were performed on undisturbed specimens. Given the nature of the soil, it was necessary to planned and carried out an appropriate specimen packaging technique which would prevent the crumbling. The steps followed to prepare all the specimens are summarized as follows:

- partial opening of the steel borehole casing and cutting part of the material (Fig. 6.3a);
- extraction of the material from the steel borehole casing, using two aluminium disks capable of ensuring the confinement (Fig. 6.3b);
- lateral confinement (Fig. 6.3c);
- infixion of the sampler steel ring (Fig. 6.3d);
- trimming (Fig. 6.3e);
- passage in the test ring (Fig. 6.3f).
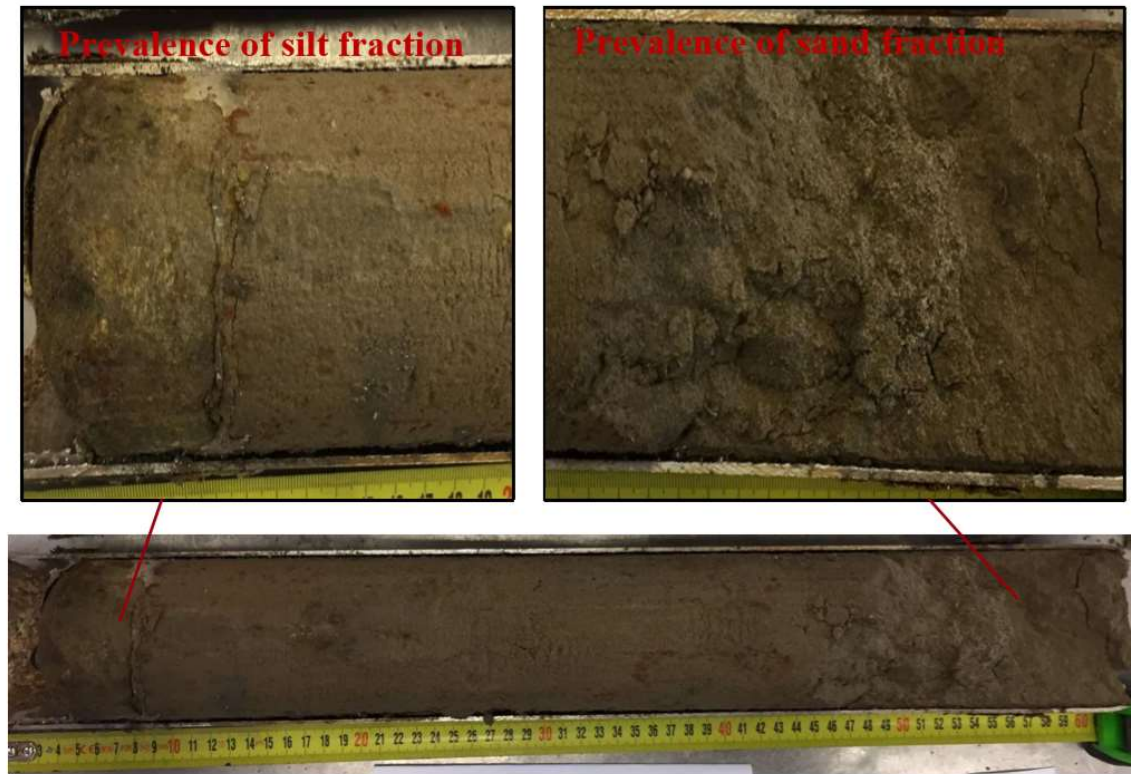
(a)
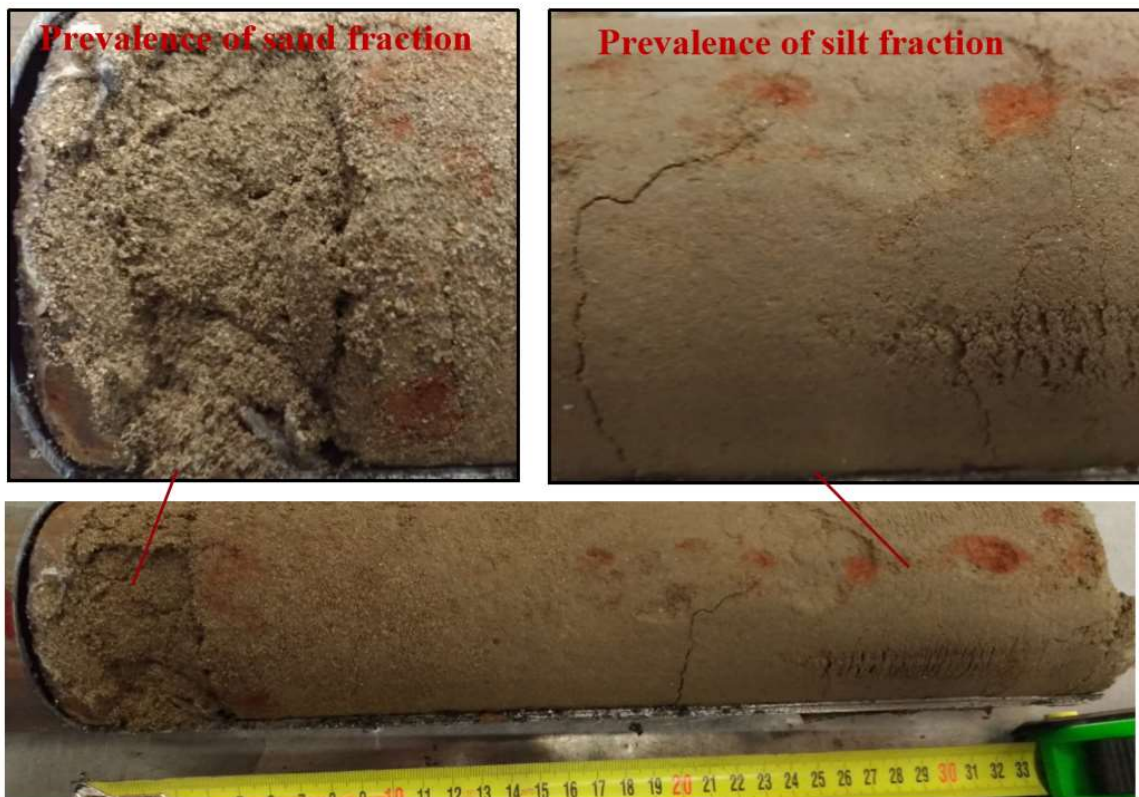
(b)

Figure 6.2. Steel borehole casing: (a) TC2-5 5.00-5.50 m; (b) TC2-6 6.20-6.50 m.

To determine the main drying branch of the water retention curve of the soil S_a three specimens were used.

The retention behaviour in the suction range of $0 \div 14.8$ kPa was obtained using the negative water column technique. One specimen with a dimension of 60 mm in diameter and 20 mm in height and an initial void ratio equal to 1.162 was sitting on a high air-entry value disk (nominal air-entry value of 100 kPa), which was connected to a burette used to impose the negative water pressure. Starting from the saturated condition, the suction was increased maintaining a constant total vertical stress of 1.75 kPa, in the same way described for the quartz sand (chapter 3.3.1). During the drying process, the measurements of the height allowed to trace the evolution of the void ratio and degree of saturation. The maximum variation in void ratio measured was -0.006.

The specimen used for the negative water column was re-cored with a ring having 50.4 mm in diameter and 10 mm in height. This specimen was used to determine the retention behaviour in the suction of $17.8 \div 53.0$ kPa using a tensiometer having a nominal air-entry value of 1500 kPa. Periodically, the specimen was exposed to the environmental condition of the room to permit evaporation. During this process, the weight and the dimensions of the specimen were monitored to trace the evolution of the degree of saturation and the void ratio. While, during the measurement, the specimen was isolated from the environment using the plexiglass confining system shown in Fig 6.4. The tensiometer permitted to determine also the initial suction of the undisturbed specimen having 50.4 mm in diameter, 10 mm in height and an initial void ratio of 0.94. The initial suction was 29.1 kPa.

The third specimen, having 60.0 mm in diameter, 20 mm in height and an initial void ratio equal to 2.24, was used to perform suction-measurement using the filter paper methods. Three filter paper disks (Whatman No. 42) were placed between the two parts of the soil specimen. The two filter papers in contact with the soil are protective filter papers while the middle filter paper is used to measure the suction.

(a)

(b)

(c)

(d)

(e)

(f)

Figure 6.3 Specimens preparation: (a) cutting; (b) extraction; (c) confinement; (d) infixion; (e) trimming; (f) passage in the test ring.

The entire system was isolated from the environment and stored in a climate chamber for 20 days.

After the equalization process, determining the water content of the middle filter paper, the suction

was estimated using the calibration curve provided by Hamblin 1981.

Additional two points for the main drying branch and six points for the main wetting branch were

obtained from the controlled-suction oedometric tests. The experimental points on the plane (Sr, s)

were fitted in Fig. 6.5(a) using the Van Genuchten's equation. The fitting parameters of the main

drying curve are $\alpha = 0.005 \text{ kPa}^{-1}$, $n = 1.00$, $m = 6.13$ and $S_{r,res} = 0.03$, while the fitting parameters

of the main wetting curve are $\alpha = 0.010 \text{ kPa}^{-1}$, $n = 1.06$ and $m = 7.31$.

The retention behaviour of the soil S_i was determined using the tensiometer (Fig. 6.4) on a specimen,

having 50.4 mm in diameter, 10 mm in height and an initial void ratio of 0.57. After the first suction

measurement, the specimen was wetted via liquid phase using a dropper.

(a)   (b)   (c)

Figure 6.4. Tensiometer: (a) view of the porous stone; (b) plexiglass system used to isolate the soil
during the measurement; (c) tensiometer during the measurement process.

After adding the water with the dropper, between one measurement and the other one the specimen

was isolated with the external environment for at least 24 hours, to allow equalization. Determined

the main wetting branch, the same specimen was also used to determine the main drying branch,

allowing periodically the evaporation between one measurement and the next, similarly to what was

done for the S_a. Figure 6.5b also shows the water retention behaviour of the soil S_i. The best-fit of the

Van Genuchten's equation was obtained using the parameters $\alpha = 0.005$ kPa^{-1}, $n = 1.60$, $m = 1.80$

and $S_{r,res} = 0.08$ for the main drying branch, and $\alpha = 0.010$ kPa^{-1}, $n = 1.70$ and $m = 1.10$ for the main

wetting branch.

As shown in Figure 6.5, both materials present limited hysteric behaviour. The main drying curves

suggest that the air-entry values are 4.2 kPa and 40 kPa for the unit S_a and S_i respectively, while the

air-exit value is equal to 3.0 kPa for the soil S_a, and 27.8 kPa for the soil S_i.

The mechanical characterization of the river embankment was performed on unit S_a which was the

main unit in the steel borehole casing analysed.
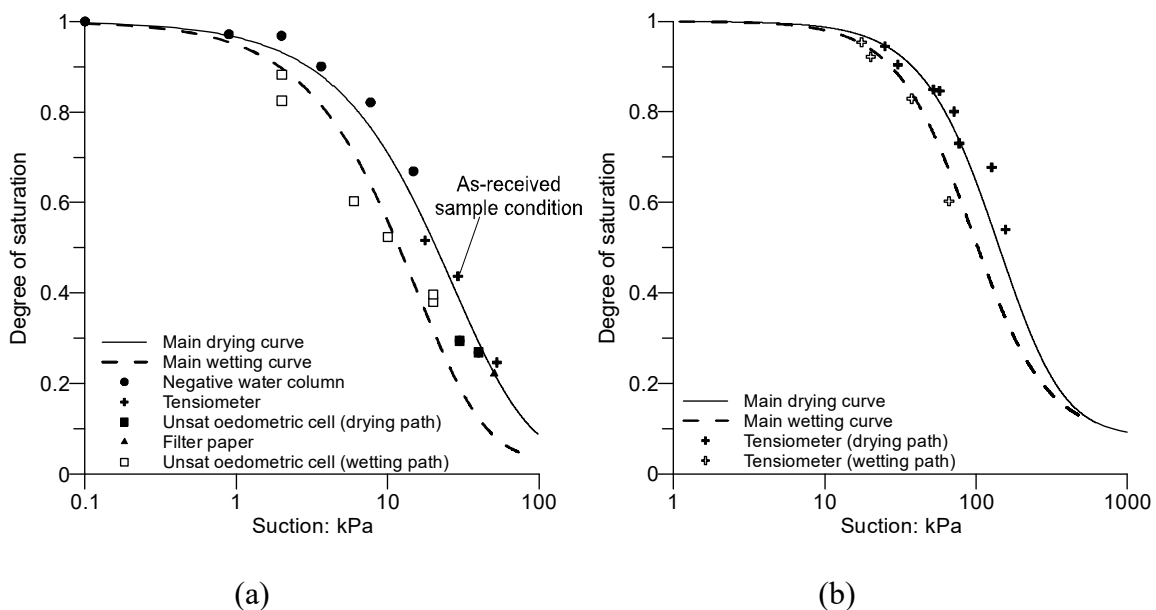
Figure 6.5 Soil water retention curve: (a) Unit S_a; (b) Unit S_i.

6.3 Test program

In order to determine the volumetric response of the river embankment when it is subjected to the

variation of the degree of saturation, two controlled-section oedometric tests, one conventional

oedometric test at saturated condition and one oedometric test at natural water content and inundation

under load were carried out. The four specimens were prepared using the same technique described
above.

The two controlled-suction tests were carried out on specimens with a diameter of 50.00 mm and a
height of 20.00 mm (initial void ratio in the range of 0.69-0.73) using the Axial Traslation Technique
(ATT). The stress paths followed in the controlled-suction oedometer are reported in the plane vertical
net stress vs suction in Fig. 6.6.
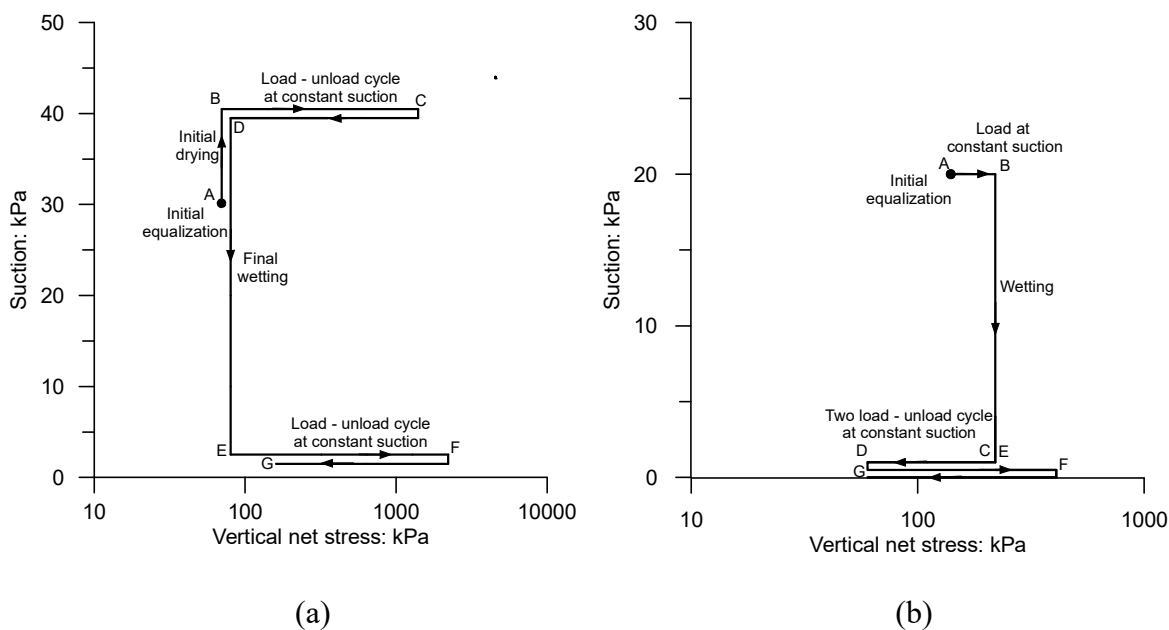
Figure 6.6 Stress paths used in the controlled – suction oedometric tests.

The stress path depicted in Fig. 6.6 (a), permits to determine all parameters of the classical model for
partially saturated, soil as the BBM (Alonso et al. 1990), using only one test.

After the first equalization to suction of 40 kPa, a first loading-unloading path (B-C-D) was performed
to assess the initial position of the Loading – Collapse curve and the values of the elastic
compressibility parameter and compressibility parameter for the virgin state. The wetting path (D-E)
was performed at low value of vertical net stress in order to prevent plastic deformations.

The loading – unloading path (E-F-G) was done to determine the yield stress and the compressibility
coefficient at 2 kPa of suction after the previous yielding, and to define the Loading – Collapse curve

in the final position. The result of this test and the result of the conventional oedometric test were allowed to calibrate the parameters of the model.

In the second test, reported in Fig. 6.6(b), the suction reduction at constant vertical net stress was carried out to assess the collapse upon wetting behaviour (B-C).

The two controlled-suction oedometric tests allowed also to determine the relative permeability of the tested soil and the test reported in Figure 6.6(b) was also used to compute the collapse potential.

The conventional oedometric test was performed on a specimen with 56.0 mm in diameter and 20.0 mm in height (initial void ratio equal to 0.79) and it was saturated by innundation. The maximum vertical total stress applied in the following loading-unloading cycle was 6.0 MPa.

The constant water oedometric specimens had 56.0 mm in diameter and 20.0, and the void ratio was 0.78. The initial water content value was 6.0 %, (corresponding range of degree of saturation 0.20). The conventional porous bases of the oedometric cell were substituted with two impermeable disks. In addition, the entire cell was isolated from the external environment by means of an impermeable membrane. The load was increased in steps up to a maximum vertical total stress of 6.0 MPa.

6.4 Test Results

6.4.1 Elasto – plastic volumetric response

The results of the oedometric tests are discussed in this section with reference to the vertical total stress. Yield stresses were determined in each performed test using the Boone's method (Boone, 2010).

Figure 6.7(a) depicts the results for the stress paths shown in Fig. 6.6(a), while Figure 6.8 reports the results obtained in saturated condition. During the initial drying, no significant deformation of the specimen was recorded. The first loading path (B-C) at constant suction (s=40 kPa) highlighted the transition from the pre-yield to the post-yield behaviour.

In addition, a new yield-point point of the Loading-Collapse curve in its final position was imposed (Point C). The unloading path (C-D) allowed to determine the elastic response of the material. During

the wetting (D-E) no deformations were recorder. The final loading – unloading path (E-F-G) shows

the yielding at low value of suction (s=2 kPa), and then a second point of the Loading – Collapse

curve in the final position.
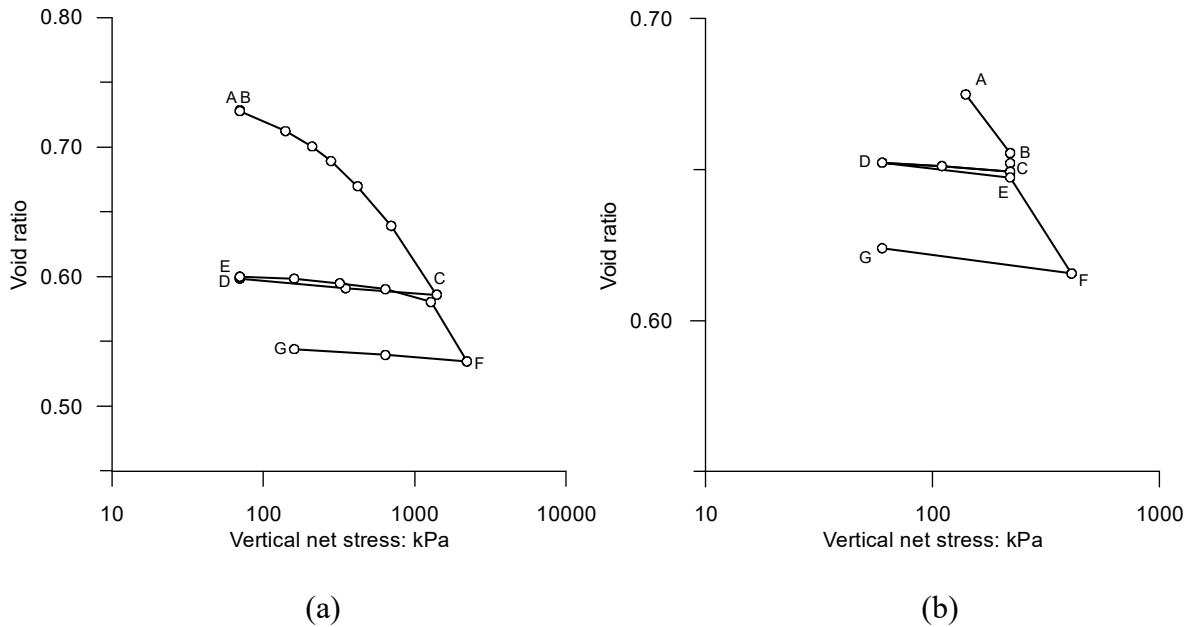
Figure 6.7. Results of the controlled-suction oedometric tests following the stress path in Fig. 6.6.

Figure 6.7(b) depicts the results obtained for the stress path depicted in Fig. 6.6(b), The loading path

(A-B) caused the yielding of the soil and the Normal Compression Line was reached. During the

wetting path (B-C) the suction changed from 20 kPa to 0 and a reduction of void ratio was registered.

This reduction of the pore volume is a result of the collapse upon wetting behaviour. The successive

unloading – loading path (C-D-E-F) confirms the new yield point caused by the previously wetting.

This reduction of the pore volume is a result of the collapse upon wetting behaviour. The successive

unloading – loading path (C-D-E-F) confirms the new yield point caused by the previously wetting.

The evolution of the compressibility coefficient with suction was modelled using the equation 4.6.
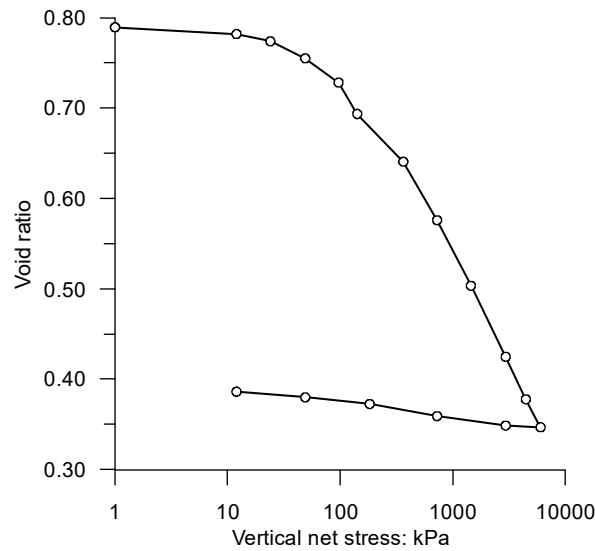
Figure 6.8. Results of the oedometric test in saturated condition.

Figure 6.9 depicts the increase of the compressibility parameter for the virgin state with the suction and the Loading – Collapse curve pre and post-yielding. As explained before, the stress path reported in Fig. 6.6(a) has been designed to determine all of the parameters needed for the model. Whether the yield stress obtained from controlled-suction oedometric test and the yield stress obtained from conventional oedometric tests cannot univocally define the Loading – Collapse curve shape in the initial position, it is possible to define the elastic domain for the undisturbed specimen starting from its yielding condition, knowing three points (two derived from the test depicted in Fig. 6.6(a), and one from the saturated test):

- the new yield stress, imposed in the stress path at s=40 kPa (point C – Fig. 6.6(a));

- yield stress of the Loading – Collapse curve in the final position, obtained during the loading path (E-F – Fig. 6.6(a));

- the saturated yield point of the Loading – Collapse curve in the final position, obtained by the Virgin Compression Line for the same void ratio $(\sigma_{v,net})_{0,f}^*$;

it is possible to define the Loading – Collapse shape in its final position.
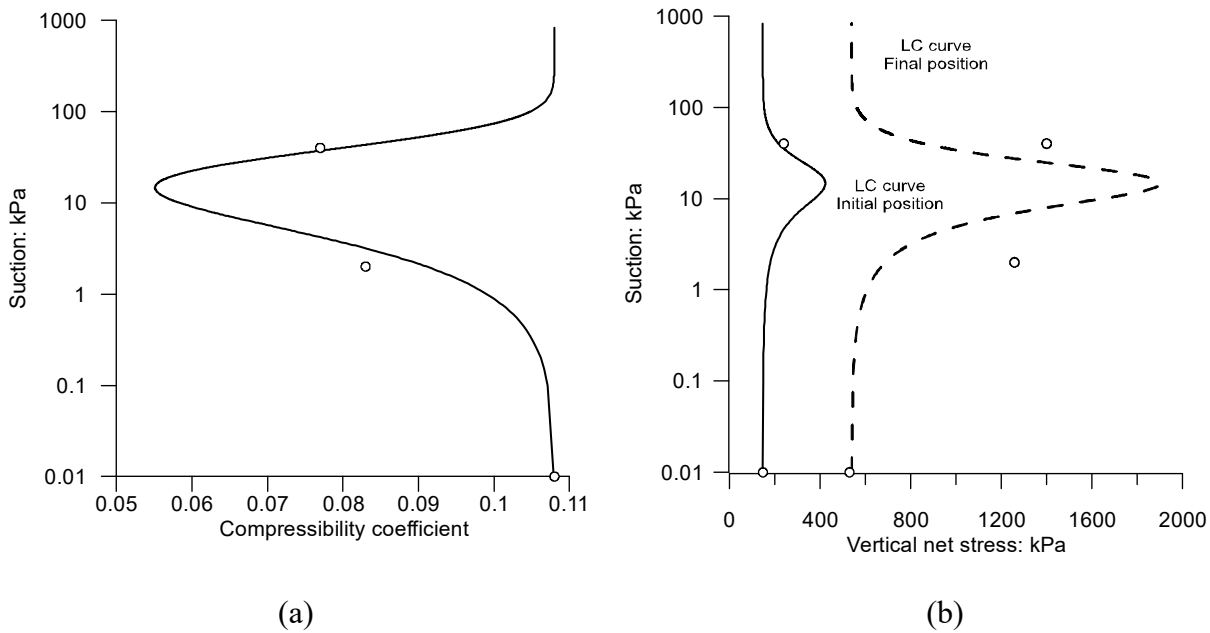
Figure 6.9. (a) Compressibility coefficient vs. suction; (b) Loading – Collapse curve, pre-yielding and post-yielding.

To determine the Loading – Collapse curve in its initial position, the same assumption proposed by Alonso et al. (1990) was used. The authors hypothesized that the yielding of the material causes a movement of the curve, but its shape remains unchanged. Therefore, knowing the shape of the Loading – Collapse curve in its final position, the yield stress in saturated condition and the yield stress obtained during the loading path B-C depicted in Fig. 6.6(a), the Loading – Collapse curve is determined. The parameters of the model are reported in Table 6.2.

6.4.2   Potential collapse

The potential collapse is an indication of the degree of bulk volume change that soils exhibit because of load and water infiltration. In one dimensional condition, the potential collapse is given by the variation in height after wetting and an applied load.

Traditionally, two methods are used to determine the potential collapse of the soil:

    (a) Single oedometer collapse test;

    (b) Double oedometer collapse test.

146

Table 6.2. Parameters of the elasto-plastic model.

Parameter	Value
α	0.01
n	1.06
m	7.31
a_s	0.15
d	0.90
i	1.40
$\left(\sigma_{v,net}\right)_0^* / \sigma_c$	3
$\left(\sigma_{v,net}\right)_{0,i}^*$ [kPa]	148
$\left(\sigma_{v,net}\right)_{0,f}^*$ [kPa]	530

The first method consists of one sample. The undisturbed soil specimen at natural moisture is loaded

to a stress level equal to 200 kPa and then a wetting path is applied (usually up to the saturation) to

induce collapse. After 24 hours, the oedometer test is carried out by increasing load to its maximum

loading. In order to determine the collapse potential of the soil using the single oedometer test, the

controlled-suction oedometer test reported in Figure 6.6 (b) was used. The correspondent oedometric

curve is depicted in Figure 6.7 (b), while the zoom in correspondence of the collapse upon wetting is

showed in Figure 6.10. Abelev (1948) defined the Collapse Index (I_e) as the potential collapse due

to wetting at applied pressure of 200 kPa (Jennings and Knight, 1975) as:

$$I_e = \frac{\Delta e_c}{1 + e_1} \tag{6.1}$$

where Δe_c is the variation of the void ratio resulting from saturation and e_1 is the void ratio just before

the inundation. The collapse index obtained from the Abelev's equation is 0.37%.

However, Jennings and Knight, 1975, defined the collapse index as:

$$I_e = \frac{\Delta e_c}{1 + e_0} \tag{6.2}$$

where e_0 is the initial void ratio, and it results equal to 0.36%.
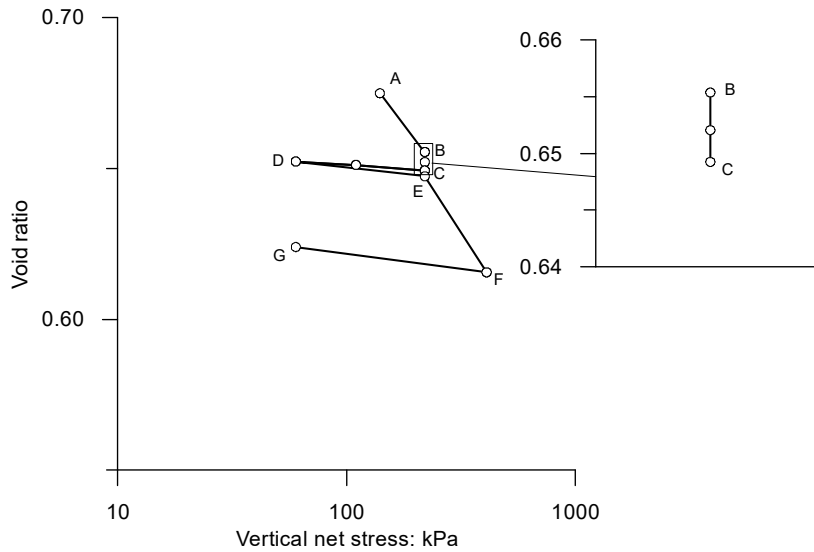
Figure 6.10 Zoom of the collapse upon wetting occurs during the controlled-suction oedometric test depicted in Figure 6.6 (b).

The doubled oedometer collapse test was proposeb by Jennings and Knight (1975) to calculate the collapse settlement using the results from two oedometric tests. In this method two specimens are placed in oedometer, one tested at constant water content (preferably at in-situ condition) and the other in saturated condition. In Figure 6.11 are depicted the two oedometric curves carried out.
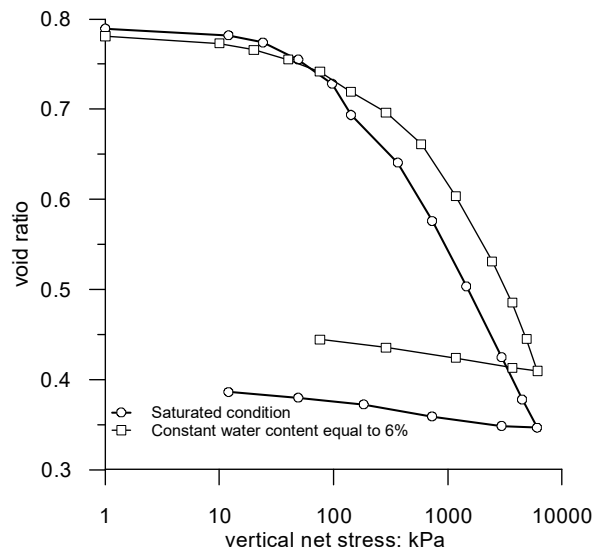
Figure 6.11 Double oedometer collapse tests; comparison between the saturated oedometric curve and the constant water content oedometric curve.

One curve refers to the constant water content test (equal to 6%), the other one is the saturated

oedometric curve also reported in Figure 6.8.

The collapse potential can be determined at any required stress level. Figure 6.12 reports a comparison

between the three curves, while in Figure 6.13 is depicted the collapse strain calculated by equations

6.1 and 6.2 at different stress levels.
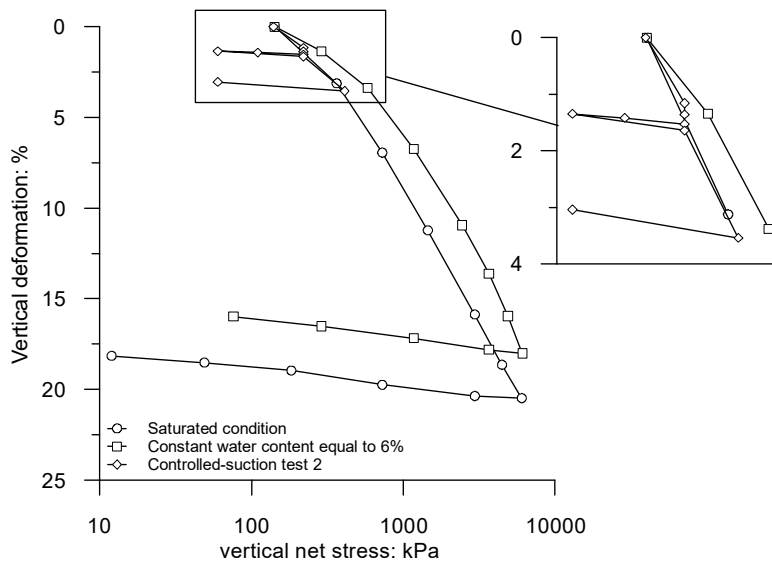
Figure 6.12 Vertical deformation vs vertical net stress.

As clearly shown in Figure 6.13, in its in-site condition (water content equal to 11%) the soil is

classified as slight collapsable (Table 6.3) (Classification of Collapse Index reported in Table 1,

ASTM D 5333-03), however, the Collapse Index increases with the water content decrease. In

particular, when the soil reaches a water content equal to 6%, the Collapse Index increases up to 2.5-

5.5% going from slight collapsible to moderate collapsible.

Table 6.3. Classification of Collapse Index from ASTM D 5333-03.

Degree of specimen Collapse	Collapse Index I_e %
None	0
Slight	0.1 to 2.0
Moderate	2.1 to 6.0
Moderately severe	6.1 to 10
Severe	>10

(a)

(b)
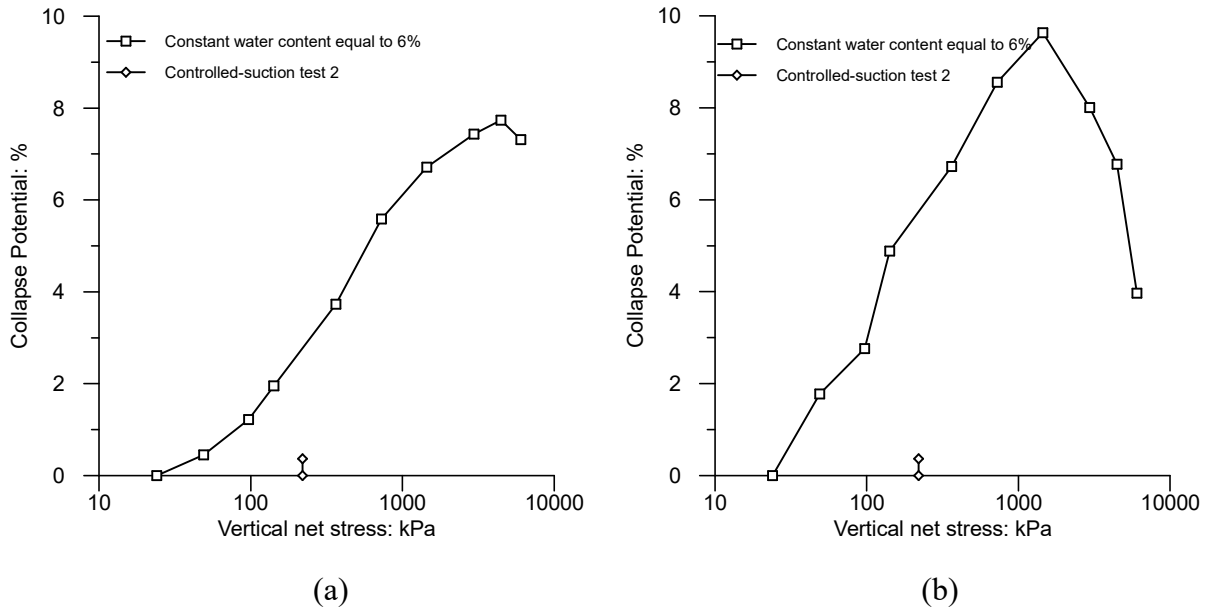
Figure 6.13 Collapse Potential – Double oedometer method: (a) Abelev (1948); (b) Jennings and Knight (1975).

6.4.3   Relative permeability function

The registration of pore water volume changes allowed determining the permeability function of the material. The hydraulic conductivity values were obtained from both wetting and drying paths, and the measured volumes were corrected to take into account the air diffusions through and water evaporation from the ceramic disc (Airò Farulla and Ferrari, 2005).

The total amount of intruded/extracted water in a suction step was expressed as follows (Kunze and Kirkham, 1962):

$$V_w(t) = \left[1 - \sum_{n=1}^{\infty} \frac{2\exp(-\alpha_n^2 D_w t / L^2)}{\alpha_n^2 (A + \csc^2 \alpha_n)} \right] V_0 \tag{6.3}$$

where V_0 is the total volume exchanged for a water pressure increments/decrement, V_w is the total volume exchanged at any time, L the specimen height, A the ratio of the impedance of the ceramic disc to the impedance of the soil $A = \dfrac{z_m}{z_s} = \dfrac{k_w e}{L k_d}$ (where e is the thickness of the ceramic disk and k_d its water permeability), and α_n the nth solution of the equation $A\alpha_n = \cot\alpha_n$ (for n=1,2,…).

The water permeability k_w is calculated from the following expression (Romero et al. 2002, Ferrari et al. 2013):

$$k_w = \frac{D_w \gamma_w V_0}{V \delta_w}$$

(6.4)

where V is the volume of the specimen.

The water volume exchanged vs time curves obtained for each suction equalization steps are depicted in Figure 6.14.

The experimental values of the water permeability in function of the degree of saturation were interpolated used the following equation:

$$k_w\left(S_r\right) = k_{w,\max} \left(\frac{S_r}{S_{r,\max}}\right)^{\zeta}$$

(6.5)

where $k_{w,\max}$ is the maximum value of the hydraulic permeability registered, $S_{r,\max}$ is the correspondent value of the degree of saturation and ζ is a fitting parameter.

The maximum value of the water permeability was carried out by mean of a conventional oedometric test in saturated condition ($k_{w,sat} = 1.3 \cdot 10^{-7}$ [m/s], $S_{r,\max} = 1$). The best-fitted value ζ was 6.2. In Figure 6.15 are depicted the measured values of the water permeability along with the fitted permeability function.

6.5 Summary and conclusion

The safety assessment of river embankments requires to consider the relevant effect of changes in suction and degree of saturation of the involved soils. In this chapter has been shown how, with a limited number of tests (two controlled-suction oedometric tests and one conventional oedometric test), it is possible to derive a comprehensive understanding of the elasto-plastic volumetric behaviour of the soil.

The suction controlled oedometric tests enabled to assess the collapse upon wetting. In fact, the tested

sandy silt has shown typical features of collapsible soils. In addition, the evolution of the yield stress

with suction was quantified and the results allowed the calibration of the constitutive model for

unsaturated soils presented in this thesis.
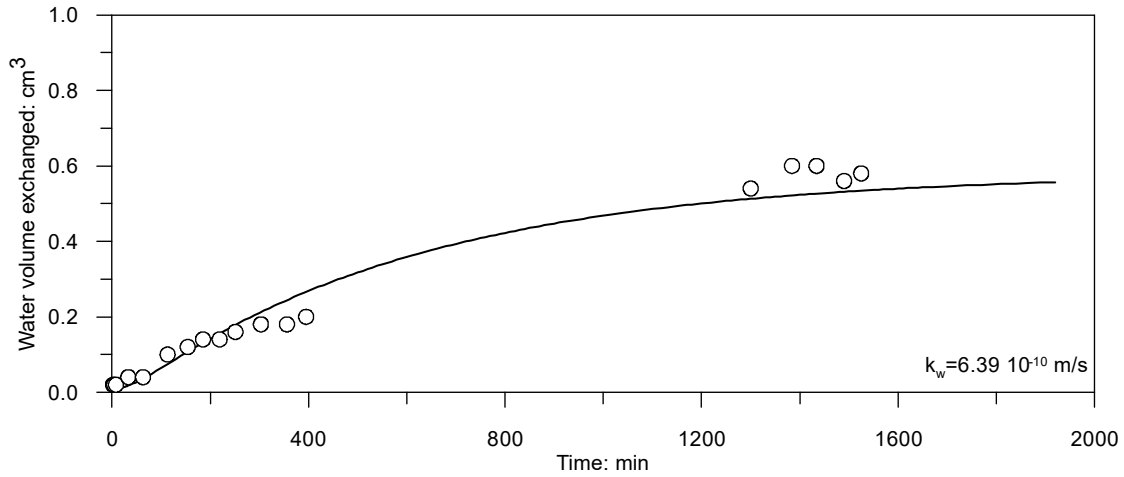
(a)
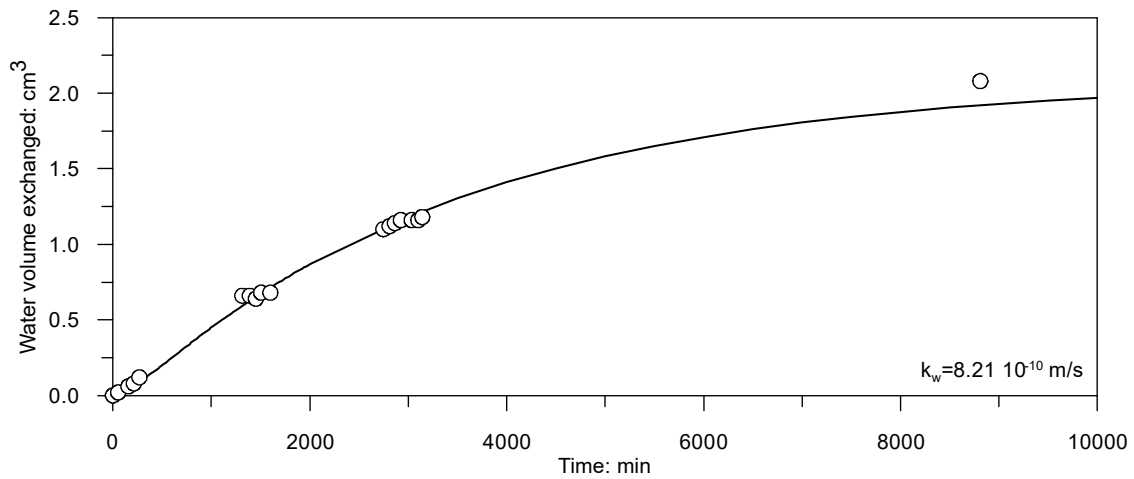
(b)
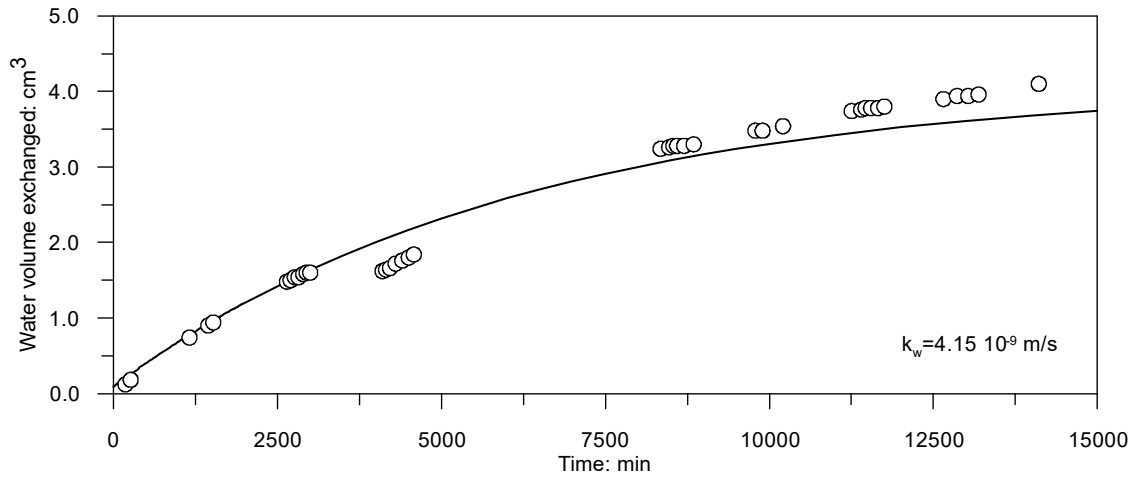
(c)
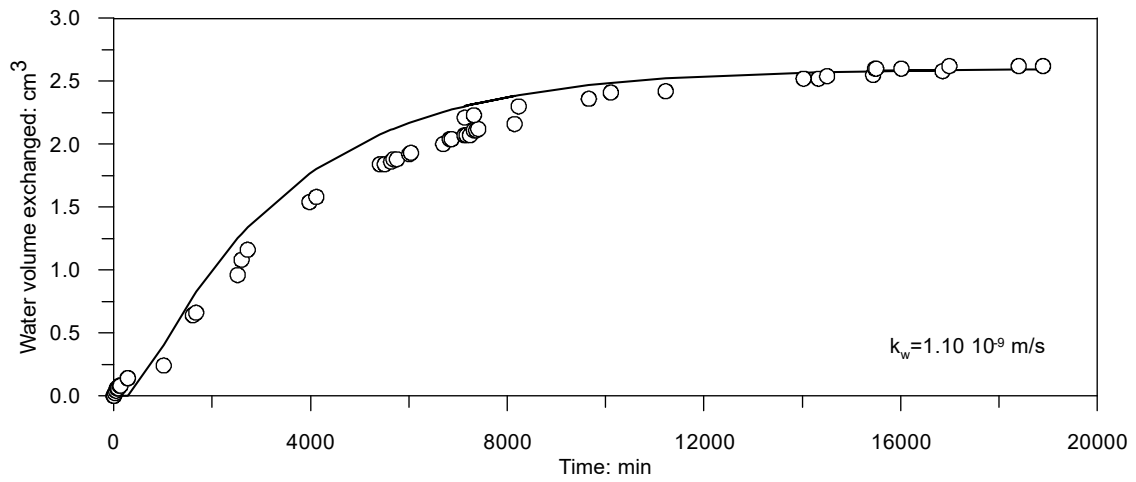
(d)

Figure 6.14 Water volume exchanged vs time: (a) controlled-suction oedometric test 1 – wetting path from 40 to 20 kPa; (b) controlled-suction oedometric test 1 – wetting path from 20 to 10 kPa; (c) controlled-suction oedometric test 1 – wetting path from 10 to 2 kPa; (d) controlled-suction oedometric test 2 – wetting path from 20 to 4 kPa.
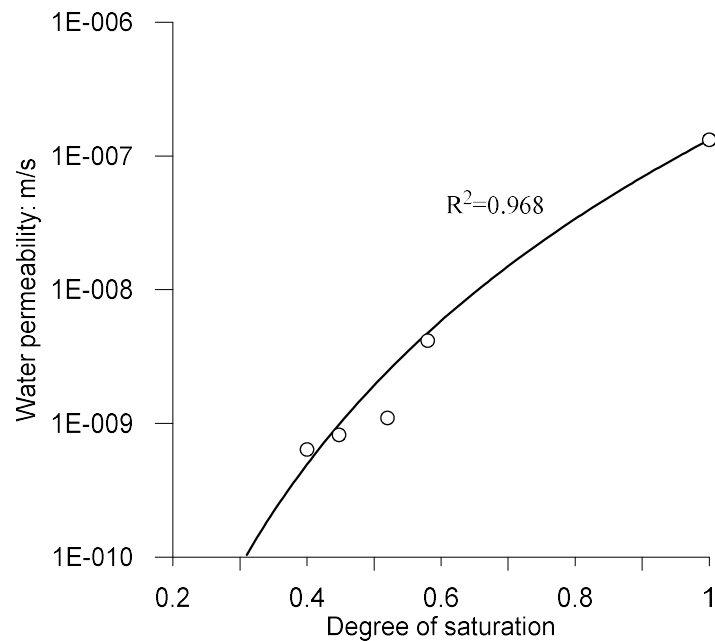
Figure 6.15 Water permeability vs. degree of saturation.

The soil characterization has shown that the river embankment is not homogeneous, but it could be defined as an alternation of silt and sandy silt, and this alternation is present also at the *"sample scale"*. Therefore, an extensive characterization was carried out and two units were identified in the explored section.

To determine the retention behaviour of the two units, expected very different one each other, various experimental technique was used, to cover the different suction range. The water retention curves showed a limited hysteretic effect and a negligible related dependence on the void ratio.

Permeability coefficient at different degrees of saturation has been determined by measuring exchanged water volume during the wetting paths of the oedometric tests. The results show that the permeability tends to be very low when the degree of saturation is in the range of what typically measured in the field, but also that it rapidly increases with the degree of saturation.

In conclusion, despite the soil of the river embankment tested in this work have proved to be potentially collapsible, the low water permeability tends to limit water content increase within the embankment. In this way the degree of saturation of the filling material is expected to undergo limited variations with the river level and only severe and persistent hydrometric peaks in association with

heavy rainfalls could cause collapse upon wetting. The monitoring of the precipitation and the river level performed before the collapse of the embankment, confirms that it was subjected to an extreme event. However, the findings of this research are particularly significant for a proper interpretation of site measurements (suction and water content monitoring) and for a reliable evaluation of the riverbank safety margins with river level fluctuations under transient flow conditions.

7. Conclusion and perspective

The understanding of the mechanics of unsaturated soils is an important component of the background for a geotechnical engineer profile. One of the most important aspects in the mechanics of partially saturated soils is represented by the volumetric behavior, where the collapse upon wetting represents the most relevant event in engineering practice.

However, the new perspective due to climate change, and the increase of the possibility that some lands will be exposed to desertification in the next years, require us to explore also the volumetric behavior when the soils approach the dry state. Consequently, the new challenges impose to adopt hydro-mechanical models able to describe the behavior of unsaturated soils in the entire range of the degree of saturation.

In this context, the investigation carried out in this thesis aimed at quantifying and understanding the volumetric response of partially saturated soils when they are subjected to very low value of the degree of saturation.

With this purpose, different materials were tested (quartz sand, Speswhite kaolin and a compacted scaly clay), in order to cover the high variability of the soils. To cover the suction range of each material different suction-control and suction-measurement techniques were used. The experimental results showed that the yield stress does not increase monotonically with suction, as provided by the classical models for partially saturated soils.

These results were also used to determine the relationship between the water retention curve and the evolution of the compressibility coefficient with suction for each material, and a new equation to model the evolution of the compressibility coefficient with suction was proposed. The new shape is able to model the experimental yield points provided for the tested material and the data provided from the literature. In addition, a strict link between the soil water retention curve and the elastic domain was demonstrated. The analysis of the new shape of the Loading-Collapse curve is consistent with the classical geomechanical point of view and it is physically correct.

To explain the evolution of the compressibility coefficient and the yield stress for the entire range of the degree of saturation at micro-scale, the evolution of Laplace pressure and capillary force of a water bridge between two grains were analysed. The high number of tests allowed also to highlight the influence of the distance between the grains on the trend of the capillary force during a drying process. The results were permitted to purpose a qualitative link between the micro- and macro-scale in order to explain the evolution of the yield stress with the suction from a physical point of view.

Finally, the new framework was used to model the behavior of natural soil from a river embankment. It was shown how, with a limited number of tests (two controlled-suction oedometric tests and one conventional oedometric test), it is possible to derive a comprehensive understanding of the elasto-plastic volumetric behaviour of the soil. The results permitted to highlight that despite the soil of the river embankment tested in this work have proved to be potentially collapsible, the low water permeability tends to limit water content increase within the embankment. In this way the degree of saturation of the filling material is expected to undergo limited variations with the river level and only severe and persistent hydrometric peaks in association with heavy rainfalls could cause collapse upon wetting.

In conclusion, the experimental work carried out in this thesis, both at macro- and micro- scale, allowed to propose a new framework to model the hydro-mechanical behaviour of unsaturated soil for the entire range of the degree of saturation. The new equation of the compressibility coefficient associated with the equation of the LC curve permits, using a very small number of tests (theoretically two tests, one saturated test, one unsaturated test and the determination of the water retention curve) to define the entire elastic domain. This result could open new scenarios in engineering practice. In fact, nowadays one of the reasons why the engineering practice does not use the elasto-plastic framework for unsaturated soils is the major number of the tests necessary to calibrate the model.

References

Abelev Y M (1948). The essentials of designing and building on microporous soil. Stroitel naya Promyshelmast 10.

Aitchison G D (1967) Generalisation and communication in modern soil engineering. Proc. Reg. Conf. Africa Soil Mech. Foundation Eng., 4th, Cape Town, 1968, 2, pp. 299-305.

Atkinson J H (1990). Discussion of session1.2. Proceedings of the conference on Engineering Geology of Weak Rock, Leeds, Cripps J M, Coulthard J M, Culshaw M G, Forester A, Hencher S R and Moon C F (eds) Balkema, Rotterdam, p. 150.

Airò Farulla C, Ferrari A (2005). Controlled suction oedometric tests: analysis of some experimental aspects. In: Proceedings of an International Symposium on Advanced Experimental Unsaturated Soil Mechanics. Edited by A. Tarantino, E. Romero, and Y.J. Cui. Trento, Italy. 27-29 June 2005. Taylor & Francis Group, London, pp. 43-48.

Airò Farulla C, Ferrari A, Romero E (2007). Mechanical behaviour of compacted scaly clay durinc cyclic controlled-suction testing. In: Schanz T (ed) Experimental unsaturated soil mechanics, Springer proceedings in physics, vol 112. Springer, Berlin, pp 345-354.

Airò Farulla C, Ferrari A, Romero E (2010). Volume change behaviour of a compacted scaly clay during suction changes. Can. Geotechnic. J. 47(6): 688-703.

Airò Farulla C, Rosone M (2011). Microstructure characteristics of unsaturated compacted scaly clay. In: Mancuso C, Jommi C, D'Onza F (eds) Unsaturated soils: research and applications. Springer, Berlin, pp 123-130.

Airò Farulla C, Battiato A, Ferrari A (2010). The void ratio dependency of the retention behaviour for a compacted clay. In: 5th International Conference on Unsaturated Soils . Edited by EE Alonso & A Gens. Barcelona, Spain, 6-8 September 2019. Taylor & Francis Group, London, pp. 417-422.

Alonso E E (1998). Modelling expansive soil behaviour. Keynote lecture, Proc. II Int. Conf. on Unsaturated Soils, UNSAT '98, Beijing, China, vol. 2, pp. 37-70.

Alonso E E, Gens A, Gehling W Y Y (1994). Elasto-plastic model for unsaturated expansive soils - Proc. 3th Eur. Conf. Num. Meth. Geot. Eng., Manchester, 1, pp. 11-18.

Alonso E E, Gens, A, High D W (1987). Special problem soils. General report. Proc. 9th European Conf. Soil Mech. Fdn Engng, Dublin, 3, 1087-l 146.

Alonso E E, Gens A and Josa A (1990). A constitutive model for partially saturated soils. Géotechnique 40, No 2, 405-430.

Alonso E E, Pereira J M, Vanaut J, Olivella S (2010). A microstructurally based effective stress for unsaturated soils. Géotechnique, 60(12):913-925.

ASTM Standard D-5333 (2003). Standard Test Methods for Measurement of Collapse Potential of Soils. Annual Book of ASTM Standards, ASTM International, West, Conshohocken, PA.

Bishop A W (1959). The principle of effective stress. Tecnisk Ukeblad, 39: pp. 859-863.

Bishop A W, Blight G E (1963). Some aspects of effective stress in saturated and partly saturated soils. Géotechnique, 12:177-197

Bishop A W, Donald I B (1961). The experimental study of partially saturated soil in the triaxial apparatus. 5th Int. Conf. Soil Mech., Paris, France, pp:13-22.

Blight G E (1965). A study of effective stresses for volume change. Proc. symposium in print Moisture Equilibria and Moisture Changes in Soils Beneath Covered Areas, Aitchinson, G.D. ed, Butterworths, Australia, pp. 259-269.

Boone S J (2010). A critical reappraisal of "preconsolidation pressure" interpretation using oedometer test. Can. Geotechnic. J. 47(3): 281-296.

Briceno S, Basabe P, Bonnard C (2007). Landslides and climate change: a world perspective, but a complex question. International conference on Landslides and Climate Change, 3-6.

Brooks R H, Corey A T (1964). Hydraulic properties of porous media. Hydrology Paper No. 3, Colorado State University, Fort Collins, Colo.

Buisson M S R, Wheeler S J (2000). Inclusion of hydraulic hysteresis in a new elasto-plastic framework for unsaturated soils. Proc. of an International Workshop on Unsaturated Soils, Trento.

Burland J (1965). Some aspects of the mechanical behaviour of partly saturated soils. In: G.D., A. (Ed.), Moisture Equilibria and Moisture Changes in the Soil Beneath Covered Areas, Australia. Butterworths.

Butt H-J, Kappl M (2009). Normal capillary forces. Adv Colloid Interface Sci, 146:48-60.

Casagrande A (1936). The determination of the preconsolidation load and its practical significance. In proceedings of the First International Conference on Soil Mechanics and Foundation Engineering, Cambridge, Mass, 3:60-64.

Collins I F, Hilder T (2002). A theoretical framework for constructing elastic/plastic constitutive models of triaxial tests. Int J Numer Anal Meth Geomech 26:1313–1347.

Collins I F, Houlsby G T (1997). Application of thermomechanical principles to the modelling of geotechnical materials. Proc R Soc Lond A 453:1975–2001.

Coop M R, Lee I K (1993). The behaviour of granular soil at elevated stresses. In: Proceedings of the C. P. Wroth Memorial Symposium: Predictive soil mechanics, London, pp:186-198.

Cornelis W M, Ronsyn J, Van Meirvenne M, Hartmann R (2001). Estimation of water retention curve of granular soils from particle-size distribution – a Bayesian probabilistic approach. Canadian Geotechnical Journal, 49, 1024-1035.

D'Alpaos L, Brath A, Fioravante V, Gottardi G, Mignosa P, Orlandini S (2014). Relazione tecnico-scientifica sulle cause del collasso dell'argine del fiume Secchia avvenuto il giorno 19 gennaio 2014 presso la frazione San Matteo.

Dehn M, Burger G, Buma J, Gasparetto P (2000). Impact of climate change on slope stability using expanded downscaling. Engineering Geology, 53(3):193-204.

Dixon N, Dijkstra T, Forster A, Connel R (2006). Climate change impact forecasting for slopes (CLIFFS) in the built environment. 10th IAEG International Congress. Geological Society of London.

Donald I B (1956). Shear strength measurements in unsaturated non-cohesive soils with negative pore pressure. 2nd Australia – New Zealand Conference Soil Mechanics Found Eng. Christchurch, New Zealand pp. 200-205

Escario V, Juca J E T (1989). Strength and deformation of partly saturated soils. Proc. 12th Int. Conf. Soil Mech. Found. Eng., Rio de Janeiro, 1, pp. 43-46.

Ferrari A, Airò Farulla C, Romero E (2010). On the volumetric response of a compacted clay subjected to wetting and drying cycles. In: Unsaturated soils: theoretical and numerical advances in unsaturated soil mechanics – Proceedings of the 4th Asia Pacific conference on unsaturated soils, pp 89-94.

Ferrari A, Eichenberger J, Laloui L (2013). Hydromechanical behaviour of a volcanic ash. Géotechnique, 63(16):1433-1446.

Fisher R A (1926). On the capillarity forces in an ideal soil; correction of formulae given by W. B. Heines, J. Agric. Sci., 16:492-505.

Frost J D, Park J-Y (2003). A critical assessment of the moist tamping technique. J. Geotechnical Testing 26 (1).

Gallipoli D, Gens A, Sharma R, Vaunat J (2003). An elasto-plastic model for unsaturated soil incorporating the effects of suction and degree of saturation on mechanical behaviour. Géotechnique, 53(1):123-136.

Geiser F (1999). Comportement mécanique d'un limon non saturé. Etude Expérimentale et modélisation constitutive. Thèse de Doctorat, École Polytechnique Fédérale de Lausanne.

Gens A (1996). Constitutive modelling: application to compacted soil. Unsaturated soils, vol 3. Balkema, Rotterdam, pp 1179–120.

Gens A, Alonso E E (1992). A framework for the behaviour of unsaturated expensive clays. Canadian Geotechnics 29, 1013-1032.

Gens A, Sanchez M, Sheng D (2006). On constitutive modelling of unsaturated soils. AG 1, 137–147.

Georgiadis K, Potts D, Zdravkovic L. (2005). Three-Dimensional Constitutive Model for Partially and Fully Saturated Soils. International Journal of Geomechanics. (DOI: 10.1061/(ASCE)1532-3641(2005)5:3(244)).

Gragnano C G, Bertolini I, Rocchi I, Gottardi G (2019). On the Stability of a Fully Instrumented River Embankment Under Transient Conditions. 7th Italian National Congress of Geotechnical Researchers.

Gragnano C G, Gottardi G, Moscariello M, Cuomo S, Rocchi I (2018). Laboratory measurement of the mechanical and retention properties of a river embankment silty soil in partially saturated condition. 7th Inter. Conf. Unsat. Soils.

Gruber S, Haeberli W (2007). Permafrost in steep bedrock slopes and its temperature-related destabilization following climate change. Journal of Geophysical research 112:F02S18.

Gottardi G, Gragnano C G, Rocchi I, Bittelli M (2016). Assessing river embankment stability under transient seepage conditions. Procedia Engineering, 158: 350-355.

Hamblin A P (1981). Filter paper method for routine measurement of field water potential. J Hydrol, 53:355-360.

Harris C (2005). Climate change, mountain permafrost degradation and geotechnical hazard. Advances in Global Change Research 23(II):215-224.

Heines W D (1926). Studies of the physical properties of soils. II. A note on the cohesion developed by capillarity forces in an ideal soil. J. Agric. Sci, 15:529-535.

Hu L B, Hueckel T, Peron H, Laloui L (2008). Desiccation shrinkage of unconstrained soil in the saturated phase. In Unsaturated Soils: Advances in Geo-Engineering, proceedings of the First European Conference on Unsaturated Soils (E-UNSAT 2008), Durham, UK, 2-4 July 2008. Edited by Toll D G , Augarde C, Gallipoli D and Wheeler S. CRC press, Taylor and Francis Group, Boca Raton, Fla., 653-658.

Hu L B, Hueckel T, Peron H, Laloui L (2009). Desiccation shrinkage and its controlling properties: multiphysics. In Proceedings of the International Conference on Computational Methods for Coupled Problems in Science and Engineering (Coupled Problems 2009), Ischia Island, Italy, 8-10 June 2009. Edited by Schrefler B, Onate E and Papadrakis M. CIMNE, Barcelona, Spain.

Hu R, Liu H-H, Chen Y, Zhou C, Gallipoli D (2014). A constitutive model for unsaturated soils with consideration of inter-particle bonding. Computers and Geotechnics, 59:127-144.

Huang J, Ji M, Xie Y, Wang S, He Y, Ran J (2015). Global semi-arid climate change over last 60 years. Clim. Dyn, 46:1131-1150.

Huggel C, Salzmann N, Allen S, Caplan-Auerbach J, Fisher L, Haeberli W, Larsen C, Schneider D, Wessels R (2010). Recent and future warm extreme events and high-mountain slope stability. Philosophical Transactions of the Royal Society A 268:2435-2459.

Hujeux J C (1979) Calcul numérique de problèmes de consolidation élastoplastique. PhD Thesis, Ecole Centrale de Paris.

Hwang S I, Yun E Y, Ro, H M (2011). Estimation of soil water retention function based on asymmetry between particle-and pore-soze distributions. European Journal of Soil Science, 62, 195-205.

Hwang S I, Choi S I (2006). Use of a lognormal distribution model for estimating soil water retention curves from particle-size distribution data. Journal of Hydrology, 323, 325-334.

Israelachvili J (1992). Intermolecular and Surface Forces. Accademic press, San Diego, USA.

Kosugi K (1994). Three-parameter lognormal distribution model for soil water retention. Water Resources Research, 30, 891-901.

Jommi C (2000). Remarks on the constitutive modelling of unsaturated soils. Experimental evidence and theoretical approaches in unsaturated soils. Balkema, Rotterdam, pp 139–153

Jennings J E, Knight K (1975). A guide to construction on or with materials exhibiting additional seattlement due to collapse of grain structure. 6th Regional Conference for Africa on Soil Mechanics and Foundation Engineering, Durban, September 1975, South Africa: 99-105.

Josa A, Alonso E, Lloret A, Gens A (1987). Stress-strain behaviour of partially saturated soils. In: IX Eur. Conf. Soil Mech. Found. Eng., Dublin. Vol. 2.

Kunze R J, Kirkham D (1962). Simplified accounting for membrane impedance in capillary conductivity determinations. Soil Sci. Soc. Am. Proc., 26: 421-426.

Laloui L, Ferrari A, Eichenberger J (2010). Effect of climate change on landslide behaviour. GEO-STRATA.

Leroueil S, Barbosa P S (2000). Combined effect of fabric, bonding and partial saturation on yielding of soils. In: Unsaturated soils for Asia. Proceedings of the Asian Conference on Unsaturated Soils, UNSAT-Asia 2000, Singapore, 18-19 May, 2000.

Liang G, Thornton C, Adams M J (1992). A theoretical study of the liquid bridge forces between two rigid spheres. Journal of Colloid Interface Science, 161:138-147.

Lins Y, Schanz T (2005). Determination of hydro-mechanical properties of sand Unsaturated Soils: Experimental Studies. Springer Proceedings in Physics (Ed T. Schanz) 93, Springer, Berlin, Heidelberg.

Loret B, Khalili N (2002). An effective stress elastic plastic model for unsaturated porous media. Mechanics of Materials 34, 97–116.

Maatouk A, Leroueil S, La Rochelle P (1995). Yielding and critical state of a collapsible unsaturated silty soil. Géotechnique, 45(3):465-477.

McDowell G R, Bolton M D (1998). On the micromechanics of crushable aggregates. Géotechnique, 48(5):667-679.

McInnes R, Jakleways J, Fairbank H, Mathie E (eds) (2007). Landslides and Climate change: International Conference on Landslides and Climate Changes, Taylor & Francis, UK.

Mesri G, Vardhanabhuti B (2009). Compression of granular materials. Can. Geotech. J. 46:369-392.

Mielniczuk B, Hueckel T, El Youssoufi M S (2014a). Evaporation-induced evolution of the capillary force between two grains. Granul. Matter, 16:815-828.

Mielniczuk B, El Youssoufi M S, Sabatier L, Hueckel T (2014b). Rupture of a liquid bridge between two grains due to its evaporation. Acta Geophys., 62:1087-1108.

Mielniczuk B, Hueckel T, El Youssoufi M S (2015). Laplace pressure evolution and four instabilities in evaporating two-grain liquid bridge. Powder Technology 283:137-151.

Molenkamp F, Nazemi AH (2003). Interactions between two rough spheres, water bridge and water vapor. Geotechnique, 53(2):255–264.

Mualem Y (1986). Hydraulic conductivity of unsaturated soils: prediction and formulas. Methods of soil analysis. No.9, Part 1. Edited by Klute A. American Society of Agronomy, Madison, Wisc. 799-893.

Nakata Y, Hyodo M, Hyde A F L, Kato Y, Murata H (2001). Microscopic particle crushing of sand subjected to high pressure one dimensional compression. Soil and Foundation 41(2):39-51.

Nuth M, Laloui L (2007). New insight into the unified hydromechanical constitutive modelling of unsaturated soils. In Proceedings of the 3rd Asian conference on unsaturated soils (UNSAT-Asia), (eds Z. Z. Yin, Y. P. Yuan and A. C. F. Chiu), pp. 109–25.

Nuth M, Laloui L (2008a). Effective stress concept in unsaturated soils: clarification and validation of a unified framework. Int. J. Numer. Anal. Methods Geomech. 32:771–801.

Nuth M, Laloui L (2008b). Advances in modelling hysteretic water retention curve in deformable soils. Comput. Geotech. 35 (6), 835–844.

Nuth M, Laloui L, Schrefler A (2010). Analysis of compaction phenomena due to water injection in reservoirs with a three-phase geomechanical model. Journal of petroleum Science and Engineering (73), 33–40.

Oertli J J (1971). The stability of water under tension in the xylem. Z. Pflanzenphysiol, 65:195-209.

Oliviero V (2016). Analisi della risposta idro-meccanica di terreni costipati di un argine del medio corso del fiume Po. Università degli Studi di Napoli, Federico II, Italy. Ph.D. thesis.

Pacheco Silva F (1970). A new graphical construction for determination of the preconsolidation stress of a soil sample. In Proceedings of the 4th Brazilian Conference on Soil Mechanics and Foundation Engineering, Rio de Janeiro, August 1970. 2(1):225–232 [in Clementino 2005].

Perrier E, Bird N G, Rieu M (1999). Generalizing the fractal model of soil structure: The pore-solid fractal approach. Geoderma 88(3-4):137-164.

Peron H (2008). Desiccation cracking of soils. Ph.D. thesis, Ecole Polytechnique Fédérale de Lausanne, Lausanne, Switerland.

Peron H, Laloui L, Hueckel T, Hu, L B (2009). Desiccation cracking of soils. European Journal of Environmental and Civil Engineering, 13:869-888.

Raghunandan M E, Juneja A, Benson Hsiung B C (2012). Preparation of reconstituted sand samples in the laboratoty International Journal of Geotechnical Engineering (6):125-131.

Rampino C, Mancuso C, Vinale F (2000). Experimental behaviour and modelling of an unsaturated compacted soil. Can. Geotechnic. J. 37:748-763.

Reynolds J F, Smith D M, Lambin E F, Turner BL 2nd, Mortimore M, Batterbury, Downing T E, Dowlatabadi H, Fernàndez R J, Herrick J E, Huber-Sannwald E, Jiang H, Leemans R, Lynam T, Maestre F T, Ayarza M, Walker B (2007). Global desertification: building a science for dryland development. Science 316:847-851.

Richefeu V, El Youssoufi M S, Azéma E, Radjai F (2009). Force transmission in dry and wet granular media. Powder Technol. 190: 258-263.

Roscoe K H, Burland J B (1968). On the generalized stress-strain behaviour of wet clay. In: Heymann G, Leckie F A, editors. Engineering Plasticity. Cambridge, UK: Cambridge University Press; pp. 535-609.

Rosone M, Airò Farulla C, Ferrari A (2016). Shear strength of a compacted scaly clay in variable saturation conditions. Acta Geotechnica 11:37-50.

Romero E, Alonso E E, Knobelsdorf J (2002). Laboratory tests on compacted sand-bentonite buffer material for the GMT emplacement project. NAGRA Project Report 02-05. Wenningen, Switzerland: NAGRA.

Romero E, Della Vecchia G, Jommi C (2011). An insight into the water retention properties of compacted clayey soils. Géotechnique, 61(4):313-328.

Romero E, Vaunat J (2000). Retention curves in deformable clays. In: Tarantino A, Mancusi C (eds) Experimental evidence and theoretical approaches in unsaturated soils. Proceedings of the international workshop on unsaturated soils, Trento. Balkema, Rotterdam, pp: 91-106.

Schaap M G, Leij F J, Van Genuchten M T (1998). Neural network analysis for hierarchical prediction of soil hydraulic properties. Soil Science Society of America Journal, 62, 847-855.

Sharma R S (1998). Mechanical behaviour of unsaturated highly expansive clays. University of Oxford, England. Ph.D. thesis.

Sheng D, Sloan S W, Gens A (2004). A constitutive model for unsaturated soils: thermomechanical and computational aspects. Comput Mech 33:453–465.

Sivakumar V (1993). A critical state framework for unsaturated soil. PhS Thesis, University of Sheffield.

Sivakumar V, Sivakumar R, Murray E J, Mackinnon P, Boyd J (2010). Mechanical behaviour of unsaturated kaolin (whit isotropic and anisotropic stress history). Part 1: wetting and compression behaviour. Géotechnique, 60(8):581-594.

Soulié F, Cherblanc F, El Youssoufi M S, Saix C (2006). Influence of liquid bridges on the mechanical behaviour of polydisperse granular materials. Int. J. Numer. Anal. Methods Geomech, 30:213-228.

Sun D A, Matsuoka H, Cui H B, Xu Y F (2003). Three-dimensional elasto-plastic model for unsaturated soil whit different initial densities. Int. J. Numer. Anal. Meth Geomech., 27, 1079-1098 (DOI: 10.1002/nag.313).

Sun D A, Matsuoka H, Yao Y P, Ichihara W (2000). An elasto-plastic model for unsaturated soil in three dimensional stresses. Soil and Foundations 40, No 3, 17-28, June 2000.

Sun, D A, Sheng D C, Sloan SW (2007). Elastoplastic modelling of hydraulic and stress-strain behaviour of unsaturated compacted soils. Mechanics of Materials, 39(3), 212-221.

Sun W, Sun D, Li J (2010). Elastoplastic modelling of hydraulic and mechanical behaviour of unsaturated expansive soils. ASCE.

Tarantino A (2003). Basic concepts in the mechanics and hydraulics of unsaturated geomaterials. In: Laloui L(eds) Mechanics of Unsaturated Geomaterials. John Wiley & Sons Inc., Hoboken, 3-27.

Tarantino A, De Col E (2008). Compaction behaviour of clay. Géotechnique, 58(3):199-213.

Tarantino A, Tombolato S (2005). Coupling of hydraulic and mechanical behaviour in unsaturated compacted clay. Géotechnique, 55(4):307-317.

Terzaghi K (1936). The shearing resistance of saturated soils and the angle between the planes of shear. International Conference on Soil Mechanics and Foundation Engineering, Harvard University Press: pp. 54-56.

Terzaghi K, Peck R B, Mesri G (1996). Soil mechanics in engineering practice. John Wiley & Sons, Inc., New York, USA.

Thu T M, Rahardjo H, Leong E, (2007) Soil water characteristic curve and consolidation behaviour for a compacted silt. Can. Geotechnic. J. 44:226-275.

Toll D G, Mendes J, Hughes P N, Glendinning S, Gallipoli D (2012). Climate change and the role of unsaturated soil mechanics. Geotechnical Engineering Journal of the SEAGS & AGSSEA, 43 (1):76-82.

Van Genuchten MT (1980). A closed-form equation for predicting the hydraulic conductivity of unsaturated soil. Soil Sci Soc Am J, 44(5): 892-898.

Vardon P J (2014). Climatic influence on geotechnical infrastructure: a review. Journal of environmental Geotechnics, 2(3).

Vaughan P R (1985). Mechanical and hydraulic properties of in situ soils-general report. Proceedings of the 1st International Conference on Geomechanics in Tropical Lateritic and Saprolitic Soils, Singapore, Brasilia, Brasilian Society for Soil Mechanics, Vol. 3, pp. 231-63.

Vaughan P R (1988). Characterising the mechanical properties of the in-situ residual soil.. Proceedings of the 2nd International Conference on Geomechanics in Tropical Soils, Singapore, Balkema, Rotterdam, Vol. 2, pp. 469-87.

Vaughan P R (1990). Discussion of session1.2. Proceedings of the conference on Engineering Geology of Weak Rock, Leeds, Cripps J M, Coulthard J M, Culshaw M G, Forester A, Hencher S R and Moon C F (eds) Balkema, Rotterdam, p. 149.

Vaunat J, Romero E, Jommi C (2000). An elastoplastic hydro-mechanical model for unsaturated soils. International Workshop on Experimental Evidence and Theoretical Approaches in Unsaturated Soils, Trento, 10-12 aprile 2000, 121-138.

Vilar O M, Rodrigues R A (2011). Collapse behavior of soil in a Brazialn region affected by rising water table. Can. Geotechnic. J. 48:226-233.

Wheeler S J (1996). Inclusion of specific water volume within an elasto-plastc model for unsaturated soils. Canadian Geotech. Journ., 33(1), pp. 42-57.

Wheeler S J, Sharma R S, Buisson M S R (2003). Coupling of hydraulic hysteresis and stress–strain behaviour in unsaturated soils. Géotechnique 53(1): 41-54.

Wheeler S J, Sivakumar V (1995). An elasto-plastic critical framework for unsaturated soil. Geotechnique 45, No 1, 35-53.

Willet Ch D, Adams M J, Johnson S A, Seville J P K (2000). Capillary bridges between two spherical bodies. Langmuir, 16:9396-9405.

Witteveen P, Ferrari A, Laloui L (2013). An experimental and constitutive investigation on the chemo-mechanical behaviour of a clay. Geotechnique, 63(3):244-255.

Young T (1805). An essay on the cohesion of fluids. Philos. Trans. Roy. Soc. London 95, 65.

Zhou A N, Sheng D, Sloan S W, Gens A (2012a). Interpretation of unsaturated soil behaviour in the stress-saturated space I: Volume change and water retention behaviour. Computer and Geotechnics 43, 178-187.

Zhou A N, Sheng D, Sloan S W, Gens A (2012b). Interpretation of unsaturated soil behaviour in the stress-saturated space II: Constitutive relationships and validation. Computer and Geotechnics 43, 111-123.

Zhou A, Wu S, Li J, Sheng D (2018). Including degree of capillary saturation into constitutive modelling of unsaturated soils. Computer and Geotechnics 95, 82-98.

Appendix A: Chapter 3
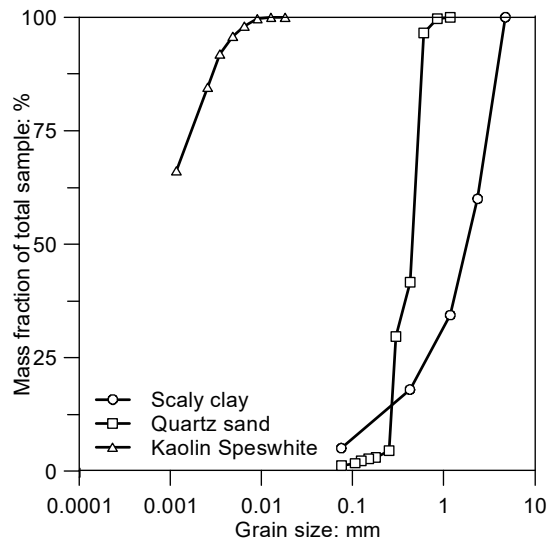
Figure A1. Grain size distribution of the tested materials.

(a)
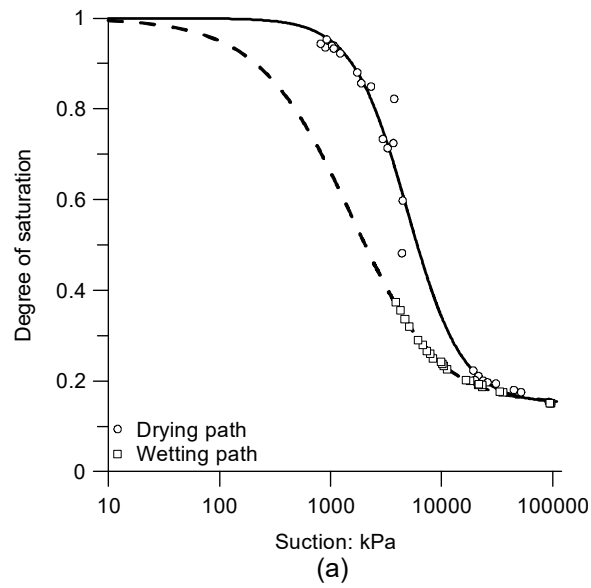
KAO04 – e=0.75	α[1/kPa]	n	m	$S_{r,res}$
Main Drying	0.0002	1.75	1.00	0.15
Main Wetting	0.0005	2.78	0.46	0.15

(b)
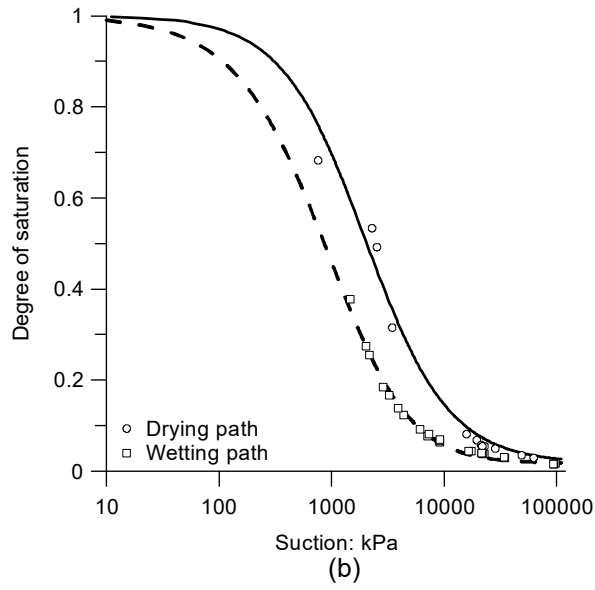
KAO05 – e=1.05	α[1/kPa]	n	m	$S_{r,res}$
Main Drying	0.0005	1.17	1.00	0.02
Main Wetting	0.0007	3.45	0.46	0.02

(c)
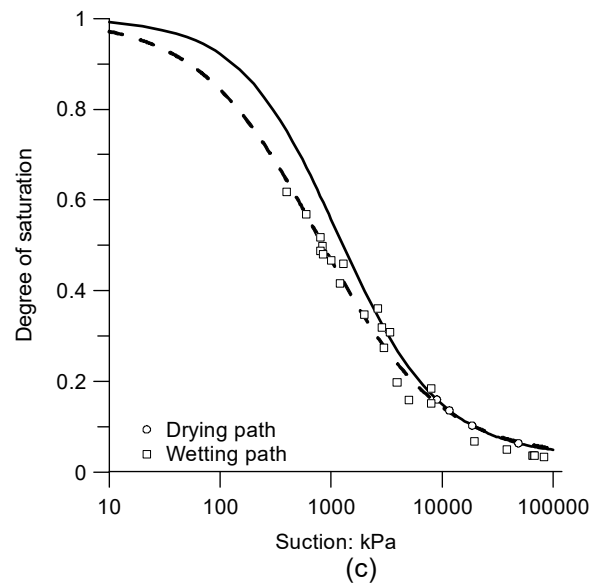
KAO20 – e=1.35	α[1/kPa]	n	m	$S_{r,res}$
Main Drying	0.001	1.11	0.80	0.03
Main Wetting	0.001	0.80	1.00	0.03

(d)
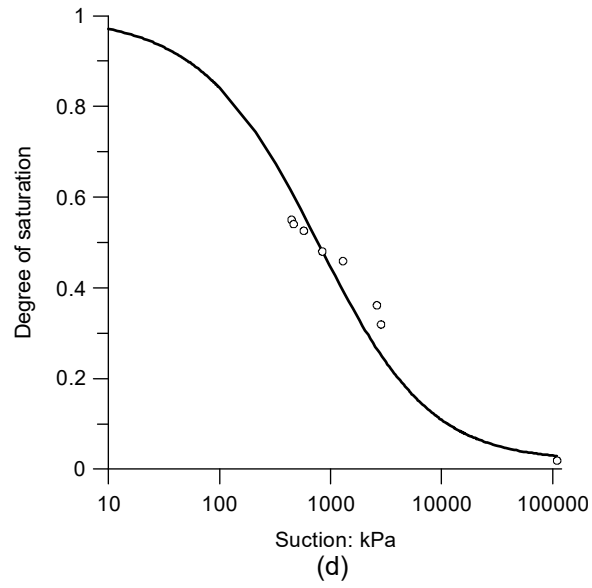
KAO08 – e=1.50	α[1/kPa]	n	m	$S_{r,res}$
Main Drying	0.001	0.80	1.2	0.02

(e)
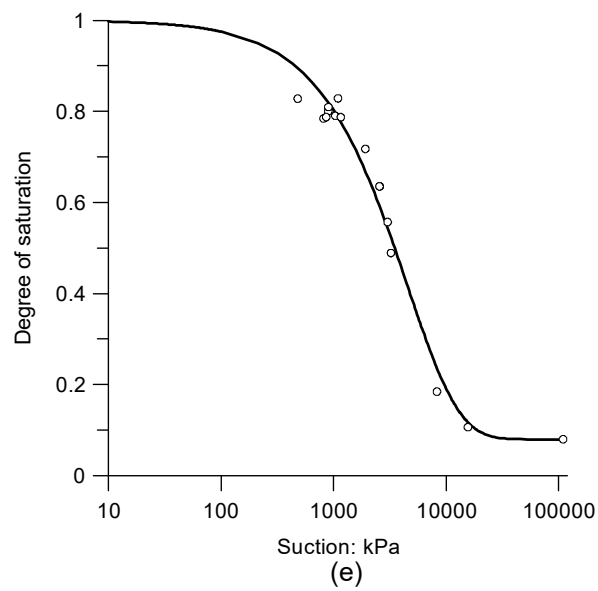
KAO09 – e=0.90	α[1/kPa]	n	m	$S_{r,res}$
Main Drying	1.9E-6	0.95	89.90	0.08

(f)
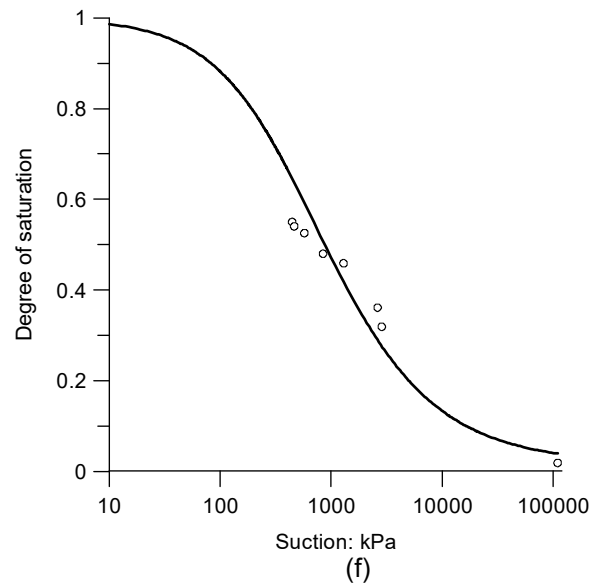
KAO11 – e=1.65	$\alpha[1/kPa]$	n	m	$S_{r,res}$
Main Drying	0.002	1.00	0.70	0.04

Figure A2. Soil water retention behavior of Speswhite kaolin for different reference void ratio.
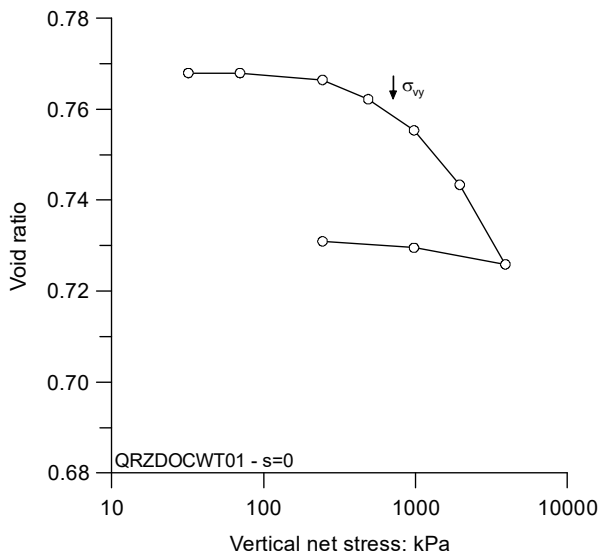
(a)
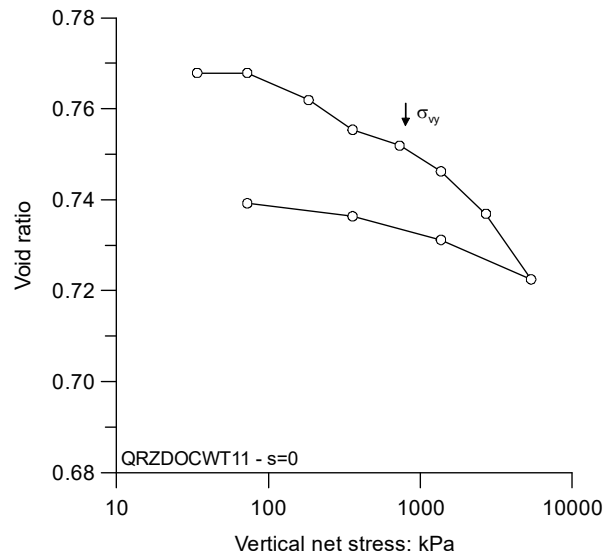
(b)
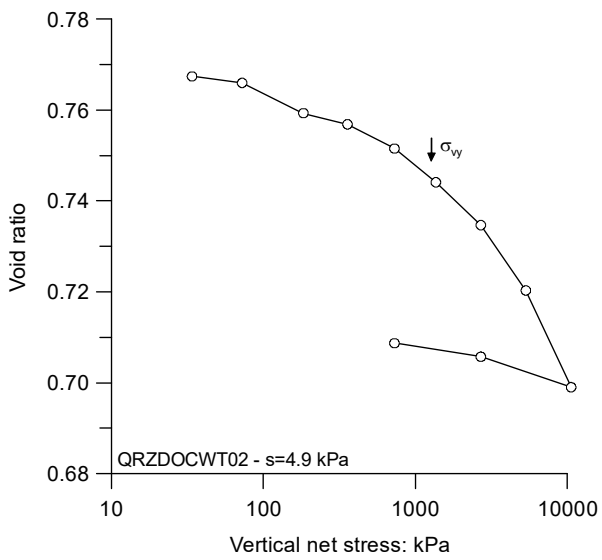
(c)
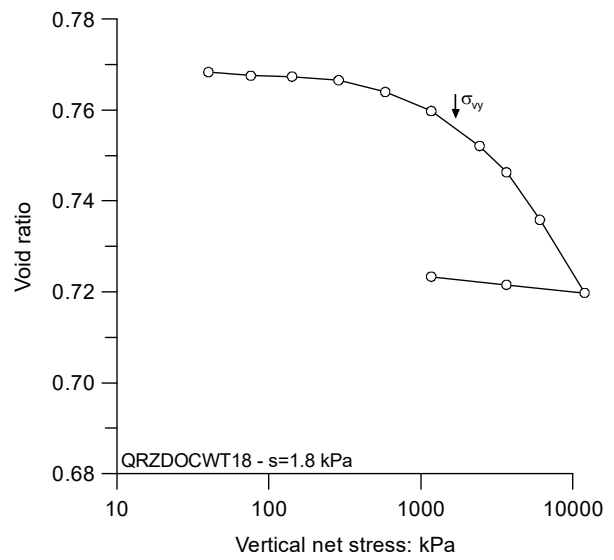
(d)
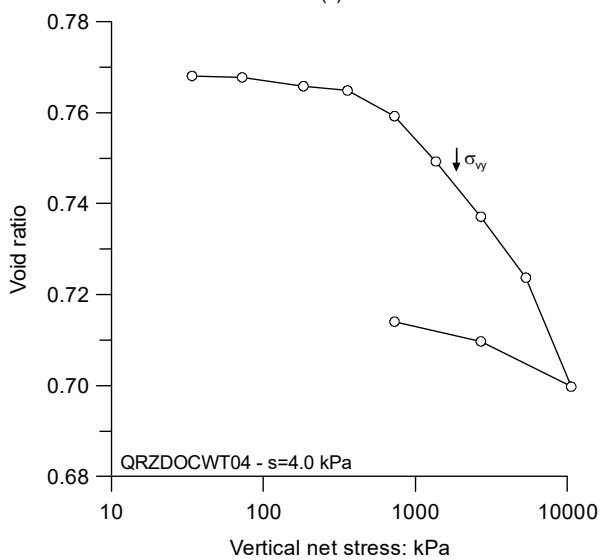
(e)
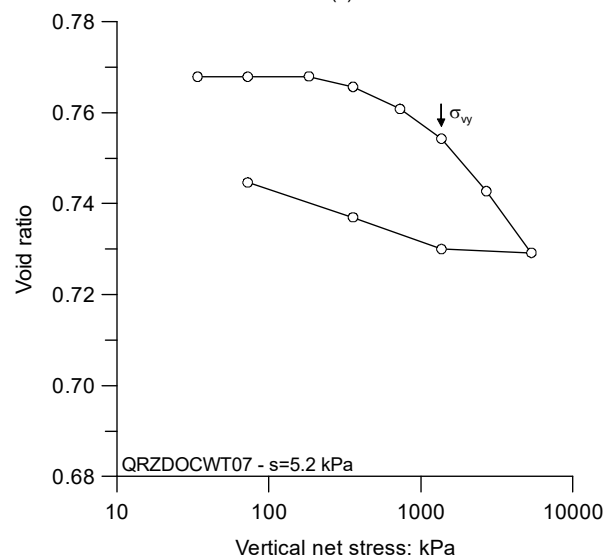
(f)
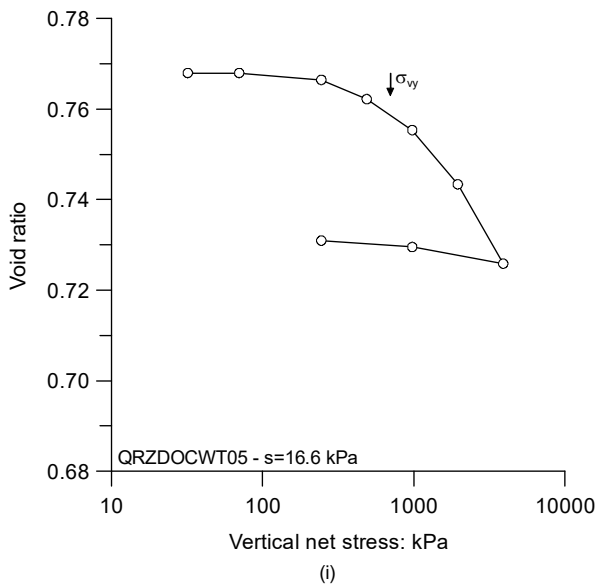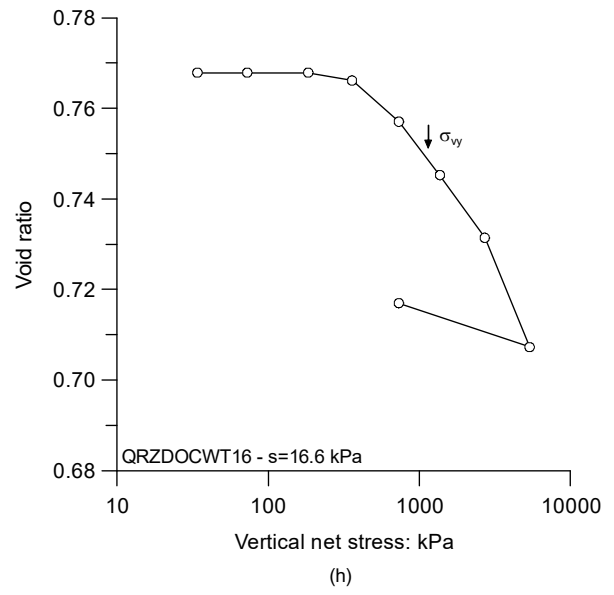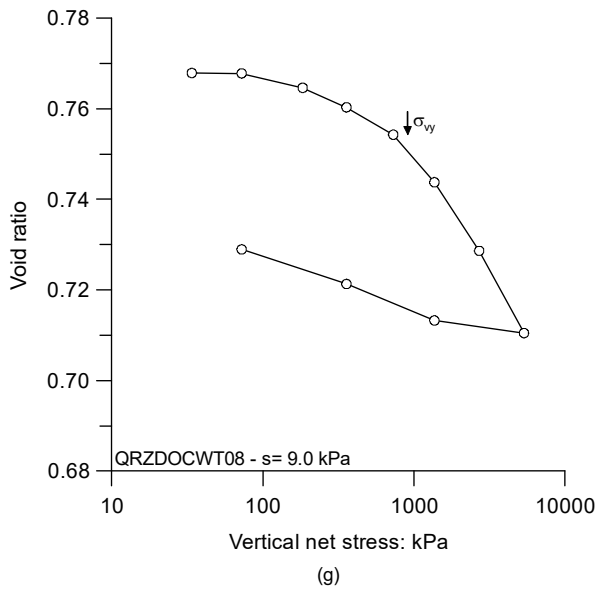
Figure A3. Controlled-suction oedometric curves operating with the negative water column

technique performed on quartz sand.

(a)

(b)

(c)

(d)

(e)

(f)

QRZDOC07 - s=16.6 kPa

(g)

QRZDOC08 - s=0

(h)

QRZDOC23 - s=2.9 kPa

(i)

QRZDOC27 - s=0

(l)

QRZDOC28 - s=4.2 kPa

(m)

QRZDOC32 - s=4.3 kPa
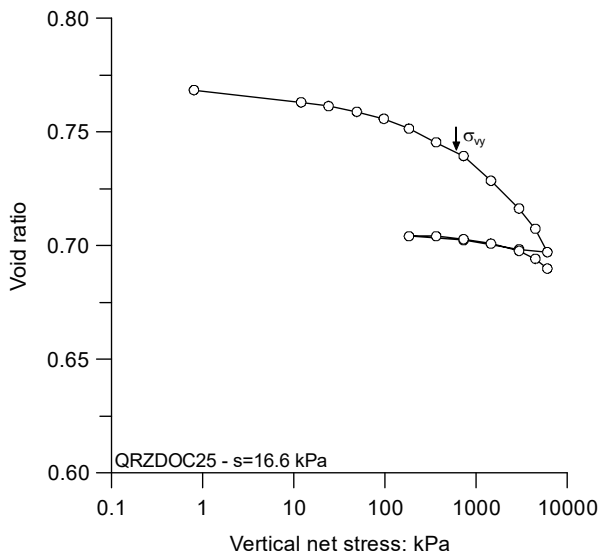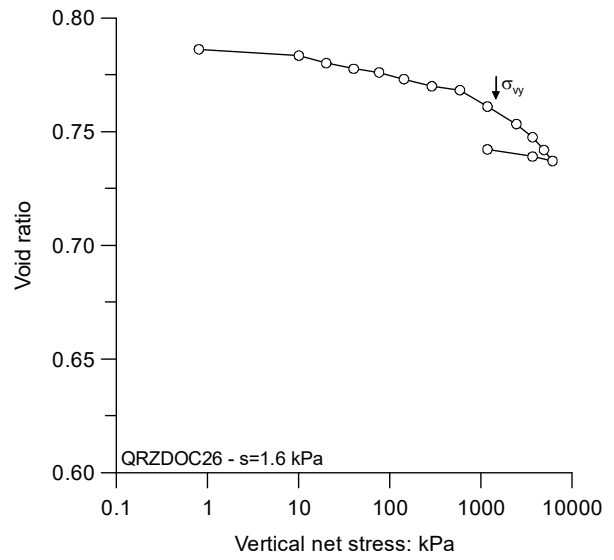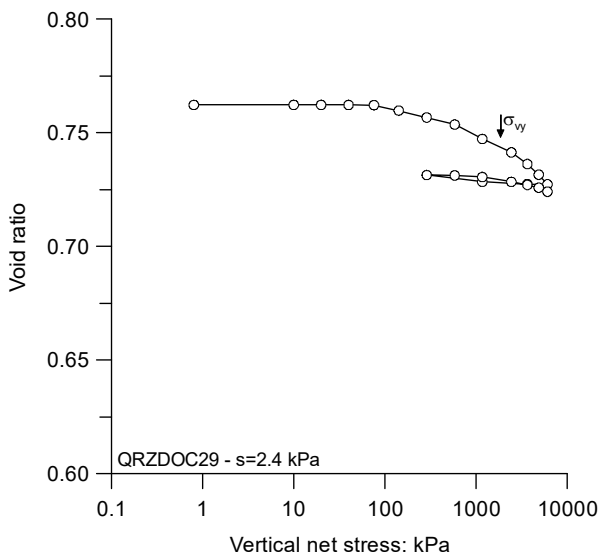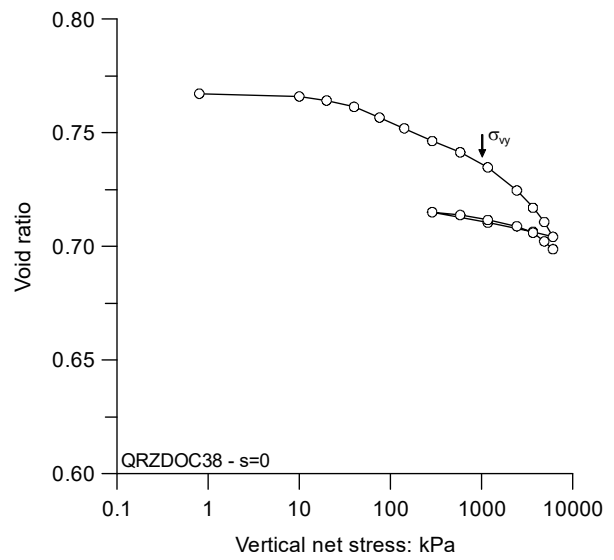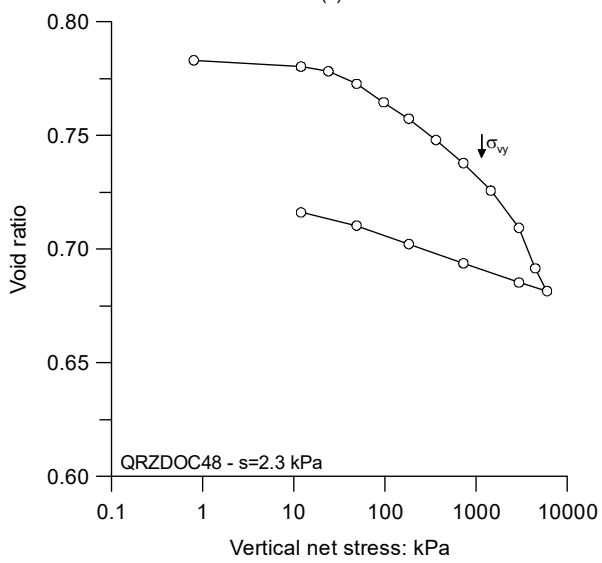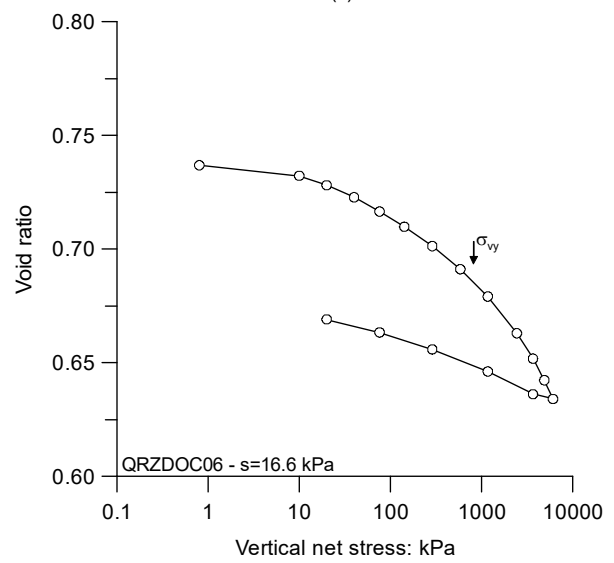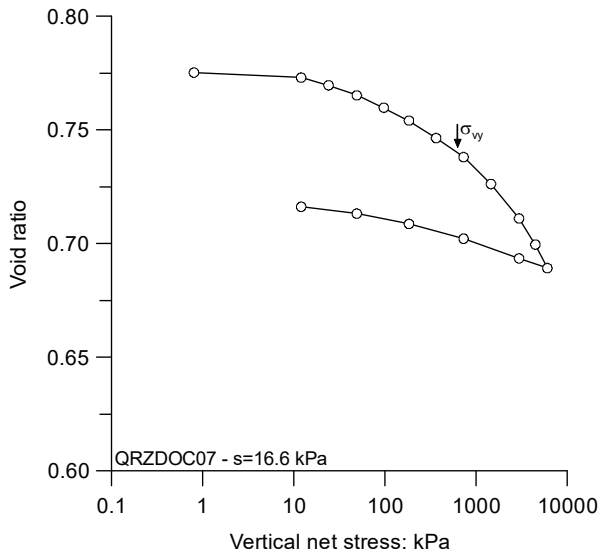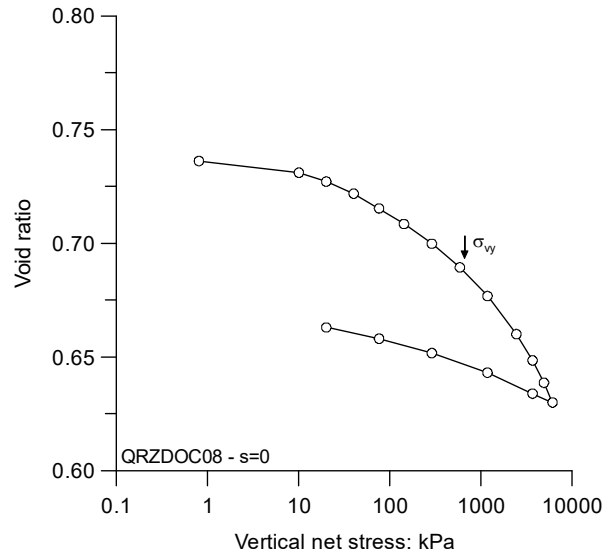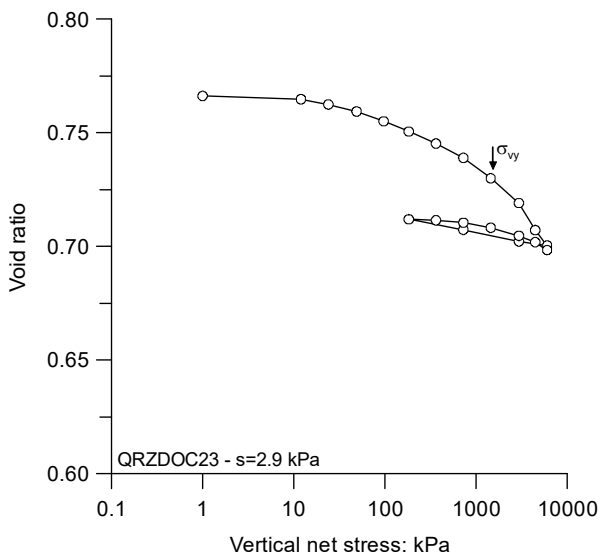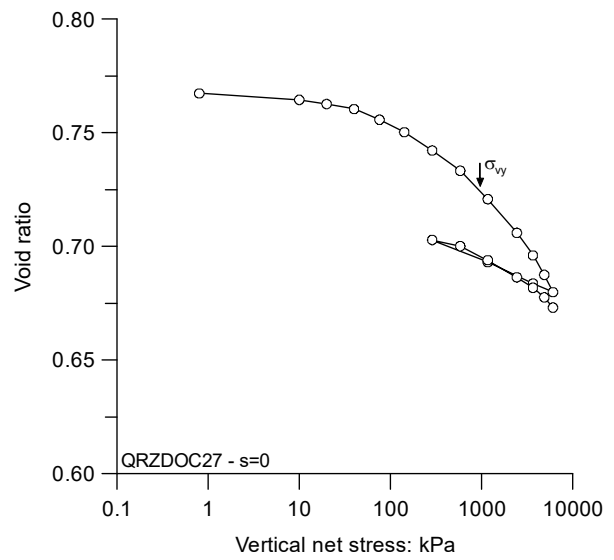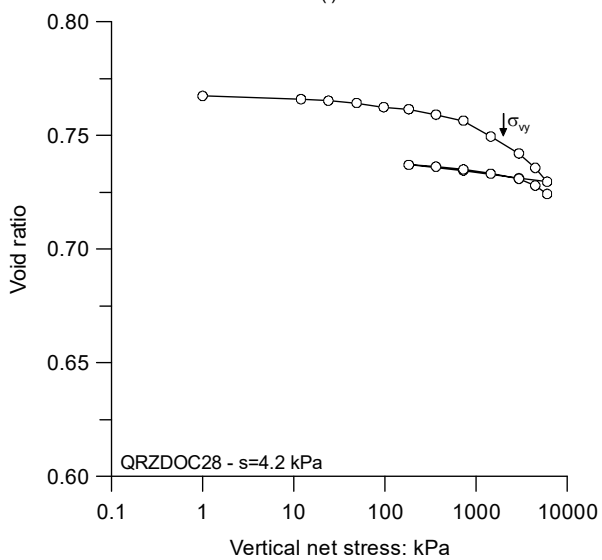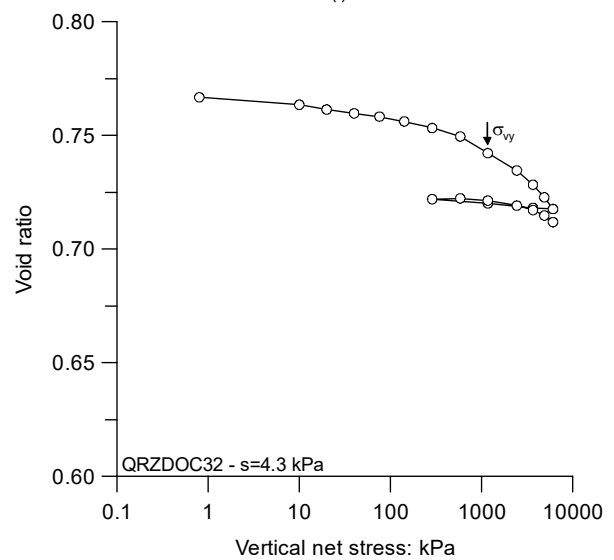
(n)
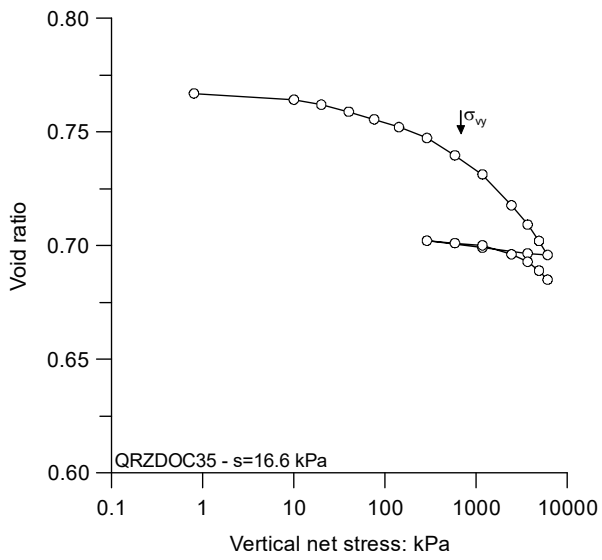
(o)
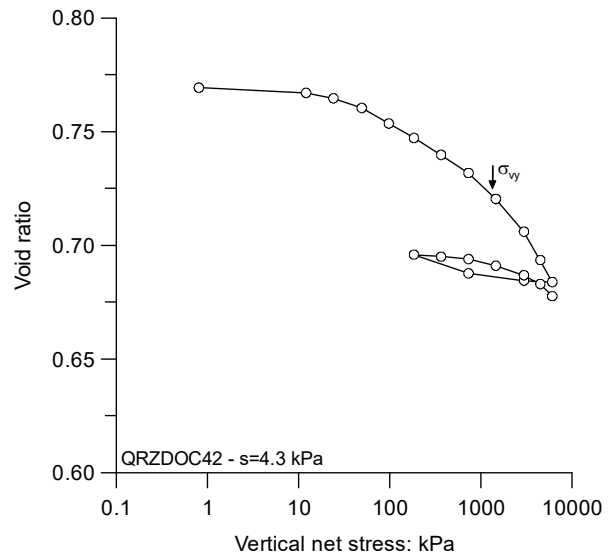
(p)
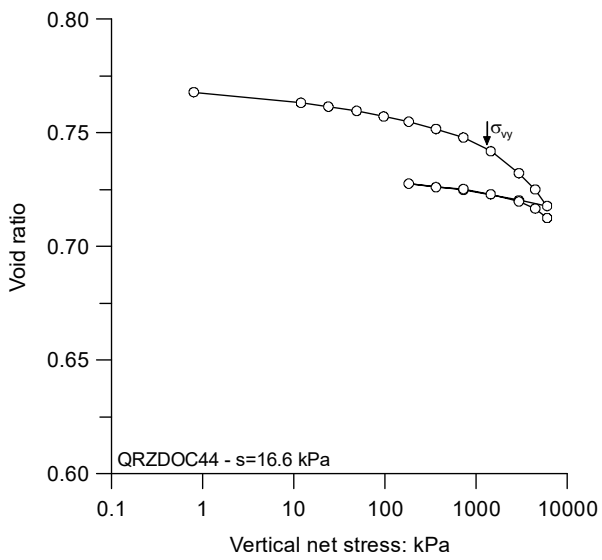
(q)
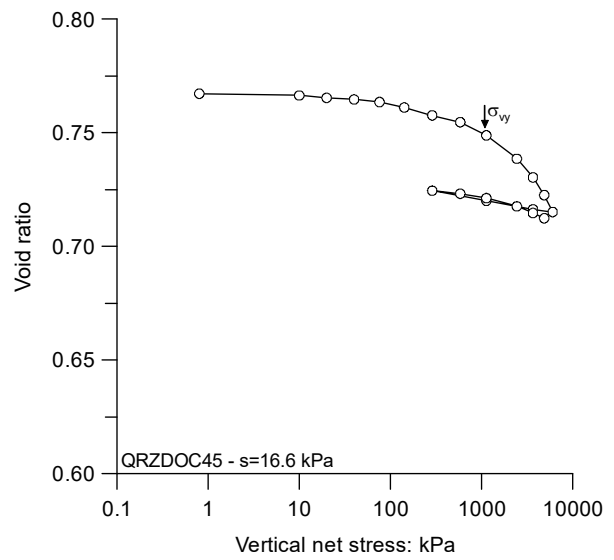
(r)
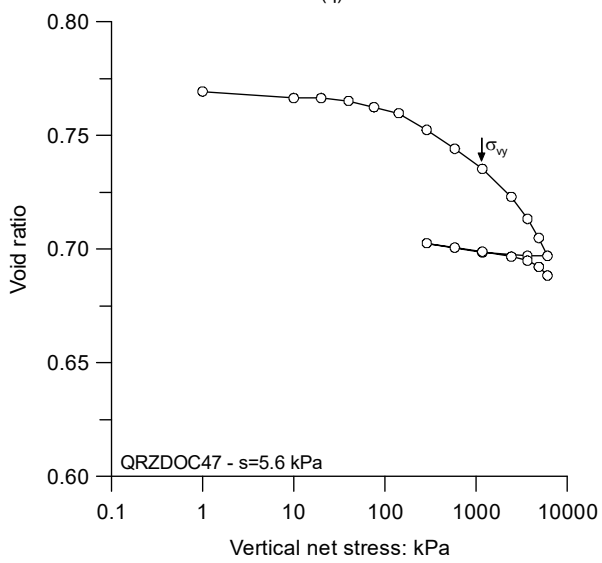
(s)
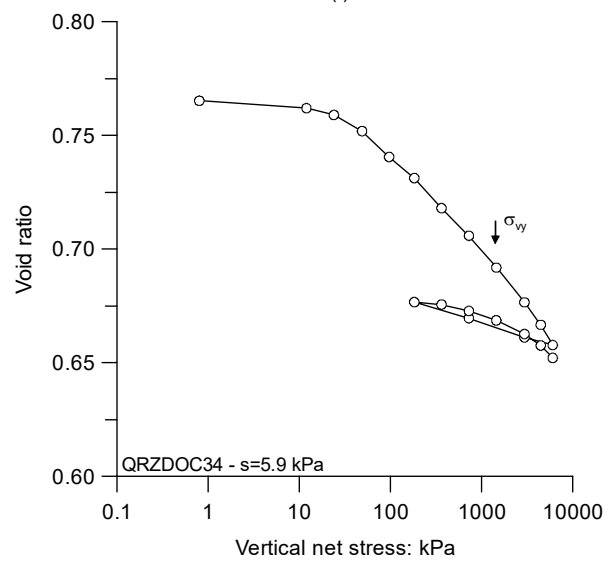
(t)
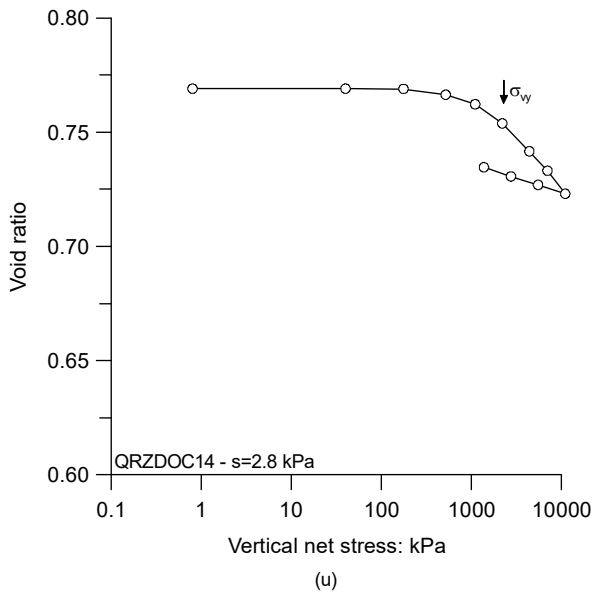
Figure A4. Constant water content oedometric curves on quartz sand.
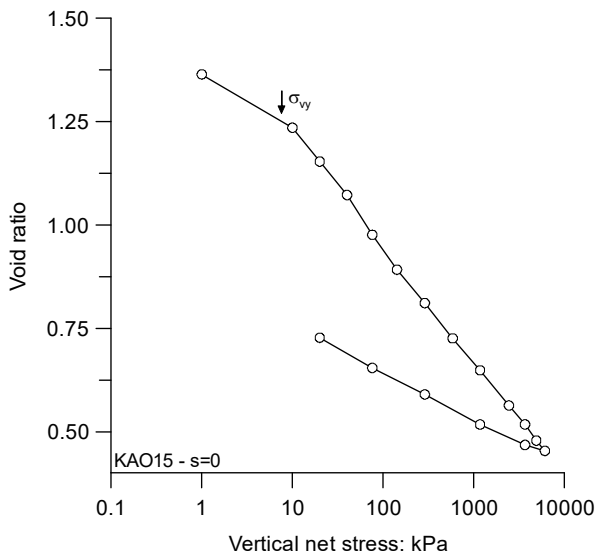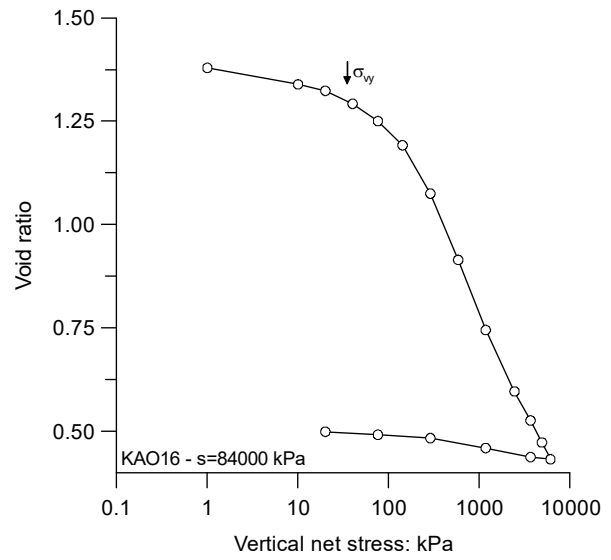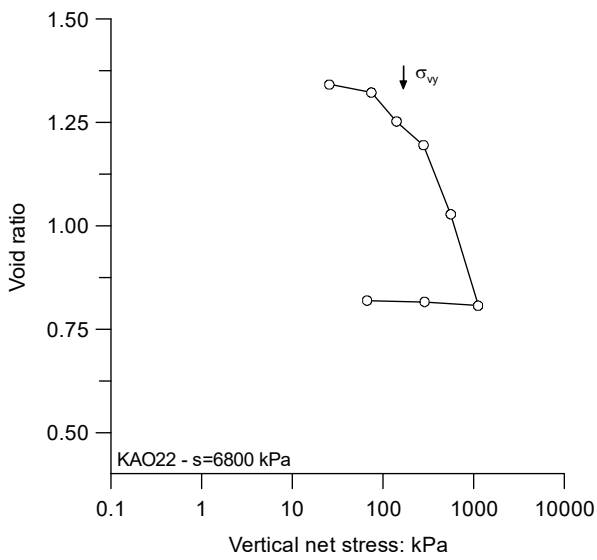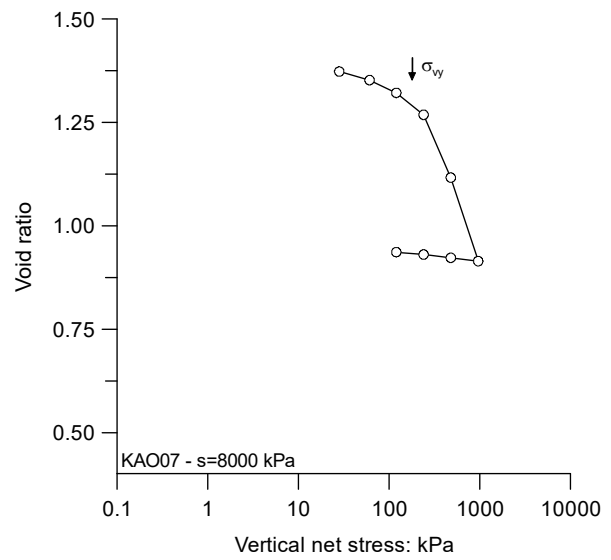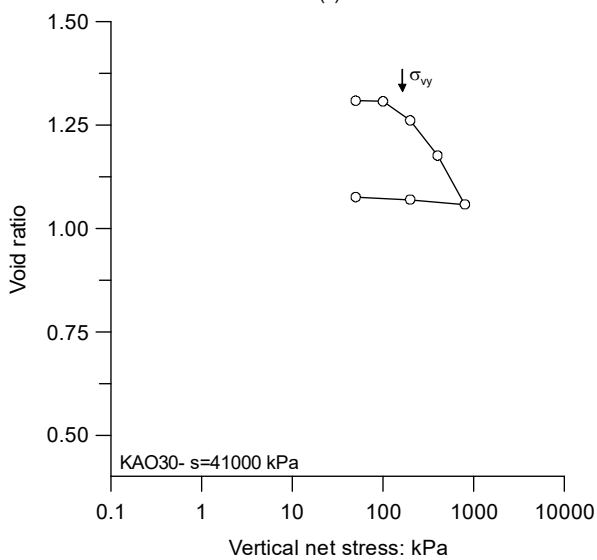
Figure A5. Controlled-suction oedometric curves operating with the vapor equilibrium technique performed on Speswhite kaolin.
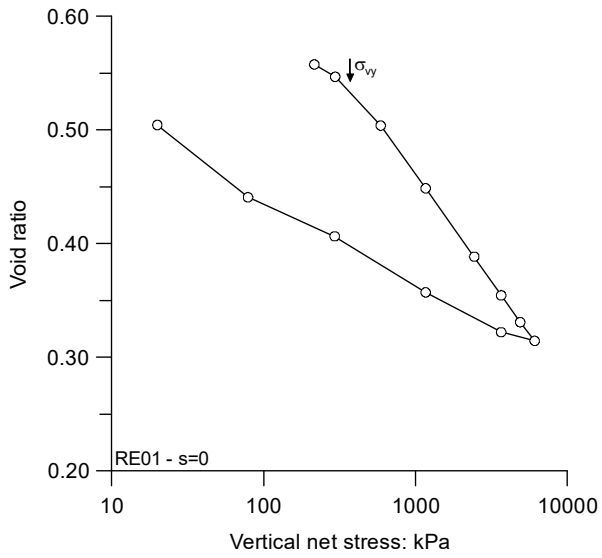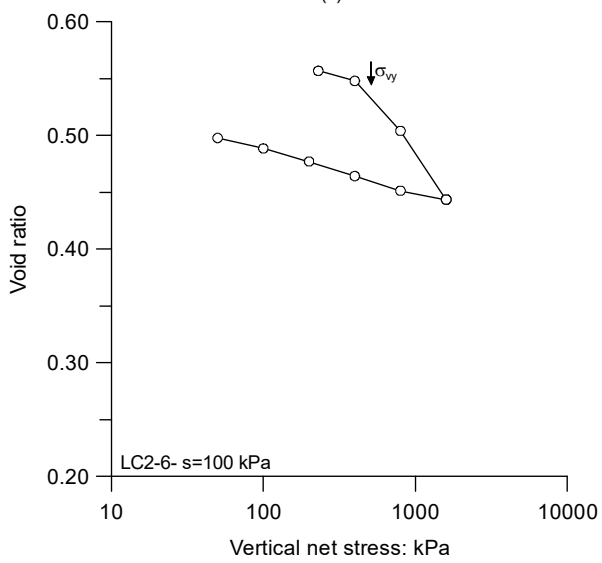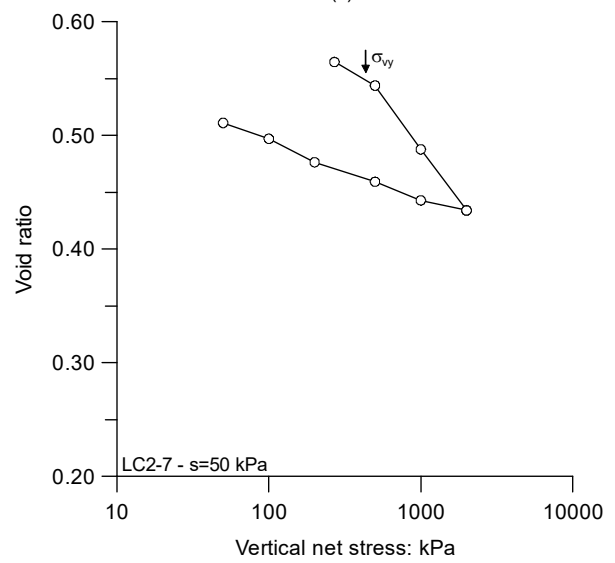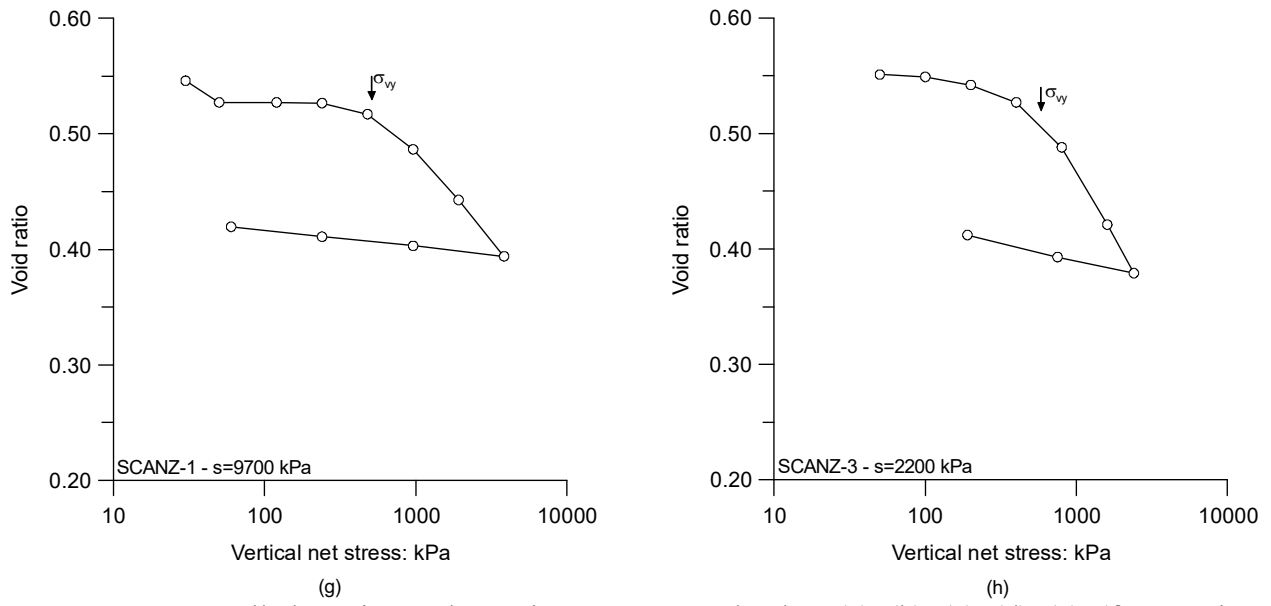
(a)
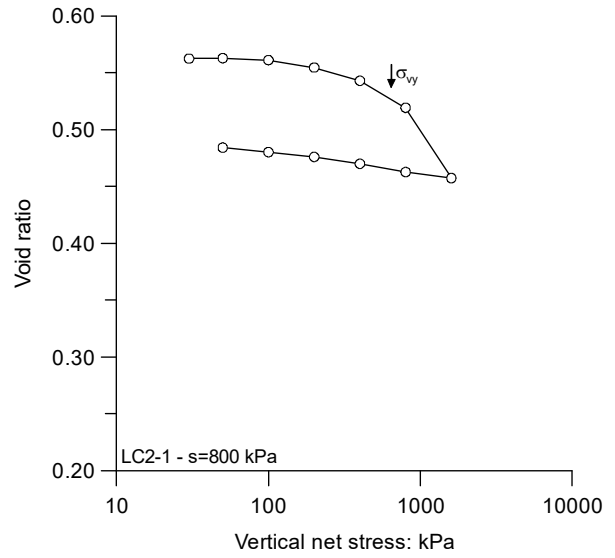
(b)
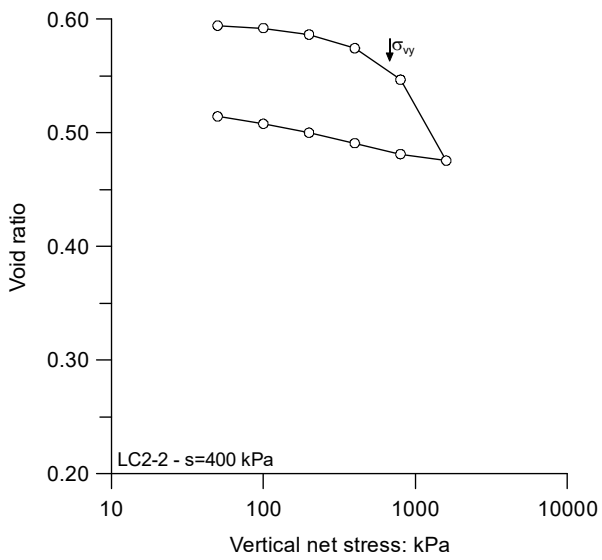
(c)
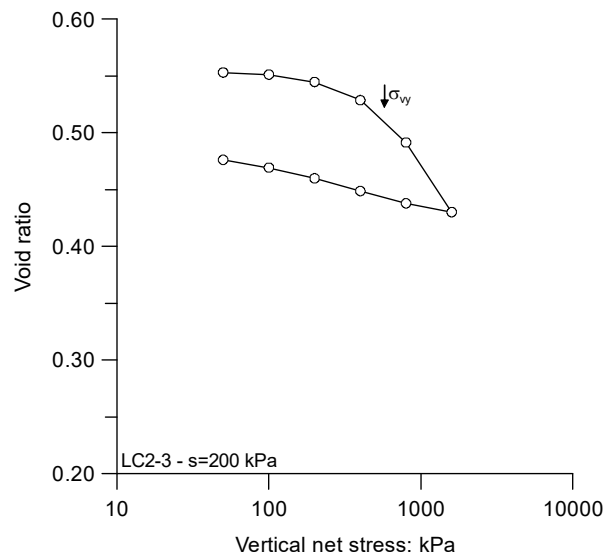
(d)

(e)

(f)

Figure A6. Controlled-suction oedometric curves on scaly clay: (a), (b), (c), (d), (e), (f) operating with the axial translation technique; (g), (h) operating with the vapor equilibrium technique.